PB80-227580

Development of Mesoscale Air Quality Simulation Models. Volume 1. Comparative Sensitivity Studies of PUFF, PLUME, and GRID Models for Long Distance Dispersion

Environmental Research and Technology, Inc.
Concord, MA

Prepared for

Environmental Sciences Research Lab.
Research Triangle Park, NC

Sep 79

U.S. Department of Commerce
National Technical Information Service
NTIS

September 1979

DEVELOPMENT OF MESOSCALE AIR QUALITY SIMULATION MODELS

VOLUME 1. COMPARATIVE SENSITIVITY STUDIES OF PUFF, PLUME, AND GRID MODELS FOR LONG-DISTANCE DISPERSION

Arthur Bass, Carl W. Benkley,
Joseph S. Scire, and Charles S. Morris

Environmental Research & Technology, Inc.
696 Virginia Road
Concord, MA 01742

NOAA Contract No. 03-6-02-35254

Project Officer

Herbert J. Viebrock
Meteorology Laboratory
National Oceanic and Atmospheric Administration
Research Triangle Park, NC 27711

OFFICE OF RESEARCH AND DEVELOPMENT
ENVIRONMENTAL PROTECTION AGENCY
WASHINGTON, DC 20460

50272-101

REPORT DOCUMENTATION PAGE

1. REPORT NO. EPA/DF-80/007d
EPA-600/7-80-056

2.

PB80-227580

4. Title and Subtitle
DEVELOPMENT OF MESOSCALE AIR QUALITY SIMULATION MODELS. Volume 1. Comparative Sensitivity Studies of PUFF, PLUME, and GRID Models for Long Distance Dispersion

5. Report Date
September 1979

6.

7. Author(s) Arthur Bass, Carl W. Benkley, Joseph S. Scire, and Charles S. Morris

8. Performing Organization Rept. No.

9. Performing Organization Name and Address

Environmental Research & Technology, Inc.
696 Virginia Road
Concord, Massachusetts 01742

10. Project/Task/Work Unit No.
N/A

11. Contract(C) or Grant(G) No.
(C) 03-6-02-35254
(G)

12. Sponsoring Organization Name and Address

Environmental Sciences Research Laboratory
Office of Research and Development
U.S. Environmental Protection Agency
Research Triangle Park, North Carolina 27711

13. Type of Report & Period Covered
Final Report

14.

15. Supplementary Notes

For magnetic tape see PB 80-227549

16. Abstract (Limit: 200 words)

This report, Volume 1 in a series entitled 'Development of Mesoscale Air Quality Simulation Models,' provides detailed comparisons and sensitivity analyses of three candidate models, MESOPLUME, MESOPUFF, and MESOGRID. This was not a validation study; there was no suitable regional air quality data base for the Four Corners area. Rather, the models have been evaluated by analyzing: model response to varying mesoscale flow regimes, model sensitivity to systematic variations in meteorological and model design parameters; and model accuracy versus computational requirements and cost.

COLOR ILLUSTRATIONS REPRODUCED
IN BLACK AND WHITE

17. Document Analysis a. Descriptors
Air pollution
Atmospheric models
Algorithms
Dispersion

b. Identifiers/Open-Ended Terms

REPRODUCED BY
NATIONAL TECHNICAL
INFORMATION SERVICE
U.S. DEPARTMENT OF COMMERCE
SPRINGFIELD, VA 22161

c. COSATI Field/Group

18. Availability Statement
RELEASE UNLIMITED

19. Security Class (This Report)
UNCLASSIFIED

20. Security Class (This Page)
UNCLASSIFIED

21. No. of Pages
221

22. Price

(See ANSI-Z39.18)

See Instructions on Reverse

OPTIONAL FORM 272 (4-77)
(Formerly NTIS-35)
Department of Commerce

DISCLAIMER

Publication of this report does not signify that the contents necessarily reflect the views and policies of the U.S. Environmental Protection Agency, nor does mention of trade names or commercial products constitute endorsement or recommendation for use.

TABLE OF CONTENTS

Page

LIST OF ILLUSTRATIONS vii

LIST OF TABLES xiii

1. INTRODUCTION 1
   - 1.1 Overview 1
   - 1.2 Mesoscale Modeling Approaches 4
   - 1.3 Integrated Mesoscale Modeling System 8
     - 1.3.1 MESOPAC 8
     - 1.3.2 MESOPLUME 13
     - 1.3.3 MESOPUFF 15
     - 1.3.4 MESOGRID 15
     - 1.3.5 MESOFILE 18
   - 1.4 Organization of Report 18
2. MODEL COMPARISON AND MODEL SENSITIVITY TESTS 22
   - 2.1 Requirement for Objective Criteria 22
   - 2.2 Test Protocol 22
   - 2.3 Initialization and Inventory Choices 25
   - 2.4 Description of Base Cases 25
     - 2.4.1 Model Design and Run Parameters 25
     - 2.4.2 Meteorological Scenarios 27
   - 2.5 Description of the Model Output Analyses 27
3. COMPARISONS OF MODEL BASE CASE RESULTS 45
   - 3.1 Qualitative Comparisons for Single and Multiple Point Sources 45
   - 3.2 Quantitative Comparisons of Model Results 73
   - 3.3 Model Simulations of Plume Fumigation 78
4. RESULTS OF MODEL SENSITIVITY TESTS 92
   - 4.1 Sensitivity to Decay and Dry Deposition Processes 92
   - 4.2 Sensitivity to Mixing Depth Variations 99
   - 4.3 Sensitivity to Systematic Variation of Wind Direction and Crosswind Growth Rate 105
   - 4.4 Model Sensitivity to Variations in Wind Speed 112
   - 4.5 Sensitivity of MESOGRID to Variations in K_z 114

TABLE OF CONTENTS (Continued)

Page

5. MODEL COST/SENSITIVITY ISSUES 120
  5.1 Overview 120
  5.2 Model Execution Cost Formulas 120
    5.2.1 MESOPAC Run Time 120
    5.2.2 MESOPLUME Run Time 121
    5.2.3 MESOPUFF Run Time 121
    5.2.4 MESOGRID Run Time 122
  5.3 Model Sensitivity to Changes in Time Step 124
6. SUMMARY, CONCLUSIONS, AND RECOMMENDATIONS 131
  6.1 Basic Model Development Objectives 131
  6.2 Model Verification 132
  6.3 Comparative Model Performance 132
  6.4 Model Sensitivity Results 133
  6.5 Adequacy of Meteorological Data 135
  6.6 Comparative Costs 136
  6.7 Recommended Model Choices 137
  6.8 Other Applications 137

REFERENCES 140
APPENDIX A MESOPLUME TECHNICAL DISCUSSION
APPENDIX B MESOPUFF TECHNICAL DISCUSSION
APPENDIX C MESOGRID TECHNICAL DISCUSSION
APPENDIX D SCALE ANALYSIS FOR TERMS IN MASS CONTINUITY EQUATION

LIST OF ILLUSTRATIONS

Figure		Page
1-1	Existing and Proposed (through 1987) Major Energy Sources in the Four Corners Region	2
1-2	The Variable Trajectory Plume Model Approach	5
1-3	The Variable Trajectory Puff Model Approach	6
1-4	Integrated Modeling System	9
1-5	Mesoscale Meteorology Package (MESOPAC)	10
1-6	Rawinsonde Stations in the General Four Corners Area	11
1-7	Mesoscale Plume Model (MESOPLUME)	14
1-8	Mesoscale Puff Model (MESOPUFF)	16
1-9	Mesoscale Grid Model (MESOGRID)	17
1-10	File Management and Analysis (MESOFILE)	19
1-11	Examples of MESOFILE Graphical Displays	20
2-1	A Schematic Representation of Episodes 1 and 2 Flow Regimes	28
2-2	Episode 1 Wind Vector and Isotach (m/s) Fields	29
2-3	Episode 1 Mixing Depth (m) Fields	33
2-4	Episode 1 PGT Stability Class Fields	35
2-5	Episode 2 Wind Vector and Isotach (m/s) Fields	37
3-1	Episode 1 Day 167 Single Source Dispersion Model Comparisons (SO_2)	46
3-2	Episode 1 Day 167 Single Source Dispersion Model Comparisons ($SO_4^=$)	49

LIST OF ILLUSTRATIONS (Continued)

Figure		Page
3-3	Episode 1 Day 169 Single Source Dispersion Model Comparisons (SO_2)	50
3-4	Episode 1 Day 169 Single Source Dispersion Model Comparisons ($SO_4^=$)	53
3-5	Episode 1 Day 167 Multiple Source Dispersion Model Comparisons (SO_2)	55
3-6	Episode 1 Day 169 Multiple Source Dispersion Model Comparisons (SO_2)	58
3-7	Episode 2 Day 124, 125, 126, and 127 Single Source Dispersion Model Comparisons (SO_2)	67
3-8	Days 167, 168, and 169 Comparison of the Different Models Results (Correlation Coefficient r)	74
3-9	Days 123, 124, 125, 126, and 127 Comparison of the Different Models Results (Correlation Coefficient r)	74
3-10	Episode 1--Comparison of the Number of Points in the Plume NP Computed by Each Model	76
3-11	Episode 2--Comparison of the Number of Points in the Plume NP Computed by Each Model	76
3-12	Episode 1--Comparison of the Different Model Results [Fractional Deviation of the Means (FDM)]	77
3-13	Episode 2--Comparison of the Different Model Results [Fractional Deviation of the Means (FDM)]	77
3-14	MESOPLUME Time Sequence of 1-hour Average SO_2 Concentrations (7 pm MST Day 166 to 1 pm Day 167)	79
3-15	Time Sequence of Mixing Depths (7 pm MST Day 166 to 1 pm Day 167)	82
3-16	MESOPLUME Mean Plume Concentration Cycle (for 1-Hour Averages)	85

LIST OF ILLUSTRATIONS (Continued)

Figure		Page
3-17	MESOPUFF Time Sequence of 1-Hour Average SO_2 Concentrations (7 pm MST Day 166 to 1 pm Day 167)	86
3-18	MESOGRID Time Sequence of 1-Hour Average SO_2 Concentrations (7 pm MST Day 166 to 1 pm Day 167)	89
4-1	MESOPLUME Sensitivity to Decay Rate and Dry Deposition Variations (Days 167-169)	94
4-2	MESOPUFF Sensitivity to Decay Rate and Dry Deposition Variations (Days 167-169)	96
4-3a	MESOPLUME Fractional Difference Field Comparison for v_d (SO_2) = 0.1 m/s Case vs. Base Case (Day 169)	97
4-3b	MESOPLUME Fractional Difference Field Comparison for v_d (SO_2) = 0.001 m/s Case vs. Base Case (Day 169)	97
4-3c	MESOPLUME Fractional Difference Field Comparison for v_d (SO_2) = 0.1 m/s Case vs. Base Case (Day 167)	98
4-3d	MESOPLUME Fractional Difference Field Comparison for v_d (SO_2) = 0.001 m/s Case vs. Base Case (Day 167)	98
4-4a	MESOPLUME Fractional Difference Field Comparison for $k_1 = -5.56 \times 10^{-5}$ Case vs. Base Case (Day 169)	100
4-4b	MESOPLUME Fractional Difference Field Comparison for $k_1 = -5.56 \times 10^{-7}$ Case vs. Base Case (Day 169)	100
4-4c	MESOPLUME Fractional Difference Field Comparison for $k_1 = -5.56 \times 10^{-5}$ Case vs. Base Case (Day 167)	101
4-4d	MESOPLUME Fractional Difference Field Comparison for $k_1 = -5.56 \times 10^{-7}$ Case vs. Base Case (Day 167)	101

LIST OF ILLUSTRATIONS (Continued)

Figure | Page

4-5 MESOPUFF Sensitivity to Mixing Depth Variations (Days 167-169) 102

4-6a MESOPLUME Fractional Difference Field Comparison for Mixing Depth Multiplier = 2.0 Case vs. Base Case (Day 167) 103

4-6b MESOPLUME Fractional Difference Field Comparison for Mixing Depth Multiplier = 0.5 Case vs. Base Case (Day 167) 103

4-6c MESOPLUME Fractional Difference Field Comparison for Mixing Depth Multiplier = 2.0 Case vs. Base Case (Day 169) 104

4-6d MESOPLUME Fractional Difference Field Comparison for Mixing Depth Multiplier = 0.5 Case vs. Base Case (Day 169) 104

4-7 MESOPLUME Sensitivity of r (——) and FDM (---) to Systematic Variations in Wind Direction $\Delta\theta$ and Plume Growth Rate $d\sigma_y/dt$ (Day 167) 108

4-8 MESOPLUME Sensitivity of r (——) and FDM (---) to Systematic Variations in Wind Direction $\Delta\theta$ and Plume Growth Rate $d\sigma_y/dt$ (Day 169) 109

4-9 MESOPUFF Sensitivity of r (——) and FDM (---) to Systematic Variations in Wind Direction $\Delta\theta$ and Plume Growth Rate $d\sigma_y/dt$ (Day 167) 110

4-10 MESOPUFF Sensitivity of r (——) and FDM (---) to Systematic Variations in Wind Direction $\Delta\theta$ and Plume Growth Rate $d\sigma_y/dt$ (Day 169) 111

4-11 Effect of Wind Speed on Idealized Plume Shape 113

4-12a MESOPLUME Sensitivity of r to Wind Speed Multiplier (a) Variations (Days 167-169) 115

4-12b MESOPUFF Sensitivity of r to Wind Speed Multiplier (a) Variations (Days 167-169) 115

4-13a MESOPLUME Sensitivity of FDM to Wind Speed Multiplier (a) Variations (Days 167-169) 116

4-13b MESOPUFF Sensitivity of FDM to Wind Speed Multiplier (a) Variations (Days 167-169) 116

LIST OF ILLUSTRATIONS (Continued)

Figure		Page
4-14	MESOGRID Sensitivity to Variations in K_z (Day 167)	117
4-15a	MESOGRID Difference Field Comparison for K_z Multiplier = 0.1 Case vs. Base Case (Day 167)	118
4-15b	MESOGRID Difference Field Comparison (Limited Grid) for Requested Time Step = 5 Minutes Case vs. Base Case (Day 167)	118
5-1a	MESOPUFF CPU Run Time (t) and Sensitivity of r to Variations in Sampling Rate and Puff Emission Rate (Days 167-169)	125
5-1b	MESOPUFF CPU Run Time (t) and Sensitivity of FDM to Variations in Sampling Rate and Puff Emission Rate (Days 167-169)	126
5-2	Variation of Correlation Coefficient with Puff Emission Rate	127
5-3	Comparative Model Run Execution Times (5-day run)	129
A-1	Schematic Representation of the Segmented Plume	146
A-2	One Possible Arrangement of Sampling and Basic Computational Grids	148
A-3	Calculation of the Trajectory of a Plume Segment Endpoint	151
A-4	Calculation of the Concentration C(i,j) by the Sampling Function	157
A-5	A Schematic Representation of Adjacent Plume Segments in Rapidly Decelerating Flow	160
A-6	A Schematic Representation of Adjacent Plume Segments in Highly Curvilinear Flow	160
A-7	Response of Two Plume Elements to Changes in Mixing Depth	164
A-8	MESOPLUME vs. the Conventional Gaussian Plume	168

LIST OF ILLUSTRATIONS (Continued)

Figure		Page
B-1	Schematic Representation of Discrete Puffs	172
B-2	One Possible Arrangement of Sampling and Basic Computational Grids	175
B-3	Calculation of the Trajectory of a Plume Segment Endpoint	178
B-4	Calculation of the Concentration C(i,j) by the Sampling Function	183
B-5	Response of Two Plume Elements to Charges in Mixing Depth	190
B-6	MESOPUFF vs. the Conventional Gaussian Plume	193
C-1	A Schematic Representation of the MESOGRID Cartesian Coordinate System	199
C-2	Vertical Structure of the MESOGRID Computation Grid Assuming Default Values	201
C-3	Scale Parameters for the Advection of a Rectangular Block of Uniformly Mixed Material	205

LIST OF TABLES

Table		Page
2-1	Model Sensitivity Test Protocol	23
2-2	Nominal Design Parameters	26
2-3	Statistical Measures Used	43
4-1	Values of the Deposition Velocities and Decay Rates Used in the Sensitivity Tests	93
4-2	Matrix of Wind Shift and Growth Rate Sensitivity Cases	106
5-1	Maximum Values of u and K_z vs. Time Step Δt	123
6-1	Recommended Model Choices	138
A-1	Coefficients for Dispersion Parameter Formulas	155
A-2	Comparison of Cu/Q Values for MESOPLUME and Turner Workbook-Computed Values	167
B-1	Coefficients for Dispersion Parameter Formulas	181
B-2	Comparison of Cu/Q Values for MESOPUFF and Turner Workbook-Computer Values	192
C-1	Inverse Monin-Obukhov Length $L^{-1}(m^{-1})$ as a Function of PGT Stability Class, for Roughness Length z_o = 25 cm (After Golder 1972)	208
C-2	Stability-Dependent Expressions for K_z in the Surface Layer and $\left.\frac{\partial K_z}{\partial z}\right\|_S$	210
C-3	Maximum Values of u and $\overline{K}_{1.5}$, $\overline{K}_{2.5}$ vs. Time Step Δt, for Nominal Model Parameters	212
C-4	Determining when MESOGRID will Modify K_z Profiles	214

1. INTRODUCTION

1.1 Overview

In response to a growing national commitment to the greatly expanded use of indigenous coal reserves to meet energy generation demands, the Four Corners region of the southwestern United States will experience increased development of coal-fired steam electric power plants and coal gasification and oil shale recovery facilities. But, as mandated by federal statutes and regulations reflecting the strong nationwide support for environmental protection, further coal-based energy resource development (ERD) will only be permitted where consistent with the maintenance of human health, welfare, and environmental quality. At the present time, the permitting of a new major coal-burning facility will be most affected by the regulations governing emissions and ambient air concentrations of criterion air pollutants, as well as by their effects on other air quality-related values, e.g., visibility and acid rain.

For major new coal-fired steam electric power plants and other coal-based major ERD point sources, the pollutant of most concern at the present time is sulfur dioxide (SO_2), especially considering the growing body of evidence linking SO_2 emissions to increased concentrations of sulfate aerosols ($SO_4^=$). Under the present statutes, the permitting of a new (or expanded) major source of SO_2 emissions is subject to both the existing National Ambient Air Quality Standards (NAAQS), as well as the new source review requirements for the Prevention of Significant Deterioration (PSD) of existing ambient air quality.

Thus, the siting and generation capacity of coal-based energy facilities in the Four Corners region will be increasingly constrained by the expected impacts of these facilities on both local and regional-scale ambient air quality. To illustrate the regional nature of the problem, Figure 1-1 displays one proposed scenario for the locations of major energy-related SO_2 point sources in the Four Corners region projected to 1987.

Suitable simulation tools are clearly needed to assess the impacts of different energy development scenarios on air quality throughout the Four Corners region. To meet this need in the public interest, the National Oceanic and Atmospheric Administration (NOAA) has sponsored a study by Environmental Research & Technology, Inc. (ERT) to develop, compare, evaluate, and exercise a number of alternative approaches to regional-scale ambient air quality modeling in the Four Corners area. A major objective of this study has been to provide a suite of air quality simulation models that are both technically sound and computationally practical for assessing regional-scale impacts of energy development scenarios.

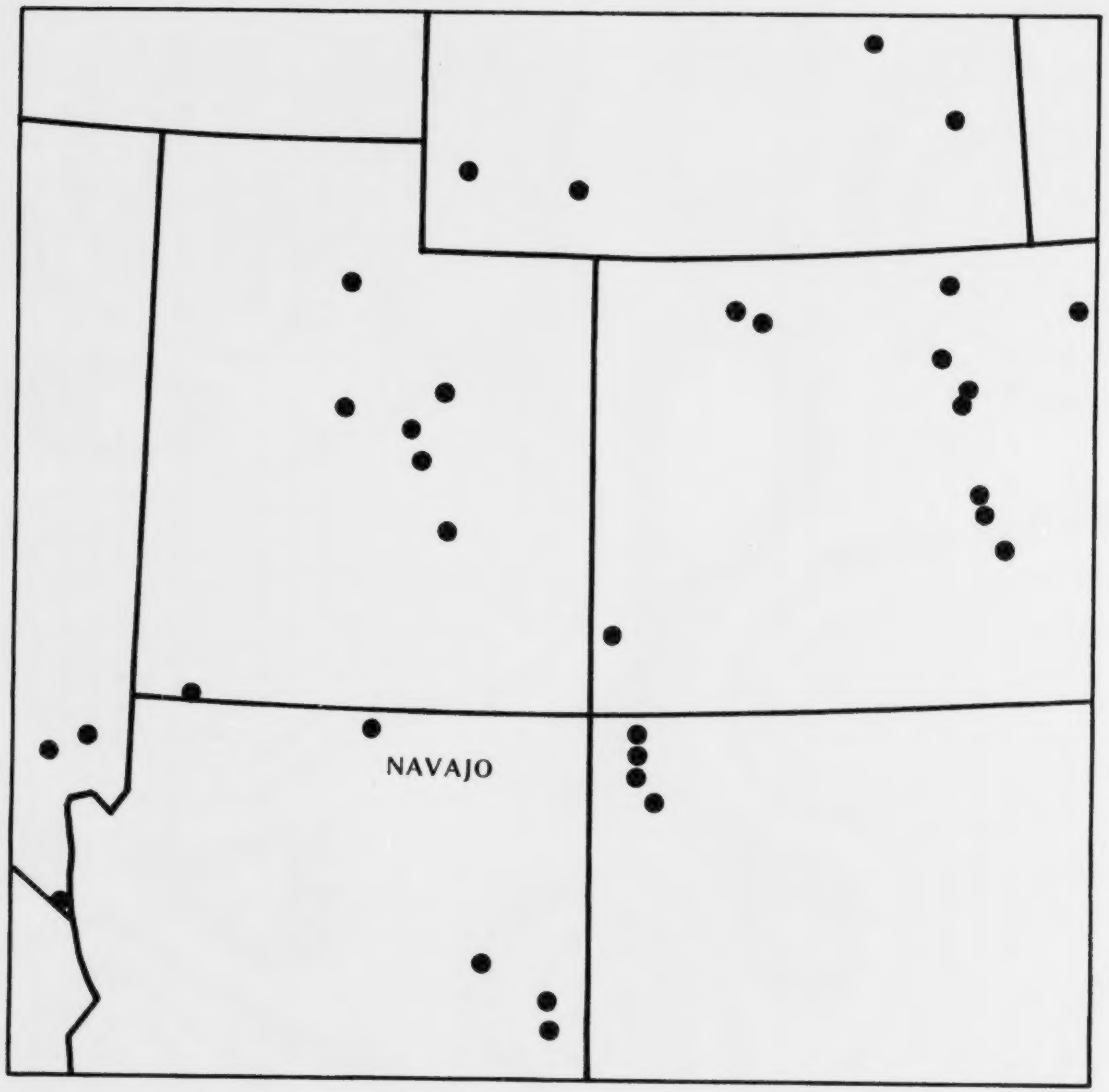

Figure 1-1 Existing and Proposed (through 1987) Major Energy Sources in the Four Corners Region

Three different air quality transport-diffusion models have been developed to address various features of point-source plume dispersion on the mesoscale [e.g., dispersion at ranges of 100 to 1,000 kilometers (km)]. The three models have been designed to meet the following objectives.

- Simulation of regional-scale aspects of plume transport and dispersion is emphasized; because model performance and resolution is optimized for the regional-scale, ambient air concentrations calculated in the near fields of sources, that is, less than 100 km, are not realistic.*
- The models are suitable for a broad range of actual meteorological dispersion conditions in the Four Corners area; and they are appropriate both for worst-case impact and for average dispersion studies.
- The models only require rawinsonde data readily available for the Four Corners region, but can accommodate other available meteorological data.
- The models are computationally practical for simulating the impacts of multiple point sources over periods of several days to several weeks.
- The models are easy to use for a variety of decision-making and regulatory applications.
- The models are intended as flexible testbeds that can be readily modified for further research, development, and simulation tasks.

These objectives were based on the following considerations: (a) the simulation of regional-scale plume transport and dispersion under different meteorological regimes requires modeling approaches that can respond to mesoscale spatial and temporal variations in wind field, mixing depth, and ambient turbulence levels; (b) the input meteorology fields necessary to drive the transport-dispersion models must be easily generated from readily available data if the models are to be useful to a wide user community; (c) the dispersion models must have moderate execution time and computer storage requirements if they are to be practical for multiple-source, multiple-day simulation exercises; (d) the model design should also allow for easy adaptation to future research needs and regulatory applications - thus, the programs should be highly modular, having components that are easily modified or readily interchanged; (e) the models must be applicable to the present regulatory environment - in particular, they must therefore be able to simulate short-term average ambient concentration values (e.g., 1-, 3-, and 24-hour averages).

---

*Subsequently, the MESOPUFF model has been augmented to provide realistic near-field impacts - see the companion report, Volume 3, 'User's Guide to MESOPUFF (Mesoscale Puff) Model'.

This report, Volume 1 in a series entitled 'Development of Mesoscale Air Quality Simulation Models', provides detailed comparisons and sensitivity analyses of three candidate models, MESOPLUME, MESOPUFF, and MESOGRID. This was not a validation study; there was no suitable regional air quality data base for the Four Corners area. Rather, the models have been evaluated by analyzing: model response to varying mesoscale flow regimes; model sensitivity to systematic variations in meteorological and model design parameters; and model accuracy versus computational requirements and cost.

1.2 Mesoscale Modeling Approaches

In a previous part of this study (Nuber et al. 1978), three candidate modeling approaches were identified for adaptation to this simulation effort. Each of the modeling approaches chosen can respond to the spatial and temporal variations in mesoscale meteorology, variations that are shown in this report to dominate plume transport and diffusion on regional scales. These modeling approaches have been implemented as three new models, namely:

- MESOPLUME, a mesoscale variable-trajectory Gaussian "plume-segment" model, adapted from the approach taken in the STRAM model (Hales et al. 1977);
- MESOPUFF, a mesoscale variable-trajectory Gaussian "puff" superposition model, adapted from the approach taken in the MESODIF model (Start and Wendell 1974);
- MESOGRID, a mesoscale Eulerian grid model based on the method of moments approach taken in the SULFA3D model (Egan et al. 1976).

Brief technical synopses of each of the three models are contained in Appendices A, B, and C, respectively; for additional information the individual model User's Guide (companion reports, Volumes 2-4) can be consulted: Benkley and Bass (1979a) for MESOPLUME, Benkley and Bass (1979b) for MESOPUFF, and Morris et al. (1979) for MESOGRID.

MESOPLUME and MESOPUFF are variable-trajectory plume models: that is, they describe a continuous plume by the transport and dispersion of fluid elements (plume segments or puffs) in a continuously deformable wind-field - see Figures 1-2 and 1-3. Variable-trajectory models of Gaussian type are natural extensions of the familiar straight-line Gaussian modeling approach (as described by Turner 1970), extensions

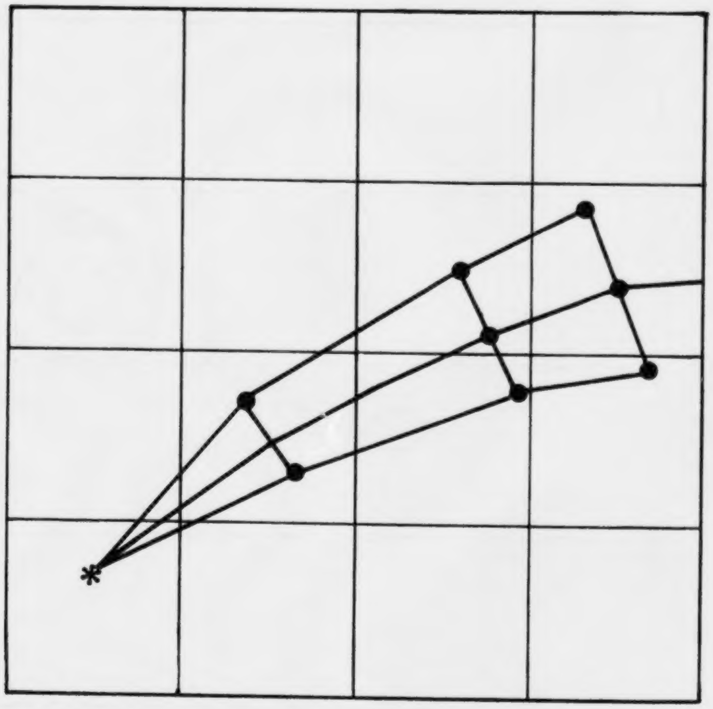

Figure 1-2 The Variable Trajectory Plume Model Approach

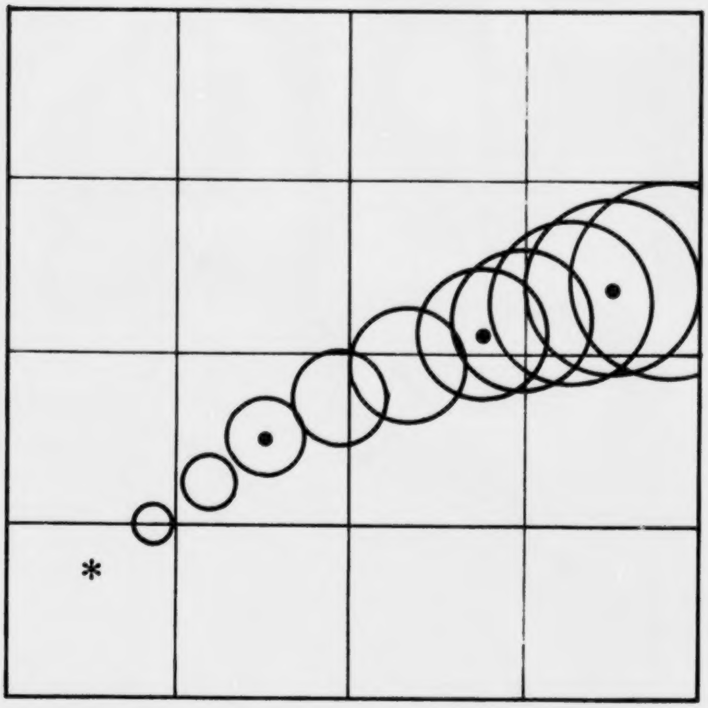

Figure 1-3 The Variable Trajectory Puff Model Approach

that take into account the often-important variability of plume trajectories, especially over regional transport scales.

Variable-trajectory models have some major advantages for regional-scale impact assessments, as compared to the conventional straight-line Gaussian models:

- Unlike the standard Gaussian plume model, the variable-trajectory model does not assume that the wind field persists uniformly over periods of many hours to days.
- On regional scales, the spatial and temporal variations in transport wind flows can produce large meanders in plume trajectories. For the models described here, meander effects can dominate plume dispersion on regional scales.
- Straight-line models are invalid for describing plume dispersion under strongly recirculating or stagnating meteorological flow conditions.

On the other hand, variable trajectory models do have disadvantages:

- They require substantially more computation time and computer resources than do straight-line models;
- The technical problem of distinguishing (a) plume dispersion effects - resulting from meander of the mean wind from (b) smaller-scale turbulent eddy-induced dispersion represented by the conventional Pasquill-Gifford-Turner dispersion coefficients - remains an open issue, and the choice of dispersion parameters for such models is still very uncertain (Nappo 1978). On balance, however, many experts advocate the use of variable-trajectory approaches when warranted by spatially and temporally varying meteorological conditions. The uncertainty in plume dispersion is, in many cases, of secondary importance - as this report will show - when compared to the uncertainties in characterizing the wind field.
- To date, little validation work has been done with variable trajectory models, principally for lack of adequate observational data bases; much more research, development and verification work should be done; some is now under way.
- These modeling approaches are new and unfamiliar. If they are to be used for regulatory applications, both the regulatory agencies and the air quality modeling community must be made familiar with their advantages and proper use for air quality impact assessments over mesoscale transport ranges.

1.3 Integrated Mesoscale Modeling System

To make as clear as possible a comparison among the respective advective-diffusive approaches, the original models were completely restructured, so that MESOPLUME, MESOPUFF and MESOGRID are identical in every aspect other than their advection-diffusion algorithms. Thus, the three new models share, where possible, the identical modules for plume rise, plume decay and deposition, plume growth with distance or travel time, and treatment of plume fumigation by entrainment within the growing mixed layer.

The dispersion models have been incorporated in an efficient, easy-to-use "integrated mesoscale modeling system". This system is schematically depicted in Figure 1-4. It consists of a closely-integrated set of independent models that perform discrete functions: meteorological preprocessing; plume transport and diffusion; postprocessing and analysis. The mesoscale meteorology preprocessor called MESOPAC (Benkley and Bass 1979c) drives any of the three mesoscale transport-diffusion models (MESOPLUME, MESOPUFF, or MESOGRID). In turn each of these models communicates its results in identical manner to the post-processing system, MESOFILE, responsible for file manipulation, display, and statistical analysis of all model output fields. Each component of this modeling system is described briefly below; complete descriptions of each of the five components are provided in the respective model User's Guides (companion reports, Volumes 2-6).

1.3.1 MESOPAC

Figure 1-5 illustrates the principal features of the mesoscale meteorological package (MESOPAC). MESOPAC is used to construct hourly time sequences of spatially variable, gridded meteorological fields. The fields produced are:

- horizontal wind components (u,v) at a user-specified level,
- mixing depth, and
- Pasquill-Gifford-Turner (PGT) stability class.

The input data required by MESOPAC are routinely available from National Weather Service (NWS) rawinsonde stations.* Figure 1-6 illustrates all the NWS rawinsonde stations in the Four Corners region. Twice-daily observational data from all of these stations were used when available. [Although the computational domain used for the dispersion model calculations is bounded by the rectangle shown in the figure, all of the rawinsonde stations shown were used in constructing the meteorological fields.]

---

*Use of MESOPAC is not restricted to the Four Corners geographic region.

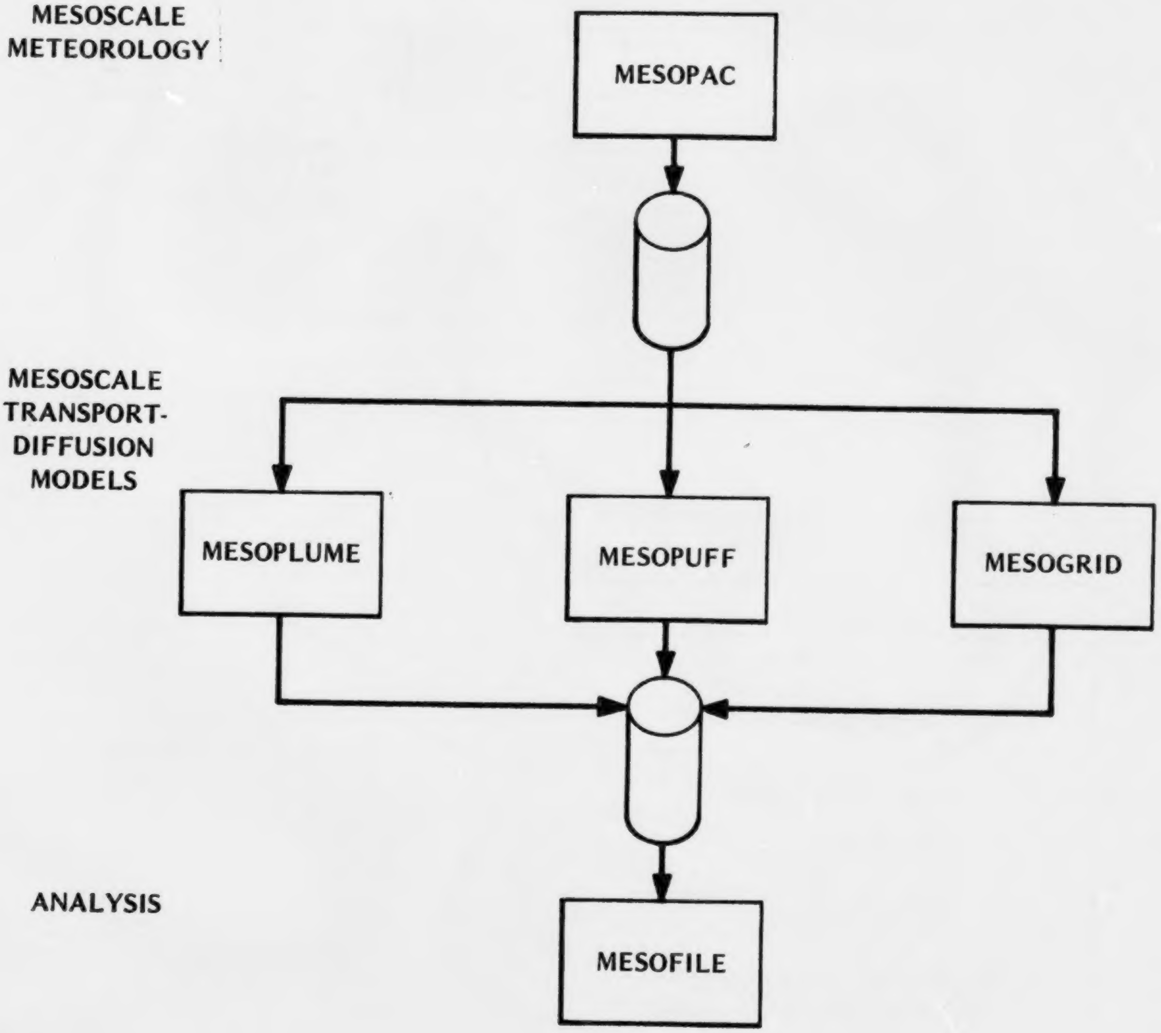
MESOSCALE METEOROLOGY
MESOPAC
MESOSCALE TRANSPORT-DIFFUSION MODELS
MESOPLUME
MESOPUFF
MESOGRID
ANALYSIS
MESOFILE

Figure 1-4 Integrated Modeling System

7901056

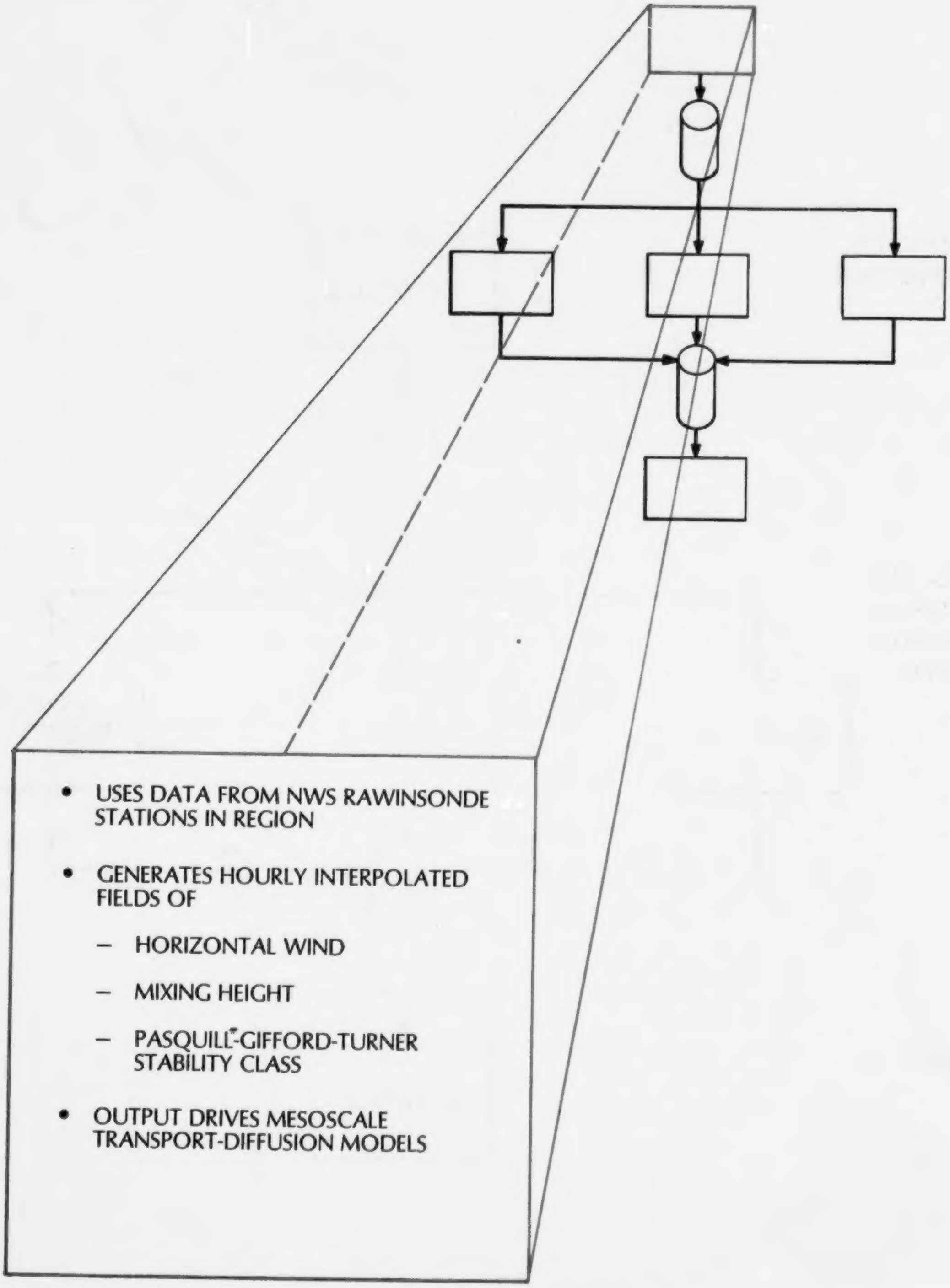

- USES DATA FROM NWS RAWINSONDE STATIONS IN REGION
- GENERATES HOURLY INTERPOLATED FIELDS OF
  - HORIZONTAL WIND
  - MIXING HEIGHT
  - PASQUILL-GIFFORD-TURNER STABILITY CLASS
- OUTPUT DRIVES MESOSCALE TRANSPORT-DIFFUSION MODELS

7901028 7901027

Figure 1-5 Mesoscale Meteorology Package (MESOPAC)

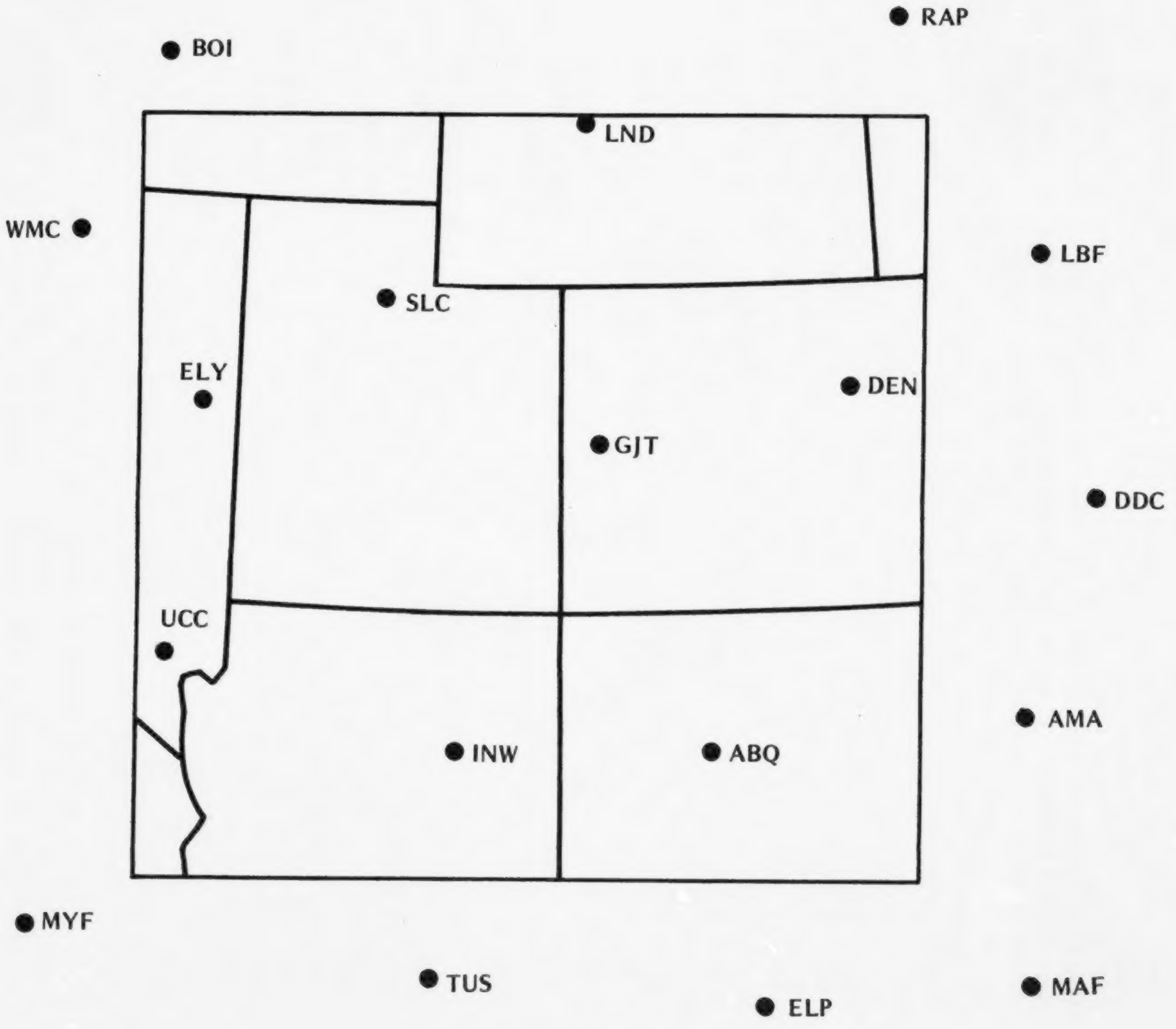
BOI
RAP
LND
WMC
LBF
SLC
ELY
DEN
GJT
DDC
UCC
AMA
INW
ABQ
MYF
TUS
ELP
MAF

Figure 1-6 Rawinsonde Stations in the Four Corners Region

The MESOPAC model generates a one-level horizontal wind field, based entirely on the observational station wind data supplied. Neither terrain channeling influences nor variations in wind with height above terrain are assumed in this model. As precedents for using single-level wind fields to make regional-scale transport-diffusion calculations, other published simulation studies of plume transport on the regional scale have used advecting wind fields invariant with height [e.g., Liu and Durran (1977) or Hales et al. (1977)]. Indeed, for the approaches typified by MESOPLUME and MESOPUFF, the use of layer-averaged winds is a practical necessity to avoid splitting plume/puff elements at each time step. Little incremental benefit is gained by using multiple-layer wind fields in simulations over rough terrain such as the Four Corners area - regions for which reliable wind field data are sparse, and for which any current interpolation scheme is conjectural.

In view of the chief objective - to provide practical modeling tools for simulations over the Four Corners region - it was decided to construct horizontal wind fields that might best describe the regional-scale advection of plumes as averaged over the mixed layer. It is not trivial to determine the appropriate level or the height interpolation method to be used: local wind circulations, induced by the complex topography of the Four Corners region, or by local thermal effects, may generate near-surface flows that are effectively uncoupled from mesoscale boundary layer transports. For application in the general Four Corners area, the rawinsonde data for the 700-millibar (mb) (mandatory) level was used to construct the horizontal wind field, because the 700-mb level frequently lies within the upper portion of the boundary layer in the western United States; and, over most of the Four Corners region, the surface pressure is less than the next mandatory level, 850 mb.*

In brief, MESOPAC interpolates gridded wind field values (u,v) to model grid points at each time step, using an inverse-square distance weighting procedure with wind data from one or more user-specified radiosonde stations. For hours other than 0000 Greenwich Mean Time (GMT) and 1200 GMT, the initial-guess wind field is synthesized by linearly interpolation with time from the bracketing 0000 GMT and 1200 GMT wind fields. It is not suggested here that such a procedure is technically preferred; only that, in the absence of a good prognostic technique (for example, a limited area fine mesh numerical weather prediction model), linear interpolation is probably a better assumption than is simple persistence. A prospective user of one or another of these models might consider the use of alternative schemes or data sources to construct the wind fields.

To help ensure pollutant mass conservation by the advection-diffusion scheme, the divergence of a wind field computed by MESOPAC can be minimized to within a user-specified absolute tolerance factor

---

*A wind data adjustment procedure based on surface wind velocities (e.g., Pack et al. 1978) was not adopted for the present study, because the surface wind velocity in regions of complex terrain is likely to be significantly different from that most representative of transport averaged over the boundary layer.

[e.g., $\leq |10^{-4}|$ (s^{-1})]. MESOPAC uses an iterative wind field relaxation scheme adapted from those of Clark and Eskridge (1977) and Liu and Goodin (1976).

The gridded field of mixing depths is generated at each time step using a technique that weights the relative importance of mechanical and convective production of turbulence, while accounting for diurnal variations. The mixing depth is assigned [following Benkley and Schulman (1979)] as the larger of two terms: (1) a mechanical value (Plate 1971); (2) a convective value computed for daytime hours as the height of the intersection of the morning temperature sounding with the adiabat extending upwards from the observed surface temperature.

The gridded field of PGT stability class is generated at each time step, using an algorithm closely paralleling that of Turner's (1970); the essential difference is that MESOPAC uses as a measure of insolation intensity the convective mixing depth value obtained above. The fields of PGT stability class are used by each of the three dispersion models in computing plume rise; and are also used by MESOPUFF and MESOPLUME to compute plume dispersion rates at downwind distances to 100 km. Stability values are also used by MESOGRID, in conjunction with mixing depth and wind speed information, to produce the spatially and temporally variable K_z profiles used in the vertical diffusion algorithm - see Appendix C.

MESOPAC is described fully in the User's Guide to MESOPAC, Volume 6 of this series (Benkley and Bass 1979c).

1.3.2 MESOPLUME

The MESOPLUME model (Figure 1-7) is a multiple point source, variable-trajectory Gaussian plume segment model driven by a Lagrangian wind field. The modeling method used in MESOPLUME has been adapted from that proposed by Hales et al. (1977). Unlike the conventional Gaussian plume approach in which the wind is invariant along the plume axis at any given time, MESOPLUME allows for deformation of the continuous plume by a temporally varying wind field.

MESOPLUME divides the Gaussian plume into contiguous segments, each segment describing a portion of plume behavior between successive time periods (Figure 1-2). The end points of each segment are advected in a Lagrangian sense. The lateral width of each segment end point depends on its distance from the source along the instantaneous plume axis, not on the distance traveled (or travel time) of the segment end point.

For the Four Corners regional study, MESOPLUME has been used with 26 by 26 horizontal grid resolution and a grid spacing of 40 km, for a

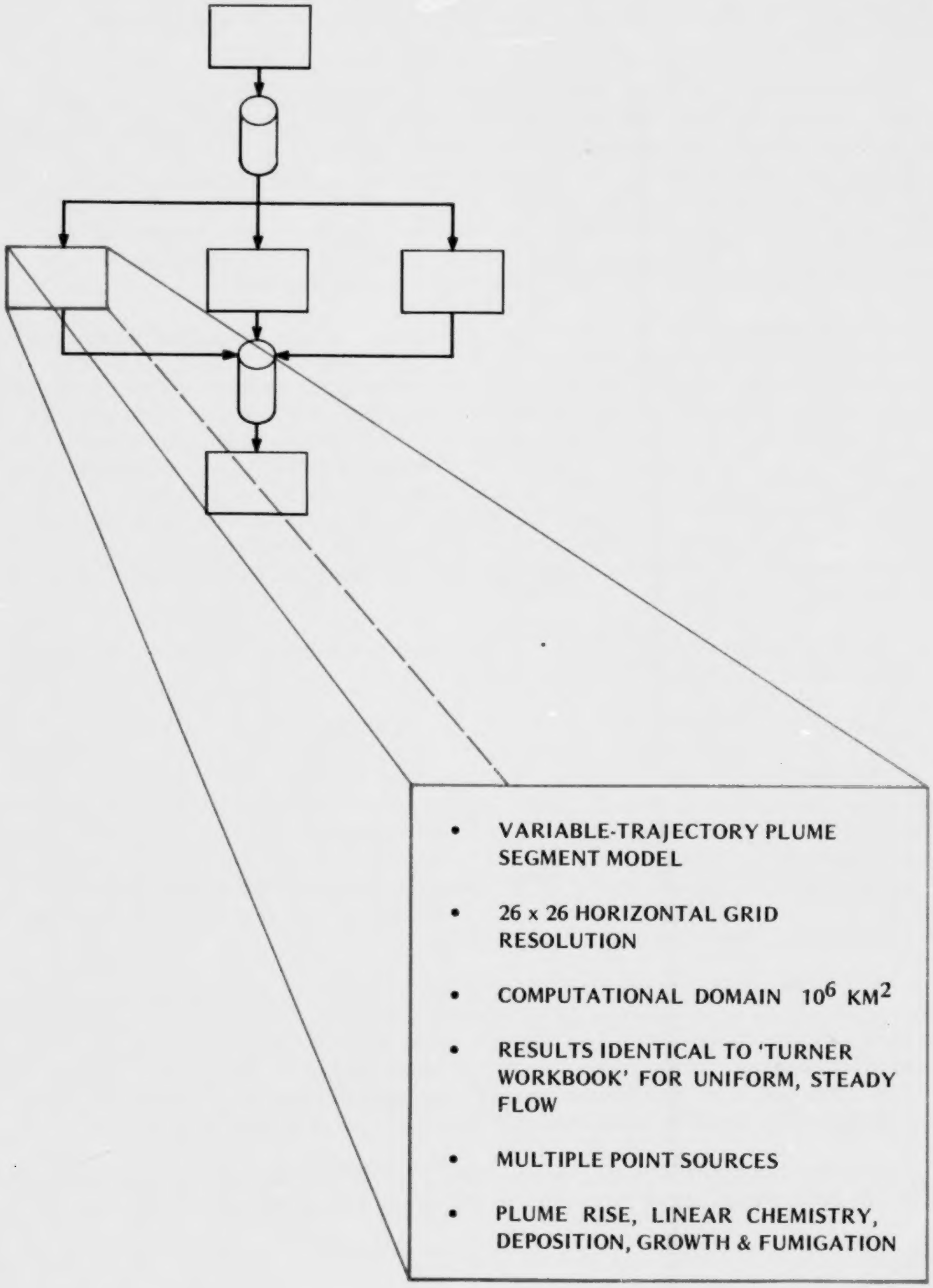

- VARIABLE-TRAJECTORY PLUME SEGMENT MODEL
- 26 x 26 HORIZONTAL GRID RESOLUTION
- COMPUTATIONAL DOMAIN 10^6 KM^2
- RESULTS IDENTICAL TO 'TURNER WORKBOOK' FOR UNIFORM, STEADY FLOW
- MULTIPLE POINT SOURCES
- PLUME RISE, LINEAR CHEMISTRY, DEPOSITION, GROWTH & FUMIGATION

7901054
7901055

Figure 1-7 Mesoscale Plume Model (MESOPLUME)

total computational domain of 10^6 Km^2.* (Both the grid point resolution and grid size are user-variable.) It accommodates multiple point sources (up to 10 per run) and includes modules for Briggs' plume rise, linear chemistry, deposition, growth, and fumigation.

MESOPLUME is described fully in the User's Guide, Volume 2 of this series (Benkley and Bass 1979a).

1.3.3 MESOPUFF

The MESOPUFF model (Figure 1-8) is a variable-trajectory, multiple point source Gaussian puff model driven by a Lagrangian wind field. The basic modeling algorithm has been adapted from that described by Start and Wendell (1974). MESOPUFF simulates a continuous plume by superposing discrete puffs (Figure 1-3). Each puff is advected in a Lagrangian sense; its time history is independent of preceding or succeeding puffs. The dimensions of an individual puff are proportional to its travel distance (or travel time).

The grid size and resolution of the MESOPUFF model can be made identical to MESOPLUME. MESOPUFF also accommodates multiple point sources (up to 10 per run) and shares the identical supporting modules for plume rise, linear chemistry, deposition, growth, and fumigation.

With appropriate choice of input parameters, MESOPUFF reproduces to a very high degree the results of the conventional straight-line Gaussian plume model, if final (equilibrium) plume rise is assumed. For the particular choice of inputs in Section B.9, for example, MESOPUFF results and straight-line plume model results agree within a few percentage points from 5 to 100 km from a point source.

MESOPUFF is described fully in the User's Guide, Volume 3 of this series (Benkley and Bass 1979b).

1.3.4 MESOGRID

MESOGRID is a hybrid Lagrangian-Eulerian advection-diffusion model based on the Egan-Mahoney method of moments (Egan and Mahoney 1972), and adapted from the SULFA3D model (Egan et al. 1976) - see Figure 1-9. The model accounts for horizontal advective transport and vertical eddy diffusion, but not for horizontal diffusion. At each time step, pollutant mass is advected and diffused in a Lagrangian sense; immediately

---

*If MESOPLUME is run with a much finer grid size (e.g., 5 km) and is driven by a uniform, stationary wind field until quasi-steady-state conditions are reached (that is, plume elements are created and fall off the grid at the same rate), it will give near-field ($\leq$ 100 km) results within a few percentage points of the Turner Workbook results in the limiting case of straight-line flow at distances for which the vertical distribution of concentration can be assumed to be uniform (see Section A.9).

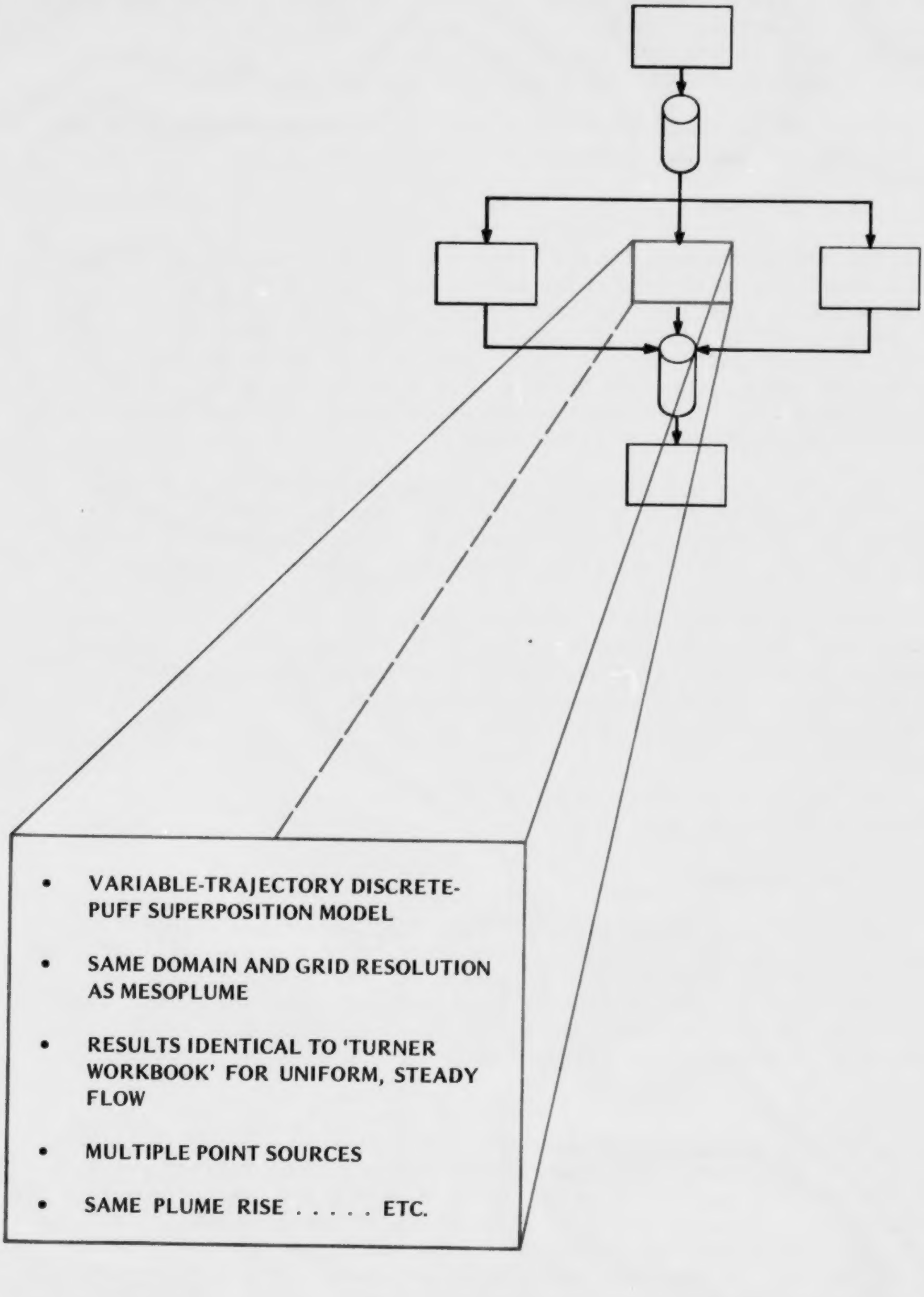

- VARIABLE-TRAJECTORY DISCRETE-PUFF SUPERPOSITION MODEL
- SAME DOMAIN AND GRID RESOLUTION AS MESOPLUME
- RESULTS IDENTICAL TO 'TURNER WORKBOOK' FOR UNIFORM, STEADY FLOW
- MULTIPLE POINT SOURCES
- SAME PLUME RISE . . . . . ETC.

7901032 7901031

Figure 1-8 Mesoscale Puff Model (MESOPUFF)

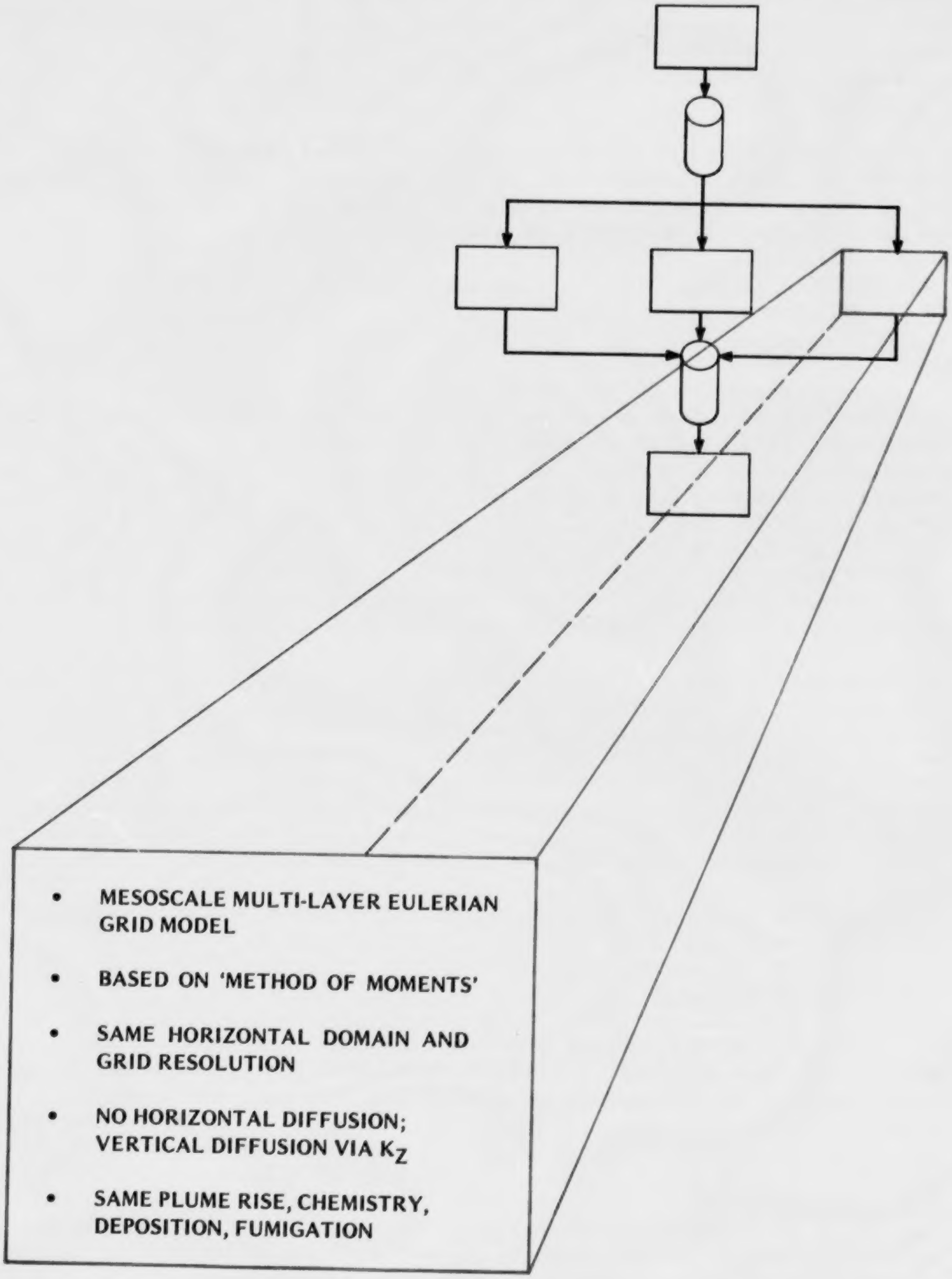

- MESOSCALE MULTI-LAYER EULERIAN GRID MODEL
- BASED ON 'METHOD OF MOMENTS'
- SAME HORIZONTAL DOMAIN AND GRID RESOLUTION
- NO HORIZONTAL DIFFUSION; VERTICAL DIFFUSION VIA K_Z
- SAME PLUME RISE, CHEMISTRY, DEPOSITION, FUMIGATION

7901030 7901029

Figure 1-9 Mesoscale Grid Model (MESOGRID)

afterwards, a mass decomposition to a stationary Eulerian grid is performed. The numerical method conserves the zeroth, first, and second moments of the pollutant mass distribution; this method minimizes pseudodiffusive errors associated with conventional finite-difference approximations.

In common with any Eulerian finite-grid model, the MESOGRID model will not conserve pollutant mass if it is driven by a wind field that (a) has significant local divergence or convergence or (b) has significant confluence, difluence or stagnation.

MESOGRID is described fully in the User's Guide, Volume 4 of this series (Morris et al. 1979).

1.3.5 MESOFILE

MESOFILE is a flexible postprocessing package consisting of: file management; file merging and manipulation; statistical analysis; and graphical display components (see Figure 1-10). The MESOFILE package records, catalogues, and archives all the relevant output from any of the mesoscale diffusion models. Its file merging features allow the user to aggregate easily the results files from any arbitrary number of separate model runs; thus, different combinations of emissions (e.g., the combined effects of existing sources and proposed sources) can be synthesized without rerunning the transport-diffusion models.

MESOFILE allows the user to specify the time averaging of the model concentration fields over any multiple of the basic time step. Wind, mixing height, PGT stability, and ambient air concentration fields can be contour plotted. Figure 1-11 illustrates the kinds of graphical displays that can be produced by MESOFILE with access to a suitable plotter. These displays, used extensively throughout this report, help greatly in describing and understanding the spatial and temporal variations in meteorology and ambient concentrations on regional scales.

MESOFILE is described fully in the User's Guide, Volume 5 of this series (Scire et al. 1979).

1.4 Organization of Report

Section 2 of this report describes the model comparison and sensitivity test protocol, including the nominal choices of model parameters for each of the models, as well as the base case meteorological scenario data. Section 3 describes the results of the model comparison runs made for both a single point source and for a set of ten point sources, for each of two multiday meteorological episodes. Section 4 describes the sensitivity of the models to systematic changes in input parameters and meteorological fields. These results are referenced to actual comparative model run costs in Section 5 for different choices of the relevant model execution parameters. Section 6 presents some

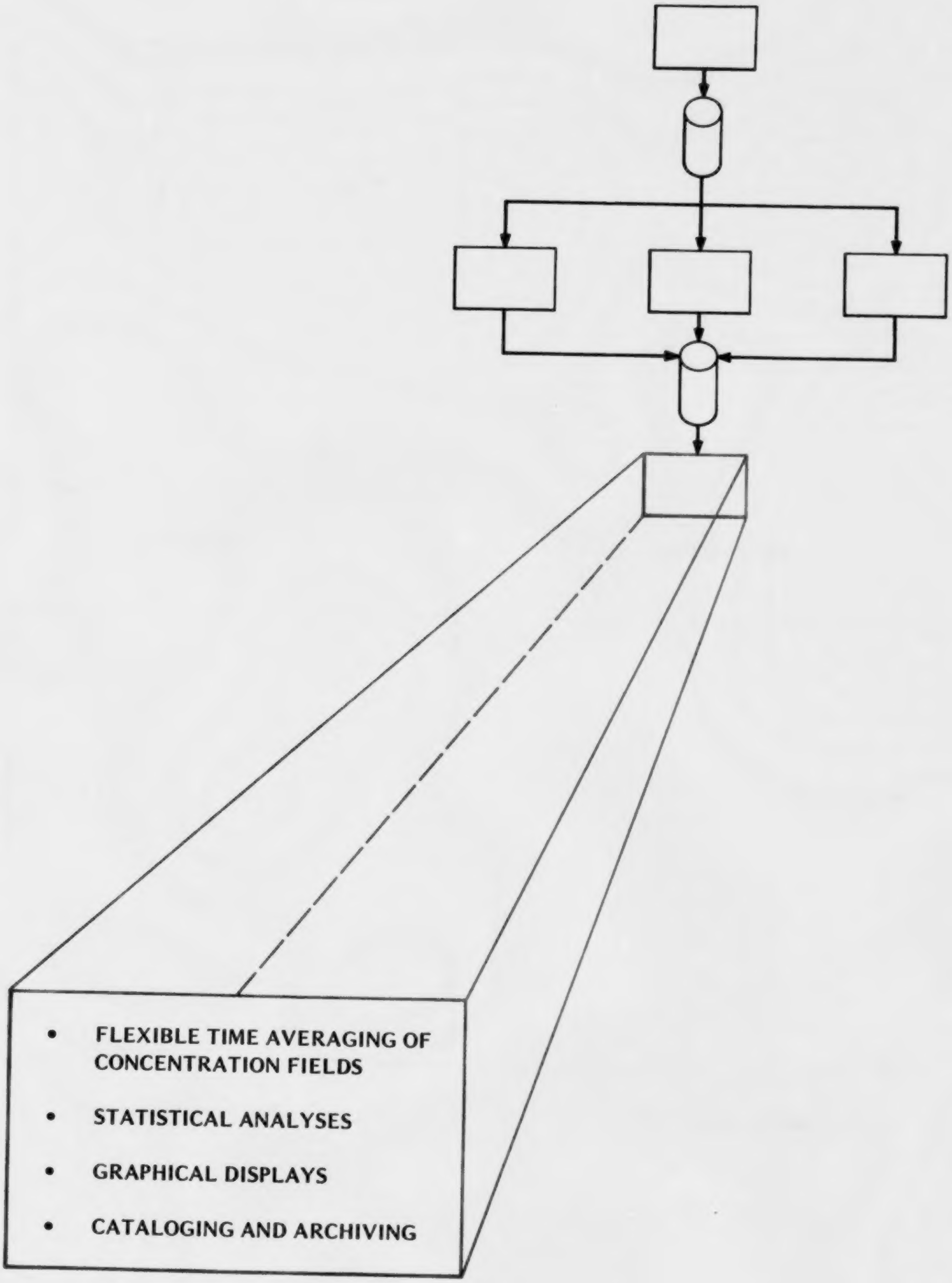
• FLEXIBLE TIME AVERAGING OF CONCENTRATION FIELDS
• STATISTICAL ANALYSES
• GRAPHICAL DISPLAYS
• CATALOGING AND ARCHIVING
7901053
7901052

Figure 1-10 File Management and Analysis (MESOFILE)

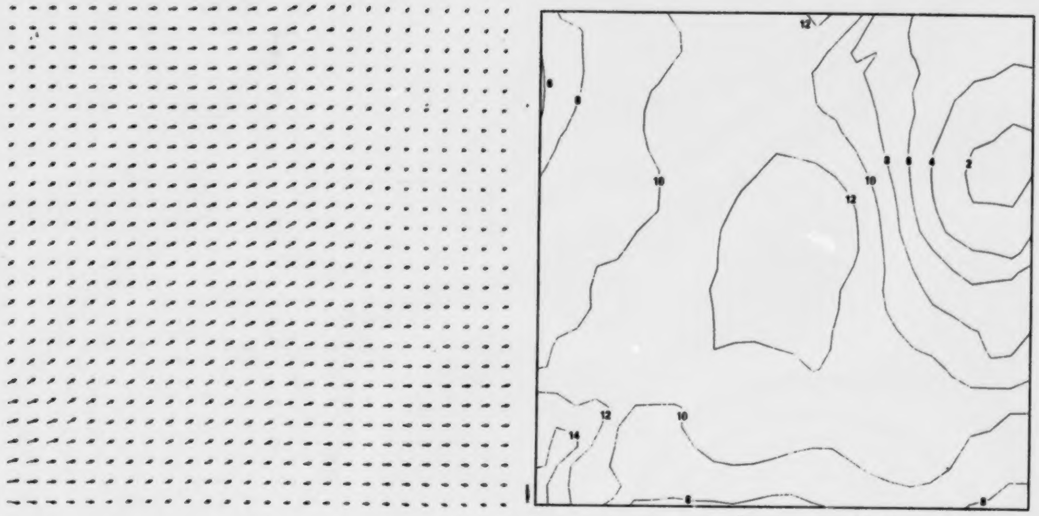

Wind Vectors

Wind Isotachs (m/s)

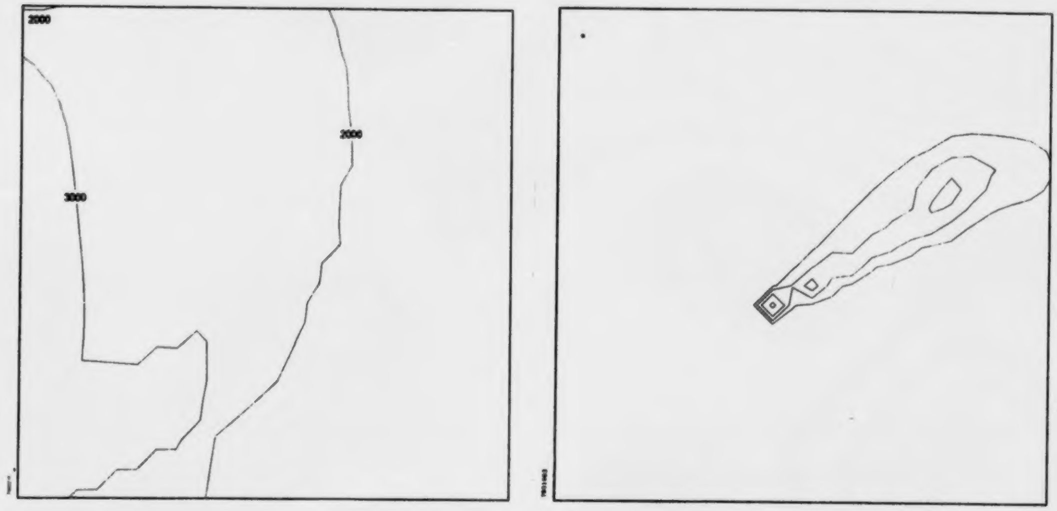

Mixing Height Field

Concentration Isopleths (μg/m³)

Figure 1-11 Examples of MESOFILE Graphical Displays

general recommendations for using one or another of these modeling approaches, based on the results of the extensive series of sensitivity tests. Appendices A, B, and C provide more detailed technical descriptions of the MESOPLUME, MESOPUFF, and MESOGRID models.

2. MODEL COMPARISON AND MODEL SENSITIVITY TESTS

2.1 Requirement for Objective Criteria

At the present time, no ambient air quality monitoring network operating in the Four Corners area seems suitable for verifying short-term regional-scale transport-diffusion models. [Such a network would be a well-distributed set of air quality monitors, situated to respond to regional-scale impacts of the point sources in the general region and not be unduly influenced by near-field major source impacts or background sources. Sheih et al. (1978) present a useful discussion of criteria for the spatial distribution of sampling networks and sampling intervals for verifying regional-scale transport models.] The lack of suitable data in the Four Corners area for regional-scale model verification is hardly unique - a comparable model development effort for the northern Great Plains area (Liu and Durran 1977) faced the same difficulty; as a result, many parameters in their model were chosen entirely on the basis of sensitivity studies.

In the absence of a suitable ambient air quality data base for model verification in the Four Corners region, the following criteria were used to provide an objective, systematic basis for comparing model performance and cost effectiveness:

- theoretical bases of the modeling assumptions,
- model performance under different realistic meteorological flow regimes,
- qualitative (graphical) and quantitative (statistical) measures of model sensitivity to different parameters,
- model sensitivity vs. execution cost tradeoffs associated with changes in the model input variables,
- computer resource requirements, and
- ease of model use and interpretation.

2.2 Test Protocol

Table 2-1 outlines the test protocol for the more than 100 multiday model sensitivity tests that were conducted. Each of the meteorological input field variables model design parameters and model run parameters were varied over the dynamic ranges indicated. It was assumed that all variables and/or parameters in Sets 1, 2, and 3 are uncorrelated. Of course, certain variables are implicitly interdependent (e.g., the rate of SO_2 deposition influences the amount of SO_2 remaining for conversion to SO_4); and other variables are explicitly interdependent (e.g., the vertical eddy diffusivity used by MESOGRID depends on the mixing depth);

TABLE 2-1

MODEL SENSITIVITY TEST PROTOCOL

Set	Category	Range of Variation
1	Mesoscale Flow Regime	
	A) Zonal flow	
	B) Recirculating flow	
	C) Stagnating flow	
2	Systematic Errors in Meteorological Input	
	A) Wind speed	± 2x
	B) Wind direction	± 22.5°
	C) Mixing depth	± 2x
3	Adjustable Modeling Design Parameters	
	A) Deposition velocity	± 10x
	B) Decay rate	± 10x
	C) Horizontal plume growth rate (MESOPLUME, MESOPUFF)	±0.5 m/s
	D) Vertical Eddy Diffusivity (MESOGRID)	± 10x
4	Model Run Parameters	
	A) MESOPLUME	
	i) Time step	1 - 12 hrs
	B) MESOPUFF	
	i) Time step	1 - 12 hrs
	ii) Puff emission rate	1/3 - 12 hrs
	iii) Sampling rate	1/3 - 12 hrs
	C) MESOGRID	
	i) "Requested" time step	5 min - 1 hour

but as a matter of practical necessity, in order to limit the number of sensitivity tests to be performed in this study, the sensitivity of the models to simultaneous variations of two or more parameters was not examined.

In the tests of model response to different mesoscale flow regimes, the three models, representing three different plume transport-diffusion modeling approaches, should be expected to perform with varying degrees of realism under different mesoscale flow regimes. The first set of sensitivity tests shown in Table 2-1 were designed to compare model performance for (A) flow regimes in which the models might be expected to compare well (e.g., highly zonal flow); and by contrast, (B,C) flow regimes in which the models should differ substantially.

The next set of sensitivity tests shown in Table 2-1, explores the influences of systematic errors in the meteorological input data. No single choice of wind level is adequate to represent plume dispersion, especially over the broad range of effective plume heights, mixing height variations, ambient turbulence levels, and terrain conditions encountered in a regional-scale simulation. Different choices of data level will produce systematically different meteorological data bases. Furthermore, a variety of different algorithms could be used to construct mixing depth and wind fields. Subgrid scale resolution problems in the data collection network will cause additional deviations in the meteorological input data used with the models. It is questionable, for example, whether interpolated grid values of mixing depth and wind speed can be estimated to much better than a factor of two, or wind direction estimated to much better than ±22.5°.

The third set of sensitivity tests shown in Table 2-1 addresses the effects of present uncertainties in model design parameters: specifically, decay rate, deposition velocity, horizontal plume growth rate (for MESOPLUME and MESOPUFF), and vertical eddy diffusivity (for MESOGRID). The ranges of variation assumed for the values of the deposition velocity and decay rate reflect the large uncertainties in these quantities. For example, estimates of SO_2 decay rates vary over approximately an order of magnitude, from ∿0.5% to ∿5.0% per hour or more (Wilson 1978). Quoted deposition velocities also vary over an order of magnitude, from ∿0.2 to ∿2.0 centimeters per second (cm/s) for SO_2 (Husar et al. 1978). For the MESOPLUME and MESOPUFF models, the long-range, time-dependent dispersion coefficients are highly uncertain; beyond 100 km transport distance, the range of horizontal plume growth rates ($d\sigma_y/dt$) may be 0.5 ±0.5 m/s [the nominal choise is from Heffter (1965)]. For the MESOGRID model, the algorithm used to create vertical profiles of K_z probably yields estimates only to within an order of magnitude at any specific location or height.

Finally, the fourth set of sensitivity tests examines the relative sensitivity benefits vs. costs for different choices of model run parameters: advective time step; plume segment or puff emission rates;

sampling time steps. For MESOPLUME and MESOPUFF, the basic time step used for the transport-dispersion calculation is varied from one hour to twelve hours. For MESOGRID, the "requested" time step (see Section C.4.4) is varied from five minutes to one hour (by reducing K_z values to ensure that the vertical numerical stability criterion is not violated). For MESOPUFF, both the puff emission rate - which also controls the frequency of puff trajectory update - and the puff sampling rate were simultaneously varied. In the cost-benefit analyses made to explore model performance with variations in time step, a very stringent (short) time step was used for the base case; then progressively longer time step(s) were chosen; in each instance, the results were compared, in terms of cost and reproducibility of important result features, with the base case results of the same model.

2.3 Initialization and Inventory Choices

In keeping with the regional-scale nature of the problems, each model run experiment consisted of a five (or seven) consecutive day simulation using hourly meteorology. The first two (or three) days of each model run were considered to be an initialization period: the analyses of model results were limited to the remaining three (or four) days of the simulation. In these experiments, the two-day initialization period is sufficient to allow the plume from any source to reach the boundary of the computational grid; thus the unrealistic effects of source start-up are largely avoided.

The model comparison experiments were performed using alternatively: (1) a single point source only; and (2) a set of ten sources chosen from the actual source distribution shown in Figure 1-1. Two different meteorological episodes were run. To keep both computational cost* and analysis efforts within reasonable bounds, the various model sensitivity tests used only a single major point source of SO_2, the Navajo power plant in northern Arizona. This source was chosen for two reasons: (a) For the two meteorological episodes considered, the winds over most of the grid area were generally westerly the plume from a source in the western portion of the grid would tend to spread eastward through a significant portion of the grid; and (b) long-range transport is the primary interest, and a source chosen for the sensitivity analysis should have significant impact at large distances - the Navajo plant has the highest emissions of any point source in the Four Corners region.

2.4 Description of Base Cases

2.4.1 Model Design and Run Parameters

The nominal base-case values chosen for the adjustable model design parameters are displayed in Table 2-2. These nominal choices are the same as those used by Hales et al. (1977). Although no assertion is

---

*The costs of operating the MESOPLUME and MESOPUFF models depend on the number of sources and a very large number of multiday sensitivity tests were required.

TABLE 2-2

NOMINAL DESIGN PARAMETERS

SO_2 Decay Rate = 2%/Hour

SO_2 Deposition Velocity = 1.0 cm s^{-1}

$SO_4^=$ Deposition Velocity = 0.1 cm s^{-1}

Plume Growth Rate (MESOPLUME, MESOPUFF):

$\leq$ 100 km, PGT coefficients

> 100 km, $\frac{d\sigma_y}{dt} = 0.5$ m s^{-1}

BASE CASE VALUES OF THE MODEL RUN PARAMETERS

MESOPLUME:

Time step = 1 hour
Meteorological fields update rate = 1 hour
Grid interval = 40 km
Computational mesh size = 26 x 26 (10^6 km^2)

MESOPUFF:

Time step = 1 hour
Meteorological fields update rate = 1 hour
Puff emission rate = 1 puff/hour
Puff sampling rate dynamically determined (see Section B.6)
Same computational mesh and grid interval

MESOGRID:

"Requested" time step = 1 hour
Meteorological fields update rate = 1 hour
Same computational mesh and grid interval

being made that these are optimal values, they are near the means of the range of values documented by the authors previously cited. The choices of model run parameter base-case values are also shown in Table 2-2.

2.4.2 Meteorological Scenarios

Two very different multiday meteorological episodes (shown schematically in Figure 2-1) were chosen for the model sensitivity tests.

Episode 1, June 14 to 18, 1978 (days 165 to 169), was chosen for its well-defined regimes of both zonal and stagnating flows. Figure 2-2 displays the wind vectors and isotach contours every 12 hours starting at 0000 GMT on day 167 (after a 2-day model initialization period). The flow on days 165 to 167 was quite steady from the west and southwest; whereas the flow on days 168 and 169 was light and disorganized, especially in the southeast portion of the grid. By the end of the fifth day, flow tended to return to zonal conditions near the source; thus, the concentration patterns on the last day should be affected by both stagnating and zonal conditions. Figure 2-3 and Figure 2-4 display the fields of mixing depth and stability class, respectively, computed for this episode.

Episode 2, May 1 to 7, 1978 (days 121 to 127), was chosen for its distinct zonal and recirculating regimes. Figure 2-5 displays the wind vectors and isotach contours every 12 hours starting 0000 GMT on day 124 (after a 3-day model initialization period). Two strong cutoff low pressure systems moved through the grid, the first from late on day 121 to day 123, and the second from day 125 to early on day 127; at other times the flow was basically zonal. Wind speeds were generally high throughout the period, except in the centers of the cutoff lows.

2.5 Description of the Model Output Analyses

Because of the large volume of model output data generated, the sensitivity analyses were designed to yield maximum information from a limited number of measures or descriptors. Qualitative (graphical) as well as quantitative (statistical) measures of the point-by-point and bulk differences between two concentration fields - a "base" (or "reference") field, and a "test" field - were used to determine the effects of "test" parameter variations on the predicted concentration field. The lowest order statistical moments - the mean and standard deviation - are normally meaningful bulk indicators of the distribution. Higher order moments can also be quantified by bulk formulas but are less meaningful - the higher order details in a concentration field are best seen in qualitative examination of the concentration isopleth patterns.

To compare two sets of concentration fields, it is useful, first, to compare the lower moments of the two distributions, and of their difference field. But since the model comparisons are also directed at

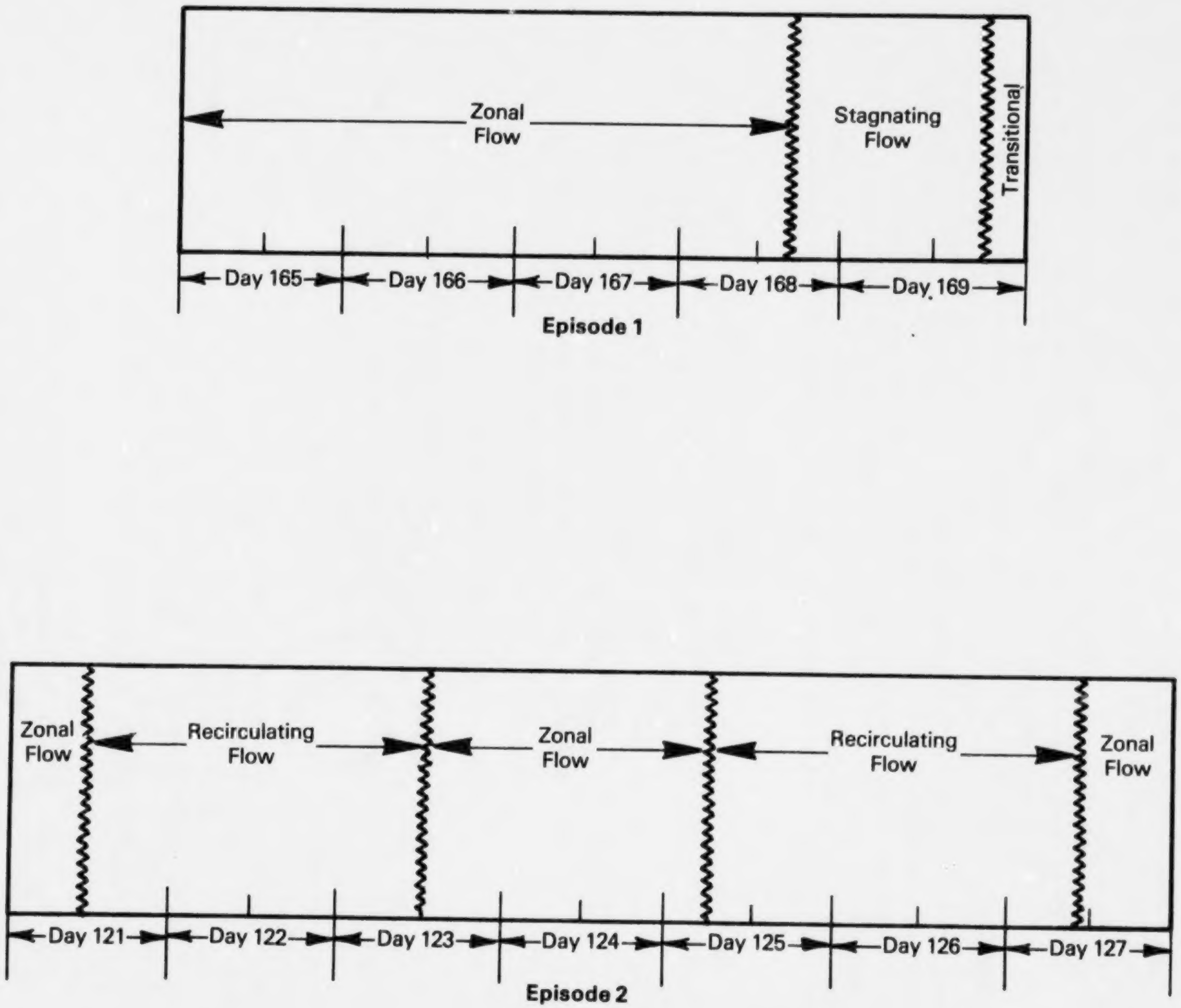
Zonal Flow
Stagnating Flow
Transitional
Day 165
Day 166
Day 167
Day 168
Day 169
Episode 1
Zonal Flow
Recirculating Flow
Zonal Flow
Recirculating Flow
Zonal Flow
Day 121
Day 122
Day 123
Day 124
Day 125
Day 126
Day 127
Episode 2

Figure 2-1 A Schematic Representation of Episodes 1 and 2 Flow Regimes

00 167 78

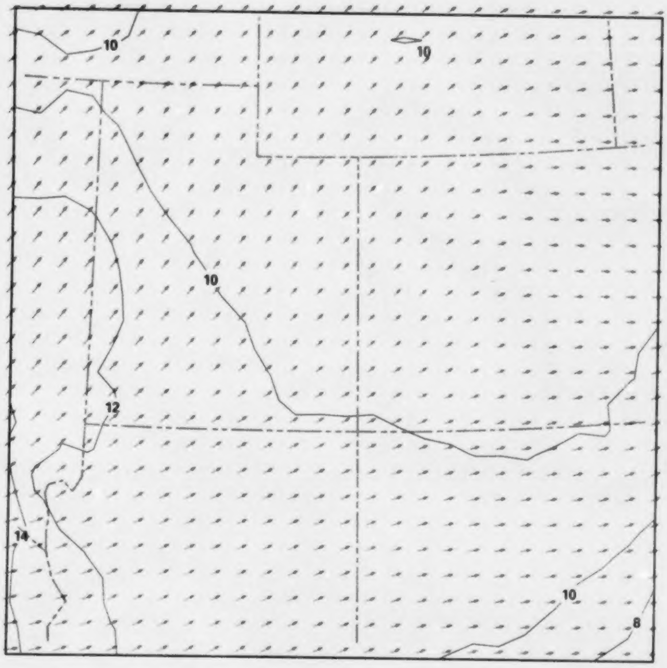
10
10
10
12
14
10
8

7902202
7901087

12 167 78

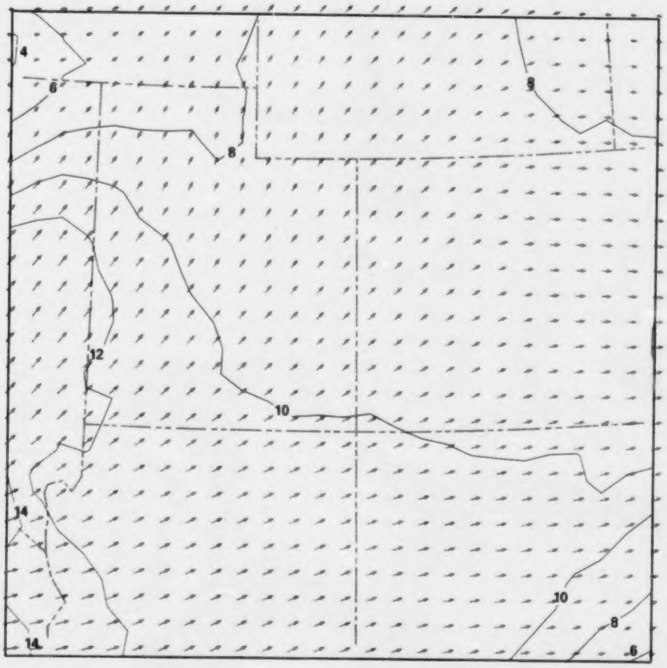
4
6
8
8
12
10
14
10
8
14
6

7902203
7901088

Figure 2-2 Episode 1 Wind Vector and Isotach (m/s) Fields

00 168 78

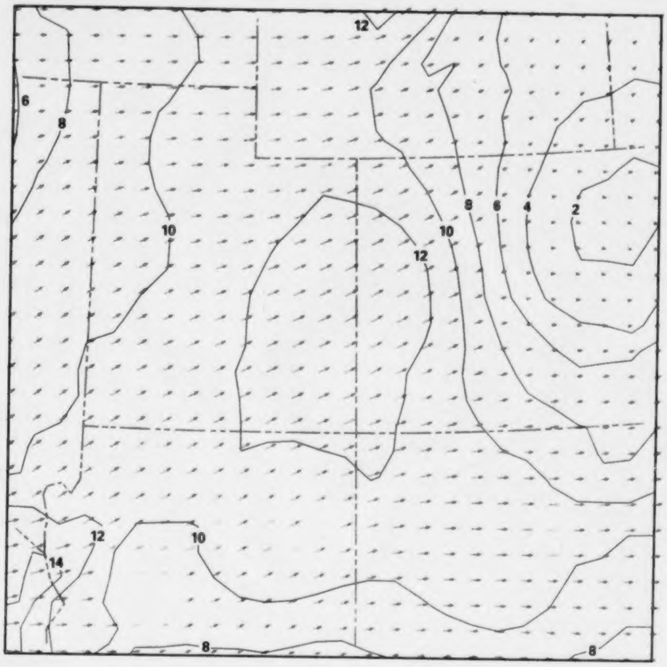
12
6
8
10
8
6
4
2
10
12
12
10
14
8
8

7902204
7901089

12 168 78

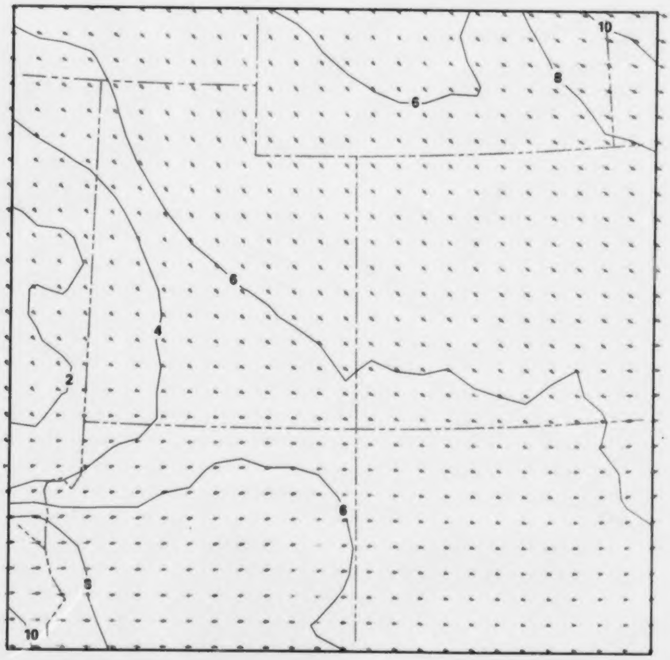
10
6
8
6
4
2
6
8
10

7902205
7901090

Figure 2-2 Continued

00 169 78

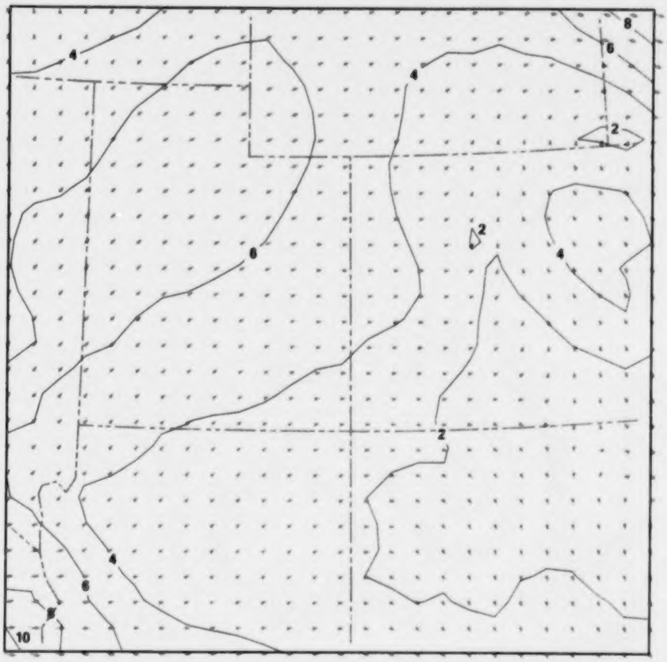
8
6
4
4
2
2
6
4
2
4
6
8
10

7902206
7901091

12 169 78

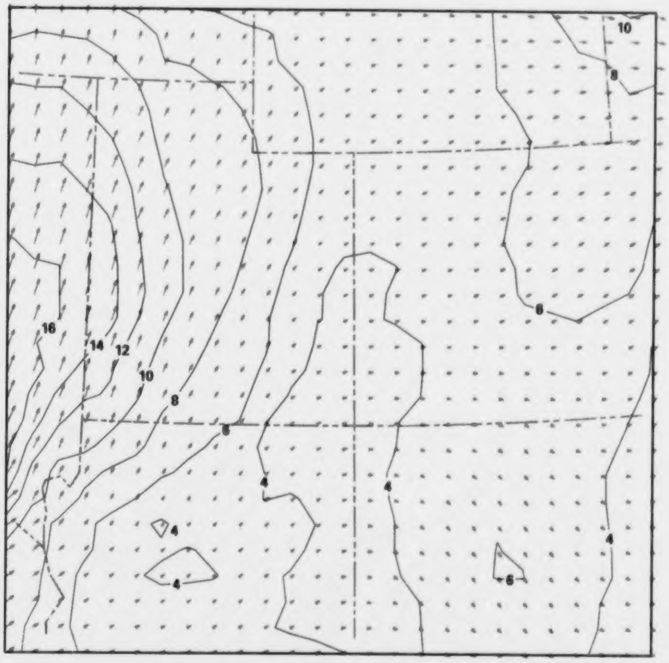
10
8
6
16
14
12
10
8
6
4
4
4
4
6
4

7902207
7901092

Figure 2-2 Continued

00 170 78

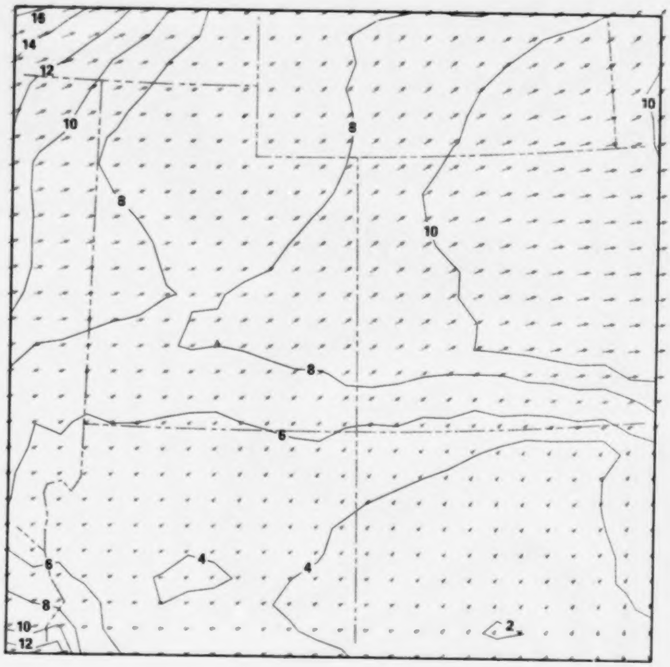
16
14
12
10
8
8
10
10
8
6
6
8
10
12
4
4
2

7902208
7901093

Figure 2-2 Continued

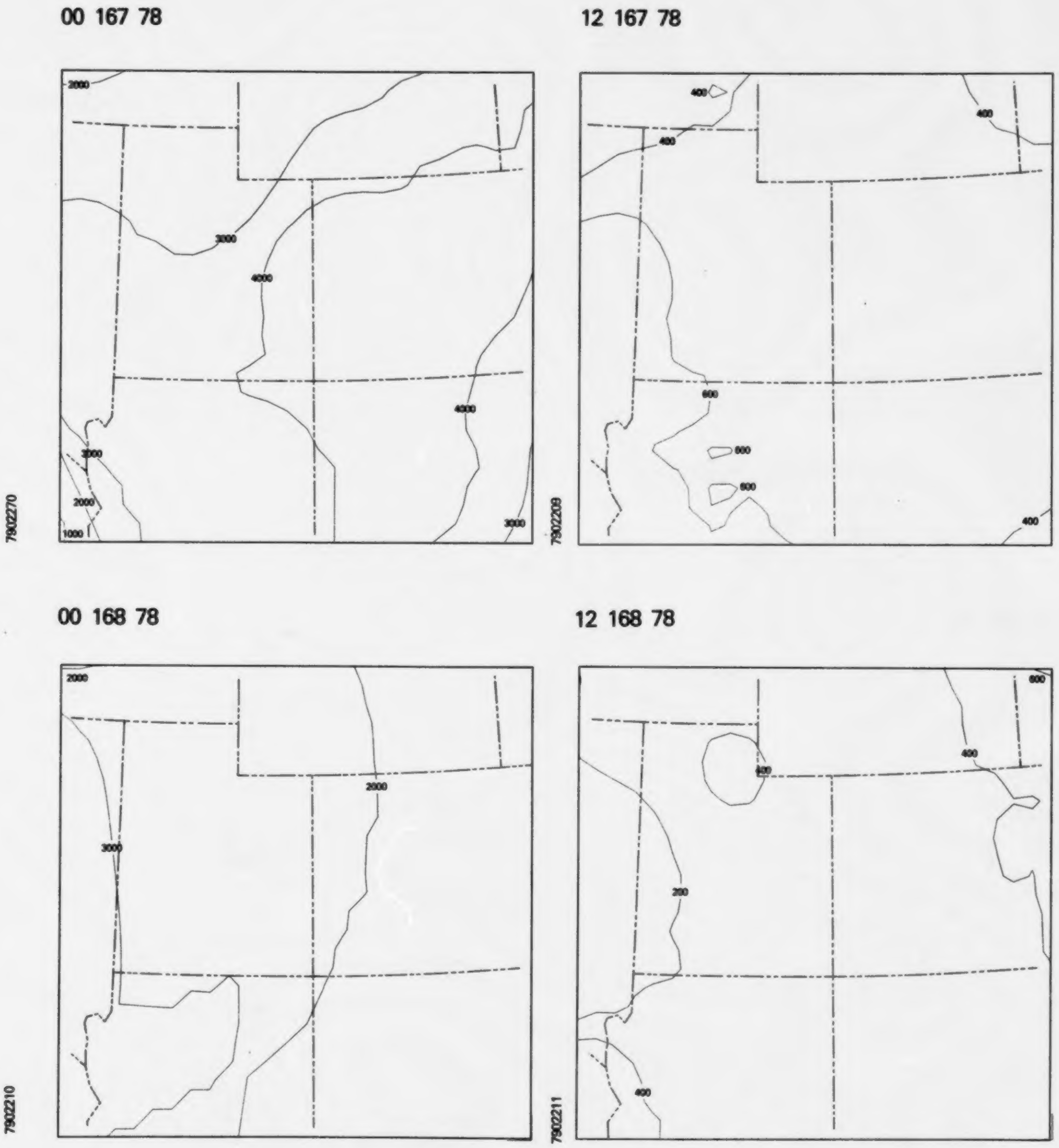
00 167 78
12 167 78
2000
3000
4000
4000
3000
2000
1000
3000
7902270
400
400
400
600
600
600
400
7902209
00 168 78
12 168 78
2000
2000
3000
7902210
600
400
400
200
400
7902211

Figure 2-3 Episode 1 Mixing Depth (m) Fields

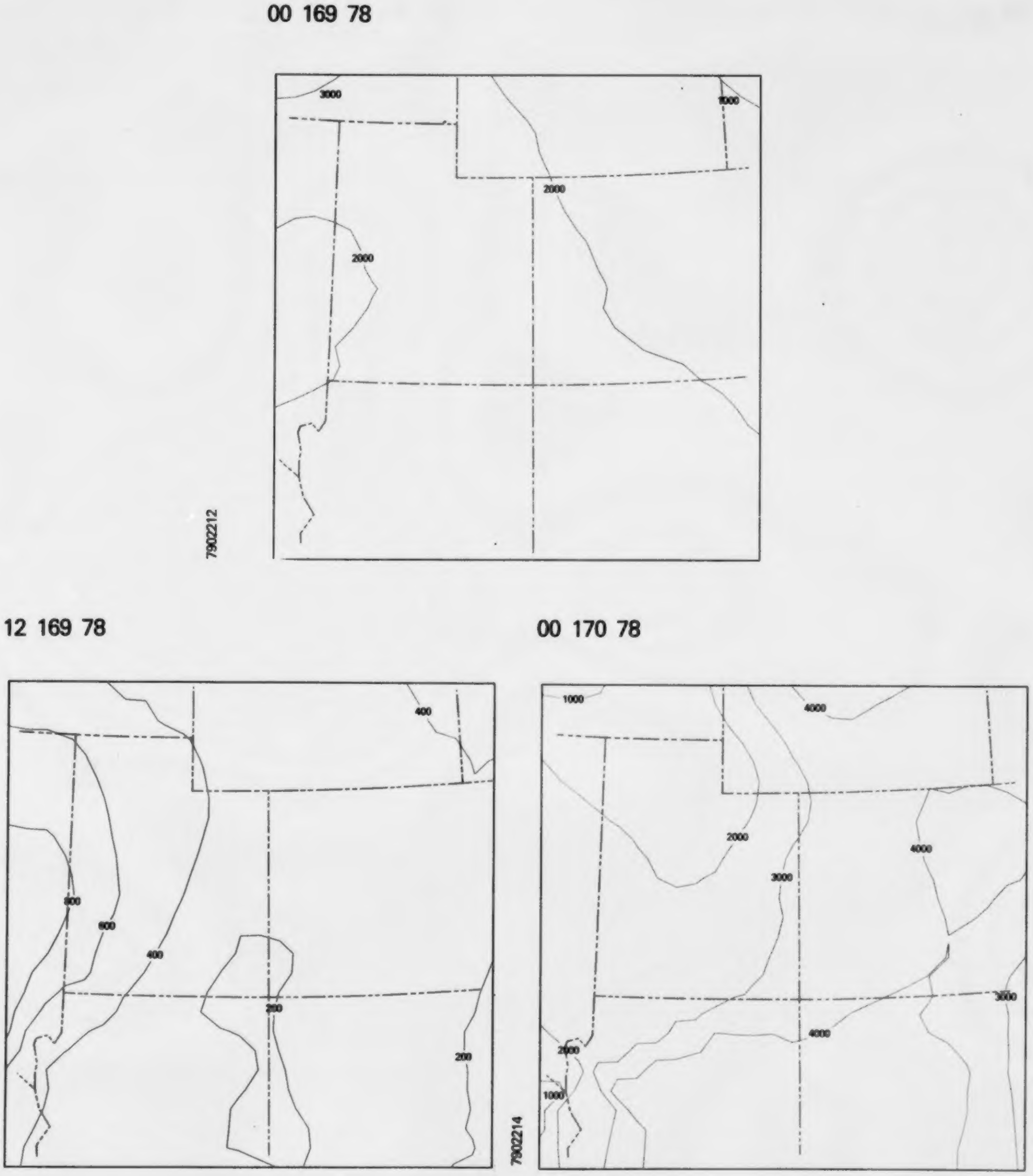
00 169 78

12 169 78

00 170 78

3000
1000
2000
2000
7902212
400
800
600
400
200
200
7902213
1000
4000
2000
4000
3000
3000
4000
2000
1000
7902214

Figure 2-3 Continued

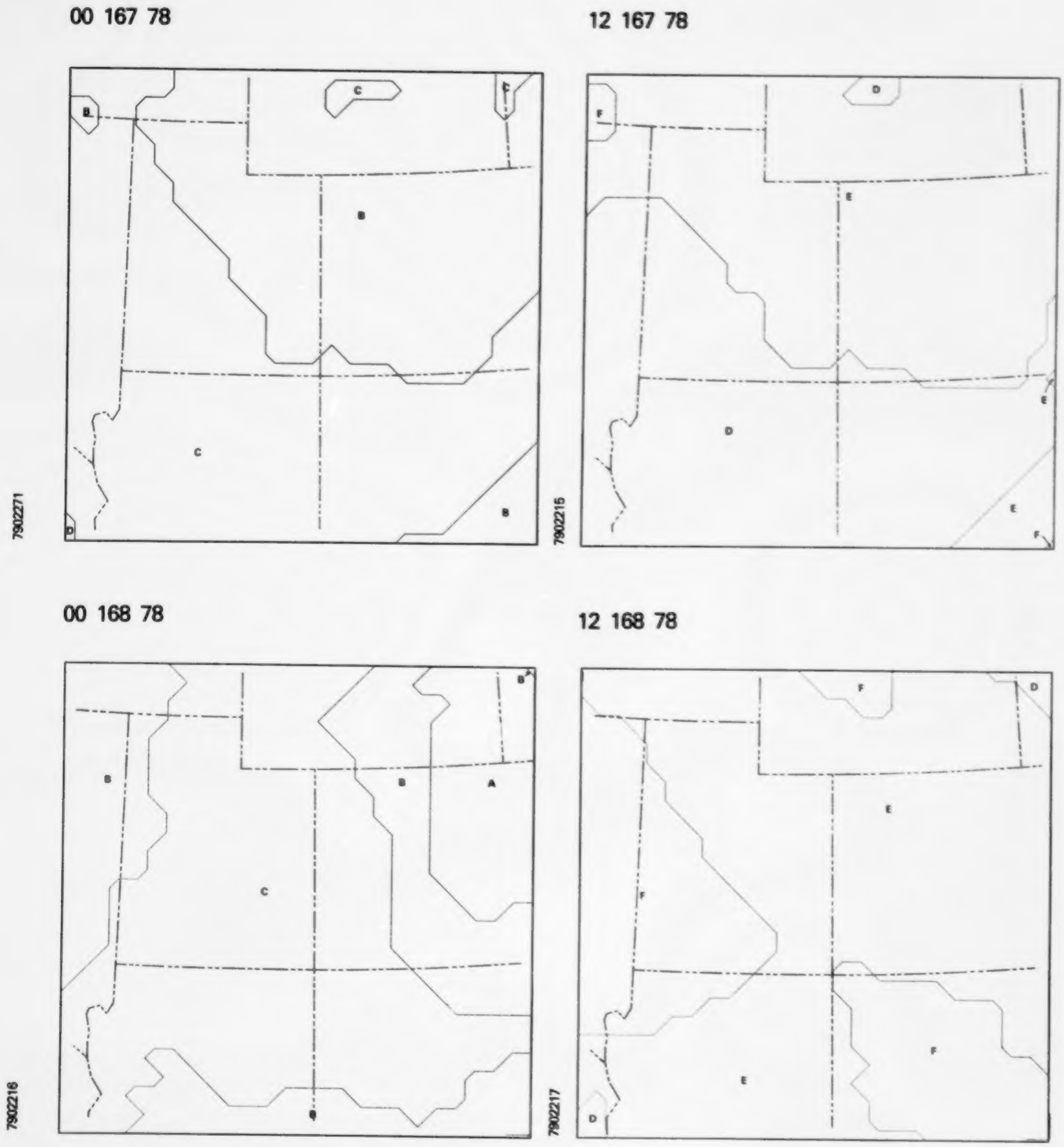
00 167 78
B
C
C
B
C
D
B
7902271
12 167 78
F
D
E
D
E
E
F
7902215
00 168 78
B
B
B
A
C
B
7902216
12 168 78
F
D
E
F
F
E
D
7902217

Figure 2-4 Episode 1 PGT Stability Class Fields

00 169 78

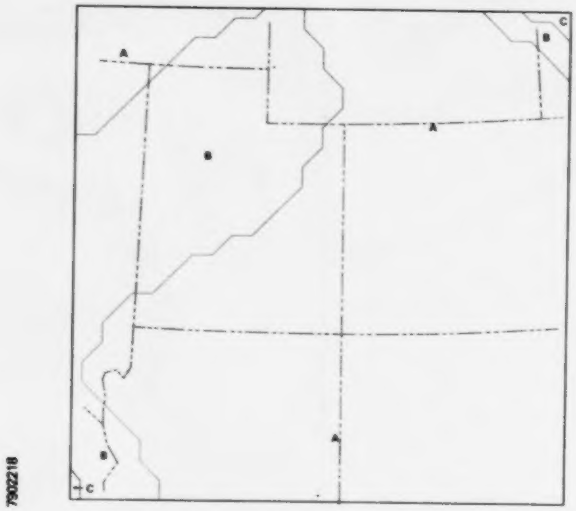
A
C
B
B
A
A
B
C
7902218

12 169 78

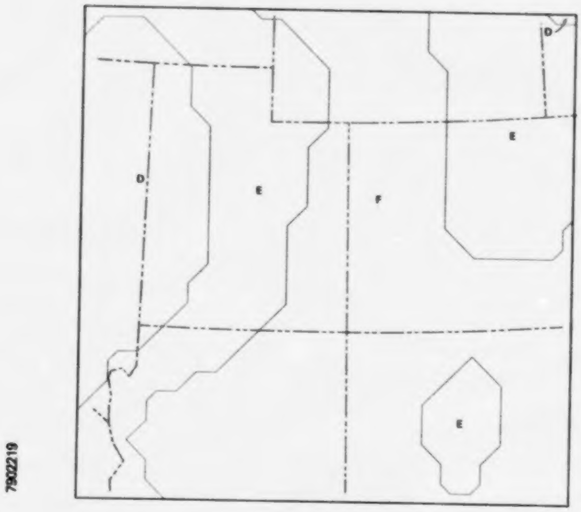
D
D
E
F
E
E
7902219

00 170 78

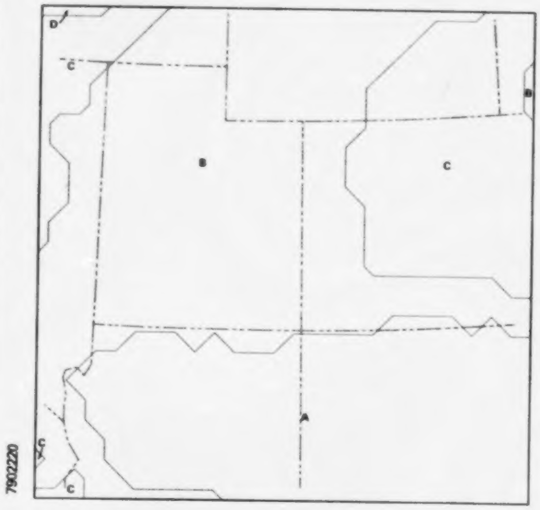
D
C
B
B
C
A
C
C
7902220

Figure 2-4 Continued

00 124 78

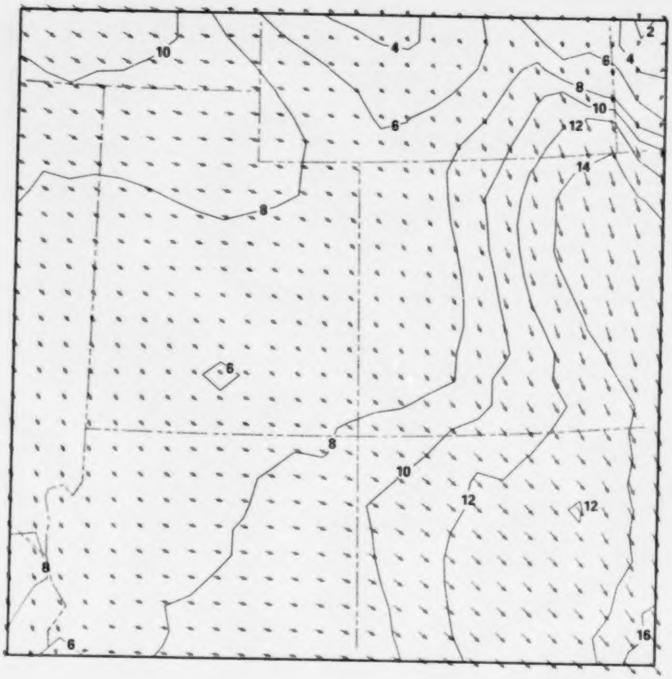
10
4
2
6
4
8
10
6
12
14
8
6
8
10
12
12
8
6
16

7902238
7902239

12 124 78

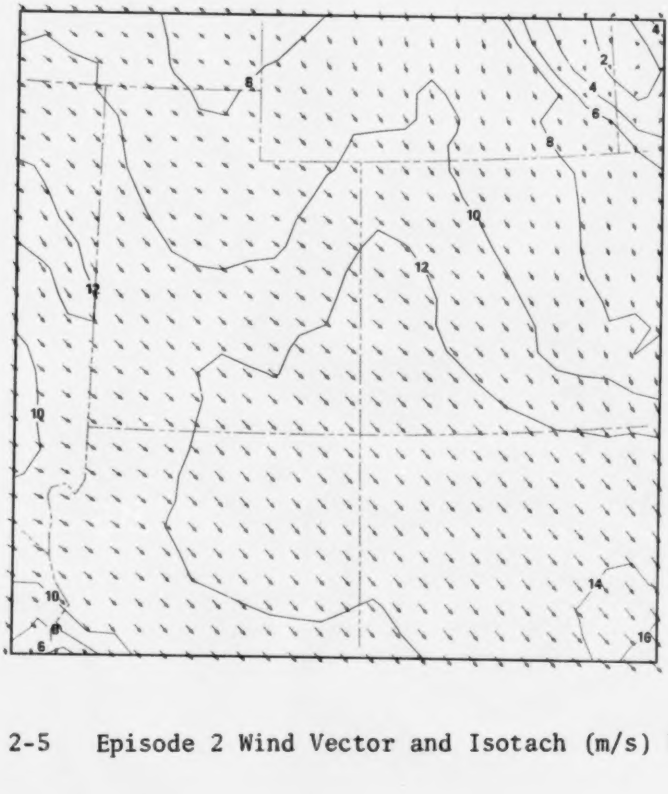
4
2
8
4
6
8
10
12
12
10
14
10
8
6
16

7902240
7902241

Figure 2-5 Episode 2 Wind Vector and Isotach (m/s) Fields

00 125 78

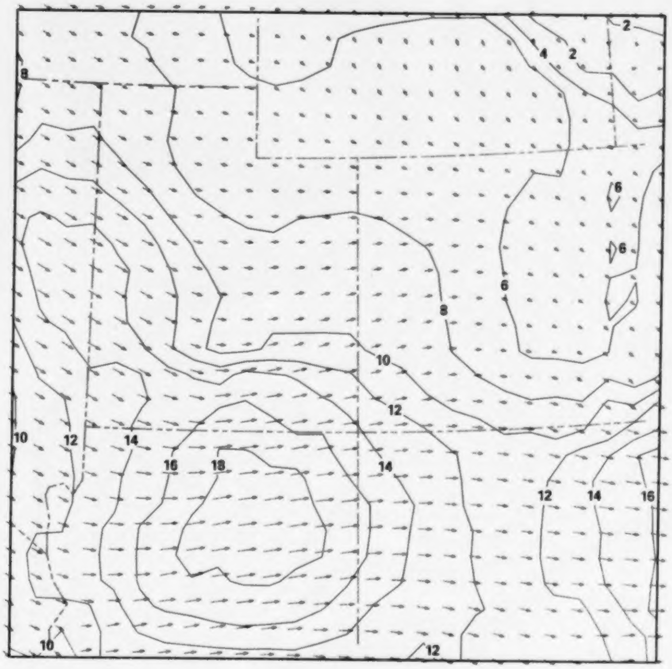
2
4
2
8
6
6
6
8
10
12
10
12
14
16
18
14
12
14
16
10
12

7902242
7902243

12 125 78

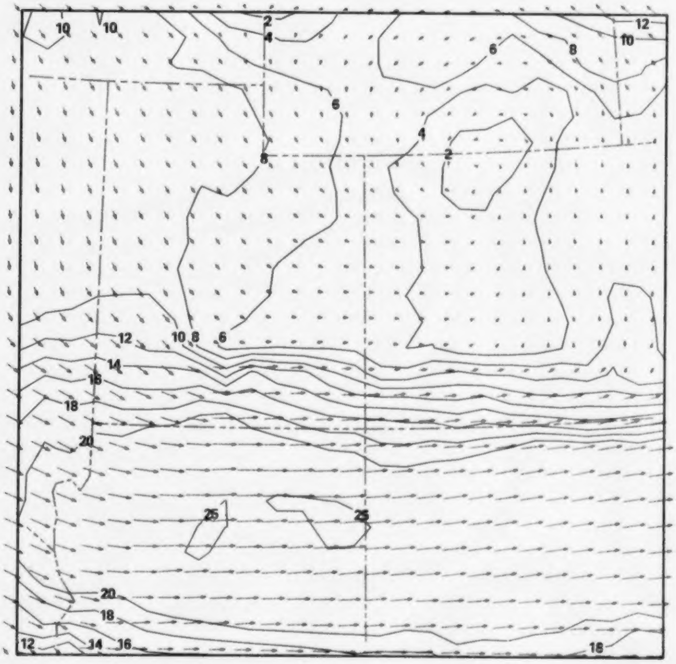
10
10
2
4
12
10
6
8
6
4
2
8
12
10 8
6
14
16
18
20
25
25
20
18
12
14
16
18

7902244
7902245

Figure 2-5 Continued

12 126 78

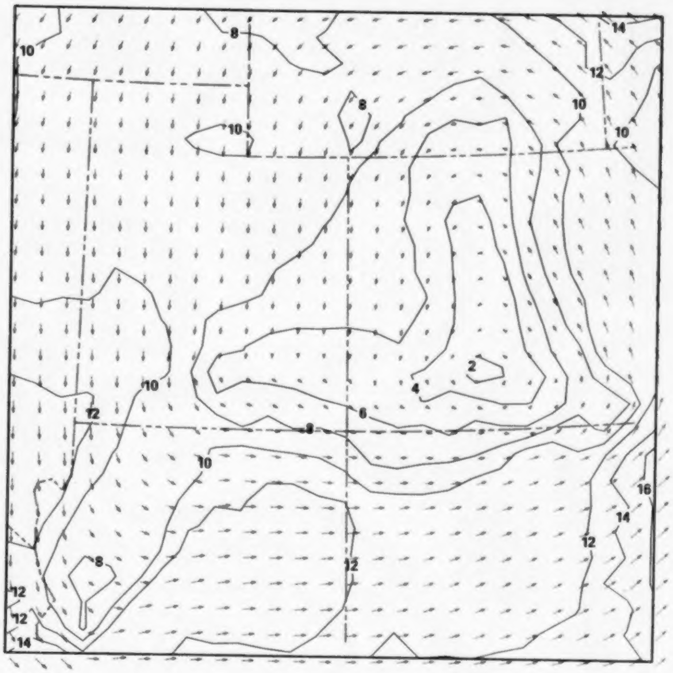
10
8
14
12
10
8
10
10
2
4
6
10
12
8
10
16
14
12
12
8
12
12
14

7902248
7902249

00 126 78

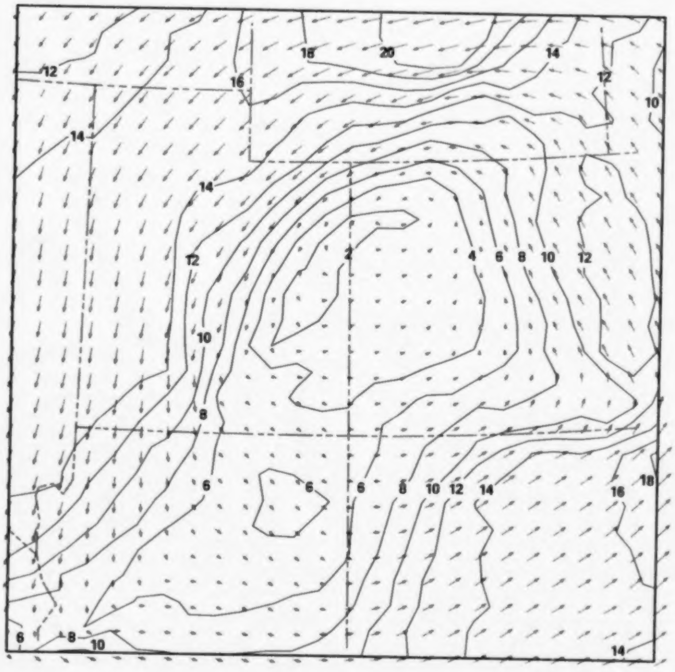
12
16
18
20
14
12
10
14
14
12
2
4
6
8
10
12
10
8
6
6
6
8
10
12
14
16
18
6
8
10
14

7902246
7902247

Figure 2-5 Continued

00 127 78

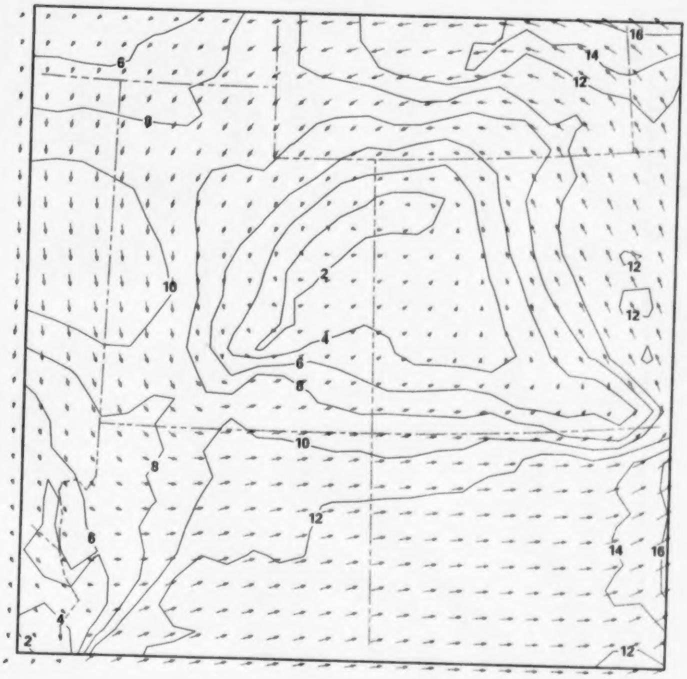
16
14
12
6
8
10
2
4
6
8
12
12
10
8
12
6
14
16
4
2
12

7902250
7902251

12 127 78

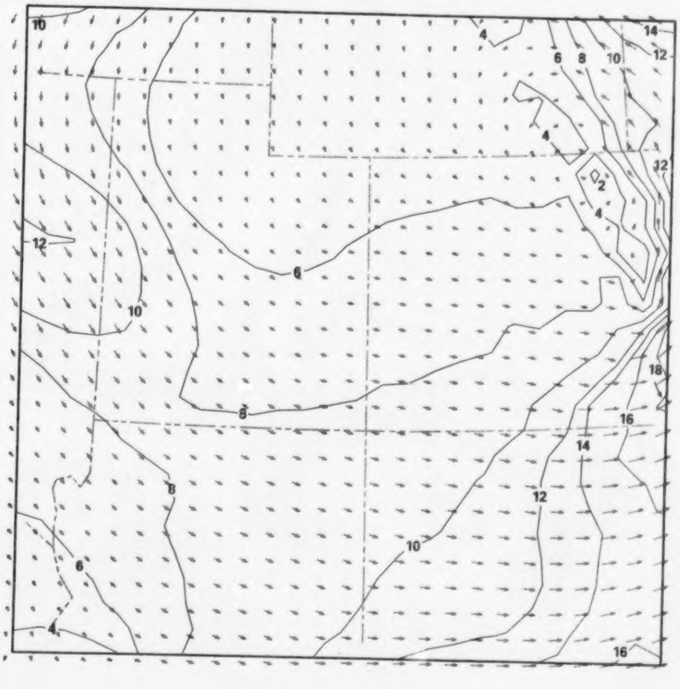
10
4
14
6
8
10
12
4
12
2
4
12
6
10
18
8
16
14
8
12
10
6
4
16

7902252
7902253

Figure 2-5 Continued

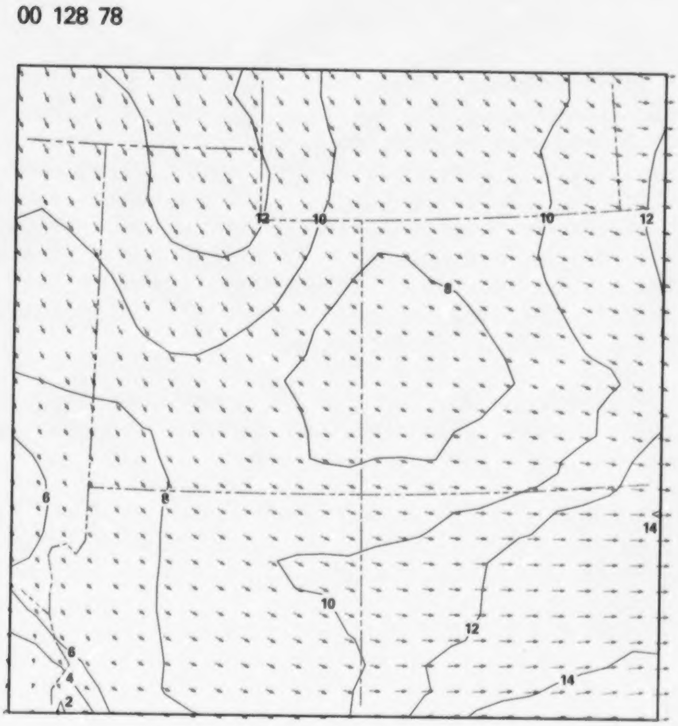
00 128 78
12
10
10
12
8
6
8
14
10
12
14
6
4
2

7902254
7902255

Figure 2-5 Continued

the more detailed structures of the respective concentration fields, point-by-point comparison measures of the two fields are also required. The relative spatial locations of the two fields should also be compared. Consider, for example, a single dispersing plume: if a base-case concentration field is defined and a test-case field is created by varying a model input parameter, the two plumes may or may not overlap. This information is especially important to possible regulatory applications, for difficult interpretation problems would arise in situations in which the test-case concentration is high and the base case concentration is low (or conversely). In summary, the statistical and qualitative (graphical) measures employed for model comparison analyses should yield the following information.

- How closely do the lower order moments of the base and test plumes compare--are the plumes of the same size and do they have the same mean concentration?
- How closely do the higher order moments of the base and test plumes compare--is a particular feature of interest similarly reproduced in both the base plume and test plume?
- How closely do the spatial location of base plume and test plume or distinct plume features coincide--do the two plumes overlap closely or do they tend to disperse in different directions?

Table 2-3 summarizes the statistics found useful in this study. Both the mean plume concentration $\overline{C}$, and the number of points NP over which the mean is computed, are useful indicators of gross plume size and magnitude of impact. The plume size NP is defined for MESOPLUME and MESOPUFF as the number of points within ±3 σ_y of the plume centerline; and for MESOGRID as the number of points experiencing at least a threshold concentration of 10^{-4} $\mu g/m^{-3}$. The standard deviation has not been included as a bulk description of individual plumes; the standard deviation was found to be more descriptive of the along-the-trajectory plume distribution than of the lateral distribution of the concentration.

Several statistics have been found useful for the bulk comparison of two plumes: the average fractional deviation (AFD), the fractional difference of the plume means (FDM), the fractional difference of number of points in the plume (FDN), and the correlation coefficient (r). The average fractional difference is most useful when every point in the test plume is also included in the base plume. However, this statistic can take on unrealistically large values when the base case concentration values at a single point become very small. Thus, this statistic is really only useful for examining the effect of an input parameter, such as decay or dry deposition, that does not affect the spatial coverage of the plumes. For other input parameter variations, the FDM or the FDN are methods by which the lowest order plume moments are

TABLE 2-3

STATISTICAL MEASURES USED

Descriptor	Definition	
I. Individual plume bulk descriptors		
1) Mean plume concentration, $\overline{C}$	$\overline{C} = \sum_{i,j} C_{i,j} / NP$	i,j range over only those points in the plume
2) Number of points in the plume, NP	For MESOPLUME and MESOPUFF, NP is the number of points within $\pm 3\ \sigma_y$ of the plume centerline. For MESOGRID, NP is the number of points experiencing at least a threshold concentration of $10^{-4}\ \mu g\ m^{-3}$	
II. Two-plume bulk descriptors		
1) Average fractional deviation (AFD)	$\mathrm{AFD} = \overline{\left\lvert \frac{\overline{C}_B - \overline{C}_T}{\overline{C}_B} \right\rvert}$	Calculated only over the intersection of the base (B) and test (T) plumes
2) Fractional deviation of the plume means (FDM)	$\mathrm{FDM} = \frac{\overline{C}_B - \overline{C}_T}{\overline{C}_B}$	
3) Correlation coefficient (r)	$r = \frac{\overline{C_B\ C_T} - \overline{C}_B\ \overline{C}_T}{\left\lvert \overline{C_B^2} - (\overline{C}_B)^2 \right\rvert \left\lvert \overline{C_T^2} - (\overline{C}_T)^2 \right\rvert}$	Calculated over the set of grid points in the union of the two plumes
4) Fraction deviation of number of points in the plume (FDN)	$\mathrm{FDN} = \frac{NP_B - NP_T}{NP_B}$	
III. Two-plume point-by-point comparisons		
1) Difference field (DF)	$(DF)_{i,j} = (C_B)_{i,j} - (C_T)_{i,j}$	i,j range over all grid points
2) Fractional difference field (FDF)	$(FDF)_{i,j} = \frac{(C_B)_{i,j} - (C_T)_{i,j}}{(C_B)_{i,j}}$	i,j range over only those grid points in the intersection of the two plumes

compared. The correlation coefficient defined in Table 2-3 is another useful statistic for comparing two-plume bulk properties. Two identical but disjoint plumes have a correlation coefficient of -1; whereas, if the two plumes are rotated into coincidence, the correlation is +1. For two nonidentical plumes spanning the identical set of grid points, r approaches unity as the respective values of the higher order moments of the two-plume concentration distributions approach each other.

No comparison of absolute maximum concentration values is included here; absolute concentration maxima are nearly always a near-field phenomenon, and the way that the long-range transport models considered here were applied does not necessarily yield accurate results at short ranges (see Section 3.1).

3. COMPARISONS OF MODEL BASE CASE RESULTS

3.1 Qualitative Comparisons for Single and Multiple Point Sources

As the mesoscale flow patterns are varied, the three models will sometimes intercompare very well, and sometimes not as well. The two meteorological episodes chosen represent some typical variations of mesoscale flow patterns that can be expected to occur over multiday, regional-scale simulations.

The first set of base-case model comparisons, Figure 3-1, depicts the isopleths of regional-scale 24-hour average ground-level concentrations of SO_2 from the Navajo power plant, as calculated by each model for day 167 of Episode 1 (the highly zonal day). Figure 3-2 depicts concentration isopleths of $SO_4^=$ from the MESOPLUME and MESOPUFF runs. In each of the concentration contour figures shown, the contour values increase inwards from the outermost (lowest) value respectively, 0.1, 0.5, 1, 2, and 5 $\mu g/m^3$.

The overall concentration patterns produced by each model are consistent with the zonal flow field on this day. Near the source, the results from MESOGRID are appreciably different from the results of the other two models. Among the factors contributing to these differences are (1) the initial dilution of the point source through a grid volume in the MESOGRID model, (2) the very different treatment of plume mixing in the vertical, (3) inadequate sampling of the lateral plume distribution by MESOPLUME and MESOPUFF when the horizontal plume size is much smaller than the grid spacing, and (4) the inability of the particular contouring package used to realistically handle point singularities.

On the regional scale, however, the three models generally intercompare closely. It should be emphasized here that unlike the other two models, MESOGRID has no explicit horizontal diffusion - evidence that plume dispersion on regional scales (at least as represented by each of these models) is not sensitive to small-scale plume diffusion.

In the next set of base case model comparisons, the 24-hour average concentrations for SO_2 (Figure 3-3) and $SO_4^=$ (Figure 3-4) from the Navajo plant are depicted for day 169 of Episode 1 (the day with highly disorganized stagnating flow conditions, particularly in the southeast corner of the computational area). By comparison with the other two models, MESOPLUME appears to produce an anomalous high SO_2 concentration region far downwind--possibly a result of the inverse wind speed dependence of the plume model (see Section C.4.3), magnified in a region where the flow rapidly stagnates. The MESOGRID algorithm is also subject to this nonphysical behavior, but because pollutant material distributed in some arbitrary manner within an individual grid cell is effectively spread uniformly over the entire grid cell for the purposes of plume sampling, MESOGRID does not show anomalous concentrations as high as those of MESOPLUME. Of the three models, the MESOPUFF results appear most realistic in the stagnating region.

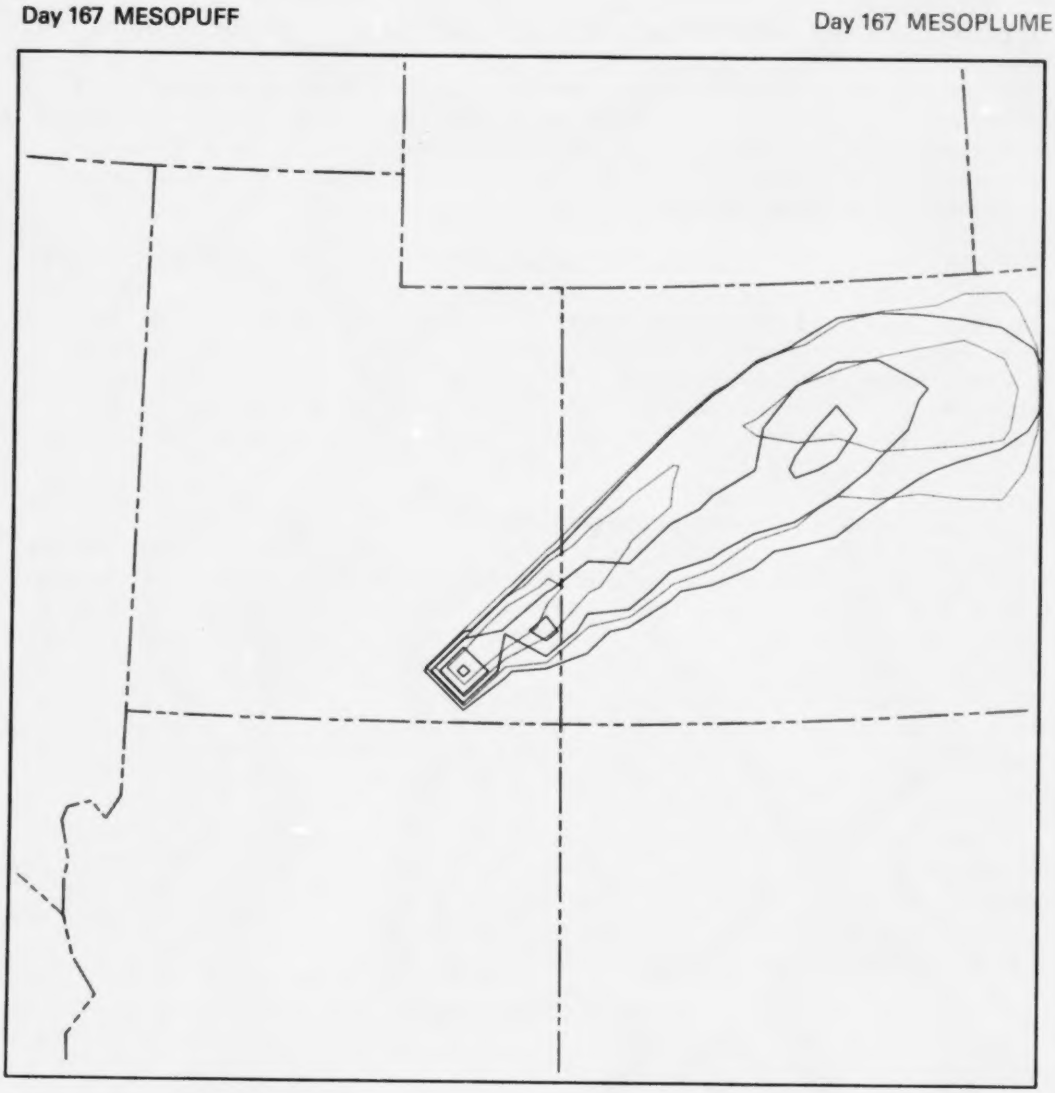
Day 167 MESOPUFF
Day 167 MESOPLUME

Figure 3-1 Episode 1 Day 167 Single Source Dispersion Model Comparisons (SO_2)

Day 167 MESOGRID

Day 167 MESOPLUME

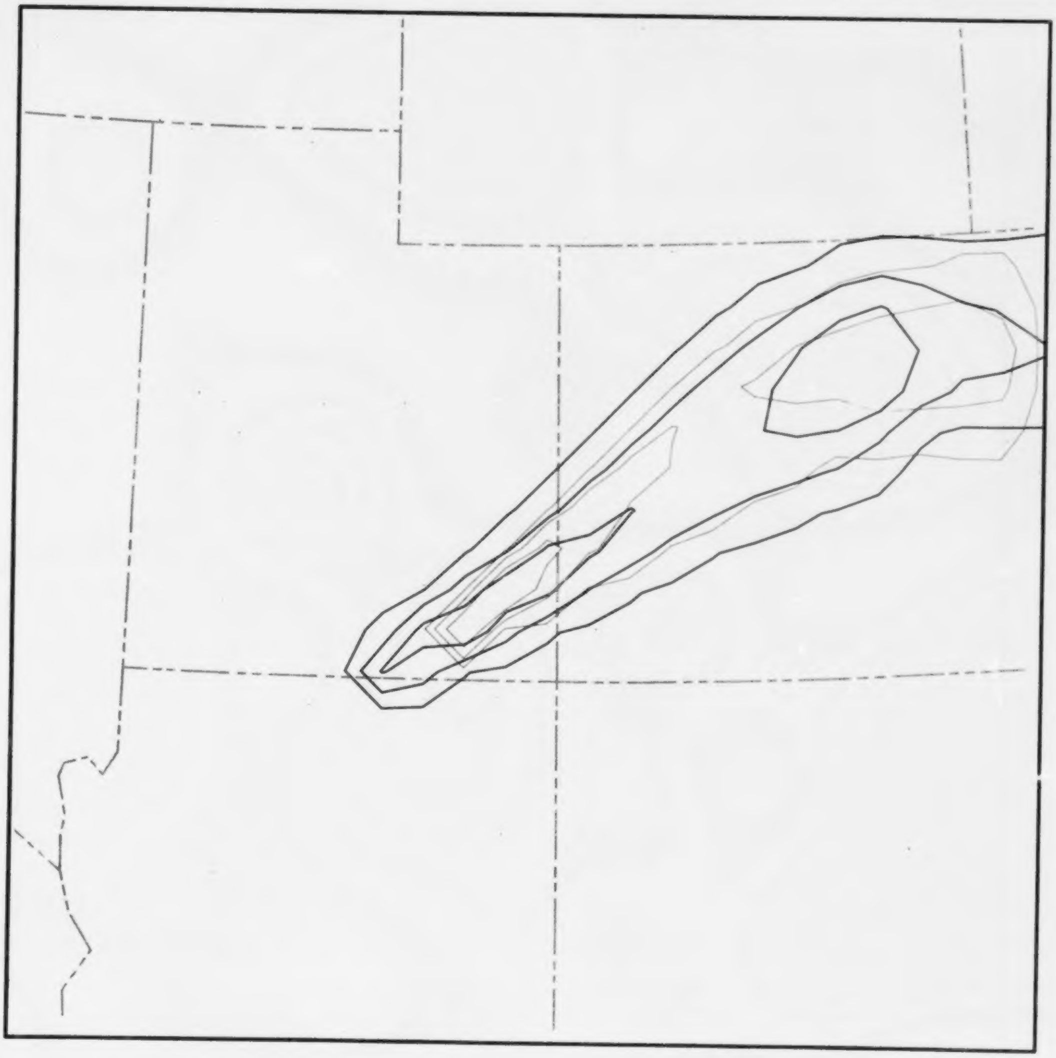

Figure 3-1 Continued

Day 167 MESOPUFF

Day 167 MESOGRID

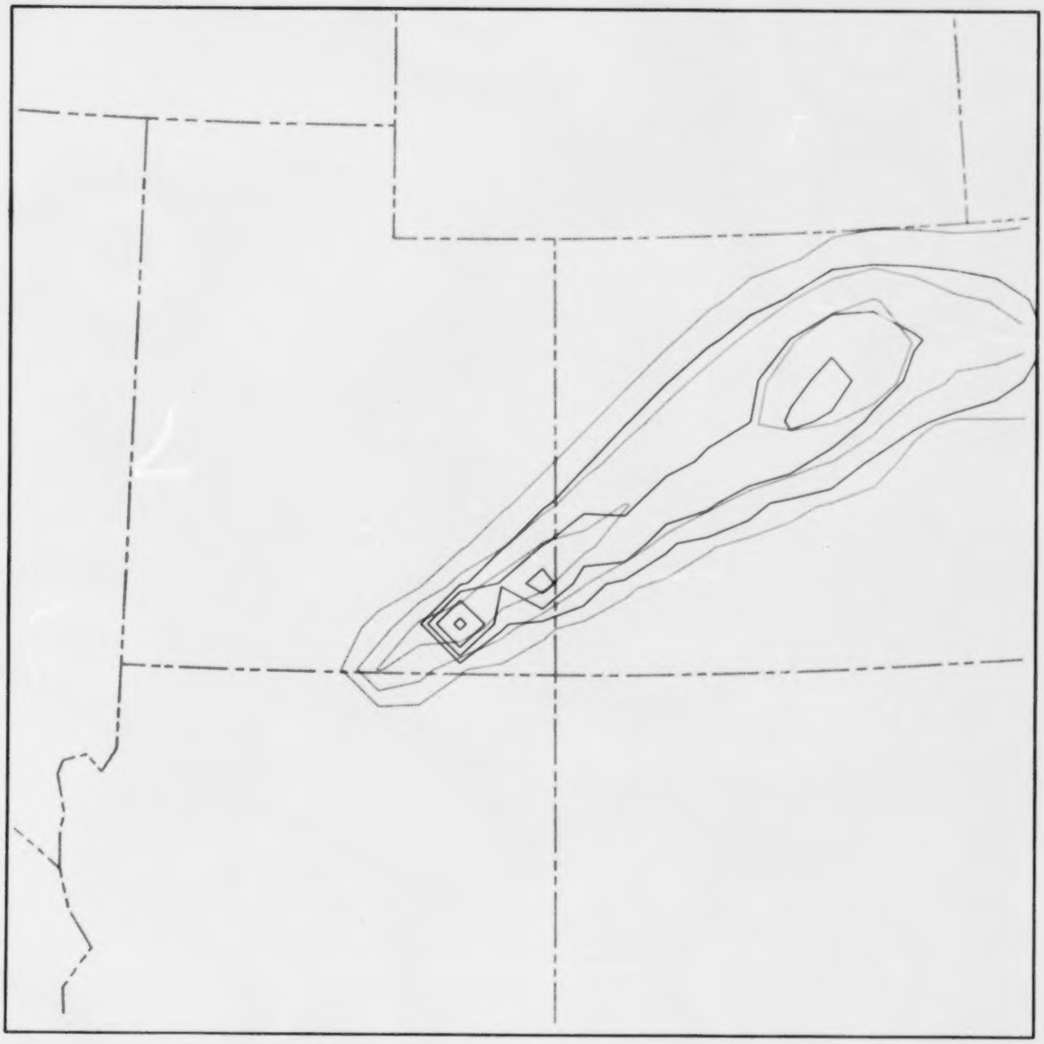

Figure 3-1 Continued

Day 167 MESOPLUME

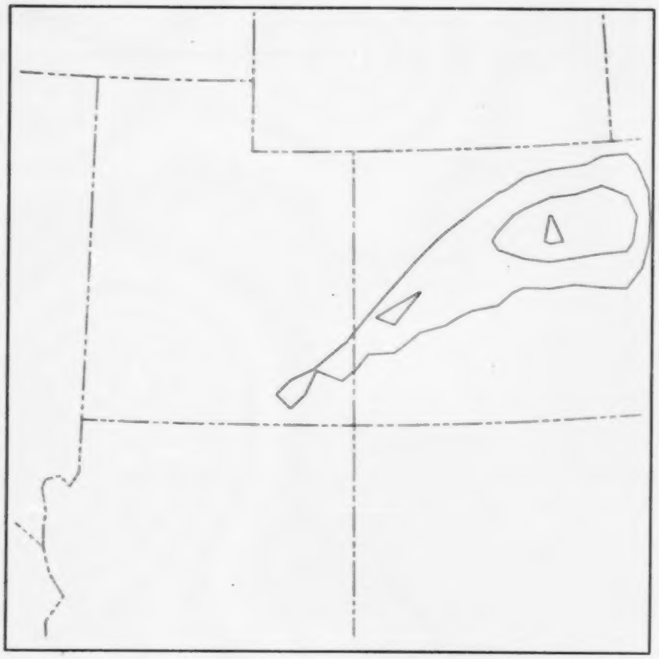

7902258

Day 167 MESOPUFF

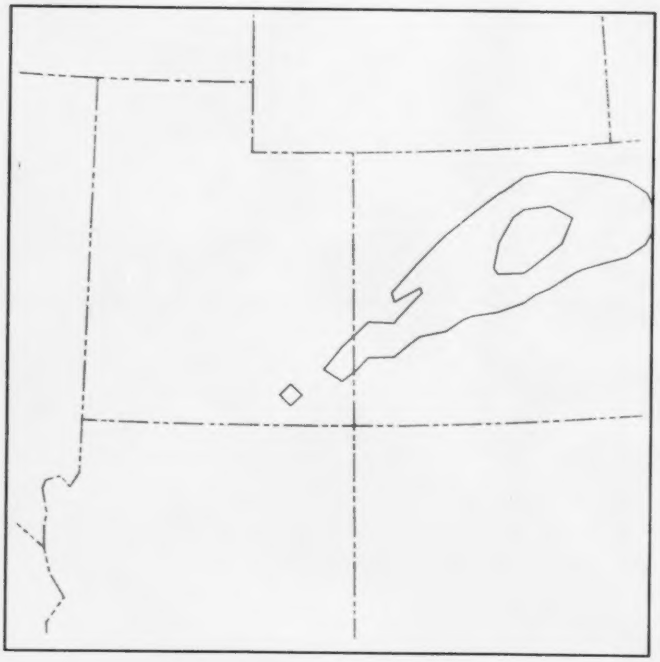

7902256

Figure 3-2 Episode 1 Day 167 Single Source Dispersion Model Comparisons (SO$_4^=$)

Day 169 MESOPUFF

Day 169 MESOPLUME

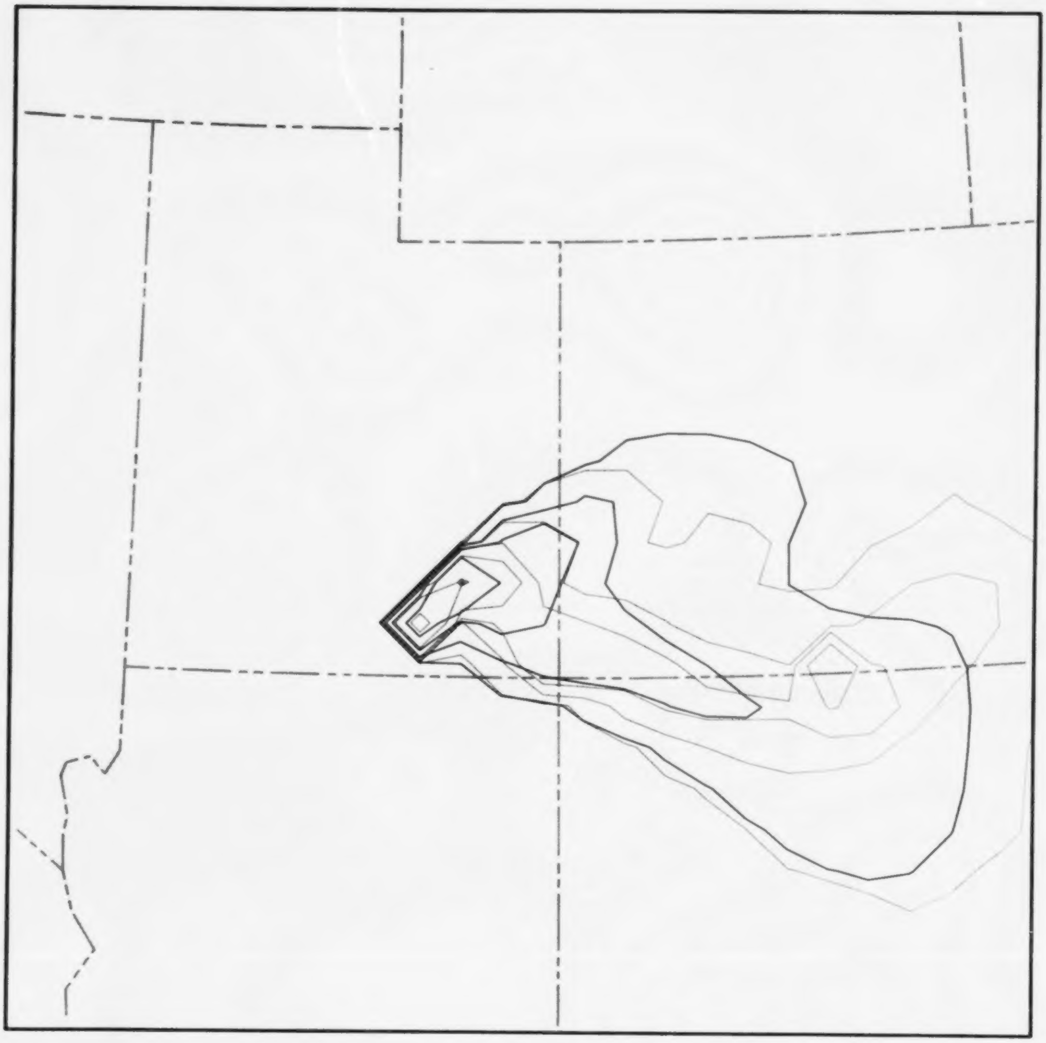

Figure 3-3 Episode 1 Day 169 Single Source Dispersion Model Comparisons (SO_2)

7901066
7901059

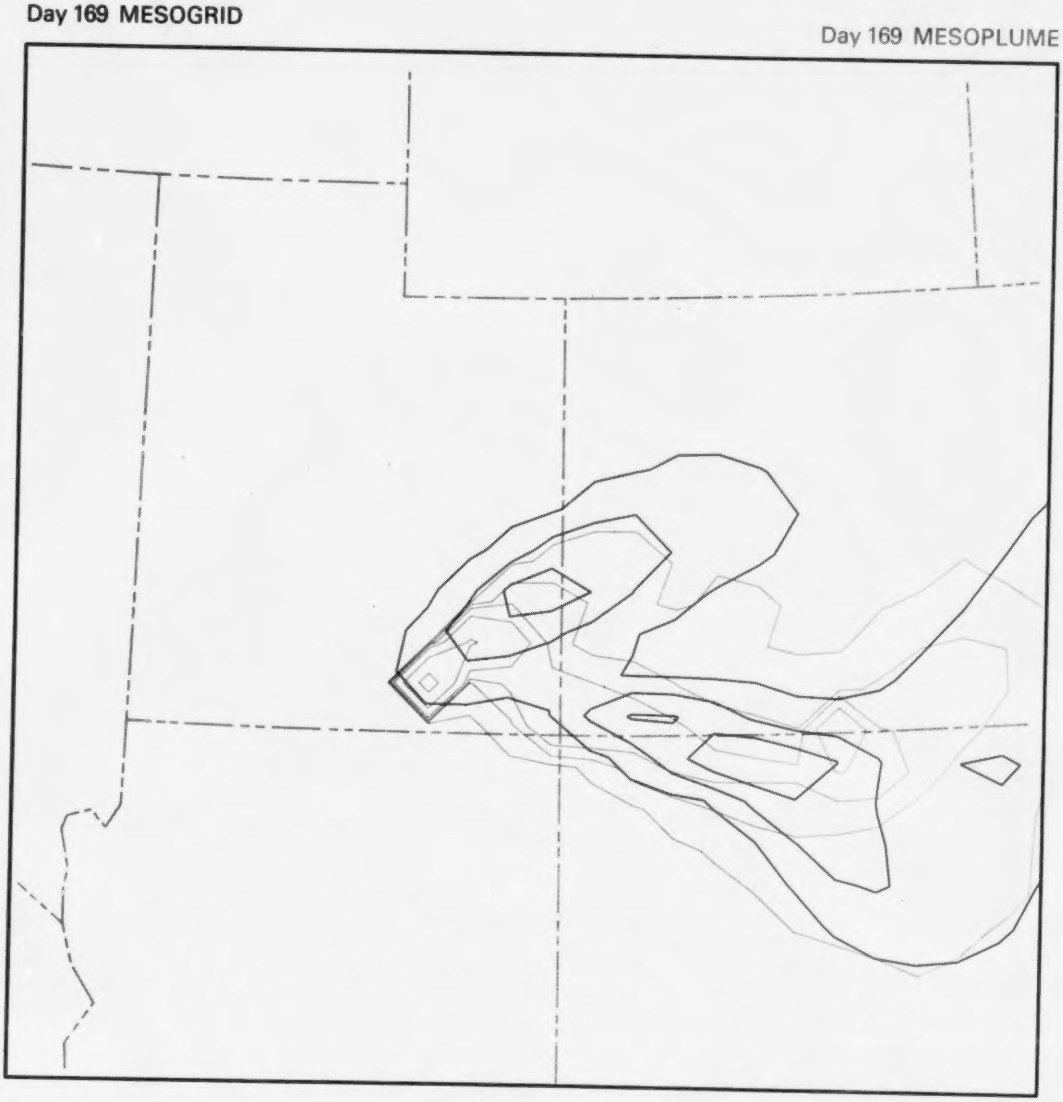
Day 169 MESOGRID
Day 169 MESOPLUME

Figure 3-3 Continued

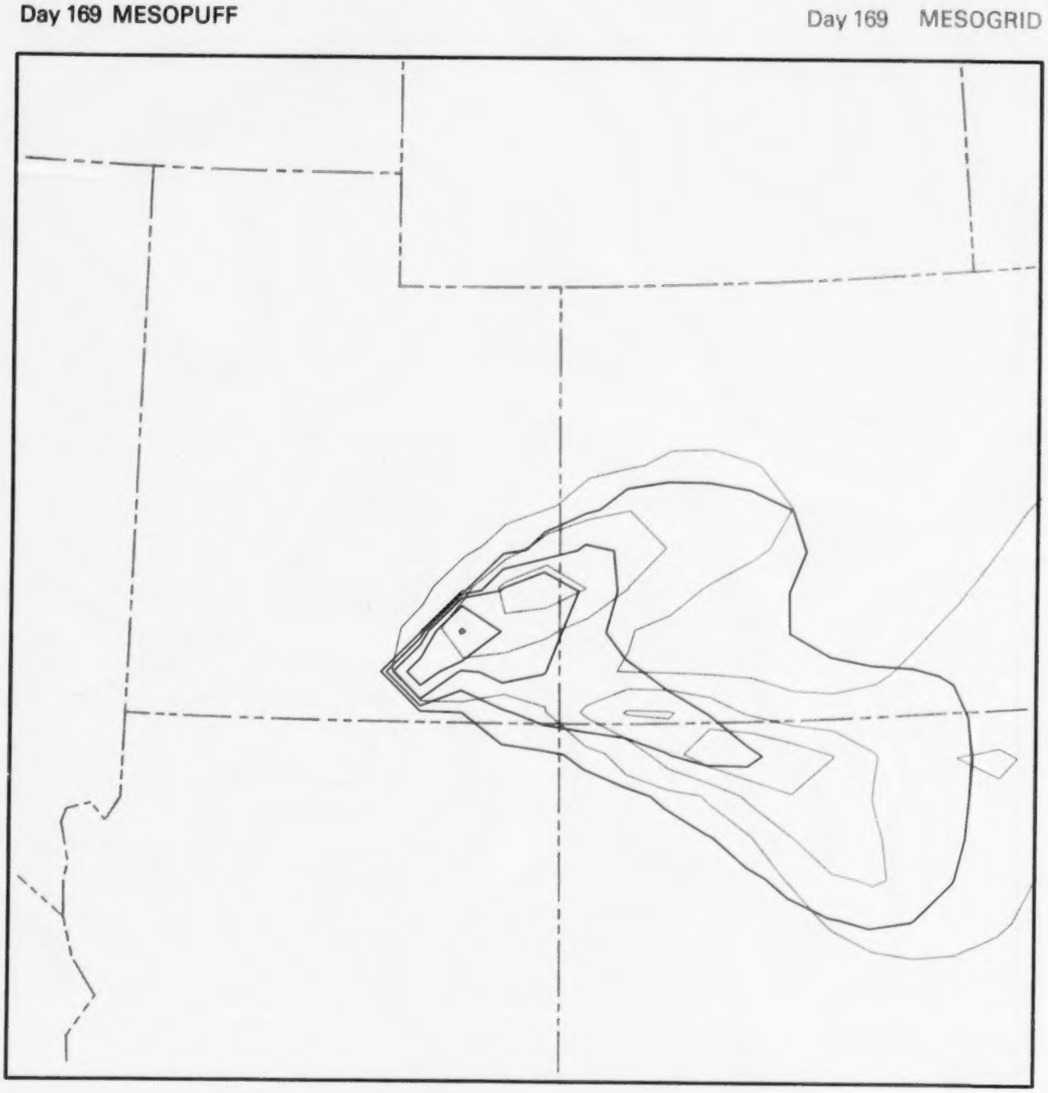
Day 169 MESOPUFF
Day 169 MESOGRID

Figure 3-3 Continued

Day 169 MESOPLUME

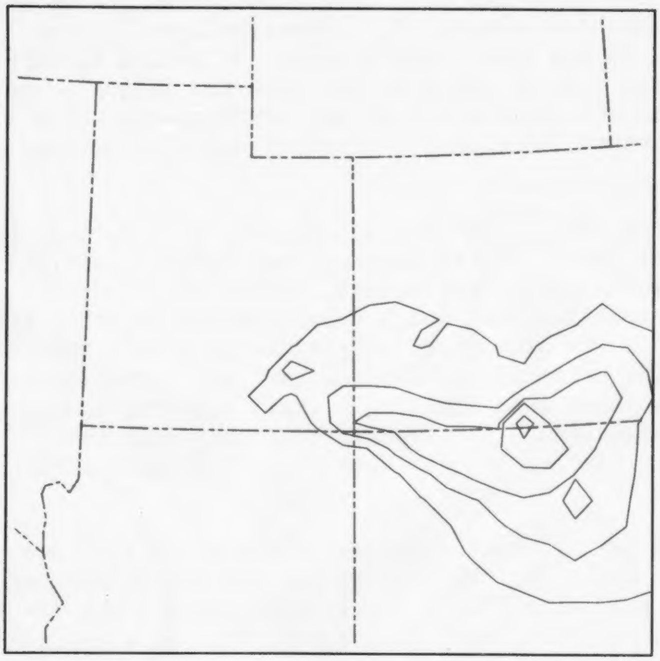

Day 169 MESOPUFF

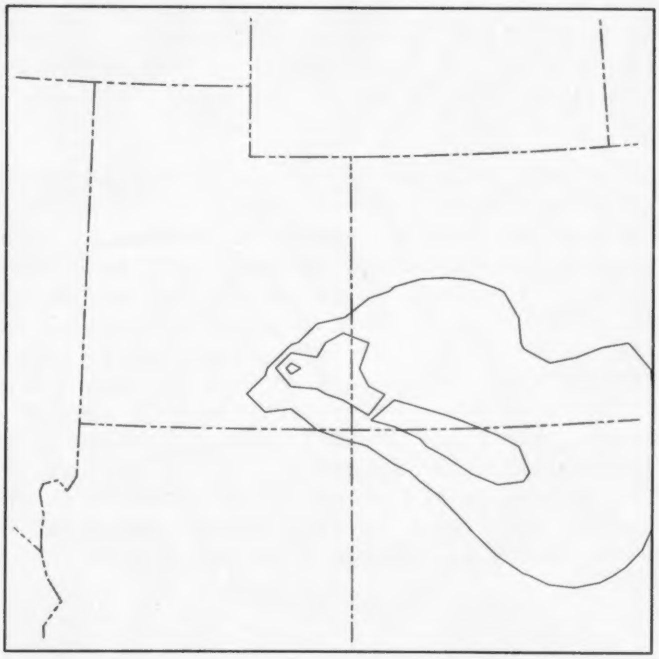

Figure 3-4 Episode 1 Day 169 Single Source Dispersion Model Comparisons ($SO_4^=$)

The multiple source base case model comparison runs using the Episode 1 meteorology are shown in Figure 3-5 which depicts, for day 167, the 24-hour average SO_2 concentrations for a set of ten major point sources in the Four Corners area. It should be emphasized that this set of ten sources was selected from the larger inventory of major SO_2 sources in the area to illustrate various aspects of model multi-source performance for a distribution of source sizes and source locations.

In general, the regional-scale impacts are, as expected, dominated by the largest point sources whose plumes remain individually discernable at distances of several hundred kilometers. Note that the 0.1 $\mu g/m^3$ contour for each model approximately envelops the middle third of the region. The plumes are aligned in about the same direction, as dictated by the uniformly zonal flow that day. The intercomparison of model results shows most strikingly that, notwithstanding differences in basic model algorithms, the overall regional-scale behavior of the three models is very similar in this case. The 0.1 $\mu g/m^3$ contour envelopes closely coincide everywhere.

The next set of model multisource comparisons, shown in Figure 3-6, correspond to day 169 of Episode 1, the day of disorganized stagnating flow. As is the case for the multisource results for day 167, the 0.1 $\mu g/m^3$ contour envelopes compare very well on the regional scale. But, as also seen in the single-source results for day 169, there are important small-scale discrepancies evident in the concentration fields produced by the three models under such adverse flow conditions. As an alternative to the two-dimensional concentration field representation, the three-dimensional perspective plots in Figure 3-6 provide a powerful comparison of the magnitudes of impact computed by the three models. These plots clearly illustrate, for example, that MESOPUFF and MESOPLUME produce large-amplitude concentration 'spikes' in the near-field, but MESOGRID does not.

Episode 2, it will be recalled, is characterized by strongly recirculating flow situations, corresponding to the passage of two migratory synoptic-scale lows throughout the region of interest. Figure 3-7 displays, for each model as previously, the 24-hour average model results for SO_2 for days 124 to 127 for the Navajo plant. Again, the gross consistency of regional-scale model results is apparent, despite the great differences in modeling approaches. Small-scale features also intercompare quite well on days 124 and 125 when the flow is quite smooth and steady. However, for the more complex flow patterns of days 126 and 127, there are important discrepancies in the higher order moments of the plume distributions. It is believed that these discrepancies are chiefly attributable to differences in the way each model behaves in the recirculating flow region around the center of the cutoff cyclone and in the stagnating flow region near the center of the cyclone.

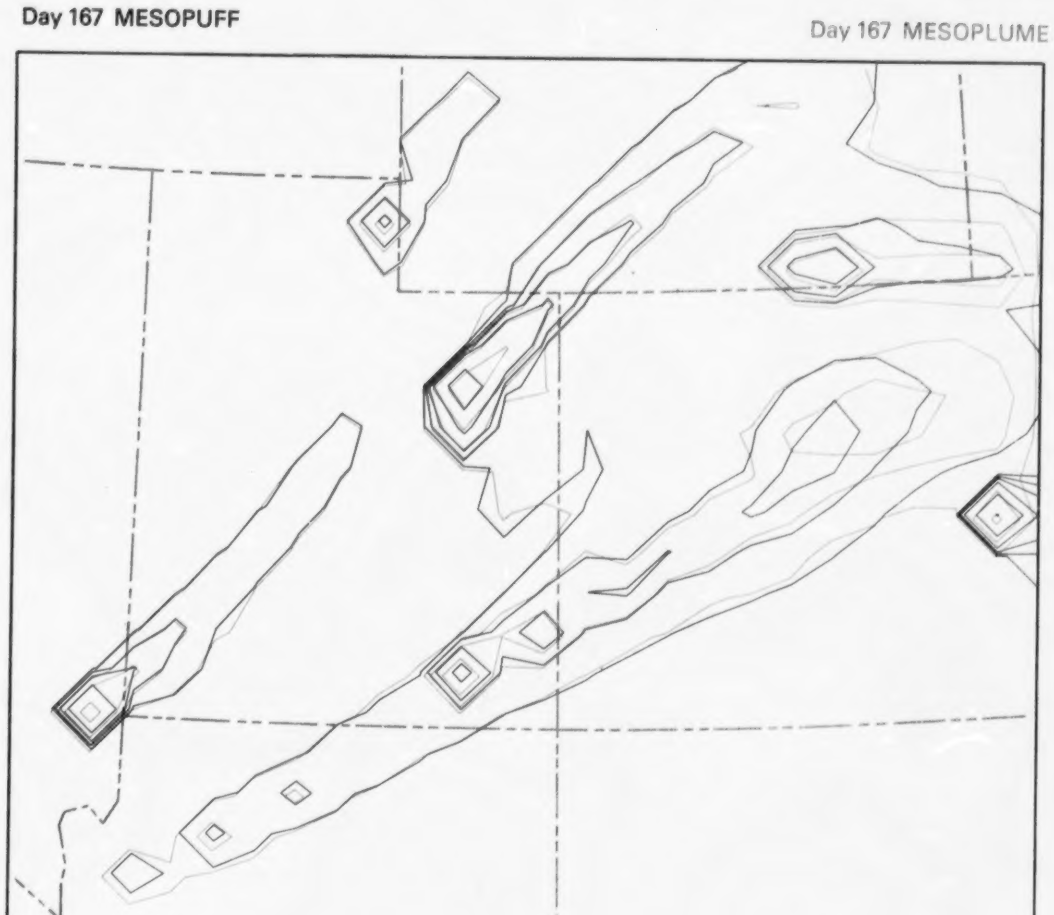
Day 167 MESOPUFF
Day 167 MESOPLUME

Figure 3-5 Episode 1 Day 167 Multiple Source Dispersion Model Comparisons (SO_2)

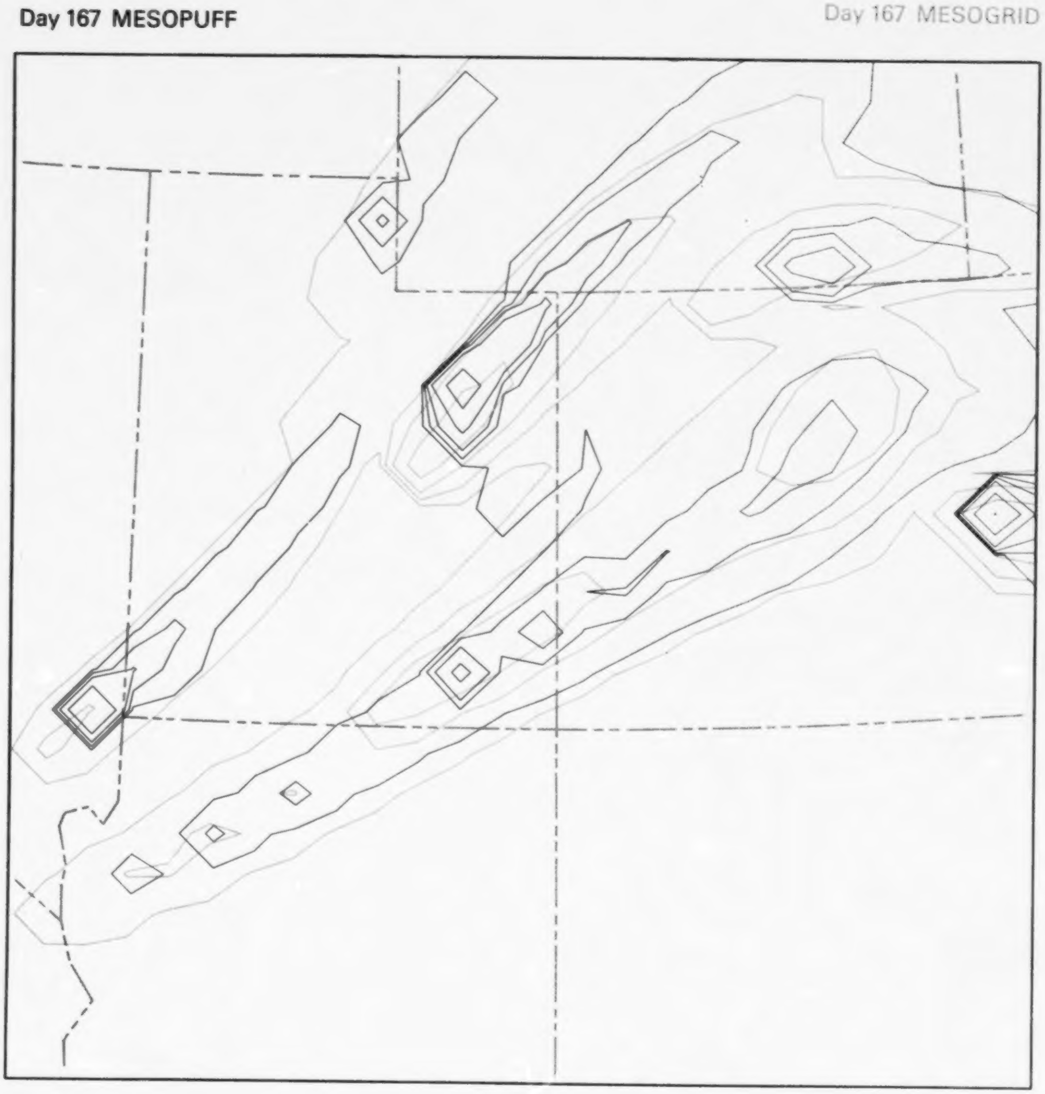
Day 167 MESOPUFF
Day 167 MESOGRID

Figure 3-5 Continued

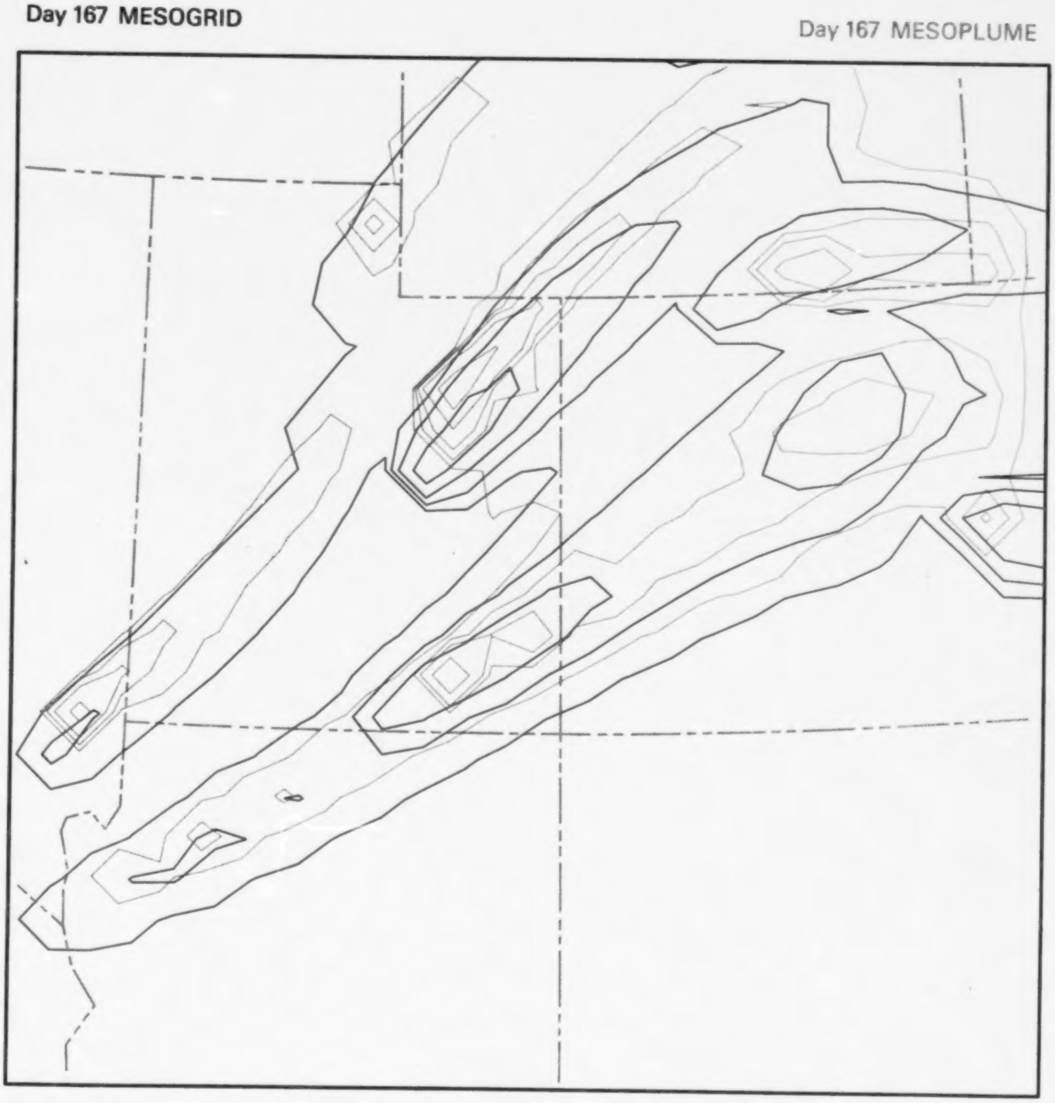
Day 167 MESOGRID
Day 167 MESOPLUME

Figure 3-5 Continued

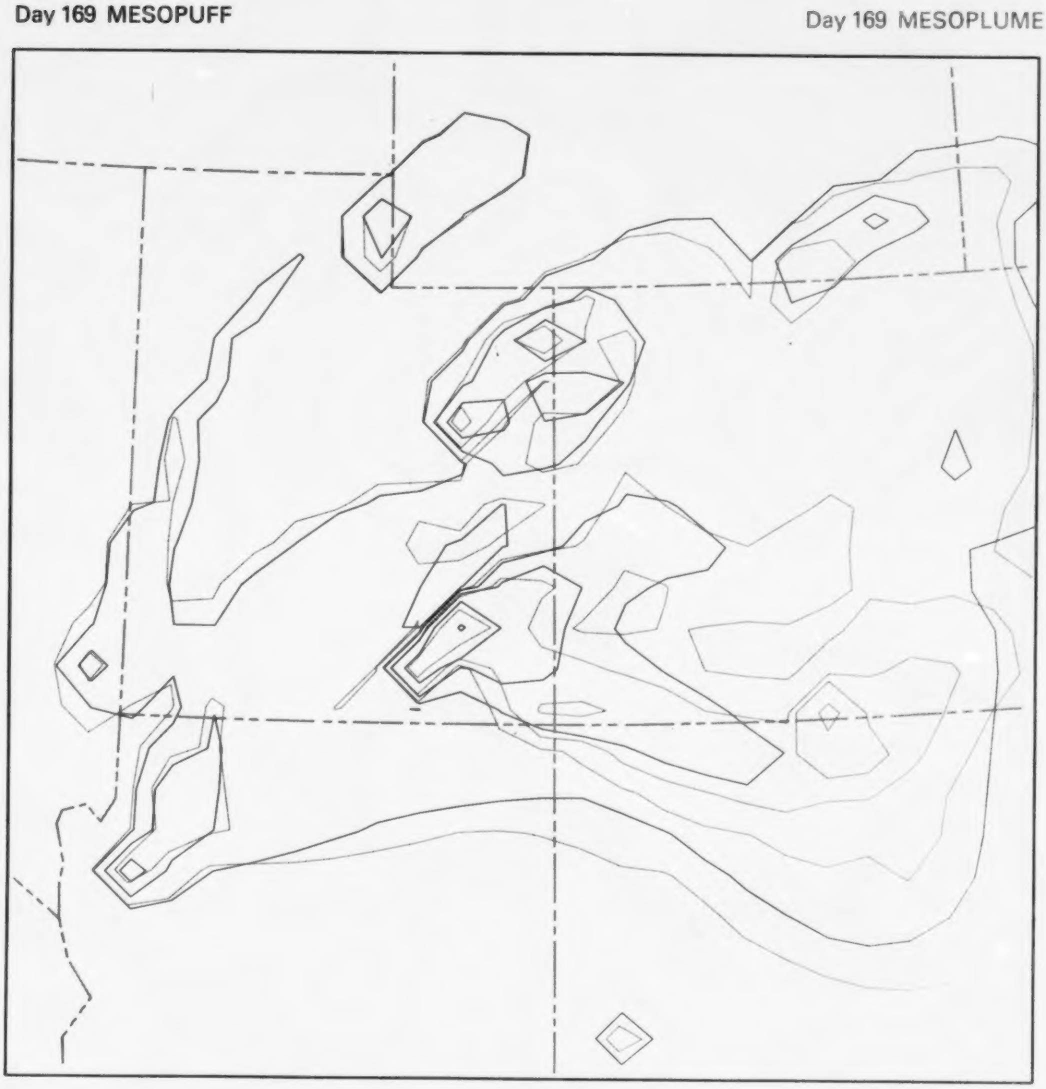
Day 169 MESOPUFF
Day 169 MESOPLUME

Figure 3-6 Episode 1 Day 169 Multiple Source Dispersion Model Comparisons (SO_2)

7901348
7901347

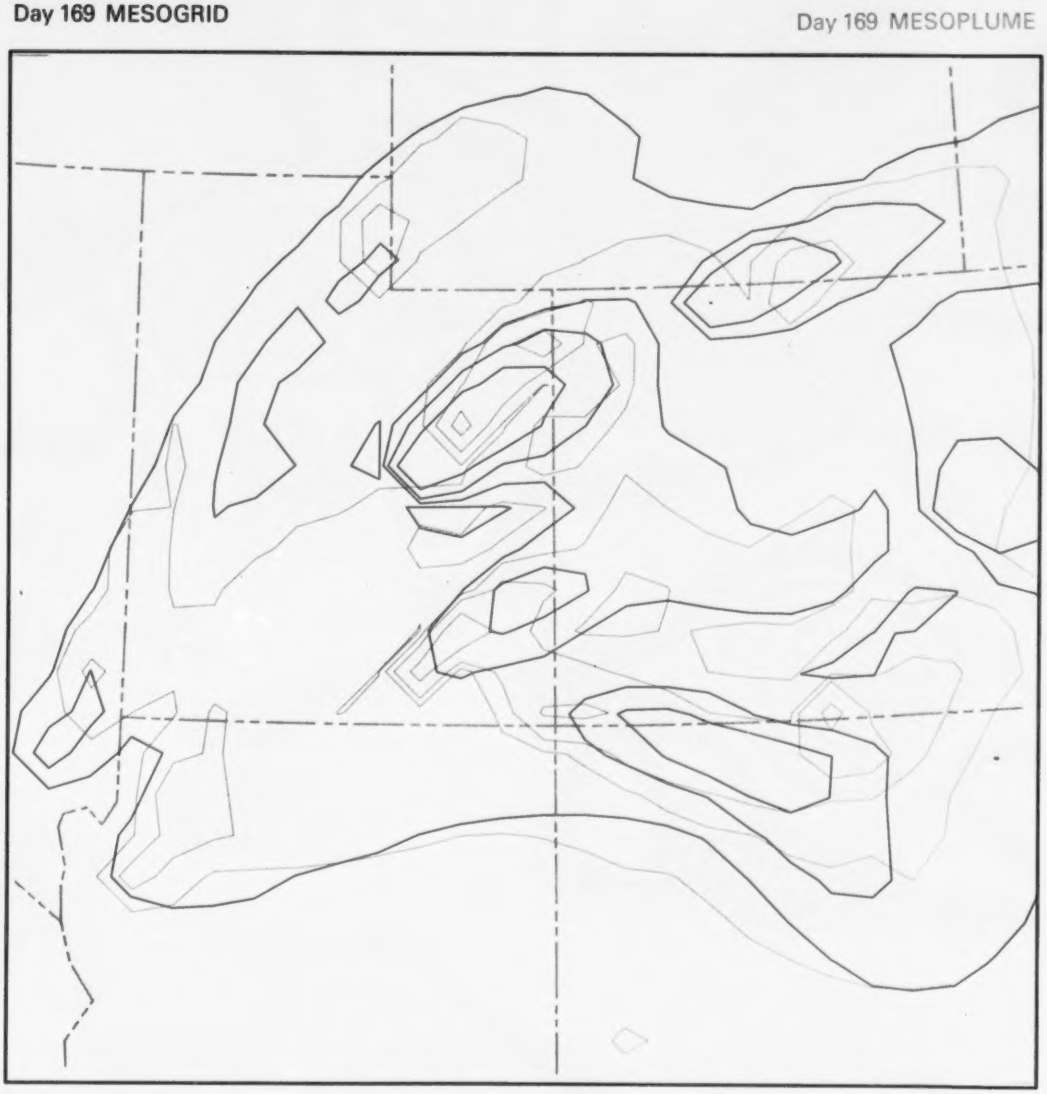
Day 169 MESOGRID
Day 169 MESOPLUME

Figure 3-6 Continued

Day 169 MESOPUFF

Day 169 MESOGRID

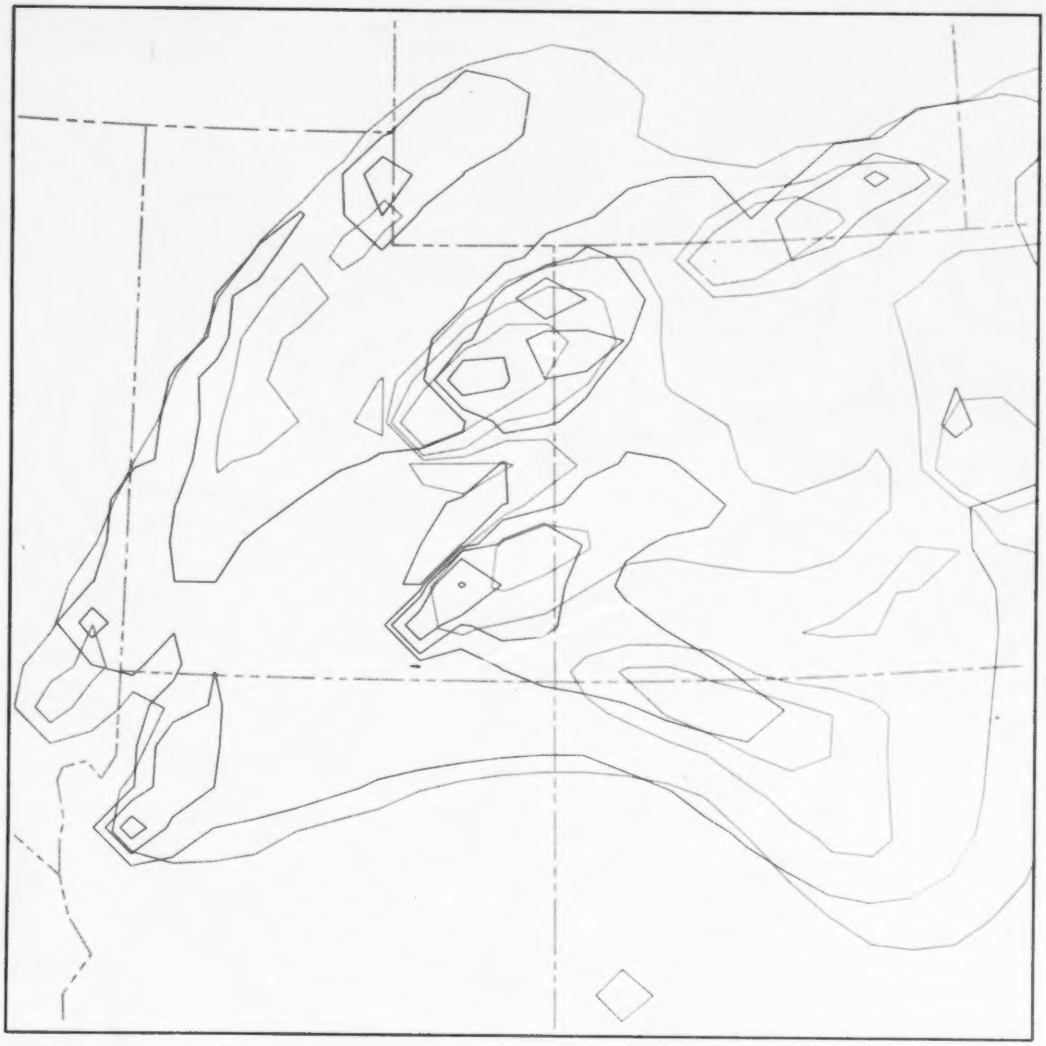

Figure 3-6 Continued

7901349

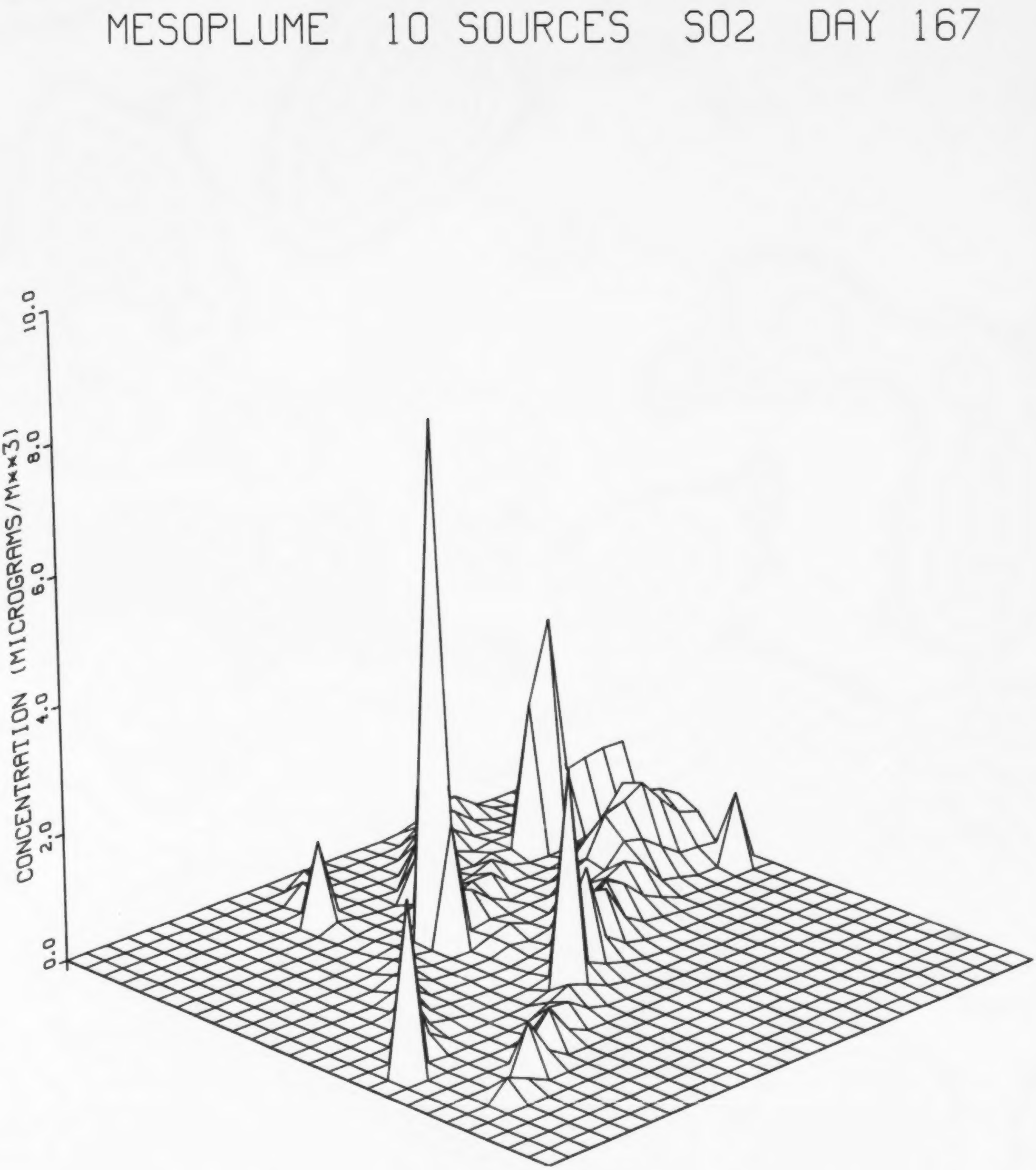

Figure 3-6 Continued

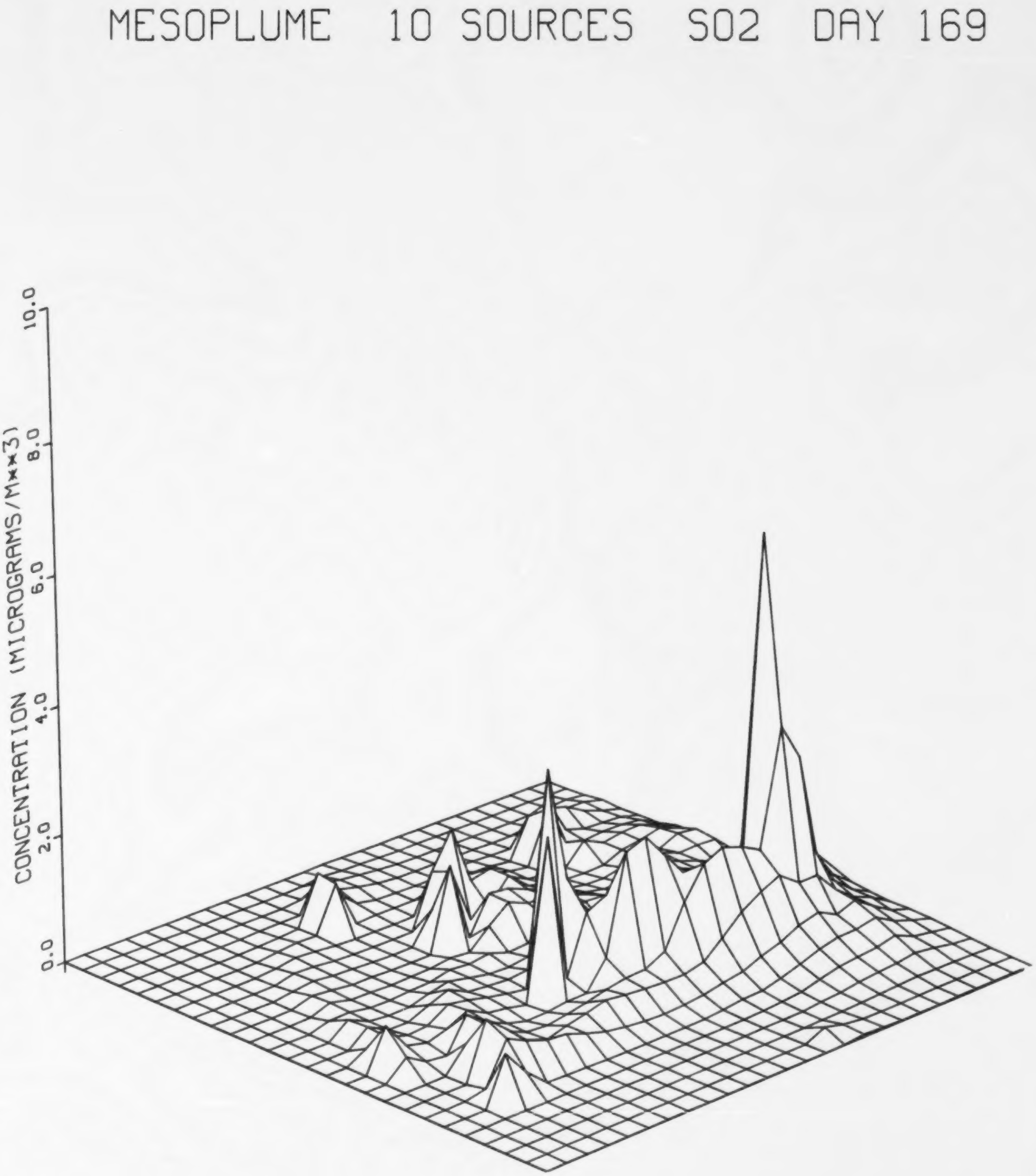

Figure 3-6 Continued

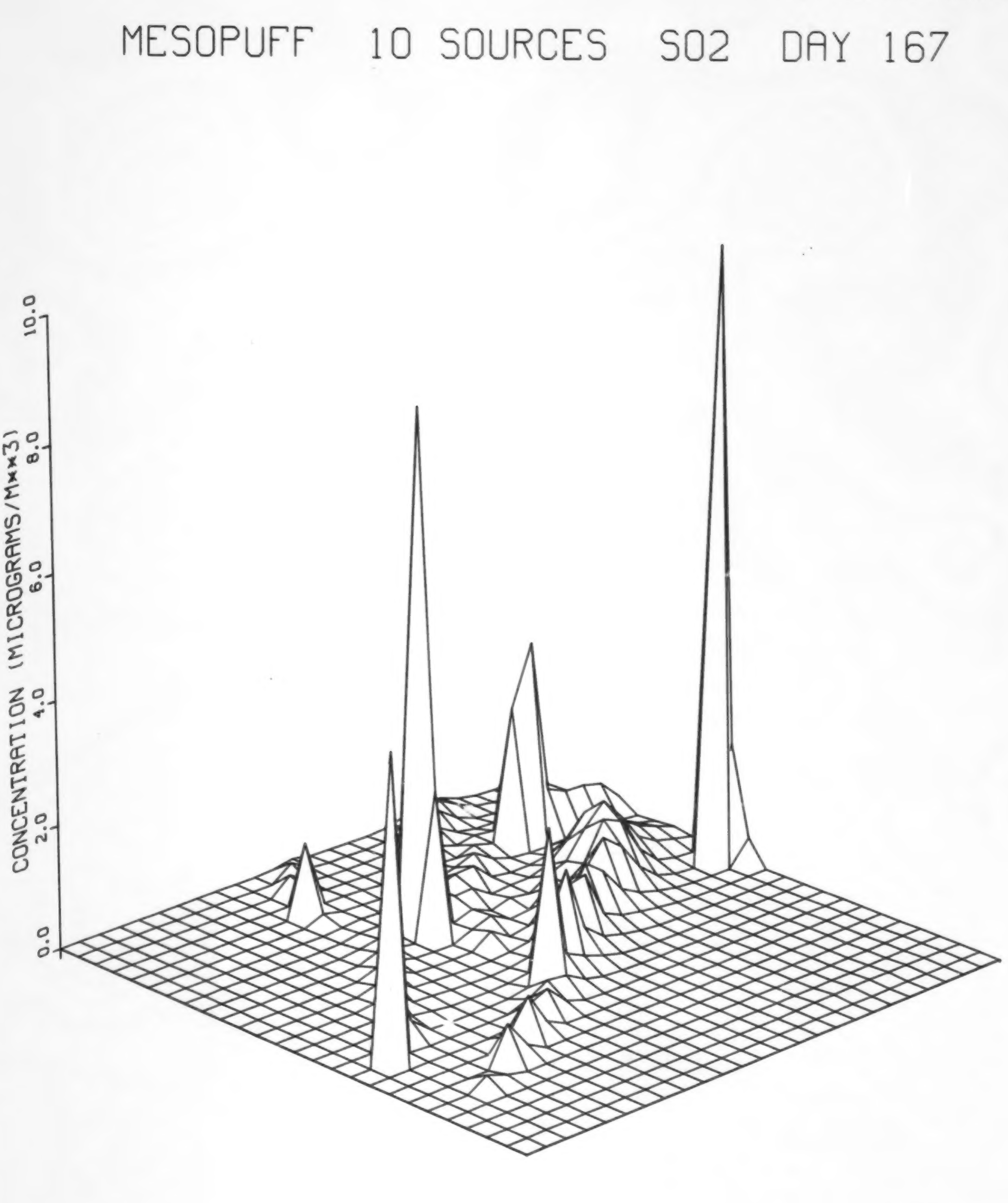

Figure 3-6 Continued

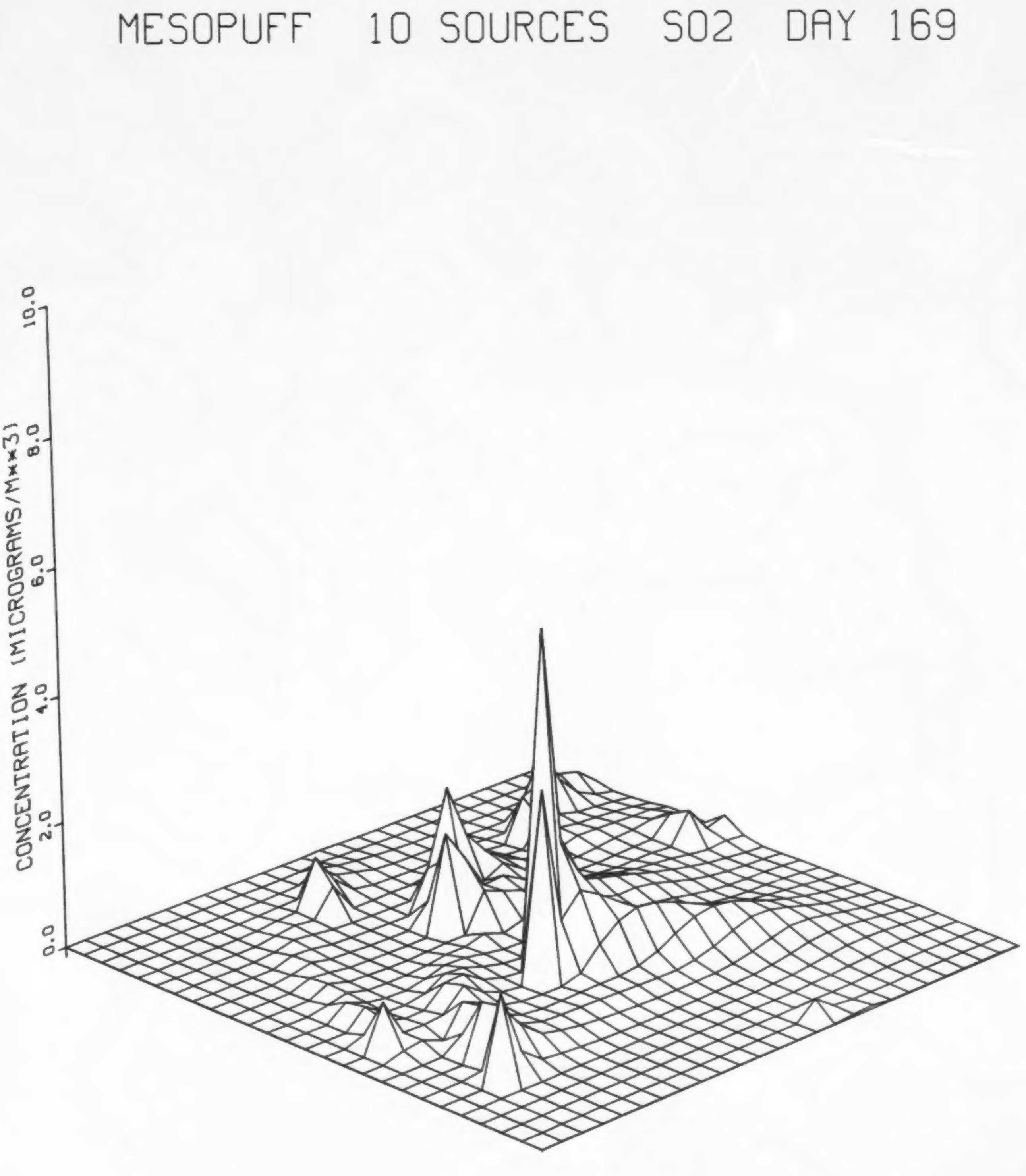

Figure 3-6 Continued

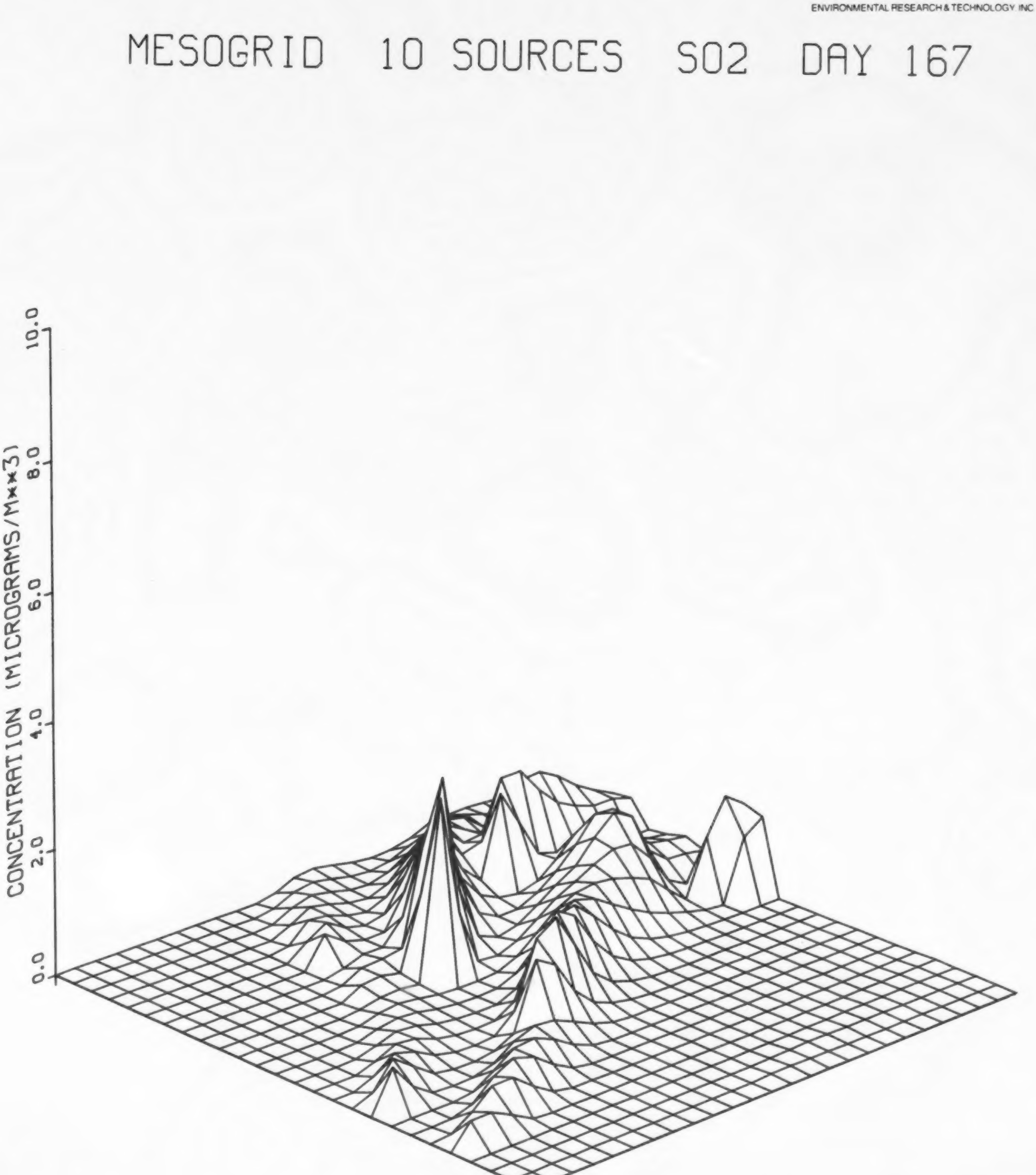

Figure 3-6 Continued

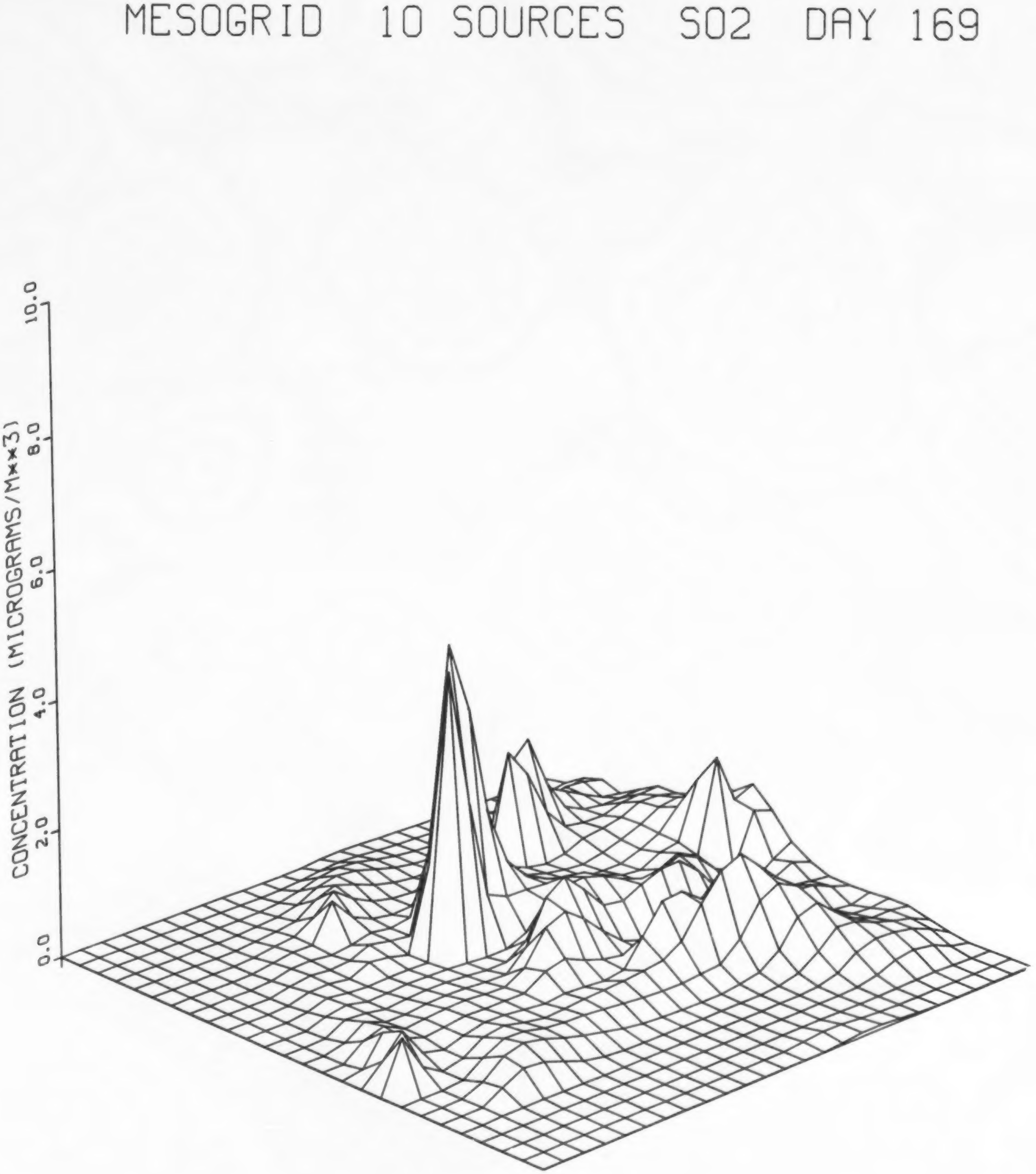

Figure 3-6 Continued

Day 124 MESOPLUME Day 124 MESOPLUME

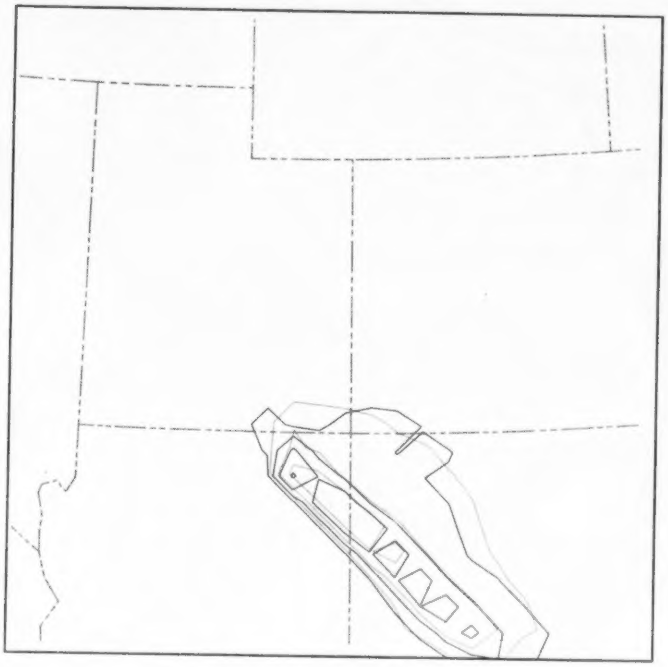
7902222
7902221

Day 124 MESOGRID Day 124 MESOPLUME

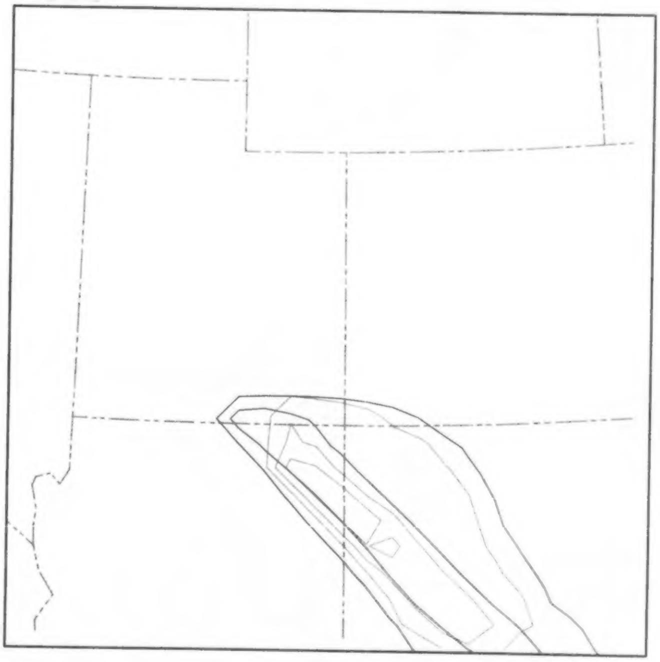
7910025
7902221

Figure 3-7 Episode 2 Day 124, 125, 126, and 127 Single Source Dispersion Model Comparisons (SO_2)

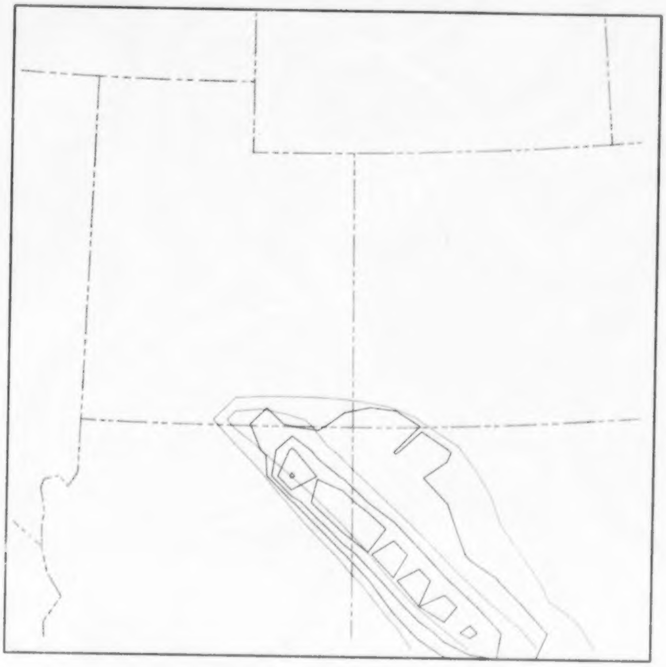

Day 124 MESOPUFF Day 124 MESOGRID

7902222
7910025

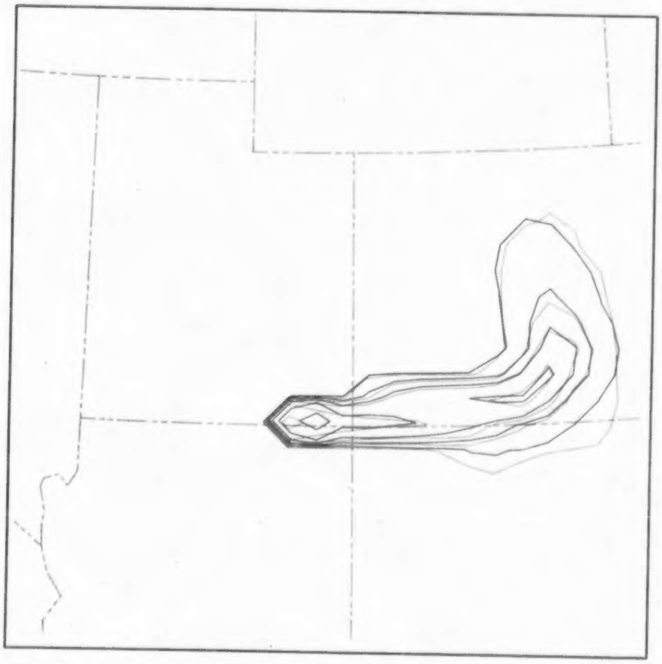

Day 125 MESOPUFF Day 125 MESOPLUME

7902225
7902224

Figure 3-7 Continued

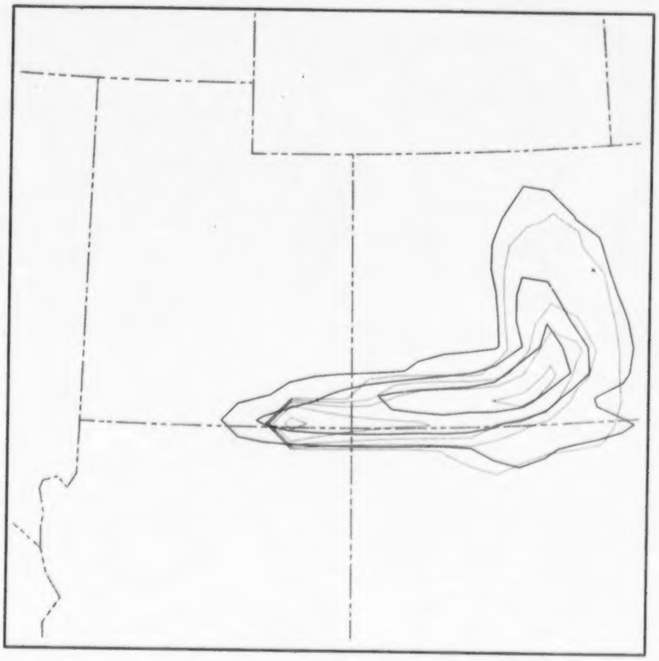

Day 125 MESOGRID Day 125 MESOPLUME

7910026
7902224

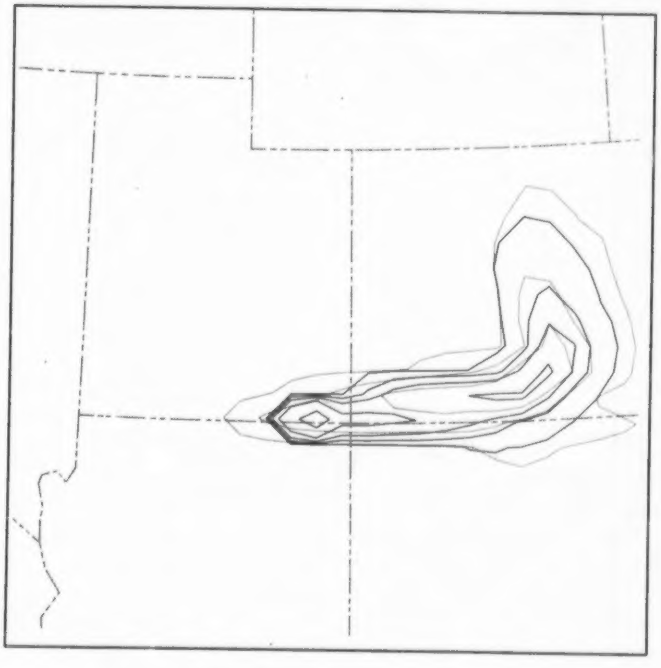

Day 125 MESOPUFF Day 125 MESOGRID

7902225
7910026

Figure 3-7 Continued

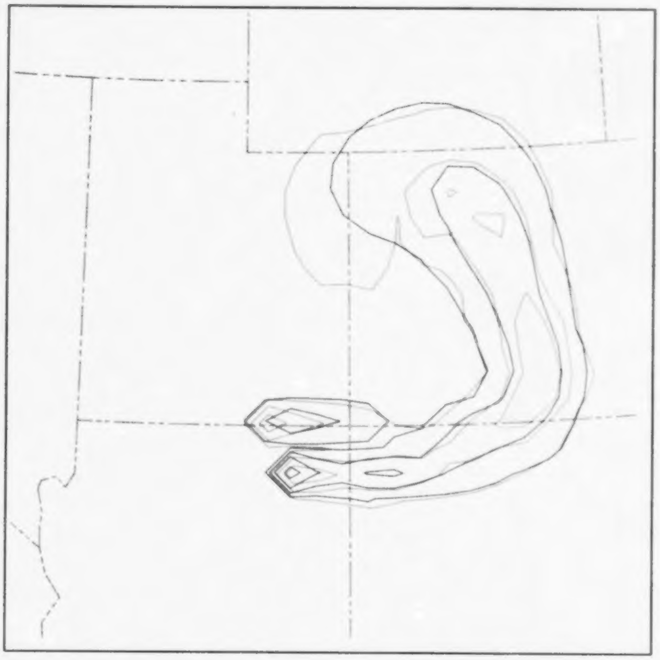

Day 126 MESOPUFF

Day 126 MESOPLUME

7902228
7902227

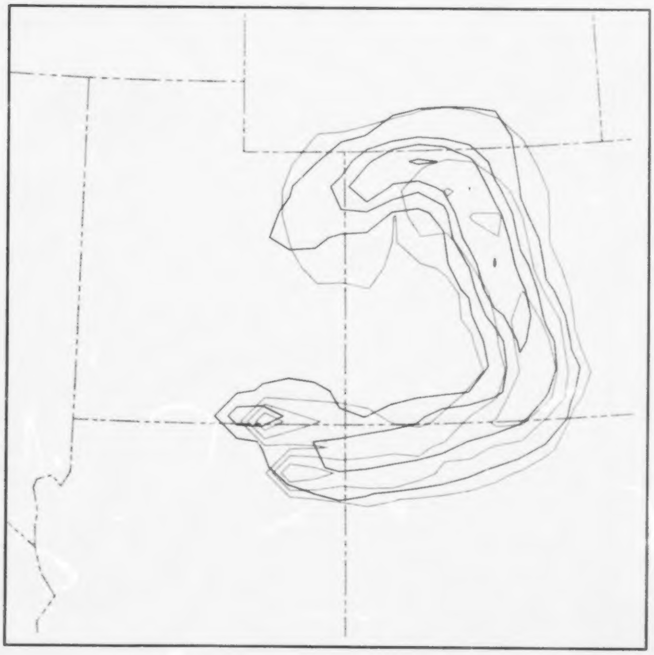

Day 126 MESOGRID

Day 126 MESOPLUME

7910027
7902227

Figure 3-7 Continued

Day 126 MESOPUFF Day 126 MESOGRID

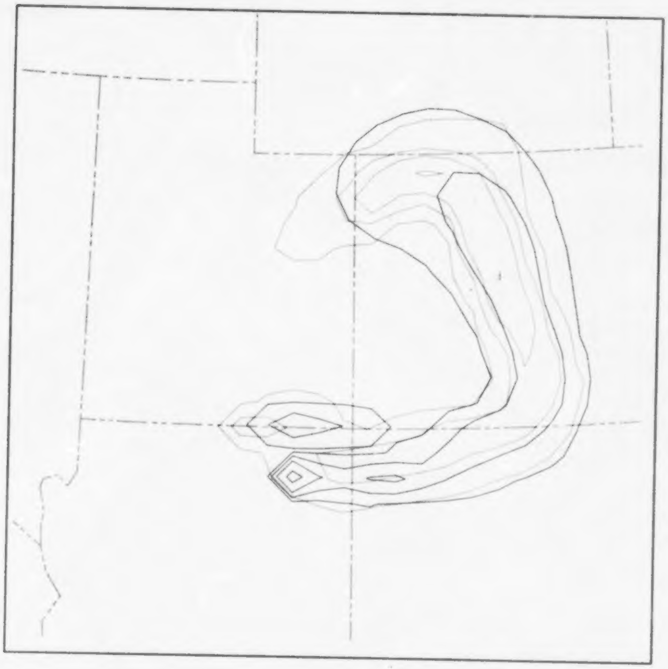

7902228
7910027

Day 127 MESOPUFF Day 127 MESOPLUME

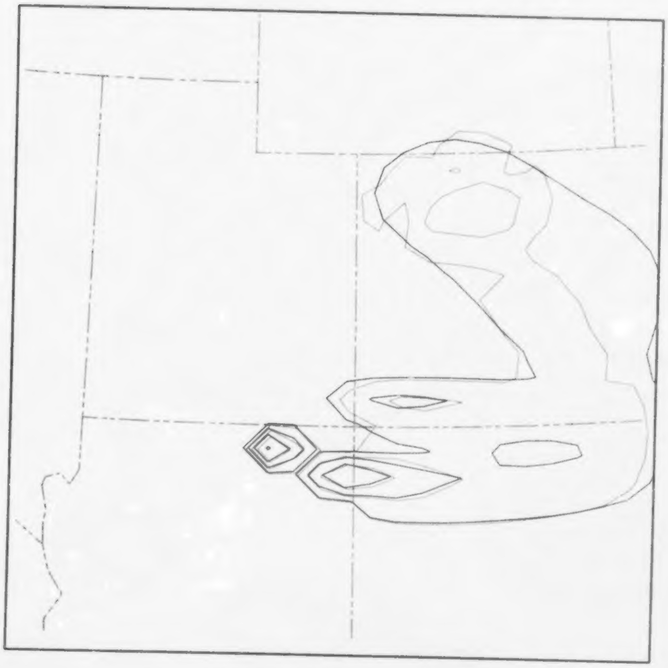

7902231
7902230

Figure 3-7 Continued

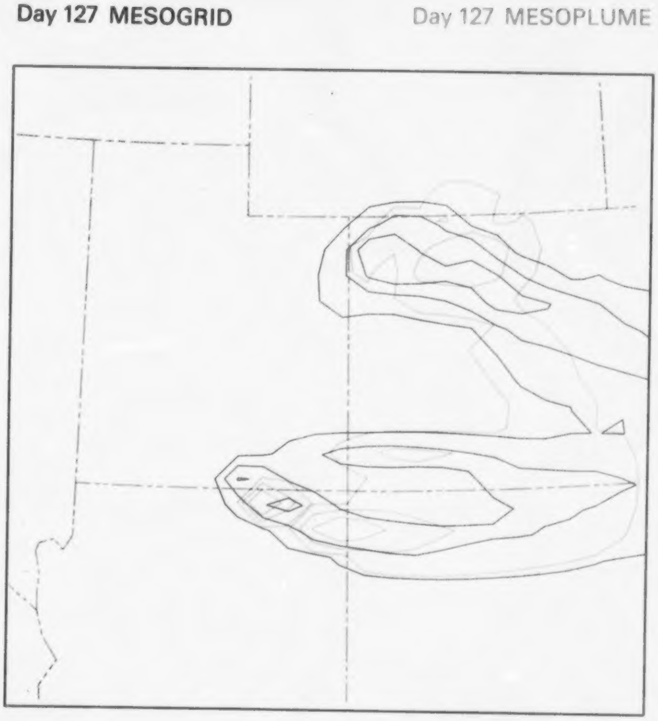
Day 127 MESOGRID
Day 127 MESOPLUME
7910028
7902230

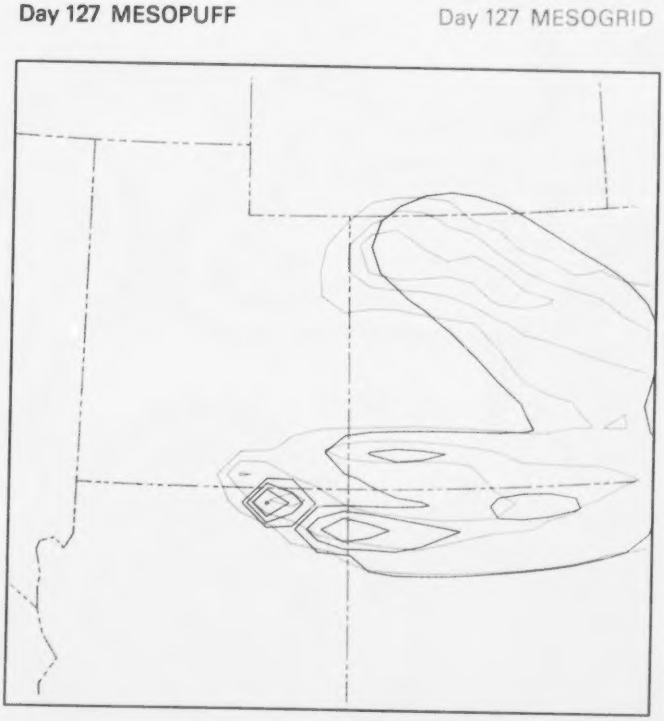
Day 127 MESOPUFF
Day 127 MESOGRID
7902231
7910028

Figure 3-7 Continued

3.2 Quantitative Comparisons of Model Results

As described in the previous section, the qualitative similarities in gross model performance are encouraging evidence for the basic validity (or at least consistency) of each of the mesoscale modeling approaches. Qualitatively, however, there are clear differences in the near vicinity of sources; and marked discrepancies in small-scale features on the regional scale. When quantitative analyses are used to compare model results, a picture consistent with the qualitative conclusions emerges. Figures 3-8 and 3-9 illustrate the correlation coefficient (r) intercomparing the results of all three sets of single-source model runs for each day during each episode.

In general, the MESOPUFF and MESOPLUME models tend to correlate best; for zonal and recirculating mesoscale flows, $r \gtrsim 0.9$, but for the highly stagnating conditions encountered during days 168 and 169 of the first episode, the correlation coefficient is as low as 0.56. The low values of correlation coefficient result, in part, because MESOPLUME predicts anomalously high concentrations in an area, about 500 km downwind from the source, in which the flow decelerates to stagnation conditions. The rapid decrease in plume segment length (associated with an inverse wind speed dependence) dramatically increases the concentrations computed by MESOPLUME. MESOPUFF does not exhibit this dramatic behavior because puff size is independent of change in wind speed.

The MESOGRID results are sensitive to the onset of stagnation conditions (probably because the two-dimensional flow field used to drive MESOGRID is locally divergent), as is indicated by the decrease in correlation coefficient with onsetting stagnation. Qualitatively, though, the hot spots that result in the MESOGRID model are not as great in magnitude as those in MESOPLUME, perhaps because in MESOGRID a pollutant mass is considered to have a particular subgrid cell distribution during the dispersion calculation, but, for the purpose of concentration field sampling the pollutant mass is considered to be spread uniformly over that grid cell.

The MESOGRID model requires a divergence-free wind field if it is to conserve strictly pollutant concentrations (in the absence of sink terms). The base-case meteorological data were processed with MESOPAC with a maximum allowable absolute wind field divergence of 10^{-4} s^{-1}. This tolerance level was chosen because a substantially more stringent level (10^{-5} s^{-1}) was found (1) to result in a loss of important subsynoptic detail in the flow pattern, and (2) to increase the costs of running the MESOPAC program by about a factor of 4. Under most circumstances, the 10^{-4} s^{-1} maximum divergence level is sufficiently low so that no significant effect is noticeable when the MESOGRID results are compared to either of the other models. It is possible under some conditions for the divergence term to be important (see Appendix D).

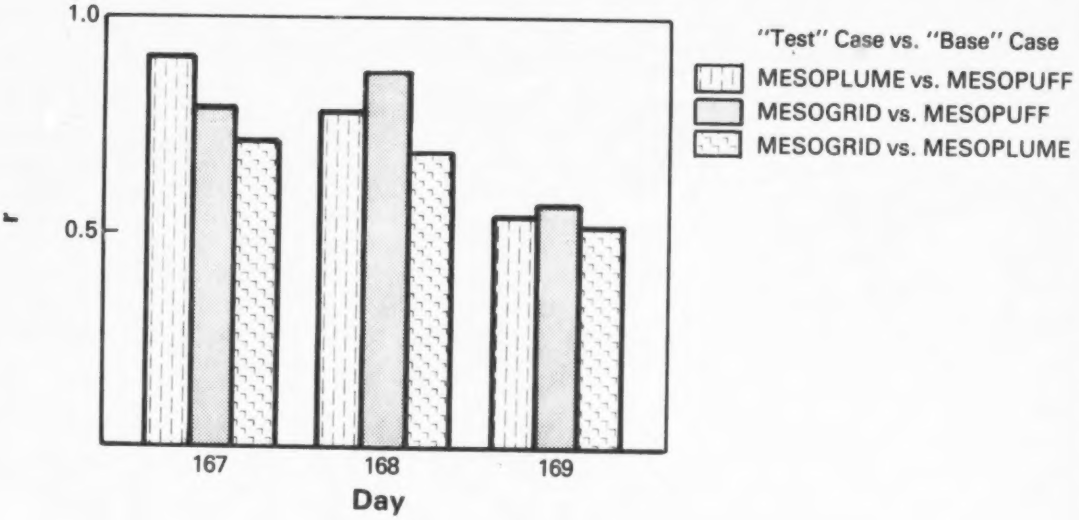

Figure 3-8 Days 167, 168, and 169 Comparison of the Different Models Results (Correlation Coefficient r)

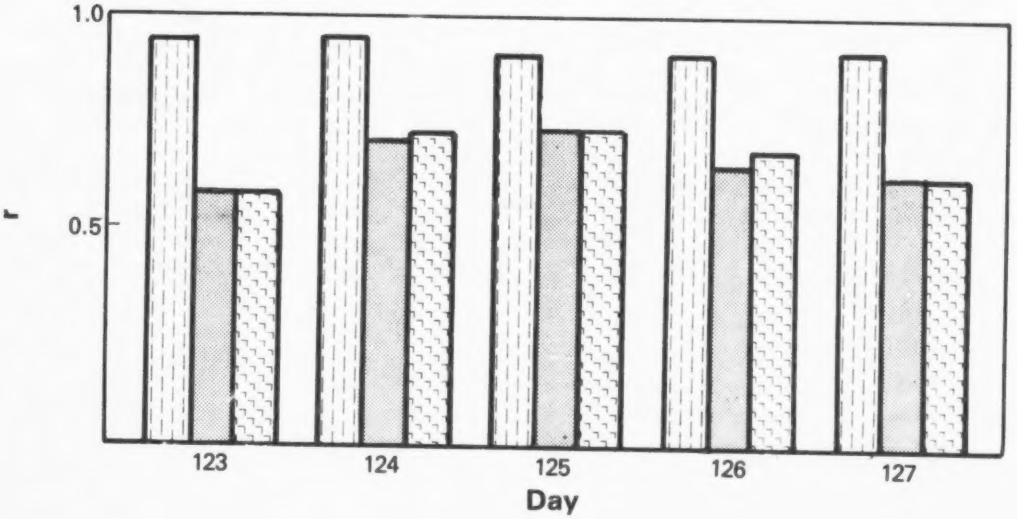

Figure 3-9 Days 123, 124, 125, 126, and 127 Comparison of the Different Models Results (Correlation Coefficient r)

Another useful quantitative criterion for model comparison is the effective size of the plume, as measured by the number of grid points with significantly nonzero concentrations. This measure is shown in Figures 3-10 and 3-11 illustrating 24-hour average plume size for each day of the two episodes. Note that (1) the MESOPLUME and MESOPUFF models calculate plume concentrations out to three horizontal standard deviations from the centerline and that (2) MESOGRID will set to zero any calculated concentration below a minimum value of 10^{-4} micrograms per cubic meter ($\mu g/m^3$). The fractional difference of number of points in the plume (FDN) is similar in all cases, with the notable exception of the MESOPUFF results for days 126 and 127 of Episode 2. This may be due to the longitudinal diffusion in MESOPUFF, tending to spread pollutant mass tangentially outward from a curved plume trajectory - the resultant MESOPUFF plume then encompasses more grid points than those of the other models. The results suggest qualitatively that horizontal dispersion is dominated by plume meander, except under special flow situations - note that the MESOGRID model, with no horizontal diffusion, yields results for plume size very similar to those of the other two models.

Figures 3-12 and 3-13 illustrate the time variation of the fractional difference of the plume means (FDM) for each 24-hour average time period during the two episodes studied. During the first episode, flow stagnation conditions in the eastern part of the grid during days 168 and 169 result in an unrealistically high concentration region in this area for the MESOPLUME model, as evidenced by the large negative values of the FDM when MESOPLUME is compared to MESOPUFF. Concentrations as large as 5 $\mu g/m^3$ occur far downwind in the region of lowest wind speeds; this occurrence is most likely the result of the inverse wind speed dependence of the MESOPLUME model. The 24-hour average plume concentration (in $\mu g/m^3$) for days 167-169 are 0.39, 0.41, and 0.40 for MESOPLUME and 0.27, 0.25, and 0.22 for MESOPUFF. During the second episode, MESOPLUME predicts high concentrations in the low wind speed area surrounding the center of the cutoff cyclone (days 126-127). The MESOPLUME-MESOPUFF 24-hour average plume concentrations are very close, however, in periods of zonal flows and moderate wind speeds during both Episodes 1 and 2.

The comparisons for Episode 1 indicate that MESOGRID produces nearly identical average plume concentrations as MESOPLUME, and somewhat higher concentrations than MESOPUFF. The absence of horizontal diffusion in the MESOGRID model is evidently not a significant factor on the regional scales considered here. The FDM results for Episode 2 are again similar for the MESOGRID and MESOPUFF models, with the exception of days 126 and 127. It is believed that the significantly higher 24-hour average plume concentrations for the MESOGRID model result from an area of convergence with low wind speeds.

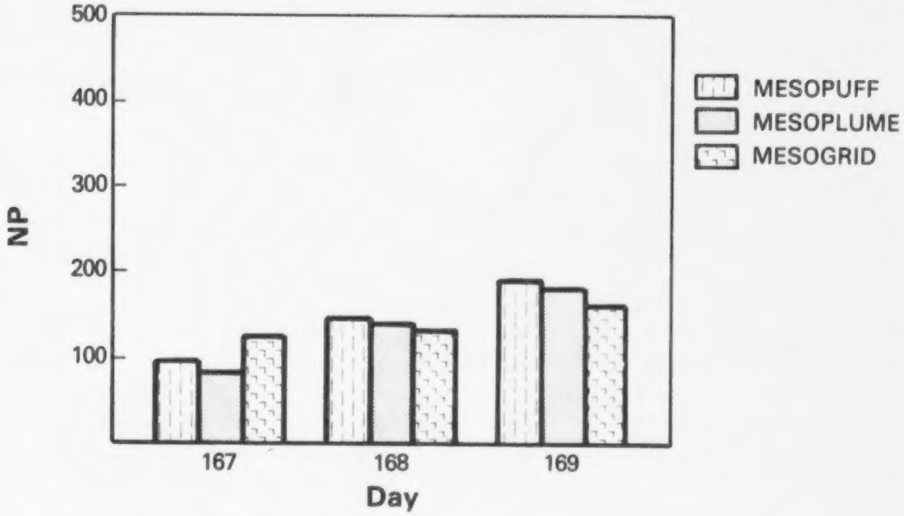

Figure 3-10 Episode 1--Comparison of the Number of Points in the Plume NP Computed by Each Model

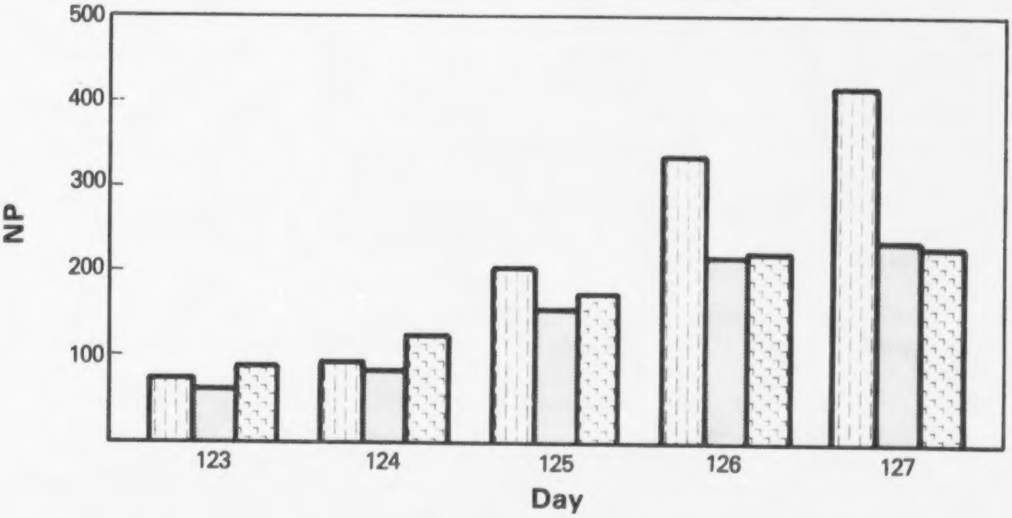

Figure 3-11 Episode 2--Comparison of the Number of Points in the Plume NP Computed by Each Model

7902311

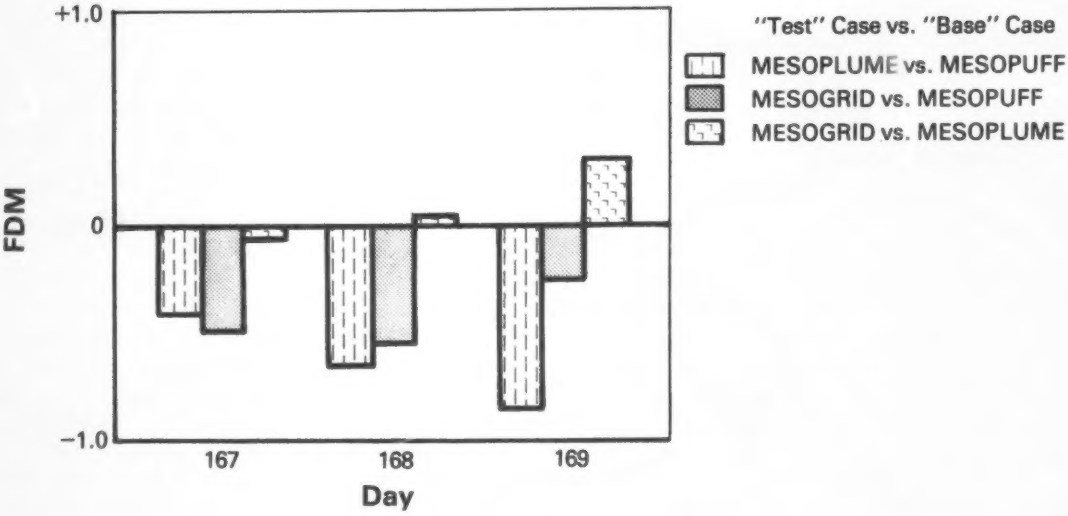

Figure 3-12 Episode 1--Comparison of the Different Model Results [Fractional Deviation of the Means (FDM)]

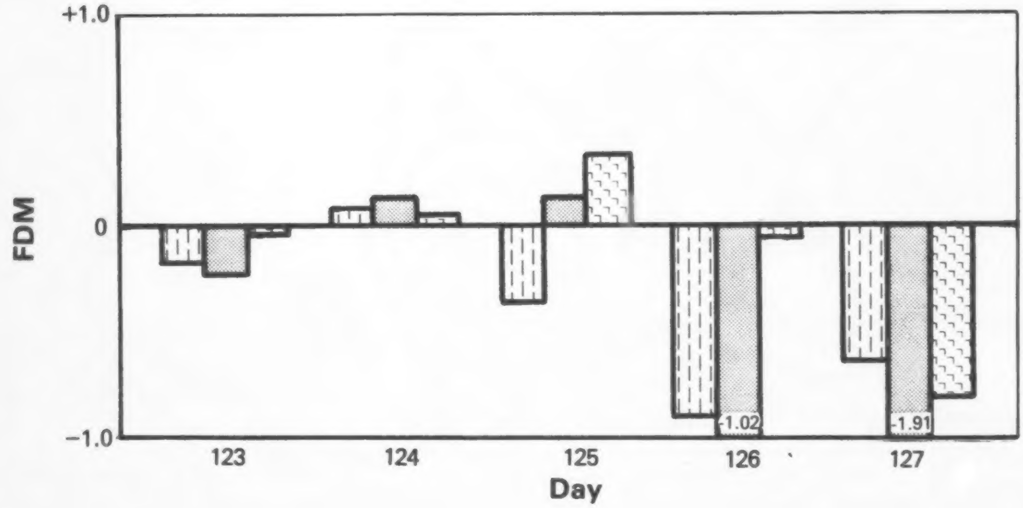

Figure 3-13 Episode 2--Comparison of the Different Model Results [Fractional Deviation of the Means (FDM)]

The model comparisons shown in these last two sections are believed to be the only such set of regional-scale comparisons of plume, puff, and grid models that have been achieved in an objective, systematically neutral manner, with uniform control over the models' external environment (that is, their meteorological, input/output, and analysis routines). These results give initial indications that for some regional-scale simulation purposes, the choice among a plume segment model, a puff element model, or a grid model may not primarily depend on the nature of the model results--the results for each model might be very similar in gross properties. Rather, the decision may be based on other issues such as relative execution cost or the regulatory acceptability of one or another modeling approach. For applications where accurate knowledge of the location and magnitude of concentration maxima is necessary, the fine-scale model behavior may be the dominant issue, especially in the near field of sources. In complicated flow situations the variable-trajectory approach used by the three models is more realistic, and therefore likely to provide more credible results, than the conventional straight-line Gaussian plume approach used for most regulatory applications at present.

The comparison of relative model performance will be explored further in Sections 4 and 5. Issues such as model sensitivity to variations in input parameters or time resolution will further illuminate the relative advantages and disadvantages of each model for various meteorological and source inventory scenarios.

3.3 Model Simulations of Plume Fumigation

As the mixing depth oscillates during a diurnal cycle, pollutant mass emitted from an elevated source may either be emitted within the turbulent boundary layer (leading directly to near-source surface impact) or may be emitted above the boundary layer (and not intersect the surface until considerably downwind of the source). On the regional scale, plumes may be transported aloft over long distances (many hundreds of kilometers) during stable nighttime hours, only to be rapidly mixed down to the surface as morning convection deepens the mixing layer. Thus, the regional-scale predictions of each of the three models will be affected significantly by the treatment provided for plume fumigation. This section provides qualitative illustrations of the treatment of fumigation by each of the models.

Figure 3-14 depicts the progression of 1-hour average ground-level SO_2 concentrations as predicted by the MESOPLUME model for the Navajo power plant during Episode 1 from 7:00 P.M. [Mountain Standard Time (MST) on day 166] through 1:00 P.M. on day 167. A set of mixing depth fields at the corresponding times is depicted in Figure 3-15. These sequences of figures can be interpreted as follows. After sunset, the mixing heights decreased to a relatively small value (a mechanically driven equilibrium value dependent on the free stream wind velocity). When the mixing height became less than the effective stack height, 7 pm MESOPLUME

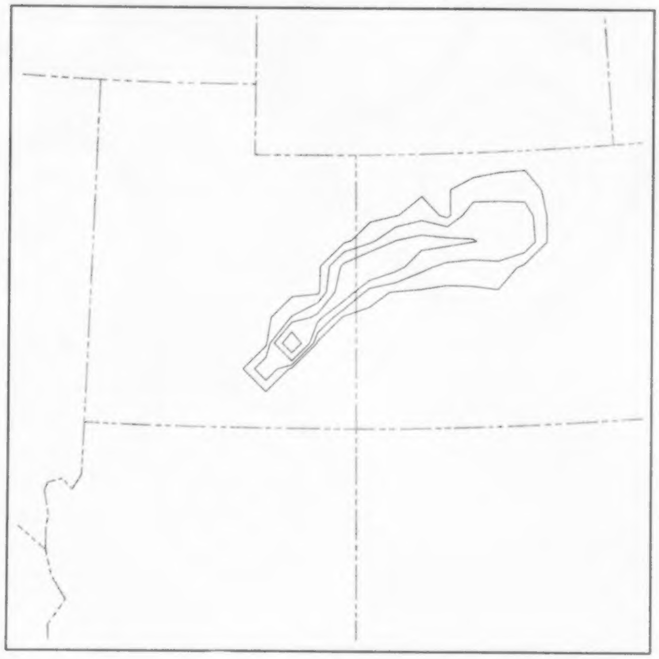

1 am MESOPLUME

7 pm MESOPLUME

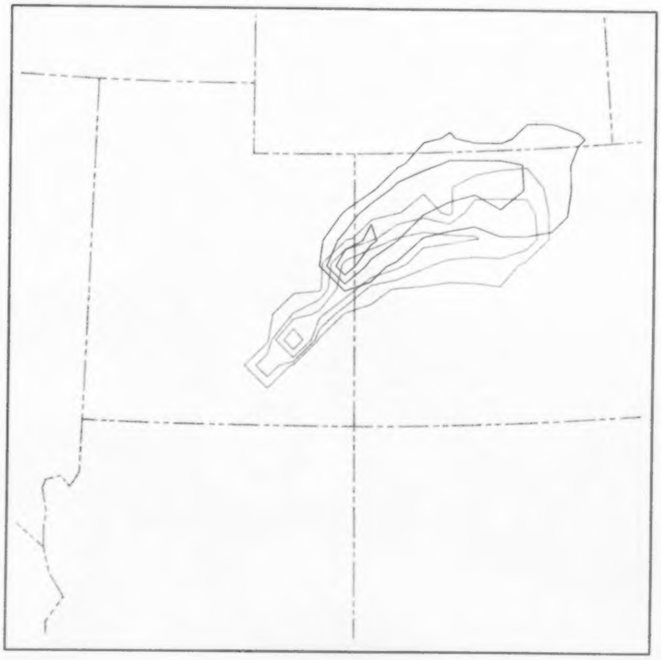
7901067
7901066

Figure 3-14 MESOPLUME Time Sequence of 1-hour Average SO_2 Concentrations (7 pm MST Day 166 to 1 pm Day 167)

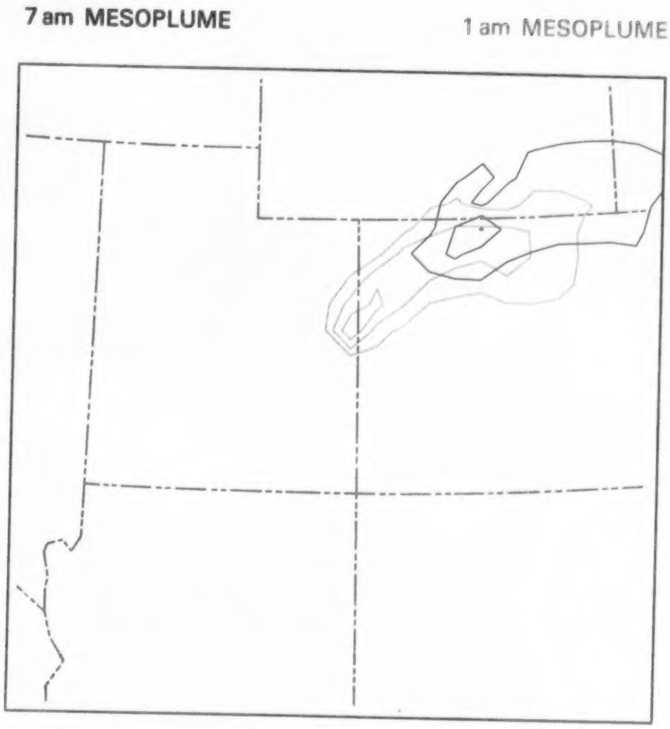
7 am MESOPLUME
1 am MESOPLUME
7901068
7901067

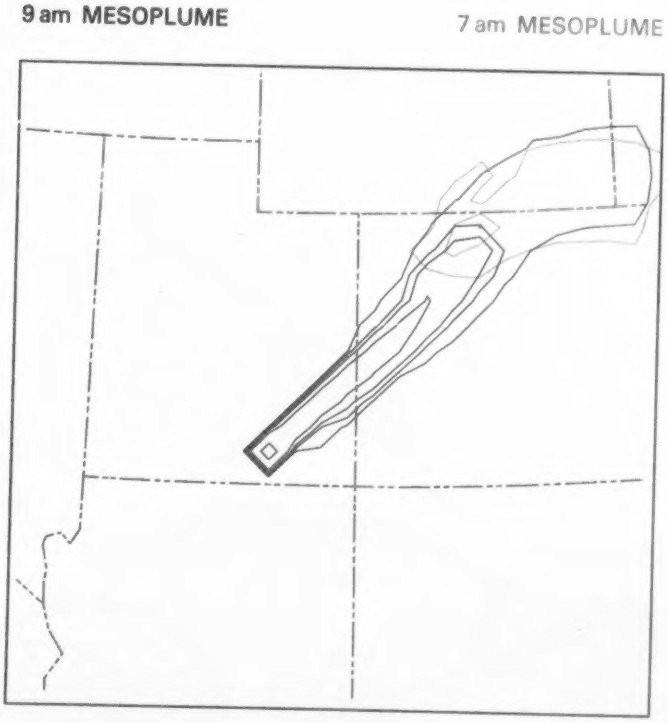
9 am MESOPLUME
7 am MESOPLUME
7901069
7901068

Figure 3-14 Continued

1 pm MESOPLUME 9 am MESOPLUME

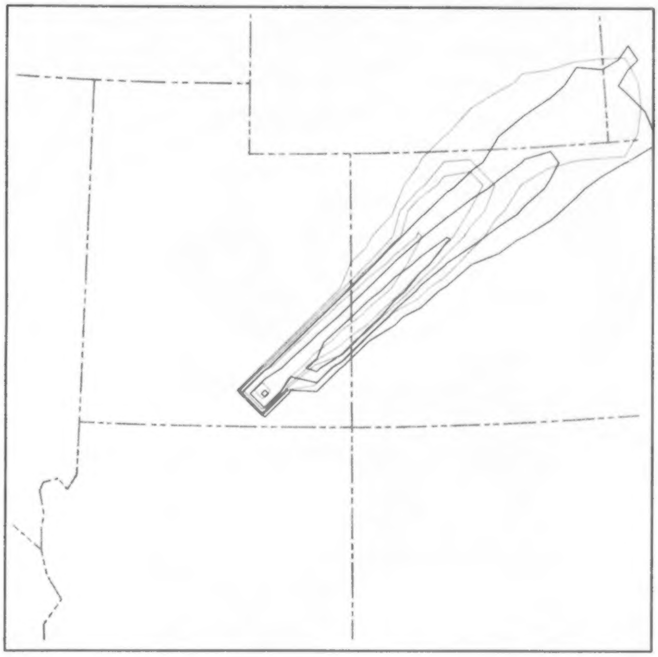

7901070
7901069

Figure 3-14 Continued

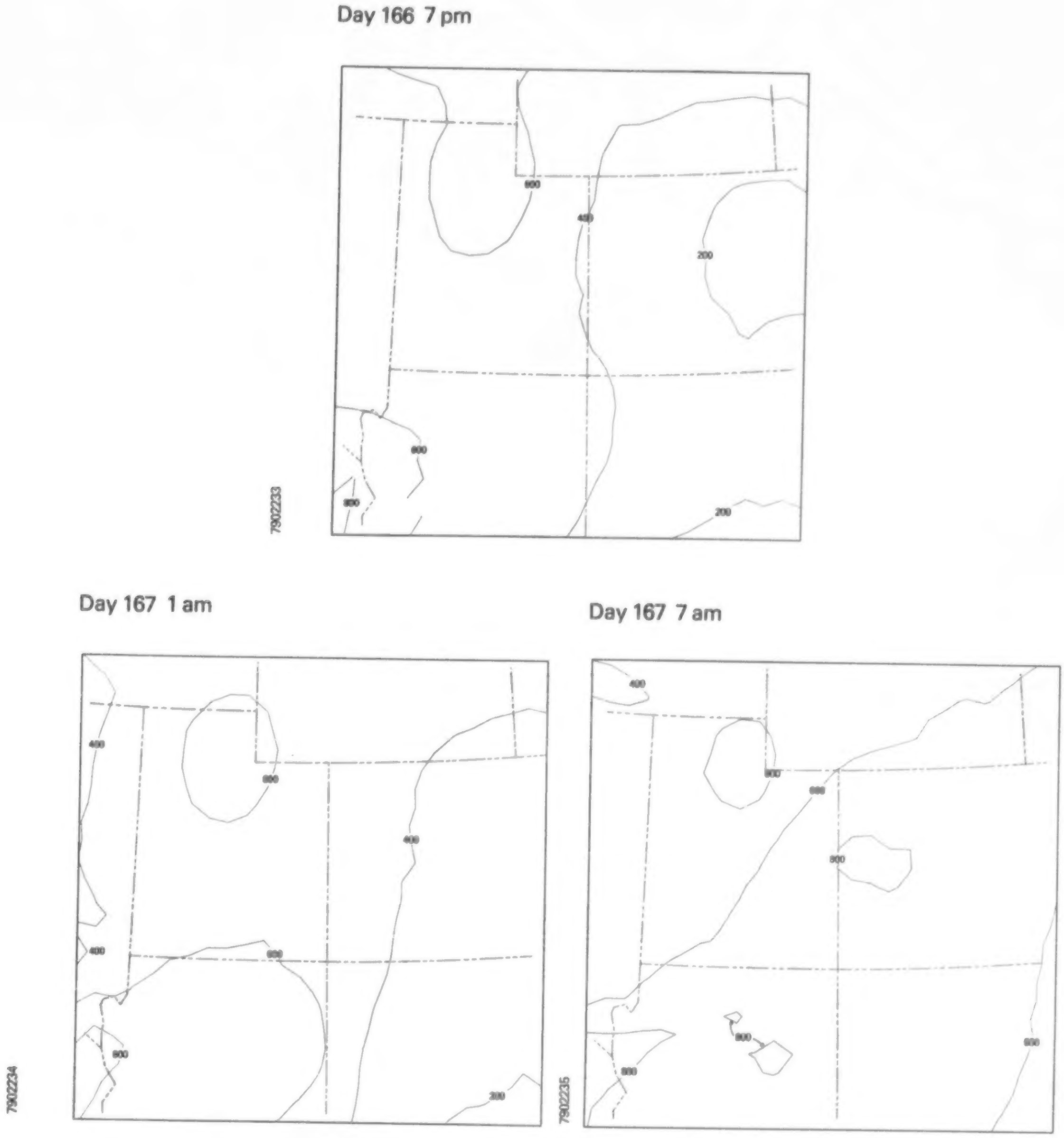
Day 166 7 pm
800
400
200
800
800
200
7902233
Day 167 1 am
400
800
400
400
800
800
200
7902234
Day 167 7 am
400
800
800
800
800
800
800
7902235

Figure 3-15 Time Sequence of Mixing Depths (7 pm MST Day 166 to 1 pm Day 167)

Day 167 9 am

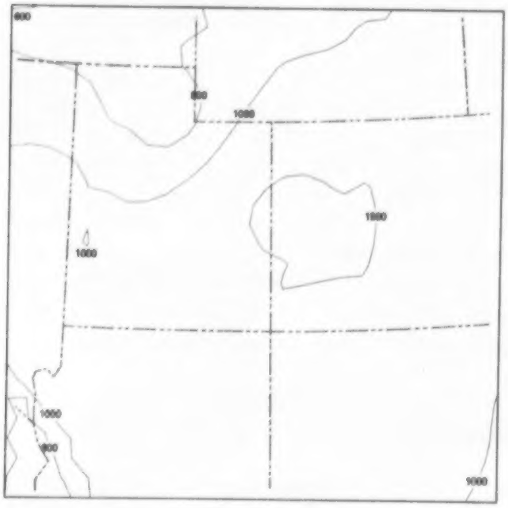
800
800
1000
1500
1000
1000
800
1000

7902236

Day 167 1 pm

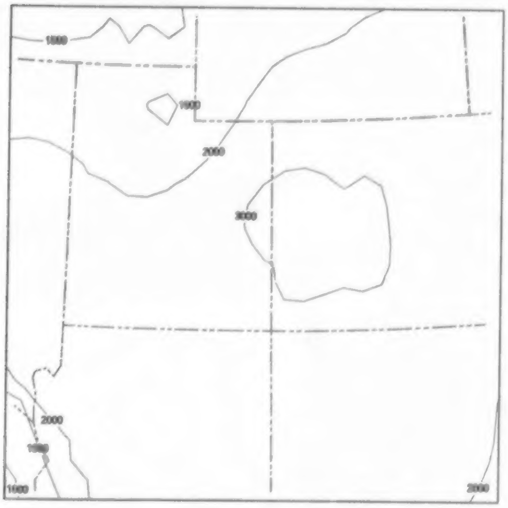
1000
1000
2000
3000
2000
1000
1000
2000

7902237

Figure 3-15 Continued

newly emitted SO_2 was no longer mixed to the ground; the SO_2 previously mixed to the surface during the day continued to be advected, diffusing slowly. Figure 3-16 illustrates the extent that dispersion and depletion of SO_2 within the plume reduces the average mass in the portion of the plume contacting the ground surface during nocturnal regional-scale transport.

After sunrise, the convective mixed layer grew rapidly and entrained the entire plume by 9:00 A.M. local time (Figure 3-14, 9:00 A.M. MESOPLUME). The plume was rapidly mixed downward to the surface. The highest concentrations of the day occurred at this time while the plume was trapped within a growing but shallow mixing layer (see Figure 3-15, 9:00 A.M. MESOPLUME). As the mixed layer height continued to grow, the emissions were diluted through an even deeper layer. After sunset, the mixed layer height collapsed, and the entire sequence of nocturnal plume transport began anew.

As shown in Figure 3-17 the MESOPUFF model displays virtually identical plume fumigation behavior as MESOPLUME.

For the MESOGRID model, however, fumigation is much less dramatic (see Figure 3-18) because vertical dispersion is determined by the K_z profile, the vertical resolution (currently three vertical layers), and the depth of each vertical layer (in the present version of MESOGRID, the cell value assigned to K_z is set to a very small number whenever the height of the grid cell exceeds the mixing height). In the MESOGRID fumigation sequence, the "old" surface plume is advected and depleted, as previously. Some continuous mixing to the surface does occur, however, and the onset of fumigation is much less abrupt, because the continuous profile of vertical diffusivity is specified by only four discrete values and usually only the lowest two values are relevant to the fumigation process. With the onset of convection in the early morning, K_z begins to increase anew as the mixing depth increases and the stability decreases; this increase leads to a more rapid but not immediate transfer of mass to the surface.

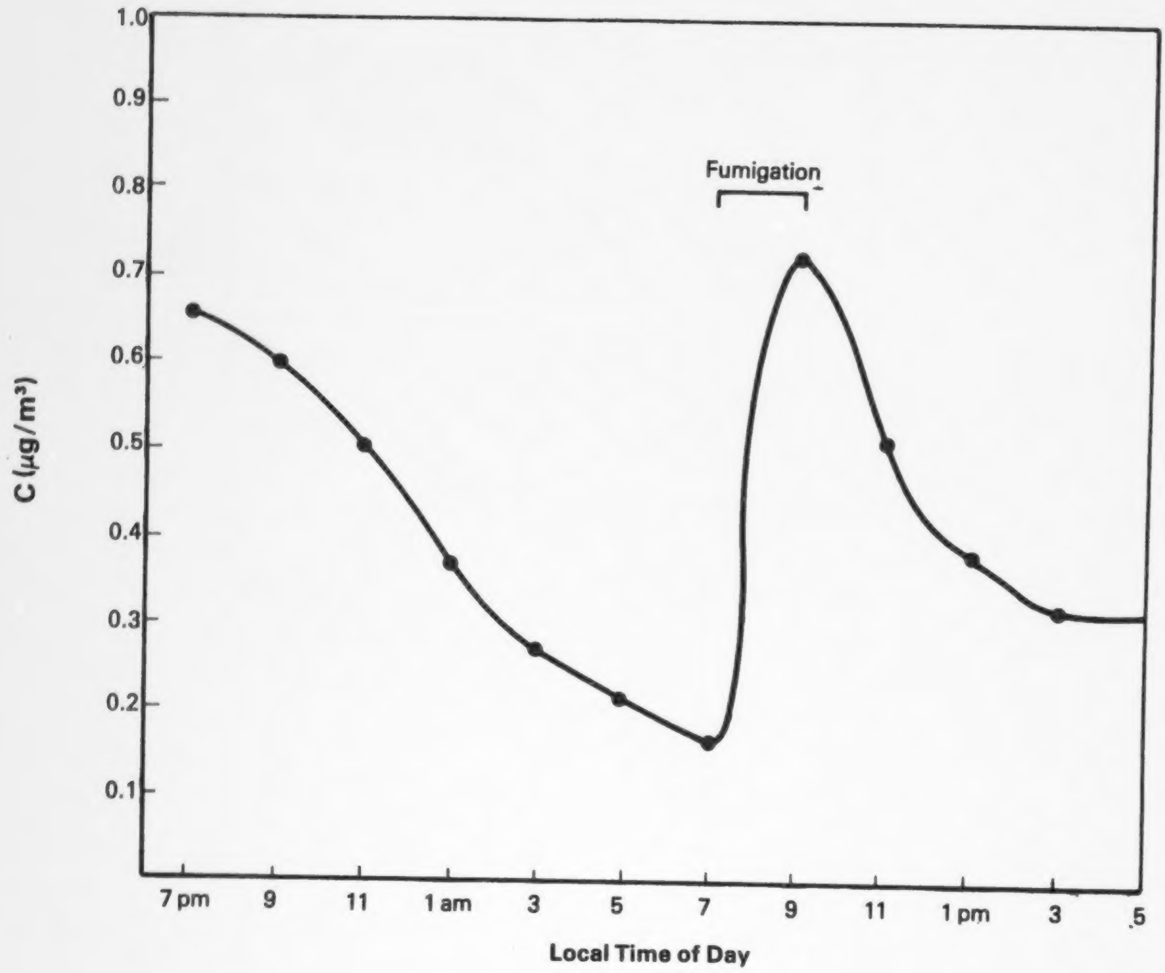

Figure 3-16 MESOPLUME Mean Plume Concentration Cycle (for 1-Hour Averages)

7 pm MESOPUFF

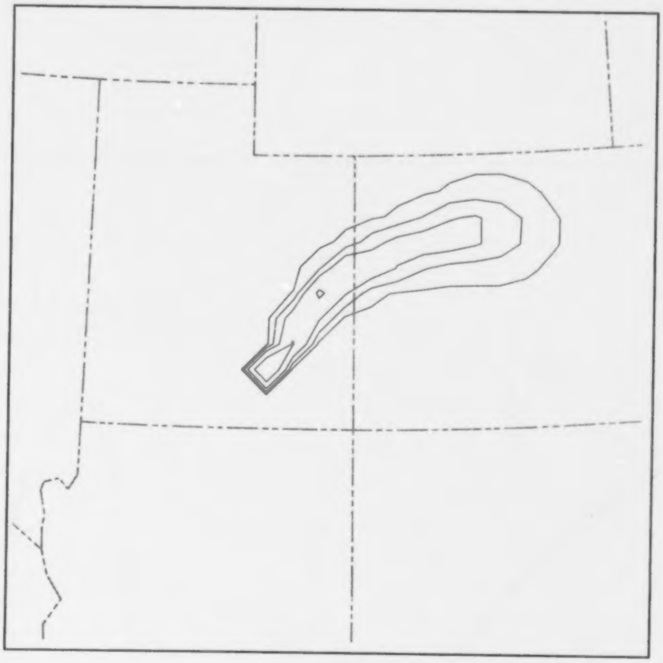

1 am MESOPUFF

7 pm MESOPUFF

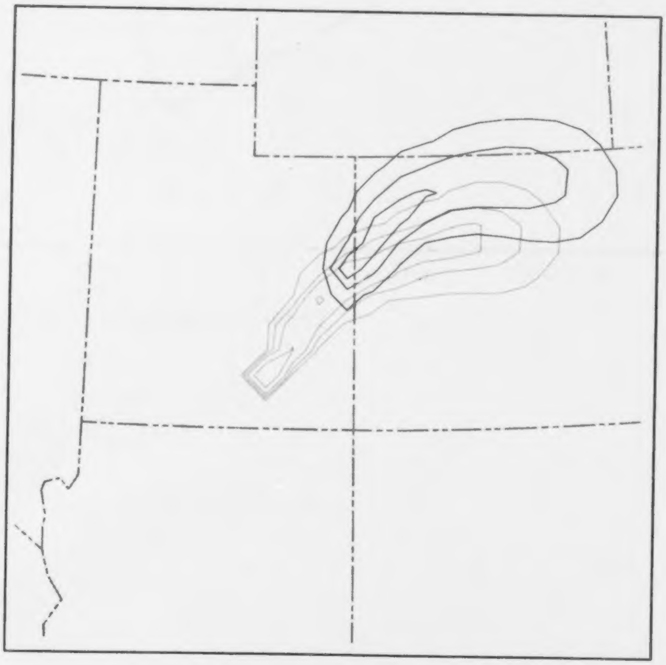
7901074
7901073

Figure 3-17 MESOPUFF Time Sequence of 1-Hour Average SO_2 Concentrations (7 pm MST Day 166 to 1 pm Day 167)^2

7 am MESOPUFF 1 am MESOPUFF

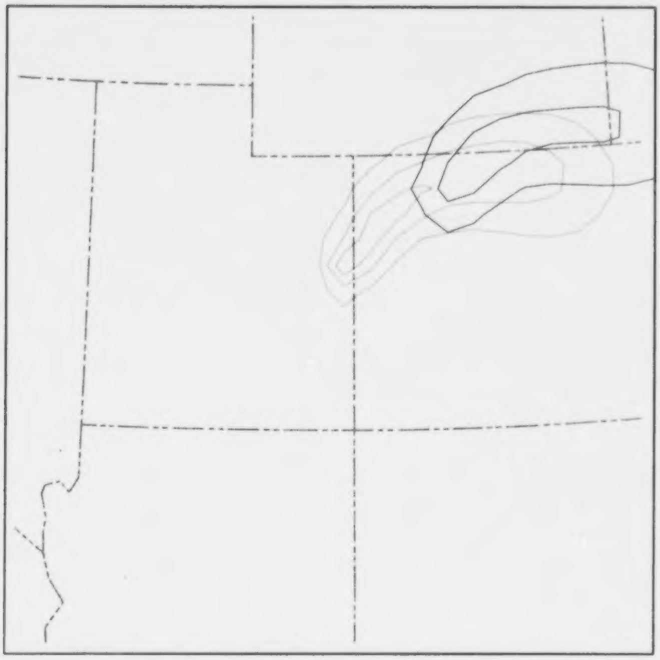

7901075
7901074

9 am MESOPUFF 7 am MESOPUFF

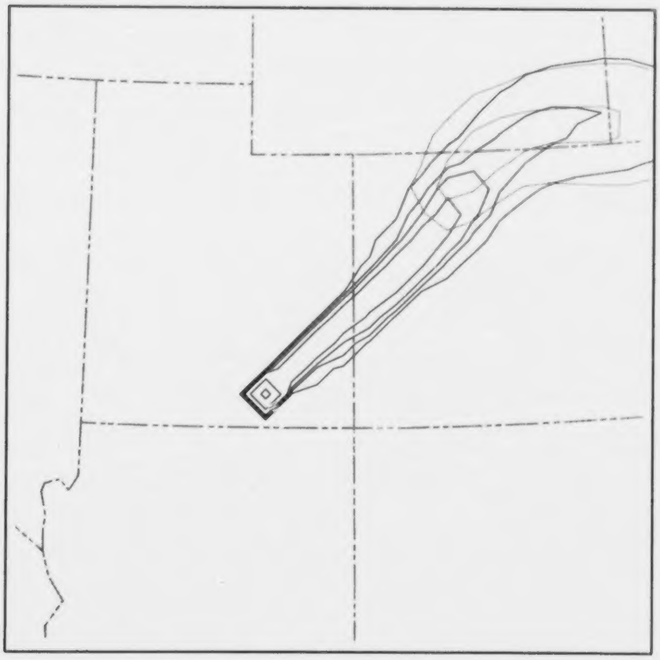

7901076
7901075

Figure 3-17 Continued

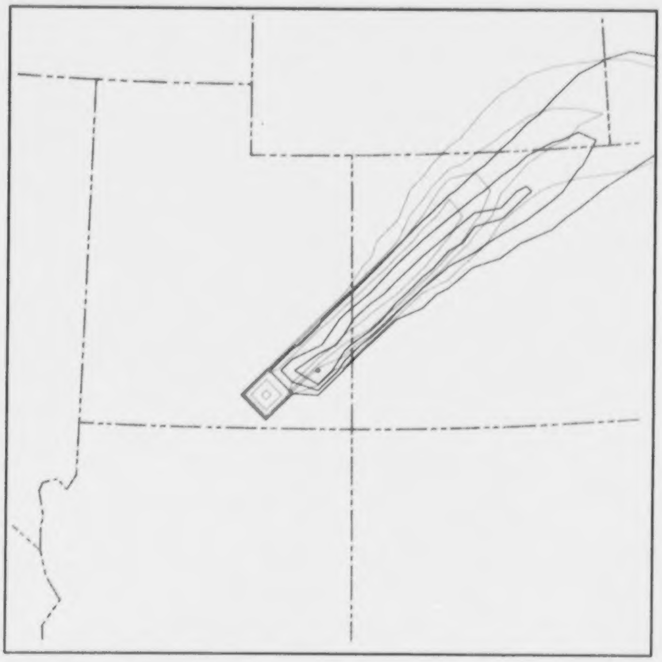
1 pm MESOPUFF
9 am MESOPUFF

7901077
7901076

Figure 3-17 Continued

7 pm MESOGRID

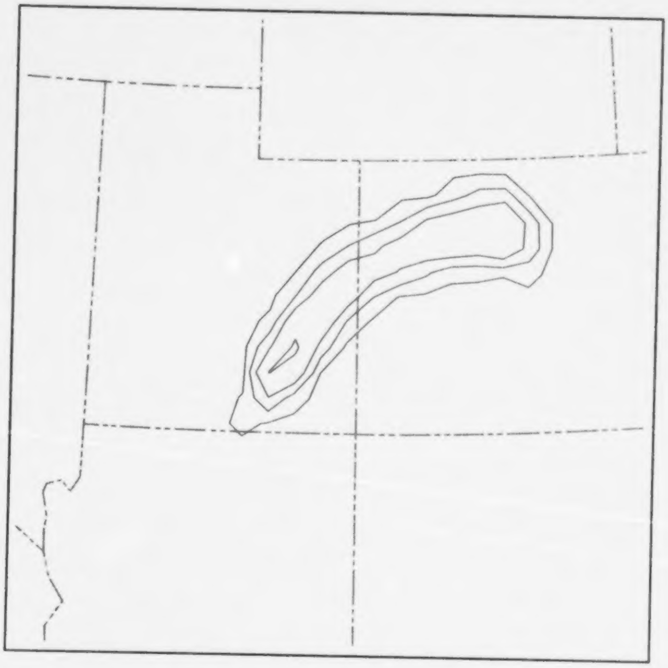
7901078

1 am MESOGRID

7 pm MESOGRID

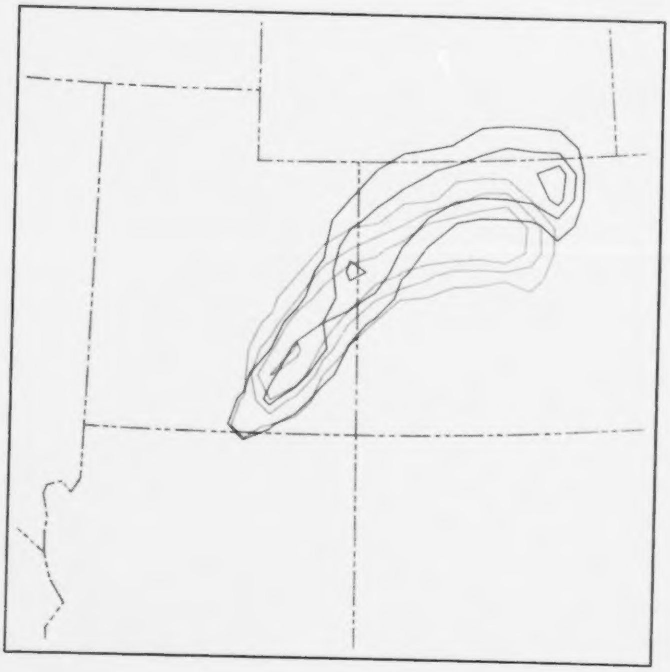
7901079
7901078

Figure 3-18 MESOGRID Time Sequence of 1-Hour Average SO_2 Concentrations (7 pm MST Day 166 to 1 pm Day 167)

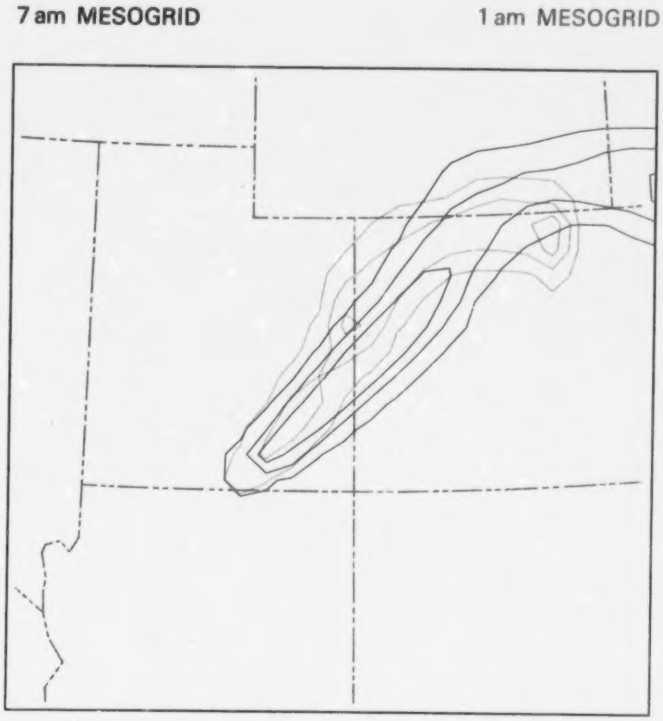
7 am MESOGRID
1 am MESOGRID

7901080
7901079

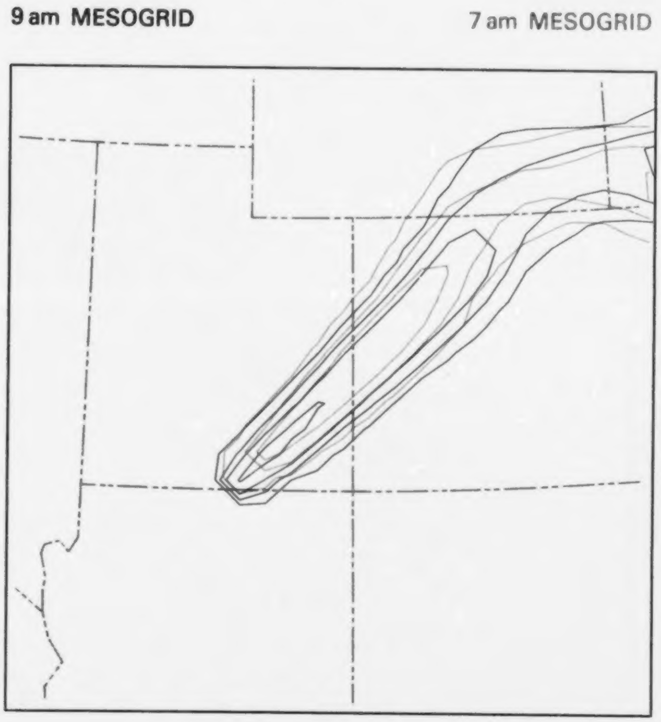
9 am MESOGRID
7 am MESOGRID

7901081
7901080

Figure 3-18 Continued

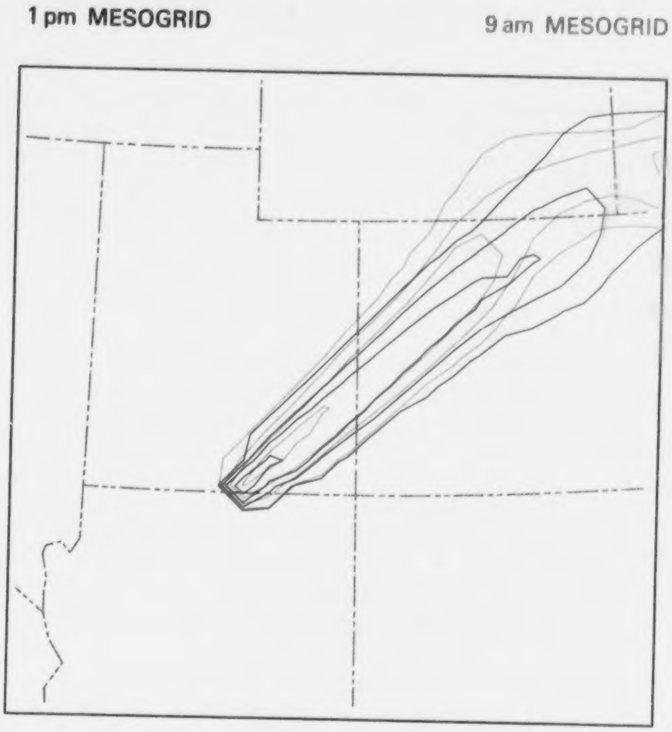
1 pm MESOGRID
9 am MESOGRID

7901082
7901081

Figure 3-18 Continued

4. RESULTS OF MODEL SENSITIVITY TESTS

This section presents some of the highlights of the more than 100 multiday model sensitivity simulation experiments performed in this study. Recalling the sensitivity test protocol described earlier in Section 2, Table 2-1 identifies the kinds of sensitivity tests conducted. Model sensitivities to differences in mesoscale flow pattern have already been discussed.

4.1 Sensitivity to Decay and Dry Deposition Processes

Plume depletion processes are important factors on regional scales. Each model permits two different depletion processes: (a) dry deposition of SO_2 and $SO_4^=$, modeled using the "deposition velocity" concept; and (b) conversion of SO_2 to $SO_4^=$, assumed to be approximated by a linear decay mechanism. The MESOPLUME and MESOPUFF model sensitivities to variations in deposition and decay rates were evaluated in detail over intervals representing the likely uncertainty in these parameters. The much higher cost of running the MESOGRID model meant that fewer MESOGRID sensitivity tests could be performed. Table 4-1 displays the pairs of values of the plume depletion parameters used in the sensitivity tests.

One effective way to display the results of an air quality model's sensitivity to variations in model parameters is the format introduced by Hilst (1970). Figure 4-1 (4-2), depicts the sensitivity of the MESOPLUME (MESOPUFF) model to variations in plume decay rate and to variations in $SO_2/SO_4^=$ deposition velocities in the Hilst format. The abscissa variable is the relative fractional difference in value chosen for the perturbed model run parameter compared to the parameter value chosen for the base case model run. For example, in one case, the perturbed case value of decay rate is chosen to be ten times larger than the base value, and the abscissa is -9; if instead the perturbed case value is chosen as one-tenth that of the base value, then the corresponding abscissal value is +0.9. The ordinate values in this figure describe the average fractional difference (AFD) in 24-hour average ground-level SO_2 concentration values computed in the base case and perturbed case runs, averaged over all grid points and over the last 3 days of Episode 1. Each of the points plotted in the figure represents, therefore, a separate 5-day run made to display this variation.

As seen from the figure, an approximate five-fold increase in the decay rate, or in the deposition velocities, leads to approximately a two-thirds decrease in the average relative fractional difference concentration field; a five-fold decrease in the decay rate, or in the deposition velocities, corresponds to only about a one-third increase in average relative difference field. This asymmetrical relative model response to variations in input parameters is very typical. MESOPLUME (MESOPUFF) also shows a somewhat greater sensitivity to changes in decay

TABLE 4-1

VALUES OF THE DEPOSITION VELOCITIES AND DECAY RATES USED IN THE SENSITIVITY TESTS

Decay Rate Coefficient, k_1	Deposition Velocity, v_d (m/s)
MESOPLUME and MESOPUFF	
$k_1 = -5.56 \times 10^{-5}$	v_d (SO_2, $SO_4^{=}$) = (0.01, 0.001)*
$k_1 = -2.22 \times 10^{-5}$	v_d (SO_2, $SO_4^{=}$) = (0.01, 0.001)*
$k_1 = -5.56 \times 10^{-6}$*	v_d (SO_2, $SO_4^{=}$) = (0.1, 0.01)
$k_1 = -5.56 \times 10^{-6}$*	v_d (SO_2, $SO_4^{=}$) = (0.0316, 0.00316)
$k_1 = -5.56 \times 10^{-6}$*	v_d (SO_2, $SO_4^{=}$) = (0.01, 0.001)*
$k_1 = -5.56 \times 10^{-6}$*	v_d (SO_2, $SO_4^{=}$) = (0.00316, 0.000316)
$k_1 = -5.56 \times 10^{-6}$*	v_d (SO_2, $SO_4^{=}$) = (0.001, 0.0001)
$k_1 = -3.89 \times 10^{-6}$	v_d (SO_2, $SO_4^{=}$) = (0.01, 0.001)*
$k_1 = -5.56 \times 10^{-7}$	v_d (SO_2, $SO_4^{=}$) = (0.01, 0.001)*
MESOGRID	
$k_1 = -5.56 \times 10^{-5}$	v_d (SO_2, $SO_4^{=}$) = (0.01, 0.001)*
$k_1 = -5.56 \times 10^{-6}$*	v_d (SO_2, $SO_4^{=}$) = (0.1, 0.01)
$k_1 = -5.56 \times 10^{-6}$*	v_d (SO_2, $SO_4^{=}$) = (0.01, 0.001)*
$k_1 = -5.56 \times 10^{-6}$*	v_d (SO_2, $SO_4^{=}$) = (0.001, 0.0001)
$k_1 = -5.56 \times 10^{-7}$	v_d (SO_2, $SO_4^{=}$) = (0.01, 0.001)*

---

*Base case values.

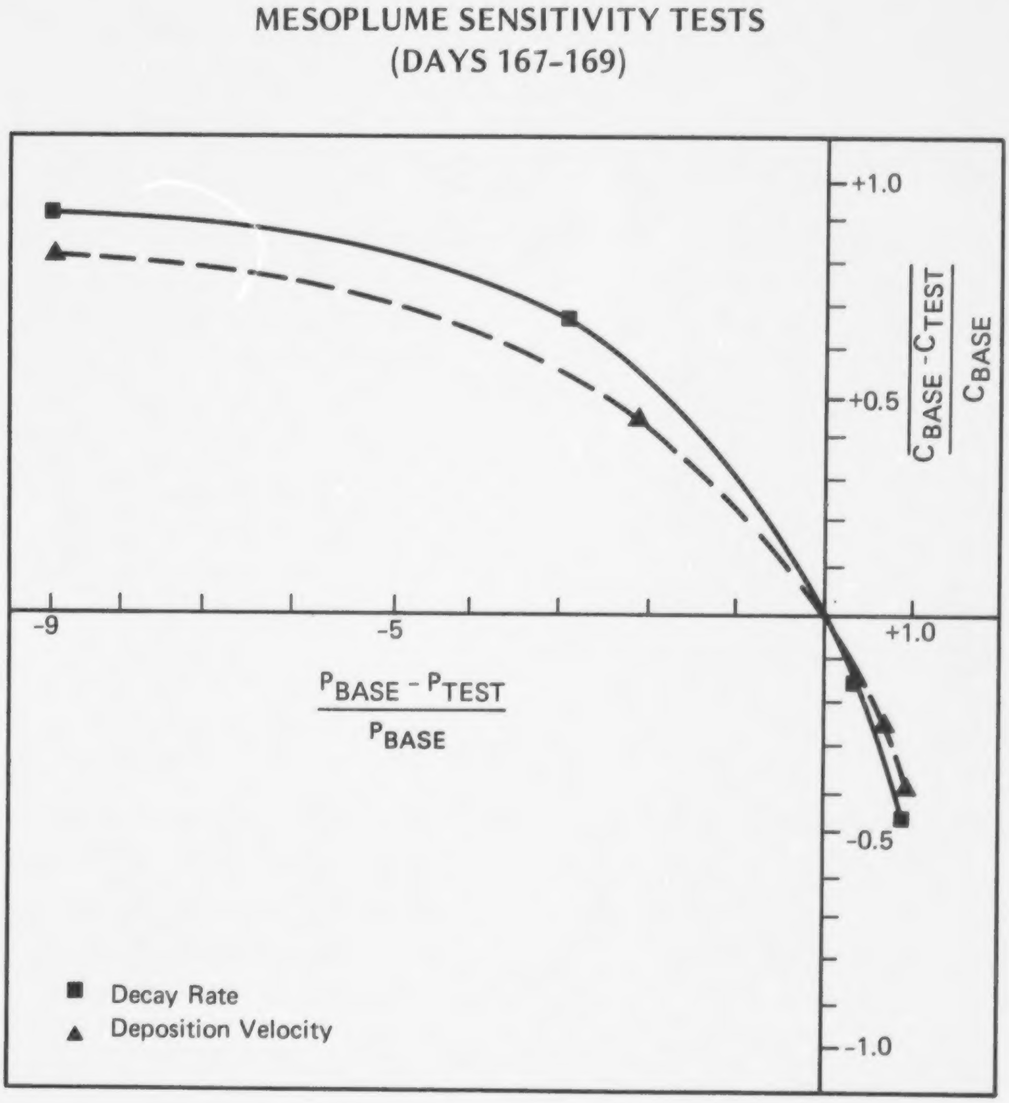

MESOPLUME SENSITIVITY TESTS
(DAYS 167-169)

P_{BASE} = Base Value

P_{TEST} = (Perturbed) Test Value

Figure 4-1 MESOPLUME Sensitivity to Decay Rate and Dry Deposition Variations (Days 167-169)

rate than to changes in deposition velocity. This sensitivity results from the diurnal fumigation cycle and the models' treatment of dry deposition and decay. For a given deposition velocity, the amount of pollutant removed by dry deposition depends on the ground-level concentration of the pollutant and the mixing depth. For the base case choices of SO_2 decay and deposition rates, the decay term dominates the deposition term whenever the plume is mixed through more than about 1,800 m in the vertical (because of the inverse-H dependence of the deposition term); when the plume is mixed through less than 1,800 m, dry deposition is the dominant process in the model. Dry deposition, however, occurs only when the plume is in contact with the ground, whereas decay processes occur continuously, even when the plume is above the mixed layer.

As seen in the previous section, the mixed layer is generally shallowest at night; new emissions may remain above the mixed layer until the plume fumigates the next morning, prohibiting dry deposition of new emissions for up to 12 or more hours each day. After plume fumigation, when dry deposition does occur, the mixing height values usually increase to greater than 1,800 m in the spring and summer in the Four Corners area, and decay processes dominate the removal.

Because the MESOPUFF model uses the identical decay and deposition algorithms, it shows virtually the same sensitivities to systematic variations in k_1, $v_d(SO_2)$, and $v_d(SO_4^=)$ as MESOPLUME (Figure 4-2). The more limited set of experiments with MESOGRID show similar results.

Figures 4-3 and 4-4 display another way in which to compare model performance (in this case, MESOPLUME) with different choices of input parameters. The contours in each figure describe the fractional difference, $(C_B-C_T)/C_B$, in concentration field (FDF) values between the 24-hour average ground-level SO_2 concentration values in the base case (C_B) and the test case (C_T). In each case, grid point concentration values less than 0.1 $\mu g/m^3$ were ignored. The first pair of figures (Figures 4-3a and b) show the effects of a ten-fold increase ($v_d = 0.1$), and a ten-fold decrease ($v_d = 0.001$) in the values of SO_2 deposition velocities, relative to the base case ($v_d = 0.01$) for the Navajo single-source case on day 169 (stagnation flow). In both instances, the fractional differences increase with distance from the source and indicate greater deviation from the base case for the choice of $v_d = 0.1$ than for the choice of $v_d = 0.001$. In contrast to Figures 4-3a and b, Figures 4-3c and 4-3d illustrate the fractional difference field for the cases $v_d = 0.1$ and $v_d = 0.001$ on day 167 (strongly zonal flow). It is noted that the fractional differences in this zonal flow situation, in which plume segments have shorter grid residence times, are considerably smaller than those of day 169. For example, for the choice of $v_d = 0.001$, there are test case values in the far-field that are more than twice those of the base case on day 169, whereas on day 167 there are no test case values even 50% greater than those of the base case.

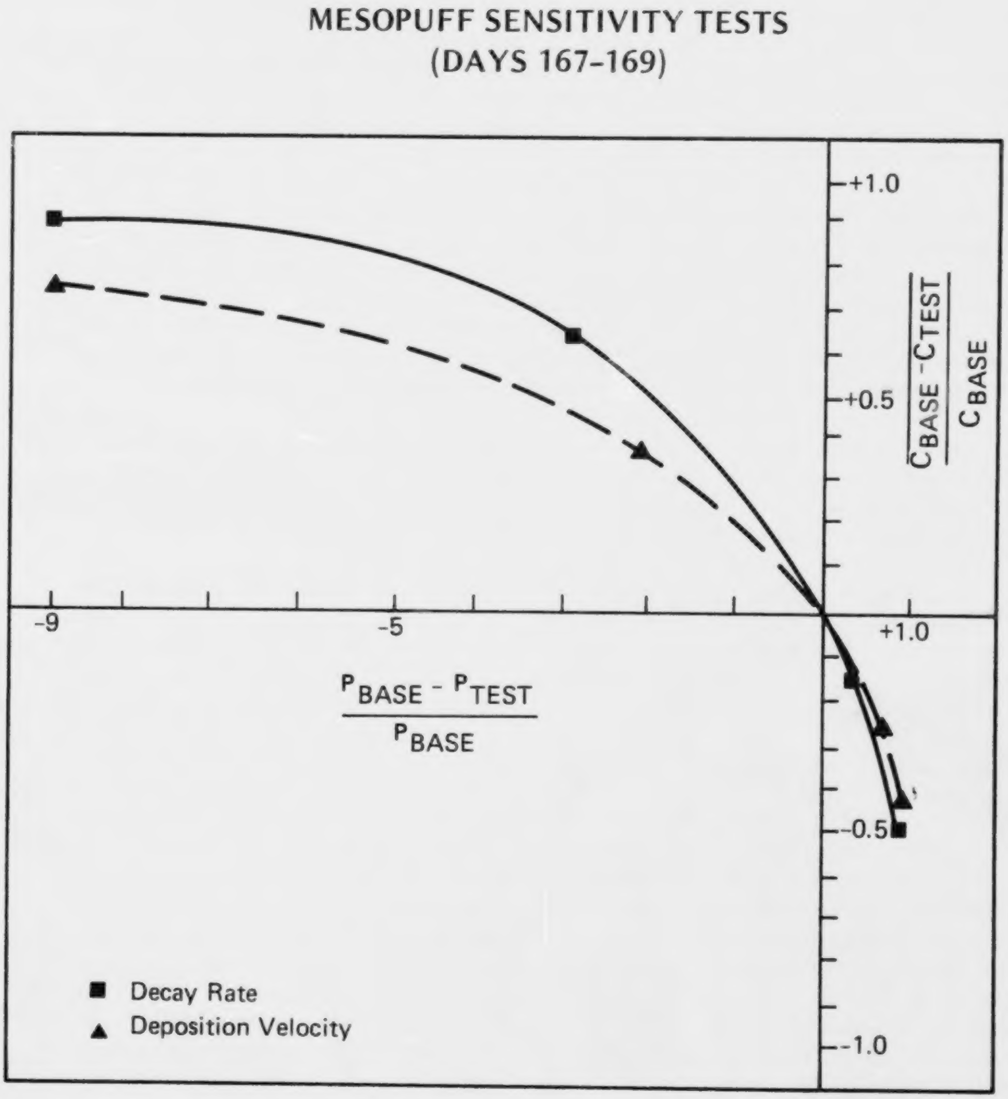

Figure 4-2 MESOPUFF Sensitivity to Decay Rate and Dry Deposition Variations (Days 167-169)

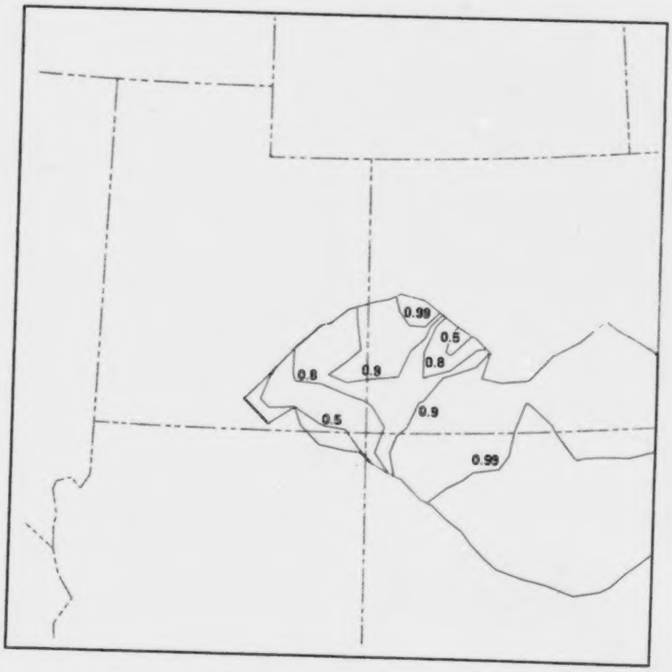
v_d = 0.1 m/s
Day 169
0.99
0.5
0.8
0.8
0.9
0.5
0.9
0.99
7904017

Figure 4-3a MESOPLUME Fractional Difference Field Comparison for v_d (SO_2) = 0.1 m/s Case vs. Base Case (Day 169)

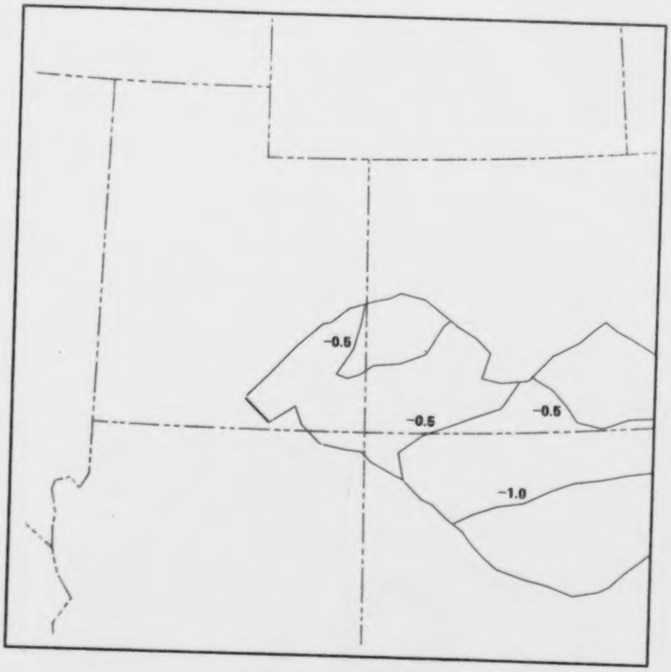
v_d = 0.001 m/s
Day 169
-0.5
-0.5
-0.5
-1.0
7904026

Figure 4-3b MESOPLUME Fractional Difference Field Comparison for v_d (SO_2) = 0.001 m/s Case vs. Base Case (Day 169)

v_d = 0.001 m/s
Day 167

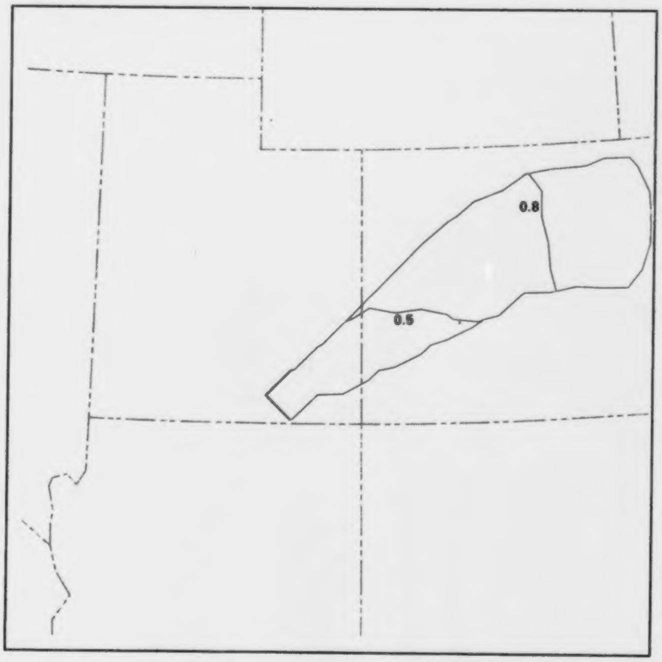

7904014

Figure 4-3c MESOPLUME Fractional Difference Field Comparison for v_d (SO_2) = 0.1 m/s Case vs. Base Case (Day 167)

v_d = 0.1 m/s
Day 167

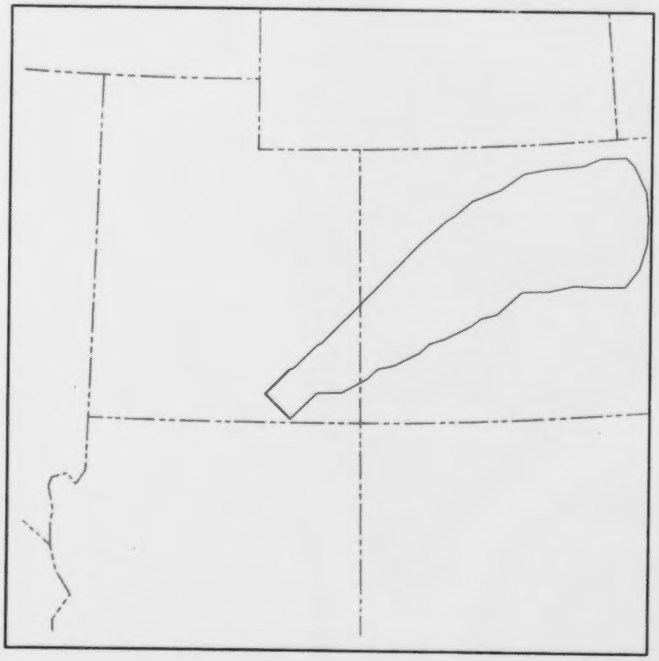

7904013

Figure 4-3d MESOPLUME Fractional Difference Field Comparison for v_d (SO_2) = 0.001 m/s Case vs. Base Case (Day 167)

This sequence of figures emphasizes that the meteorological regime can exert a great influence on the sensitivity of the model to different choices of deposition velocity. Although only the MESOPLUME model is illustrated here, the other models also show comparably wide variations in deposition velocity sensitivity as the meteorology changes.

The next set of figures (Figures 4-4a through 4-4d) show the corresponding fractional difference results of the MESOPLUME model for ten-fold increases and decreases in decay rate k_1, relative to the base case, both for the stagnating conditions (day 169) and the zonal conditions (day 167). The strong dependence on meteorological flow regime, evident in the deposition velocity tests, is also seen here.

4.2 Sensitivity to Mixing Depth Variations

The sensitivity of the models to systematic variations in the mixing depth was evaluated by varying the mixing height by simple multiplicative factors--the values used were 0.5, 0.67, 1.5, and 2.0. If the plume is assumed to be entrained by the mixed layer under all base and test conditions and if dry deposition is ignored, a doubling of the mixing depth corresponds to a halving of the average concentration (FDM = 0.5) with perfect correlation of base and test cases ($r = 1.0$). Likewise, a halving of the mixing depth means a doubling of the average concentration (FDM = -1.0) and again $r = 1.0$. In actuality, the behavior of FDM and r are very different, as illustrated in Figure 4-5 for the MESOPLUME 24-hour average SO_2 concentrations (Navajo single source). For Episode 1, the FDM values seem only weakly correlated with the mixing depth multiplier, and r becomes much less than unity for the largest mixing depth multiplier. These results may be explained by differences in the nocturnal behavior of the plume in the base and test cases. If in the base case the plume is above the mixed layer, then increasing the test case mixing depth may cause plume entrainment; therefore, rather than the average plume concentration halving when the mixing depth doubles, the ground-level concentration could actually increase, which did occur on day 168.

The fractional difference fields (Figure 4-6 a, b, c, and d) on days 167 and 169, show that the sensitivity of the models (here, specifically, MESOPLUME) to mixing depth variations is highly episode-specific. For the examples shown, raising (lowering) the mixing depth lowers (raises) the plume concentrations in the very far field, because plume elements far from the source will have experienced at least one diurnal mixing depth cycle and will have therefore been entrained. [This process occurs even in the case of the 0.5 mixing depth multiplier, because in the Four Corners region the summer mixed layer is generally very deep (recall Figure 2-3)]. In contrast, no such definite relationship can be assumed in the near field because of the episode-specific nature of plume entrainment.

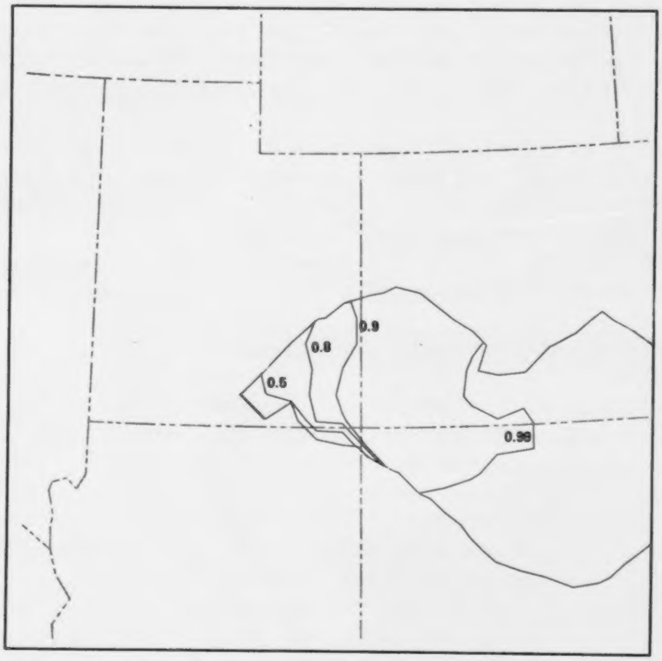
k1 = 5.56 E-5
Day 169
0.5
0.8
0.9
0.99
7904025

Figure 4-4a MESOPLUME Fractional Difference Field Comparison for $k_1 = -5.56 \times 10^{-5}$ Case vs. Base Case (Day 169)

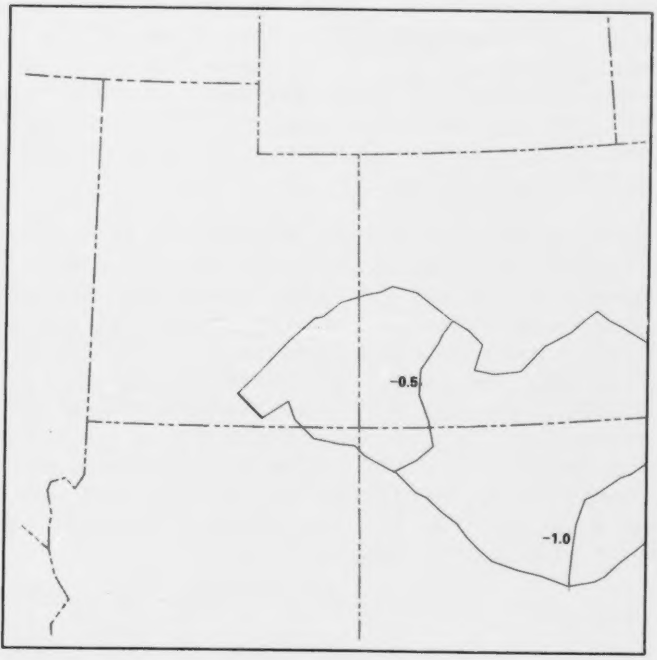
k1 = -5.56 E-7
Day 169
-0.5
-1.0
7904024

Figure 4-4b MESOPLUME Fractional Difference Field Comparison for $k_1 = -5.56 \times 10^{-7}$ Case vs. Base Case (Day 169)

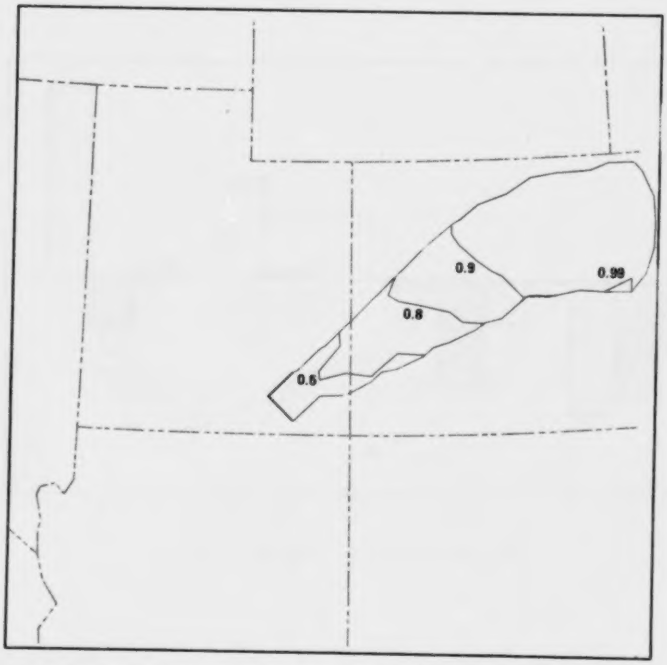
k_1 = -5.56 E-5
Day 167
0.9
0.99
0.8
0.5
7904022

Figure 4-4c MESOPLUME Fractional Difference Field Comparison for $k_1 = -5.56 \times 10^{-5}$ Case vs. Base Case (Day 167)

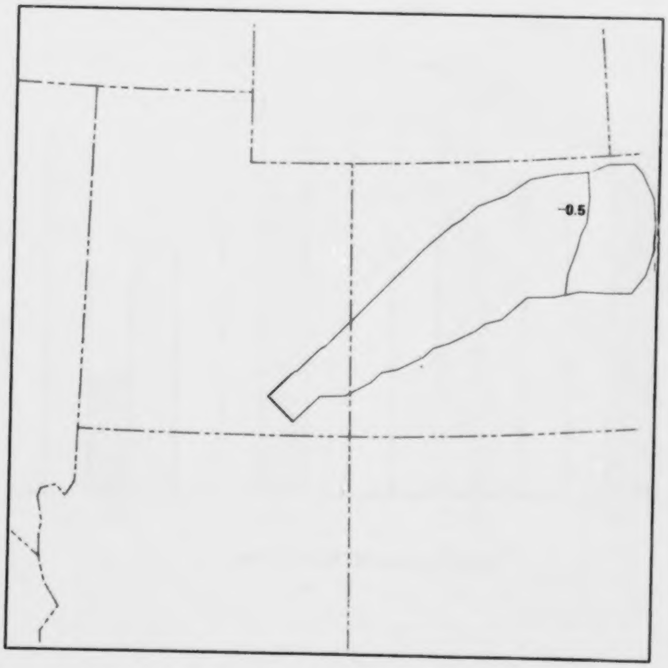
k_1 = -5.56 E-7
Day 167
-0.5
7904023

Figure 4-4d MESOPLUME Fractional Difference Field Comparison for $k_1 = -5.56 \times 10^{-7}$ Case vs. Base Case (Day 167)

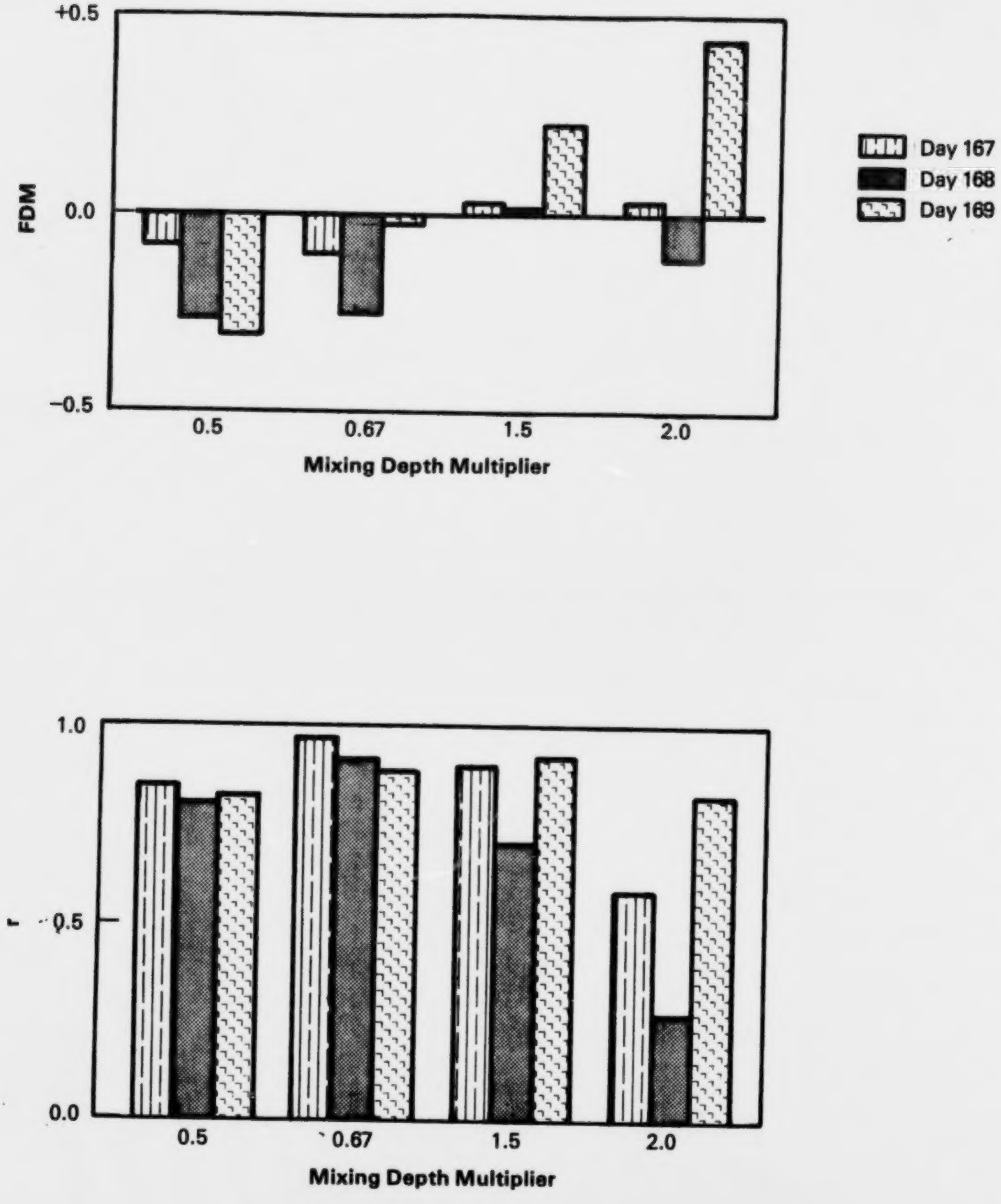

Figure 4-5 MESOPUFF Sensitivity to Mixing Depth Variations (Days 167-169)

PBLDEL = 2.0
Day 167

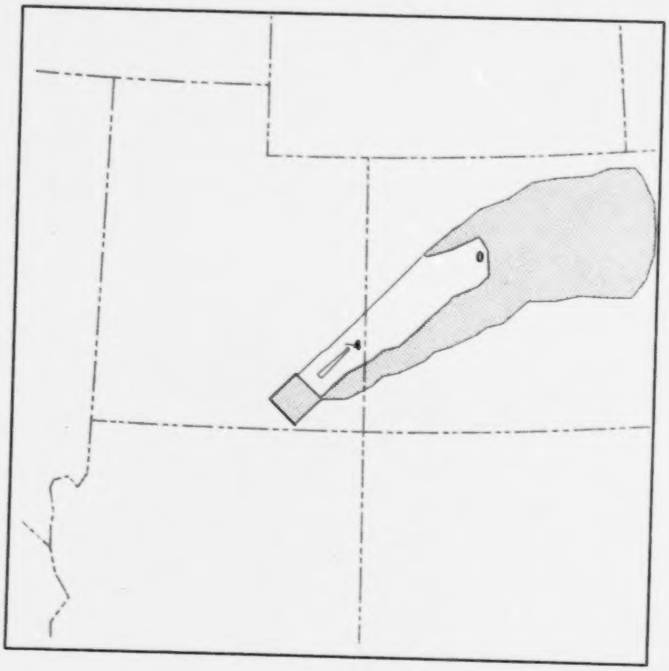

7904021

Figure 4-6a MESOPLUME Fractional Difference Field Comparison for Mixing Depth Multiplier = 2.0 Case vs. Base Case (Day 167)

PBLDEL = 0.5
Day 167

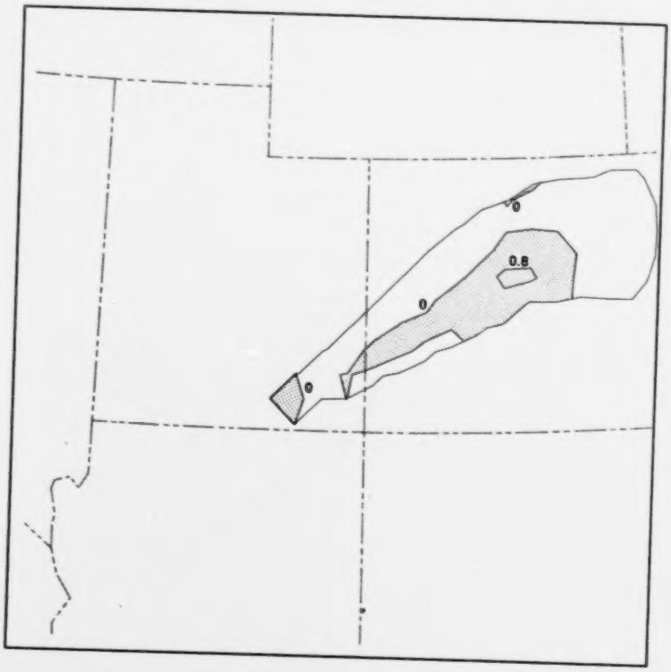

7904020

Figure 4-6b MESOPLUME Fractional Difference Field Comparison for Mixing Depth Multiplier = 0.5 Case vs. Base Case (Day 167)

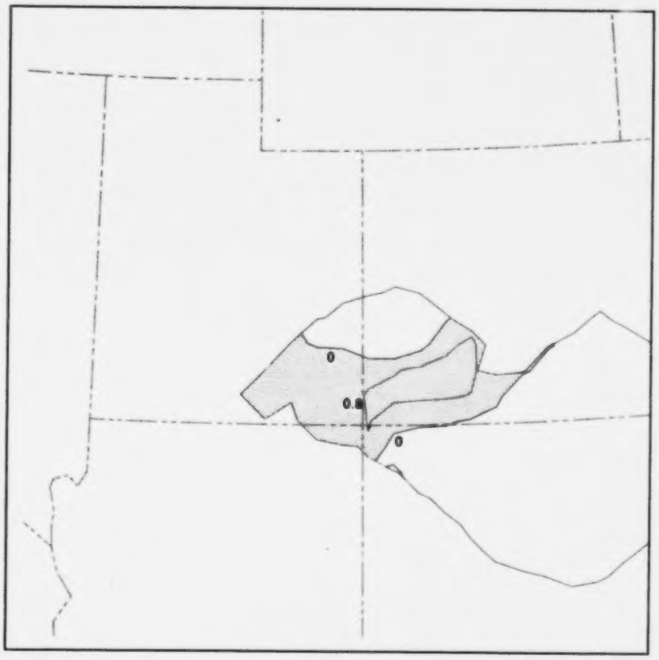
PBLDEL = 2.0
Day 169
0
0.
0

7904019

Figure 4-6c MESOPLUME Fractional Difference Field Comparison for Mixing Depth Multiplier = 2.0 Case vs. Base Case (Day 169)

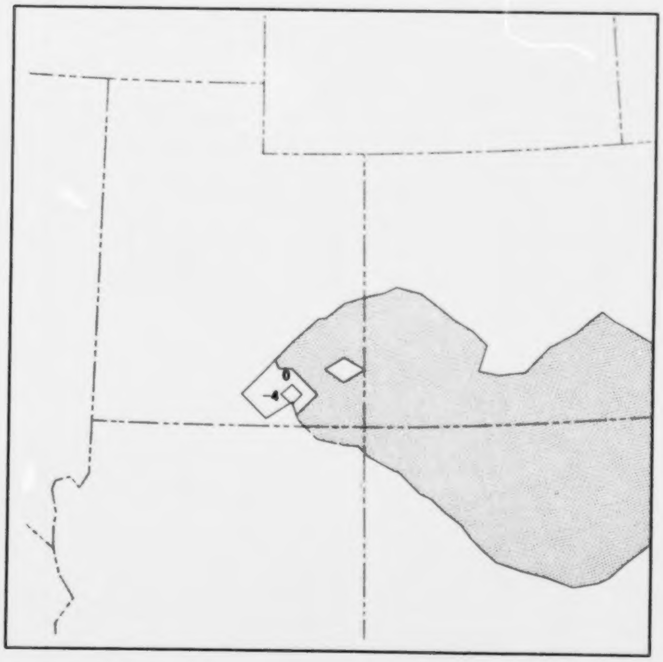
PBLDEL = 0.5
Day 169
0
-4

7904018

Figure 4-6d MESOPLUME Fractional Difference Field Comparison for Mixing Depth Multiplier = 0.5 Case vs. Base Case (Day 169)

4.3 Sensitivity to Systematic Variation of Wind Direction and Crosswind Growth Rate

A series of sensitivity tests were performed with the MESOPLUME and MESOPUFF models to compare the relative importance of (1) horizontal crosswind plume growth and (2) systematic wind direction variations. This set of sensitivity tests was performed by adding a constant angular shift factor to the base case wind direction at each grid point and, simultaneously, using a multiplicative scaling factor to adjust the horizontal, time-dependent plume growth rates [used for the plume or puff elements at travel distances beyond 100 km only]. (Both MESOPLUME and MESOPUFF use the PGT sigma curves for travel distances $\leq$100 km.)

These tests have three specific objectives:

(a) they investigate the sensitivity of the model to changes in plume growth rate. The results suggest that plume meander (resulting from large-scale fluctuations in the mesoscale wind field) dominates small-scale turbulent dispersion (as represented by plume diffusion coefficients). If this is generally true, more exact parameterizations of small-scale dispersion may not be necessary.

(b) they try to determine how much systematic wind direction variations influence the orientation and shape of a given plume, because large systematic errors can occur when the driving wind field is initialized. For example, the direction of the 700-mb station wind used in this study as input to MESOPAC could differ significantly from the wind direction most representative of plume altitude for the particular dispersion problem at hand. This wind direction initialization error could produce concentration patterns very different from the real situation.

(c) they examine the relative importance of plume growth rate vs. wind shift. This could be useful in determining whether, for example, the effect of lateral plume growth is great enough to override the effect of a systematic wind shift. The matrix of sensitivity cases run with each model for meteorological Episode 1 is shown in Table 4-2. For each model, the base case run is defined by no wind shift and a plume growth rate of 0.5 m/s.

Note that the sensitivity of the models to random variations in wind direction (such as those caused by improper initialization of the subsynoptic scale wind field) was not studied, at least not directly. Because the primary result of random wind variation is the enhancement of plume diffusion, it was felt that the effect of imposing random wind variations can be adequately represented by increasing the crosswind plume growth rate.

TABLE 4-2

MATRIX OF WIND SHIFT AND GROWTH RATE SENSITIVITY CASES

Plume Growth Rate (m/s)	Angular Wind Shift		
	5.625°	11.25°	22.5°
0.0	x	x	x
0.5	x	x	x
1.0		x	x

The two statistical measures found to be most useful in evaluating the results were the correlation coefficient (r) and the fractional deviation of the plume means (FDM). The correlation coefficient, r, is useful because it is a measure of the degree of overlap among the concentration fields of two plumes. The FDM statistic is also useful because it is a measure of the gross first-order moment difference between plume structures, without regard to differences in their spatial orientations.

The next set of figures shows the results for the zonal day (167) and stagnating day (169), both for the MESOPLUME model (Figures 4-7 and 4-8) and for the MESOPUFF model (Figures 4-9 and 4-10). Each figure contains subjectively sketched curves of approximately constant correlation coefficient (r) (shown as solid lines) as well as the FDM (shown as dashed lines). These curves are seen to be more or less orthogonal, because two plumes with very comparable mean values (FDM $\sim$0) and high correlation coefficient when the directions coincide (r $\gtrsim$0.75), rapidly become uncorrelated with only very modest angular shifts in wind direction.

As illustrated next, the sensitivity to variations in wind direction is quite dependent on the meteorological episode. A comparison of Figure 4-7 with Figure 4-8, and Figure 4-9 with Figure 4-10, shows that during the moderate wind speed zonal flow conditions (day 167), a small, systematic wind direction shift results in a test plume uncorrelated with the base case plume; whereas, the light variable winds during the stagnating flow period (Day 169) lead to results that are appreciably less sensitive to the imposed variations in wind direction.

Wind direction shifts had very little effect on the FDM, especially during the stagnating flow conditions. Systematic variations in the wind direction do cause plumes to pass through different sections of the grid and, therefore, experience somewhat different mixing height and stability fields, but, in this case, the slight FDM dependence on wind direction variations probably reflects the fact that these fields are homogeneous.

The sensitivity of the MESOPLUME and MESOPUFF models to variations in the plume growth rate, $d\sigma_y/dt$, also shows a dependence on the mesoscale flow pattern. For growth rates less than the base case (0.5 m/s), the FDM is much more sensitive to changes in the growth rate, when flow conditions are zonal (relatively steady), than when stagnating (variable). The results also indicate that once a nominal growth rate is reached, further increases of the growth rate do not substantially change the mean plume structure. The plume growth rate appears to be important only until the plume reaches a size large enough to be influenced by the mesoscale flow structure. Thereafter, the plume dispersion is dominated by the larger (meso-) scales of the flow; horizontal plume dispersion from small-scale turbulent diffusion is no longer of primary

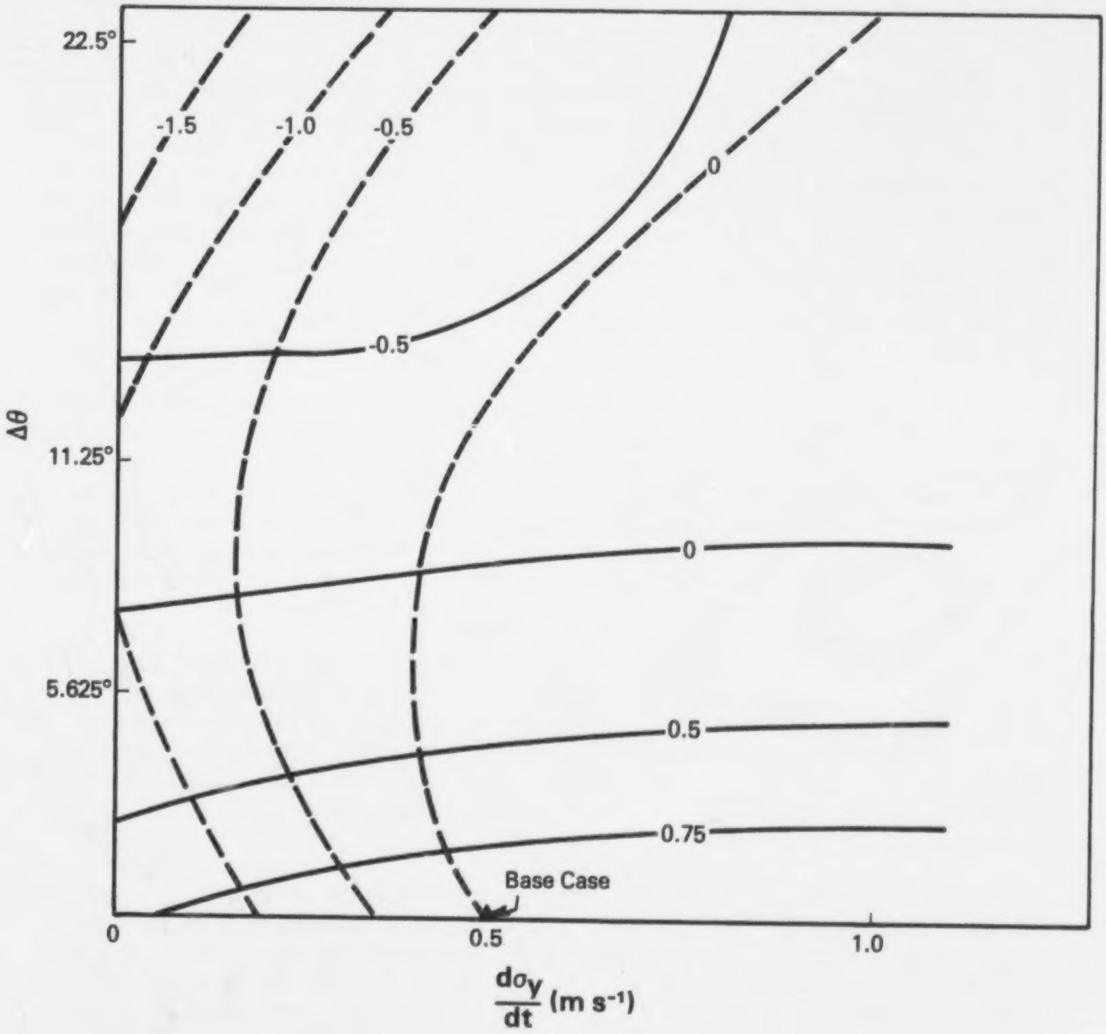

Figure 4-7 MESOPLUME Sensitivity of r (——) and FDM (---) to Systematic Variations in Wind Direction Δθ and Plume Growth Rate $d\sigma_y/dt$ (Day 167)

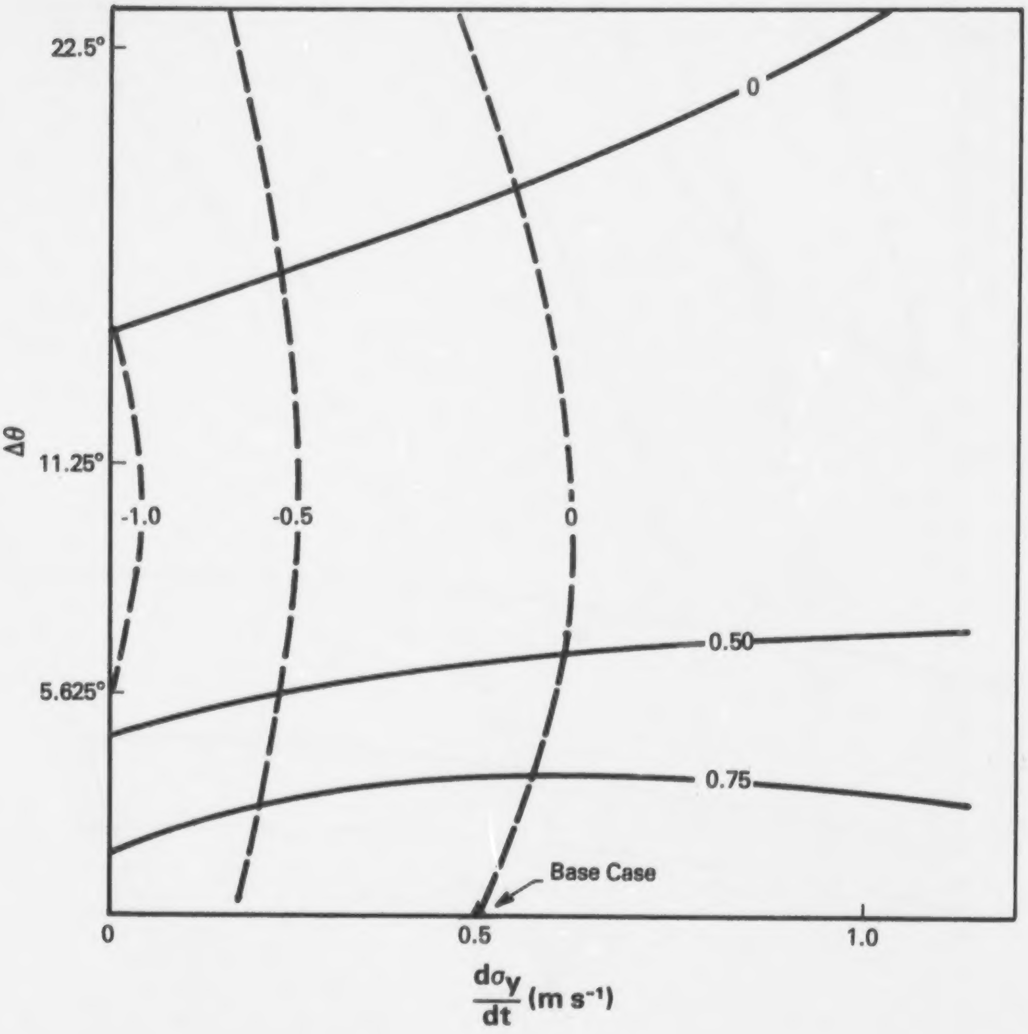

Figure 4-8 MESOPLUME Sensitivity of r (——) and FDM (---) to Systematic Variations in Wind Direction Δθ and Plume Growth Rate $d\sigma_y/dt$ (Day 169)

7902505

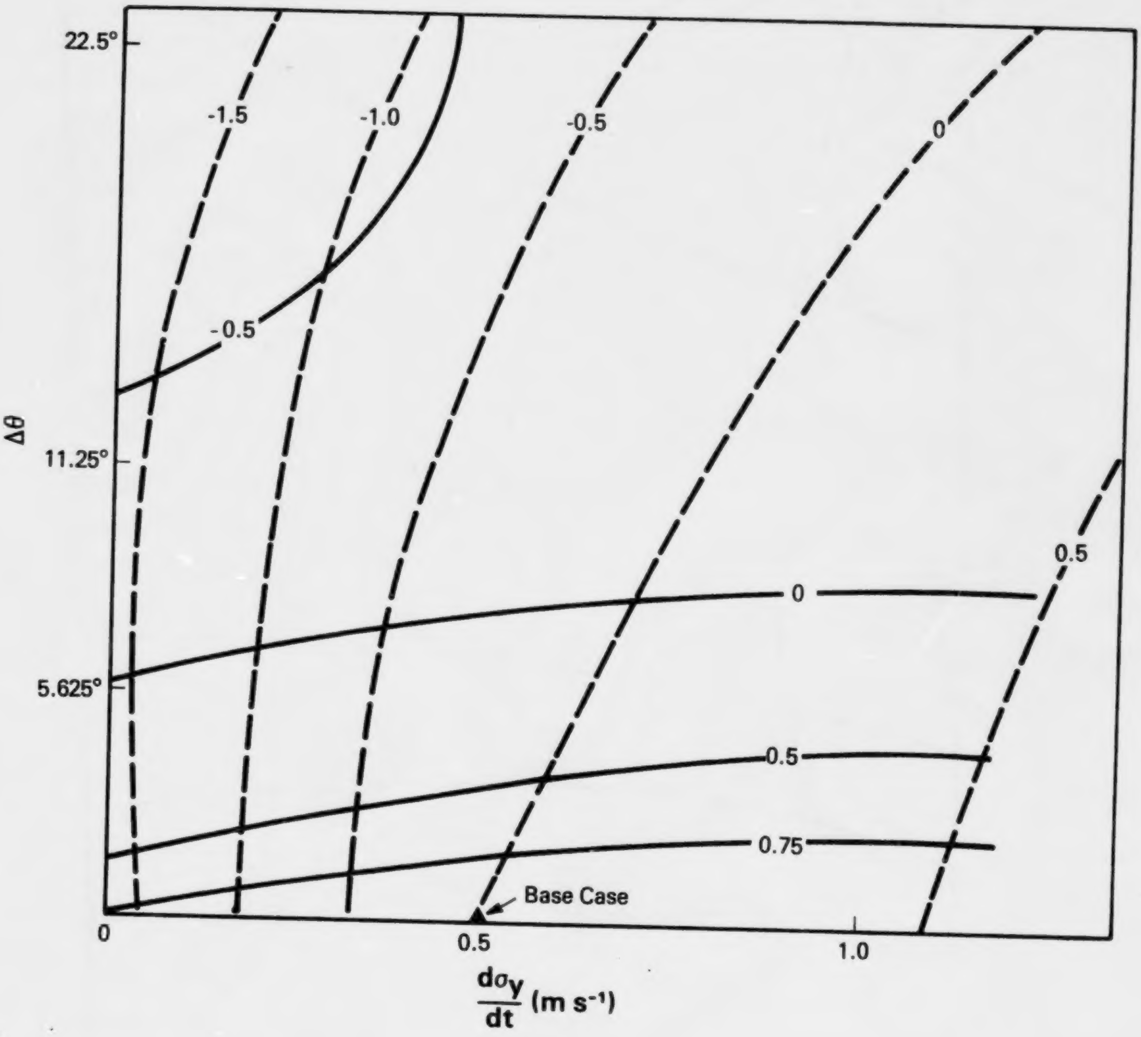

Figure 4-9 MESOPUFF Sensitivity of r (—) and FDM (---) to Systematic Variations in Wind Direction Δθ and Plume Growth Rate $d\sigma_y/dt$ (Day 167)

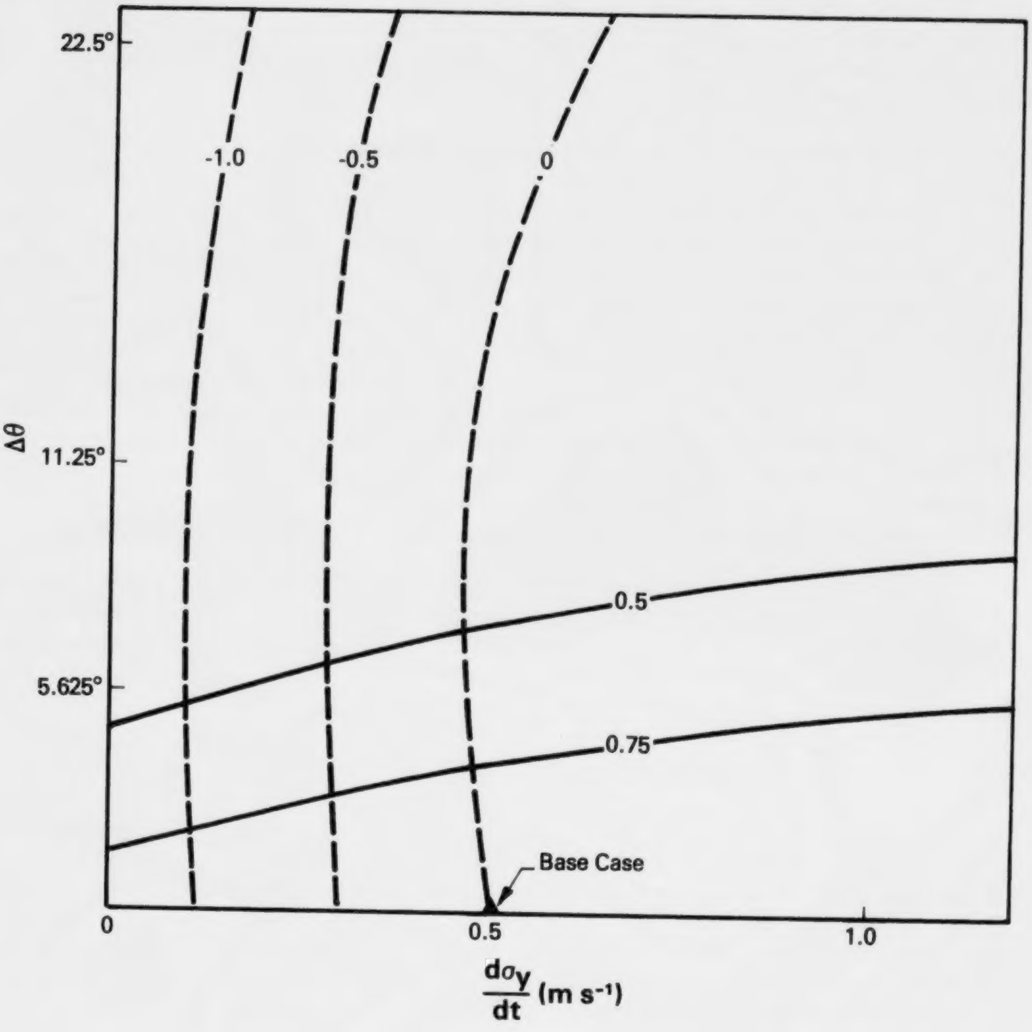

7902304

Figure 4-10 MESOPUFF Sensitivity of r (——) and FDM (---) to Systematic Variations in Wind Direction Δθ and Plume Growth Rate $d\sigma_y/dt$ (Day 169)

importance. The correlation coefficient is remarkably independent of variations in $d\sigma_y/dt$ - even in the extreme case of no plume growth beyond 100 km ($d\sigma_y/dt = 0$), the correlation coefficient is at least 0.75.

Thus, for regional-scale transport and dispersion as simulated by these models, the specific nature of the wind field is critical - chiefly because the mesoscale flow features appear to play the dominant role in plume dispersion on these scales.

4.4 Model Sensitivity to Variations in Wind Speed

Just as in the case of wind direction, the initialization scheme can introduce appreciable systematic errors in transport wind speeds. To understand the effect of a systematic variation of wind speed on the plume or puff model results, consider the idealized situation represented in Figure 4-11, Case A. Assume that the wind field is horizontally uniform and steady, and that it takes t hours for the emissions from a point source to reach the edge of the grid. Doubling the wind speed at each grid point will halve the travel time to the end of the grid (Case B). The mass of pollutant integrated over the entire plume is twice as large for Case A as for Case B (assuming no removal), because the plume in Case A contains t hours of emissions (assumed constant) and the Case B plume contains only t/2 hours of emissions.

The centerline concentrations, however, should be approximately the same in both cases; this may be understood as follows. The MESOPLUME model assumes the centerline concentration C_c is inversely proportional to $u\sigma_y$:

$$C_c \propto \frac{Q}{u\sigma_y H}$$

For travel distances greater than 100 km, C_c is roughly independent of the wind speed because the plume segment width (σ_y) at a given distance from the source is approximately linearly related to the elapsed travel time t; and, therefore, inversely related to the wind speed u. Both the mass of pollutant contained in the plume as well as the volume occupied by the plume are roughly twice as large in Case A; therefore, the average concentrations are also about the same in both cases.

In real meteorological situations, systematic wind speed variations have more complicated episode-dependent effects. Increasing or decreasing the wind speed will cause alterations in the plume trajectory; thus, the plume will occupy different sections of the grid and will be affected by different wind vectors, mixing heights, and stability classes. In addition, the amount of removal by dry deposition and decay depends on plume segment (or puff) age - and, thus, wind speed variations will also affect the amount of pollutant depleted from the plume. Also, plume rise calculations are dependent on wind speed. For these reasons, the sensitivity of each of these models to systematic variations in wind speed can be expected to be highly episode-dependent.

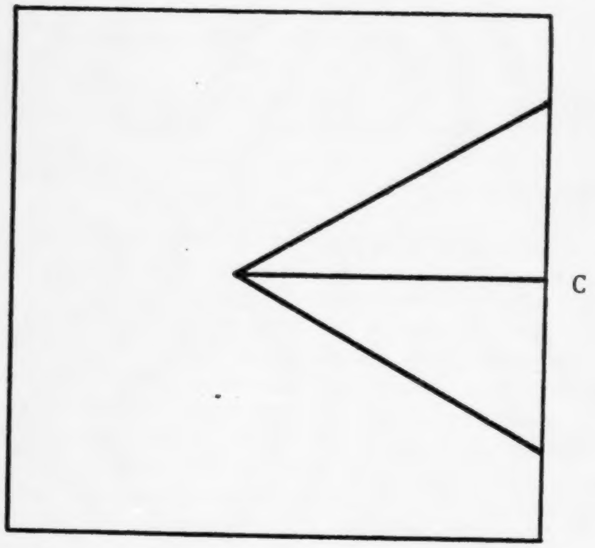

Case A

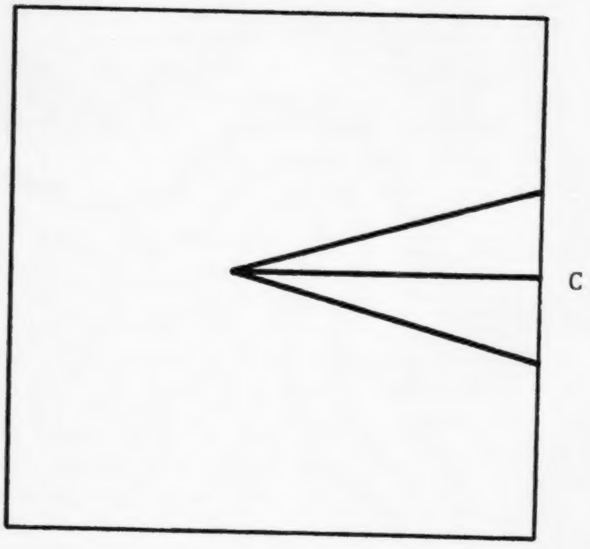

Case B

Figure 4-11 Effect of Wind Speed on Idealized Plume Shape

The wind speed sensitivity tests were conducted by adjusting the wind speed at each grid point with a multiplicative factor in each model run. The factors used were 0.5, 1.5, and 2.0, relative to the base case. Note that, for these sensitivity tests, the MESOPAC-generated mechanical mixing depths and stability classes were not recomputed whenever the wind speeds were changed.

Figures 4-12 a and b display the correlation coefficient r as a function of the wind speed multiplier for wind speed sensitivity runs MESOPLUME and MESOPUFF. The results are similar for both models; meteorology-dependent behavior is seen in the day-to-day variations of the results. Increasing or decreasing the wind speed by a factor of two causes about a two-fold reduction in the correlation coefficient. As was seen in the analysis with the correlation coefficient, day-to-day variations of the fractional difference of the means (Figures 4-13 a and b) are highly episode-dependent. Large FDM values are sometimes produced when a change in the wind speed multiplier leads to a change in the plume trajectory that exposes the plume to radically different wind vectors, mixing depths, and stabilities. But even with the occurrence of these large deviations, no well-defined FDM/wind speed multiplier trend can be extracted from the analysis. Implicit dependencies on the spatial and temporal variations in meteorology override any explicit trends in the data.

4.5 Sensitivity of MESOGRID to Variations in K_z

A series of tests has been performed to determine the sensitivity of MESOGRID to variations in K_z values. The concern here is to illustrate how well test case concentration fields, produced by altering some or all of the K_z values, reproduce a base case concentration field generated using a predetermined K_z criterion. The base case K_z criterion was chosen such that the MESOGRID "requested time step" is one hour. Thus, all overly-large values of K_z are truncated to the threshold value, which ensures numerical model stability in the vertical for a one-hour time step (see Section C.4.4 for a complete discussion).

Two methods of varying K_z field values were adopted in the present sensitivity study. The first method involved the direct reduction of K_z values by a K_z multiplier (less than unity). In Figure 4-14, this method was used to produce the portion of the sensitivity curve that lies to the right of the ordinate axis. It is seen that reducing all K_z values by as much as 90% causes a significant reduction in the average concentration of the plume. Figure 4-15a supports this contention--when K_z values are reduced by an order of magnitude, ground-level concentrations are decreased [Fractional Difference (FD) field values are positive) everywhere except in the very far field. (Note that, in Figures 4-15a and b only, MESOGRID plume concentrations as small as

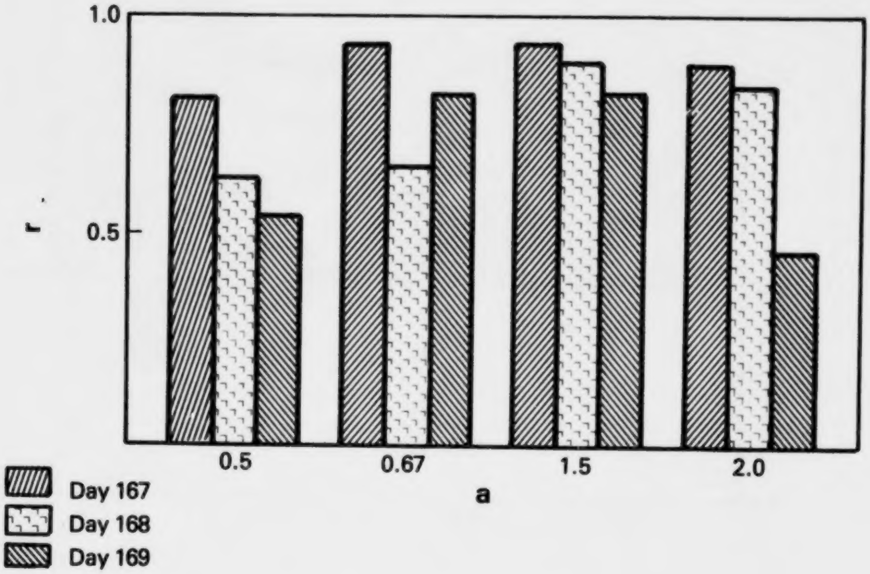

Figure 4-12a MESOPLUME Sensitivity of r to Wind Speed Multiplier (a) Variations (Days 167-169)

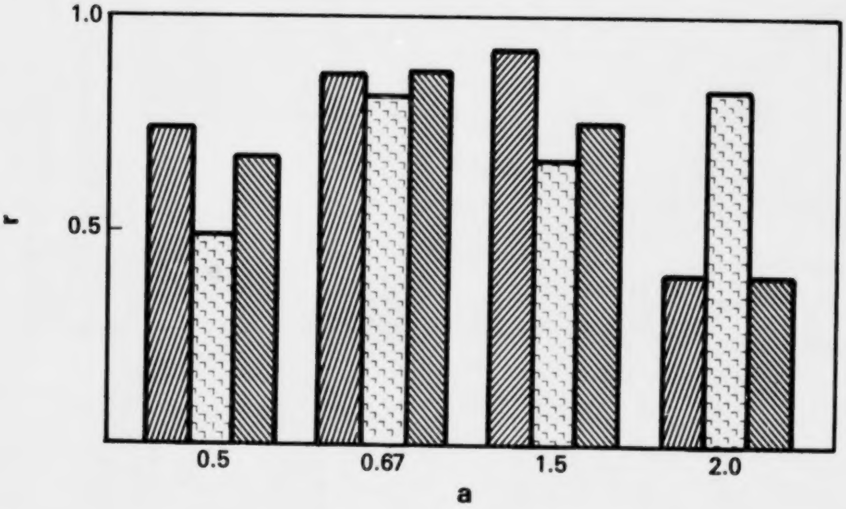

Figure 4-12b MESOPUFF Sensitivity of r to Wind Speed Multiplier (a) Variations (Days 167-169)

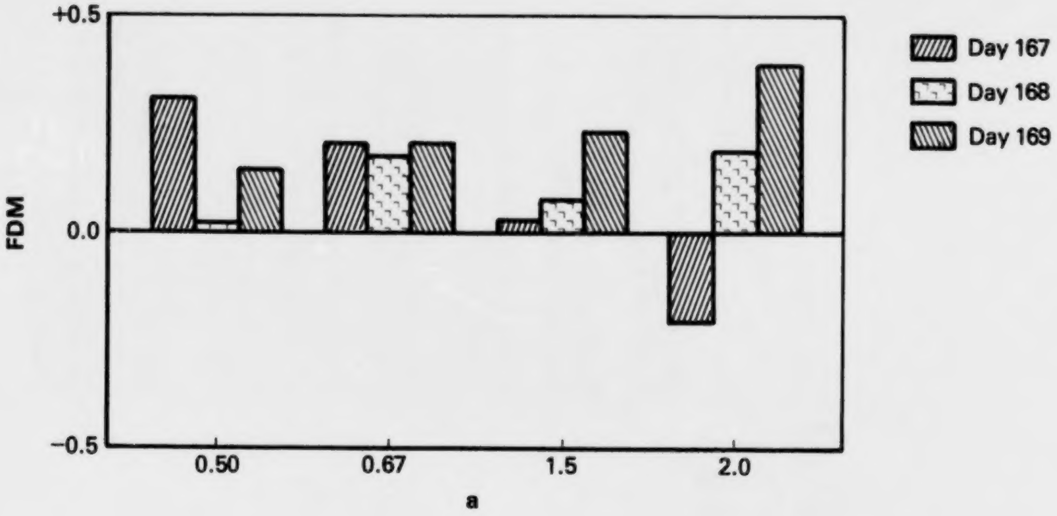

Figure 4-13a MESOPLUME Sensitivity of FDM to Wind Speed Multiplier (a) Variations (Days 167-169)

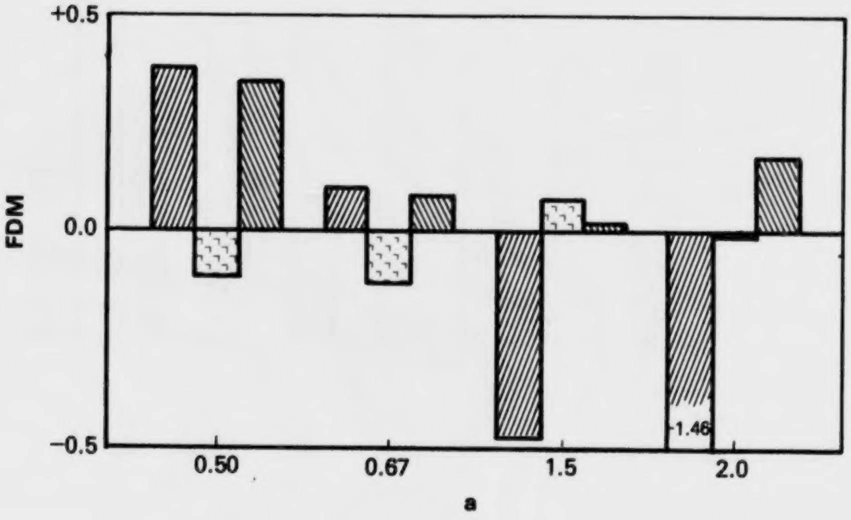

Figure 4-13b MESOPUFF Sensitivity of FDM to Wind Speed Multiplier (a) Variations (Days 167-169)

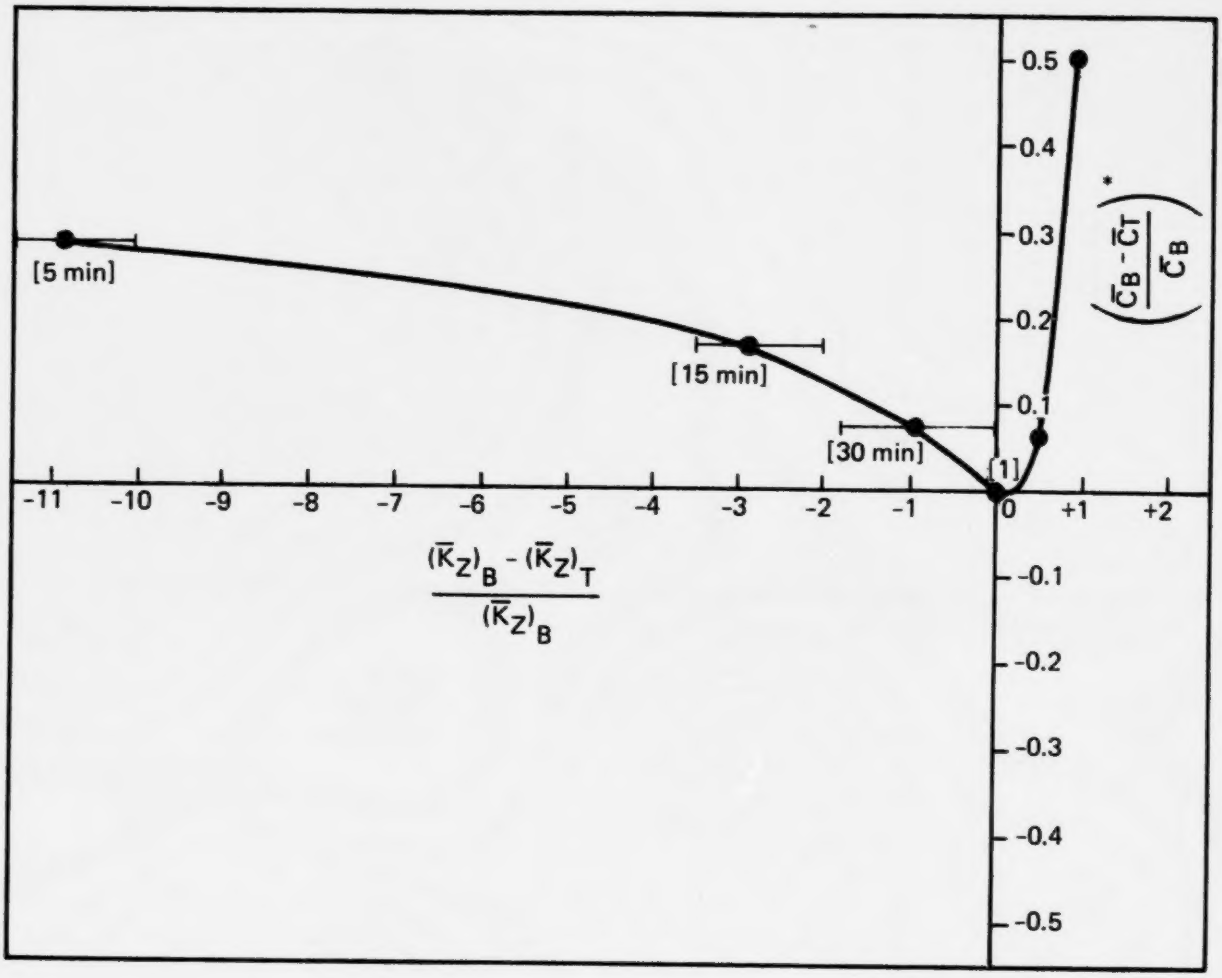

* Fractional Deviation of the Mean Concentration of the Base and Test Case Plumes (FDM)

Figure 4-14 MESOGRID Sensitivity to Variations in K_z (Day 167)

7901097

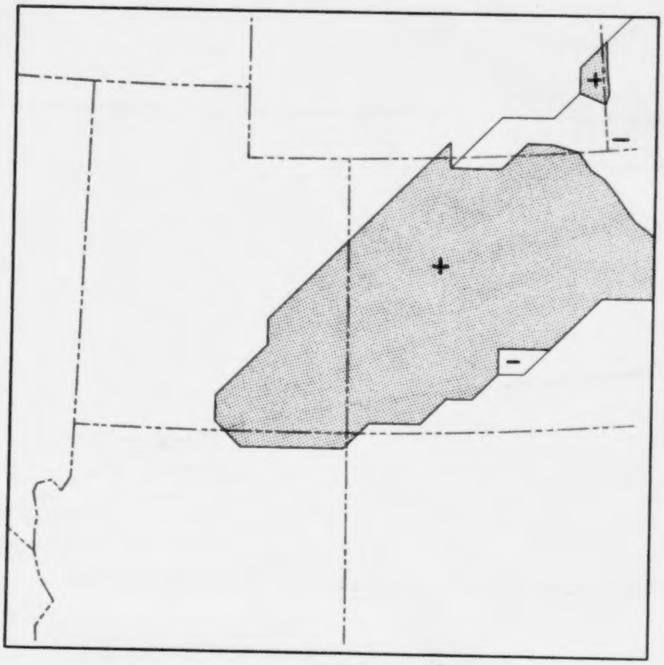

Figure 4-15a MESOGRID Difference Field Comparison for K_z Multiplier = 0.1 Case vs. Base Case (Day 167)

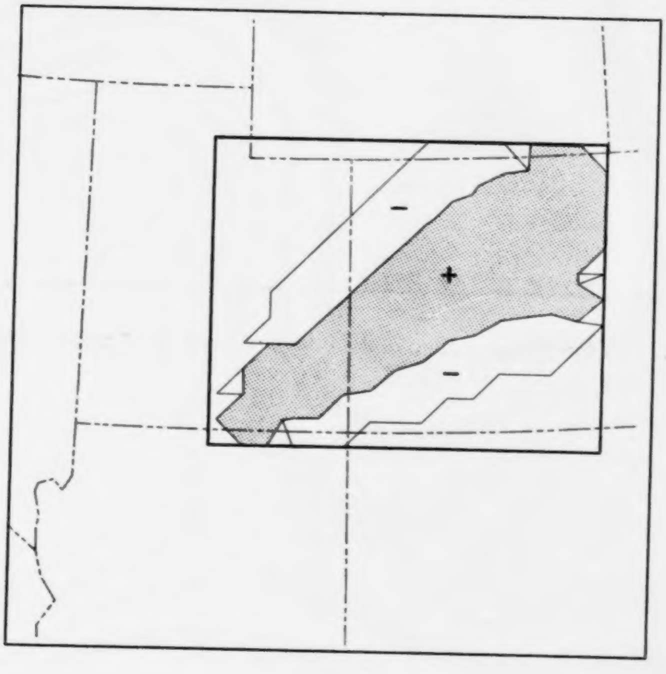

Figure 4-15b MESOGRID Difference Field Comparison (Limited Grid) for Requested Time Step = 5 Minutes Case vs. Base Case (Day 167)

10^{-4} μg m^{-3} are included.) Apparently, reducing K_z values directly decreases the rapidity of vertical mixing; pollutant material in the upper two grid levels will take longer to diffuse to the lowest layer, thus resulting in lower surface concentrations. But, reducing the surface concentration reduces the rate of removal by dry deposition, leaving more pollutant mass in the atmosphere; thus, after long travel times, ground-level concentrations in the "reduced-K_z" cases may actually become greater than those in the base case.

The second method of varying K_z involved the indirect modification of overly large values of K_z by reducing the "requested time step." This method was used to produce the portion of the sensitivity curve to the left of the ordinate axis in Figure 4-14. In practice, in parts of the Four Corners study, K_z values up to 1,000 m^2/s were found to be produced in strongly convective conditions by the algorithm discussed in Section C.4.3. These very large values, unless truncated, would force the model to use a time step even smaller than 5 minutes. Values of K_z that exceeded the limits of the requested time steps (respectively, 30 minutes, 15 minutes, and 5 minutes) were automatically truncated. Because of the truncation, there is some uncertainty in the values of K_z at each grid point. The FDM fields also reflect the effects of truncation, which are expressed as estimated error bases on the K_z values.

It is curious that allowing K_z values to increase apparently results in reduced surface concentrations--one would rather expect stronger vertical mixing to increase the rate at which material from above is mixed to the surface. The fractional difference field in Figure 4-15b compares the 5-minute "requested" time-step test case to the 1-hour "requested" time-step base case. This comparison is a useful adjunct in determining the cause of the K_z versus plume concentration relationship. (Note that a somewhat smaller computational grid has been used here to reduce the cost of a MESOGRID simulation for a 5-minute requested time step.) It can be seen that near the plume centerline, base case values exceed test case values (FD is positive), whereas away from the centerline, the opposite is true (FD is negative). Apparently, when a much shorter time step is used, pseudodiffusion effects resulting from multiple time steps are appreciable and tend to spread the plume laterally. For a 5-minute "requested" time step, this effect is enough to reduce mean plume concentrations by about one-third.

In the example shown, the resultant tradeoff of the two competing mechanisms, horizontal pseudodiffusion and vertical explicit diffusion, yields the most conservative plume concentrations when a "requested" time step of approximately one hour is used.

5. MODEL COST/SENSITIVITY ISSUES

5.1 Overview

The model sensitivity information presented in Section 4 is necessary but not sufficient to base a choice of the respective modeling techniques most appropriate to a given situation - particularly in the context of regulatory applications, serious issues of relative time and cost are also encountered. The use of an expensive, complicated method with extensive time and cost requirements should be questioned if a simpler, less costly method can produce similar results for the given application.

To gain more insight into these issues, a set of sensitivity tests was performed to study individual model performance vs. execution time requirements and to compare the cost/sensitivity results for the three models. The following questions, among others, were addressed.

- Which parameters control the cost of a given model simulation? What are the cost factors? How do these vary with meteorology, emissions inventory, and model run parameters?
- How do the model simulation costs compare for identical input conditions?
- Which factors and parameters can be modified or relaxed to produce substantial savings in model simulation costs, yet with only minimal deviations in output concentration fields?
- How do the costs of running each of the three regional-scale dispersion models compare to the costs of collecting and preprocessing the meteorological input data and the costs of postprocessing and analyzing the model output concentration fields?

5.2 Model Execution Cost Formulas

5.2.1 MESOPAC Run Time

Execution cost of the MESOPAC model (Benkley and Bass 1979c) is determined principally by:

- the number of time steps,
- the number of grid points, and
- the wind field divergence "tolerance factor".

The simulation run time is directly proportional to the number of time steps and the number of grid points. It is also strongly dependent on the tolerance factor, the magnitude of which determines the number of iterations required to produce the divergence-minimized wind field. The run time is only weakly dependent on the number of rawinsonde stations included, because the rawinsonde data is used only to compute the first-guess wind field and convective mixing value field.

The MESOPAC runs used in this report were made on a 26 by 26 grid, with 18 input rawinsonde stations and with a tolerance factor of $10^{-4}s^{-1}$ (which did not cause more than three relaxation iterations, even in recirculating meteorological regimes). For these conditions, MESOPAC required about 5 seconds CPU time (IBM 370/158) per simulated hourly time step; a 7-day simulation using a 1-hour time step required 14 minutes CPU time. For other test purposes a tolerance factor of $10^{-5}s^{-1}$ was used, causing an average of 25 iterations, or about 18 seconds per time step, almost 4 times longer.

MESOPAC may require a significant amount of input data preparation - for example, manual preparation of one week of Service C teletype rawinsonde data for input to MESOPAC required nearly two person-days. The cost of manual data preparation can quickly become prohibitive, if lengthy model simulations are to be undertaken, MESOPAC input data should be reduced and concatenated from the National Climatic Center (NCC) Upper Air (5600 format) tapes for each of the rawinsonde stations to be included.

5.2.2 MESOPLUME Run Time

MESOPLUME simulation time is directly proportional to the number of time steps N and varies linearly with the number of sources S. However, various meterorological factors - for example, lower transport wind speeds - cause an increase in the average number of plume segments resident on the grid and therefore a direct increase in running costs. For typical meteorological conditions within the Four Corners grid, and with the spatial extent and grid resolution used for these experiments, MESOPLUME model run times on an IBM 370/158 were described by:

$$t(\text{sec}) = 0.17(S)(N) + 0.40(N) \tag{5-1}$$

5.2.3 MESOPUFF Run Time

The time required for a MESOPUFF simulation depends on:

- the number of time steps N,
- the number of puff releases n_p per source per time step,
- the number of puff samples n_s per time step,

- the number of sources S, and
- various meteorological factors that control the average number of puffs resident on the grid.

The MESOPUFF model allows for the specification of puff release and puff sampling substeps (see Section B.9). These substeps can be chosen to ensure that discrete puffs emitted consecutively from a source will overlap sufficiently to simulate a continuous plume. For a single source, the following relationship for MESOPUFF execution time was found useful for estimating run time for typical meteorological conditions in the Four Corners area:

$$t(\mathrm{sec}) = 20 + 0.5N + 0.003\,(n_p - 1)\,N^2 + 0.002\,(n_s - 1)\,N^2 \qquad (5\text{-}2)$$

Note that while both n_p and n_s can be varied to simulate a continuous plume, frequent sampling is often less costly than frequent puff releases. For one puff release per time step (n_p=1), and with sampling frequency dynamically determined (see Section B.6), MESOPUFF execution time (on an IBM 370/158) over the Four Corners computational grid and typical meteorological conditions used is given by:

$$t(\mathrm{sec}) = 0.38\,(S)(N) + 0.43\,(N) \qquad (5\text{-}3)$$

For runs with more than a few sources (so that the second term on the right hand side of (5-3) is negligible), the MESOPUFF model is about twice as expensive to run as MESOPLUME.

5.2.4 MESOGRID Run Time

The run time required for a MESOGRID simulation is determined by the number of time steps, the number of grid points, and various meteorological factors that control the time step Δt satisfying the horizontal and vertical computational stability criteria (see Section C.4.4). Note especially that MESOGRID execution time varies directly with the number of grid points but is independent of the number of sources. MESOGRID becomes cost-effective compared to the plume and puff models only when many sources are to be included. The execution time (on an IBM 370/158) of MESOGRID for the Four Corners computational grid (and typical meteorological conditions) is described by:

$$t(\mathrm{sec}) = \frac{300\,N^*}{\Delta t} \qquad (5\text{-}4)$$

where N* is the total number of time steps (of duration Δt minutes) in a MESOGRID simulation. Table 5-1 lists the maximum values of u and K_z consistent with various choices of Δt, assuming a horizontal grid interval of 40 km and vertical layer thicknesses of 500, 1,000 and 2,500 m. The values of $\overline{K_z}$ shown are the averages of the values of K_z at the adjacent integer levels, e.g., $\overline{K_z}\,(1.5) = 0.5\,(K_z(1) + K_z(2))$.

TABLE 5-1

MAXIMUM VALUES OF u AND K_z VS. TIME STEP Δt

Δt (min)	Advective Stability Criterion u_{max} (m/s)	Maximum K_z (m^2/s) Allowed by the Vertical Diffusive Stability Criteria	
		Level 1.5	Level 2.5
5	-	625	2,916
15	-	208	972
30	22.2	104	486
60	11.1	52	293

5.3 Model Sensitivity to Changes in Time Step

As seen in the preceding section, for a specified number of sources, grid size, and meteorological conditions, model execution time varies approximately inversely with length of the time step used. It may be expected, however, that as time steps are lengthened to save execution time, a model will no longer reproduce the results obtained when a very small time step was used. This section examines the reproducibility of model results as the time step is changed. For model runs made with different time steps, the 24-hour average SO_2 concentration fields are compared.

Figures 5-1 a and b illustrate in highly condensed form the results of numerous cost/sensitivity tradeoff experiments made with MESOPUFF. The figures display the execution cost (in IBM 370/158 CPU minutes) and either the correlation coefficient (r) or the absolute value of the fractional difference of the mean (|FDM|), as puff sampling rate and puff emission rate are relaxed from "special" base case values of 20 minutes each. Here, the correlation coefficient r (given as the average of the three correlation coefficients computed individually for each of the last 3 days of the simulation) is used as a measure of the extent to which a "test" case would reproduce the results of the "special" base case. The execution time of the base case was about 6 minutes for the 5-day Episode 1 run with the Navajo power plant. In contrast, a test run made with sampling and puff emission rates of 2 hours took only 43 seconds (an 8-fold savings in run time); yet, qualitatively at least, the test run reproduced the base case results very closely ($r = 0.88$, $|FDM| = 0.06$). This suggests that computationally "optimal" values of puff sampling rate and puff emission rates can often be chosen (at least for this episode).

In Figure 5-2, the MESOPLUME and MESOPUFF models are compared for departure from their respective base case results when only the plume segment (or puff) emission rate is varied; the sampling rate is dynamically determined and therefore nearly constant in each case. The correlation coefficient r is again used to measure reproducibility of model results (expressed as 24-hour average SO_2 ground level concentrations). The figure indicates that as the plume segment or puff emission rate is increased (from a base case rate of 1 hour), the MESOPUFF model, for the most part, reproduces its base case results with more precision than MESOPLUME. Indeed, the MESOPUFF results for a 4-hour time step show a correlation of $r = 0.9$ with the results for the base case; by contrast, for a 4-hour time step, MESOPLUME shows a correlation of only about 0.6. Model execution times are, of course, significantly reduced when using a longer time step--for the 4-hour time step simulations, MESOPUFF required 40 seconds (compared to 97 seconds for its base case), and MESOPLUME required 36 seconds (compared to 76 seconds for its base case).

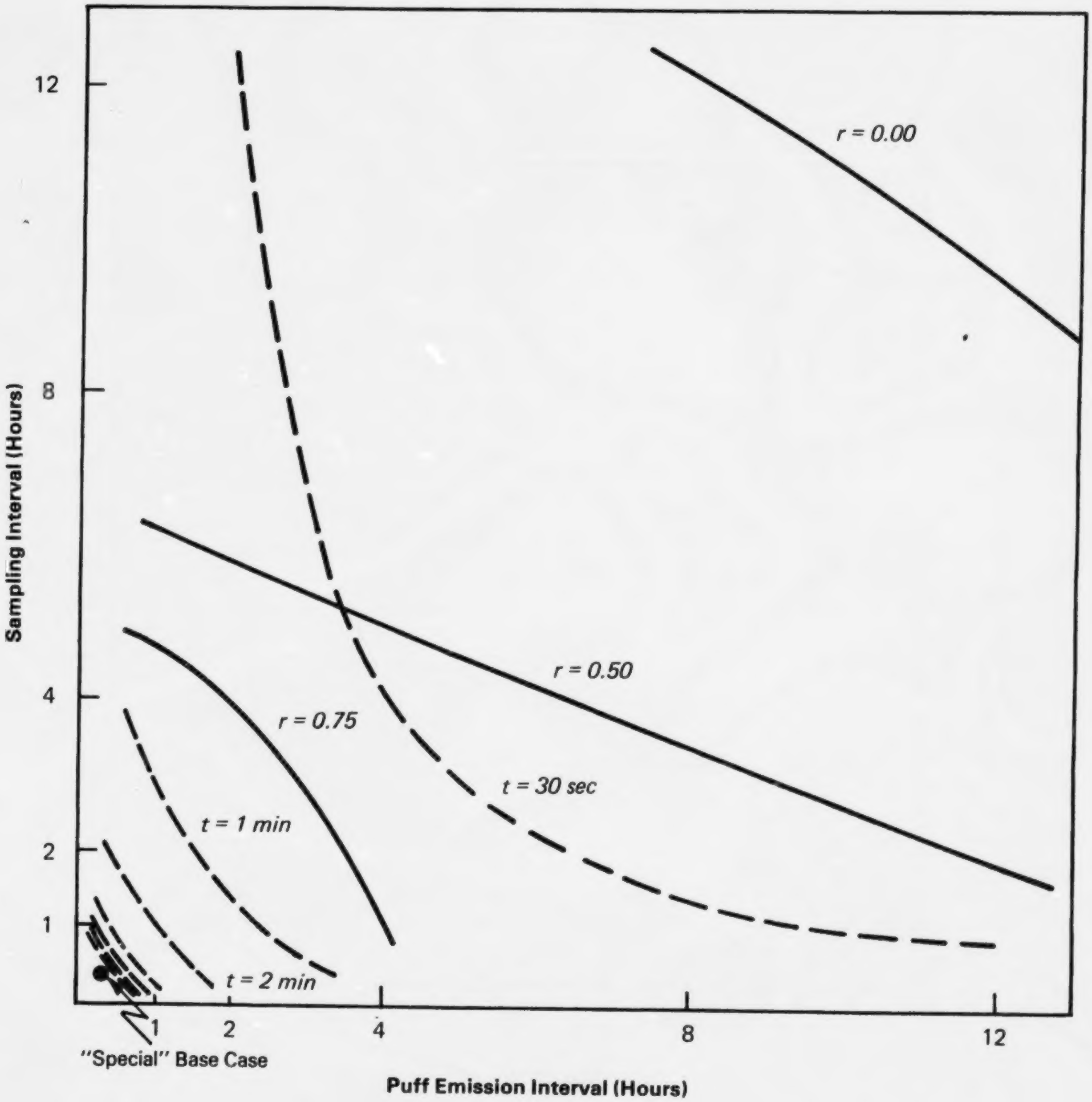

Figure 5-1a MESOPUFF CPU Run Time (t) and Sensitivity of r to Variations in Sampling Rate and Puff Emission Rate (Days 167-169)

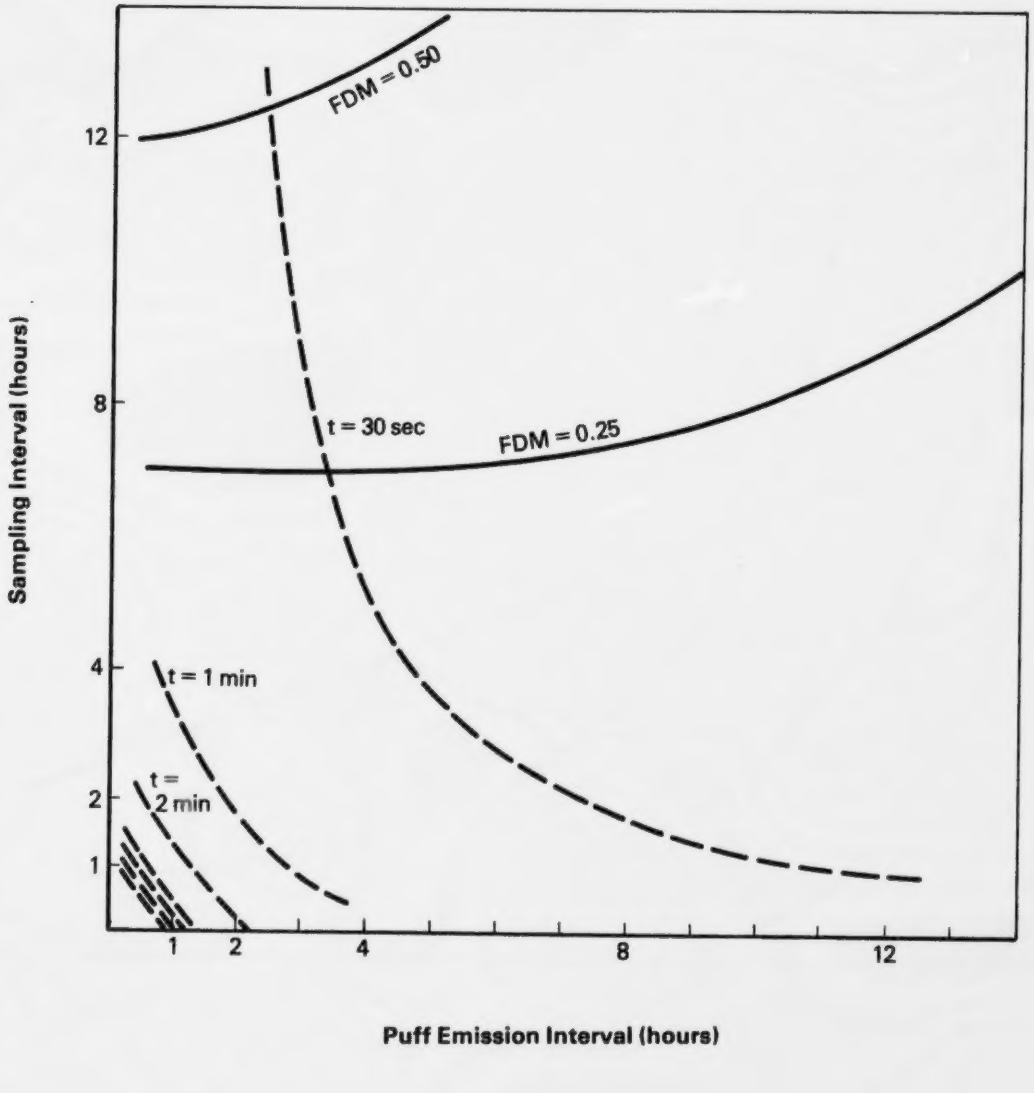

Figure 5-1b MESOPUFF CPU Run Time (t) and Sensitivity of FDM to Variations in Sampling Rate and Puff Emission Rate (Days 167-169)

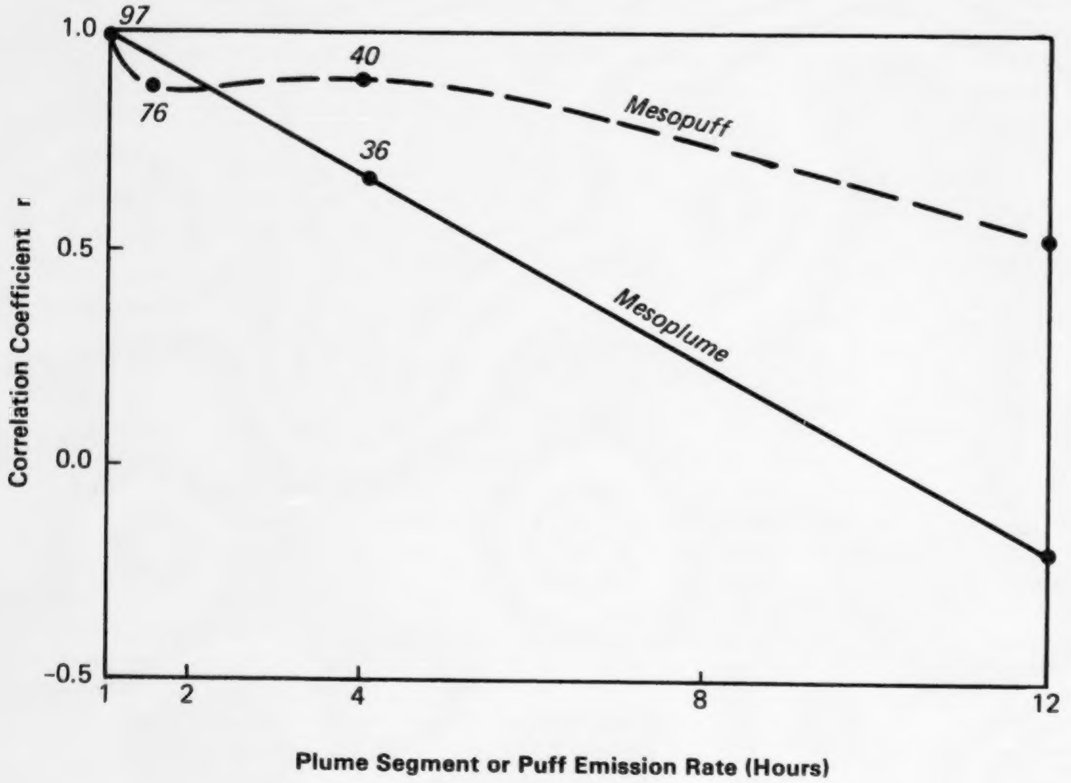

Figure 5-2 Variation of Correlation Coefficient with Puff Emission Rate

For the MESOGRID model, the only way to increase the time step (thereby decreasing simulation cost) is to reduce the maximum values of K_z at any time step, so that no K_z values exceed the maximum allowable value for a certain "requested" time step. Section 4.5 demonstrated that maximum K_z values could be reduced to be consistent with a 1-hour requested time step without significantly affecting reproducibility of results on regional scales. MESOGRID execution costs can be minimized by requiring that the model time step be solely determined by the advective stability criterion (the Courant condition). In the first episode, the maximum wind field velocities at each time step forced the model to use a 30-minute time step during 80% of the simulation and a 60-minute time step during the remaining 20% of the simulation. Total execution time was 18 minutes (IBM 370/158) for the 5-day meteorological episode.

In all cases, the costs associated with archiving, combining, analyzing, and producing hard copy plots of output results (using the MESOFILE postprocessing system) are negligible when compared to the costs of running one of the dispersion models.

Figure 5-3 compares the execution time required by each model to simulate Episode 1, days 165 to 169, 1978, as a function of the number of sources included in a simulation. The MESOPLUME, MESOPUFF, and MESOGRID curves are based on Equations 5-1, 5-3, and 5-4. Thus, for this episode, MESOGRID becomes competitive with MESOPUFF when about 40 sources or more are included in a simulation, but about 80 sources must be included before MESOGRID becomes competitive with MESOPLUME. [Note that the MESOPLUME and MESOPUFF models as currently configured will actually accommodate a maximum of 10 sources per run (to save on computer storage requirements). For either model, the costs of performing, for example, 4 simulation runs with 10 sources each and then merging the results files using the MESOFILE System are only negligibly greater than the costs of actually running the models with a 40-point source inventory; and restriction to 10 sources produces substantial savings in needed core storage. MESOGRID is currently restricted to a maximum of 50 sources per run, but this restriction could be easily changed.]

The comparative run costs shown are based on time steps and other model run parameters chosen to optimize the reproducibility of results of base case runs made with very small time increments. The costs shown are therefore somewhat higher than necessary; in particular, the time step(s) used by the plume and puff models can be increased by a factor of two or even four with minimal loss of reproducibility. [Note that if modeling of only SO_2 (and not $SO_4^=$) is desired, it is possible to run MESOGRID for SO_2 alone and thereby reduce MESOGRID execution time by almost a factor of two.]

Finally, the possibly substantial cost of generating the necessary meteorological inputs to the dispersion models should be emphasized. In practice, the cost of running MESOPAC per simulated day of hourly time

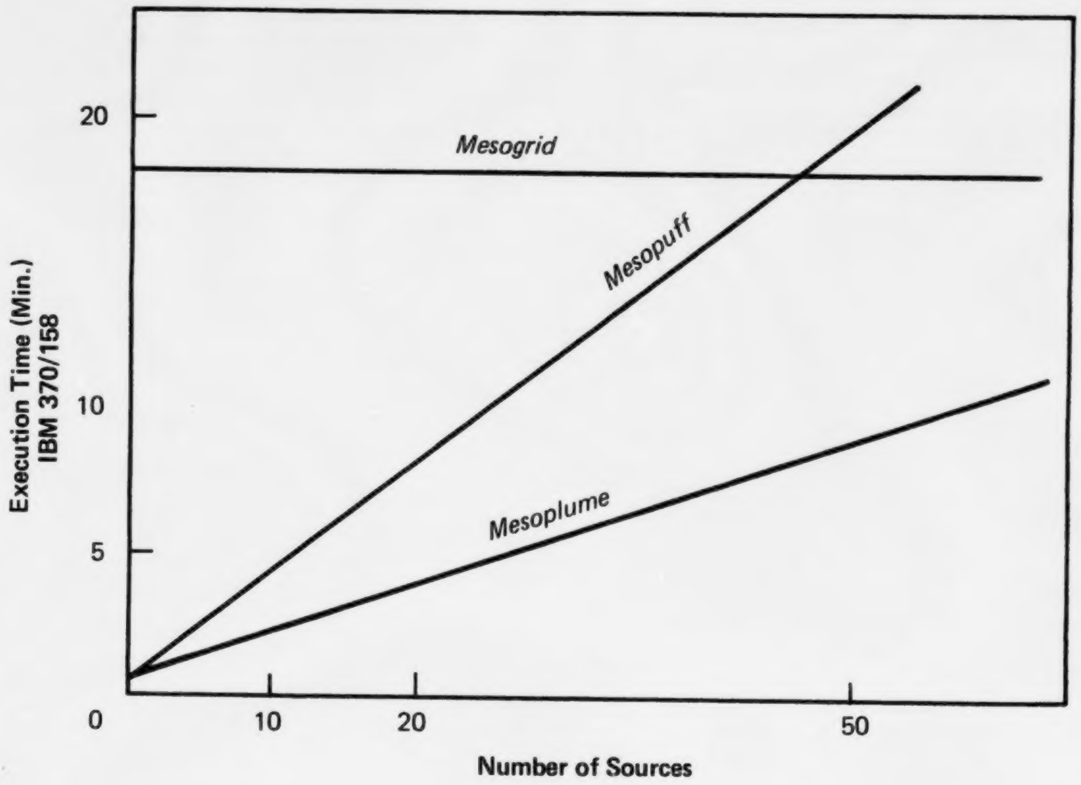

Figure 5-3 Comparative Model Run Execution Times (5-day run)

7901104a

steps is about one-third that of MESOGRID, or comparable to a 20-source, 1-day simulation by one of the other models. If a lengthy set of meteorological data is to be generated by hand and then used for only a few simulations by one or another of the dispersion models, the labor costs associated with manually reducing and concatenating the raw rawinsonde data will probably dominate the total cost (labor plus computer time) of the entire simulation. In such an instance, using MESOGRID rather than MESOPLUME or MESOPUFF would yield only a negligible increase in total simulation cost.

6. SUMMARY, CONCLUSIONS, AND RECOMMENDATIONS

6.1 Basic Model Development Objectives

As shown by the many model comparison, model sensitivity, and model cost analyses presented or summarized in the preceding sections, the basic model development objectives have largely been realized. When used and interpreted appropriately, each of the new models appears to be a practical tool for simulating regional-scale air quality impacts of energy-related major point sources of SO_2 in the Four Corners area. These different models provide the user with a range of performance vs. cost tradeoffs from which to choose; the choice of model best suited to a specific application depends on (1) size of inventory, (2) characteristic or dominant meteorological regimes, and (3) importance of small-scale plume dispersion and plume fumigation to regional scale impacts.

Each of these variable trajectory models takes into account the important mesoscale variations in the meteorological fields governing long-range plume dispersion in the Four Corners region. The meteorological input data are readily constructed from available rawinsonde data using the MESOPAC preprocessor; use of alternative meteorological preprocessing schemes (in place of MESOPAC) is easily achieved because of the uniform meteorological interface structure built into each of the three transport-diffusion models.

The contiguous plume segment approach adopted in MESOPLUME, and the puff superposition approach adopted in MESOPUFF, have each been presented as generalizations of the conventional straight line Gaussian plume model, useful for situations dominated by spatial and temporal variations in wind fields, mixing heights, and atmospheric turbulence levels. In the limit of uniform, steady flows, both MESOPLUME and MESOPUFF can reproduce well the results of the straight-line model. This feature of these models should aid in their general acceptance by the air quality community.

Other important features that contribute to the usefulness of these models for regulatory and other applications include:

- the ease with which model design and run parameters and algorithms can be changed to facilitate use for a range of model validation research and development projects;
- the ease with which the models can be used to simulate short-term average ambient ground-level concentrations, and the ease with which the postprocessing system can analyze and display model results; and

- the complete freedom to change the geographic extent and resolution of each model and to modify (replace) the meteorological preprocessing system.

6.2 Model Verification

For lack of a suitable regional-scale data base in the Four Corners region, the performance of these new models has not been verified to date against actual ambient air quality in the region. However, the basic computational method used in the MESOGRID model has been previously verified to a limited extent on regional scales by MESOGRID's parent model SULFA3D in the first phase of the Electric Power Research Institute's Sulfate Regional Experiment (EPRI/SURE).

6.3 Comparative Model Performance

All three models compare extremely well on regional scales when meteorological flow conditions are such that each of these modeling approaches is appropriate. Even when the nature of the meteorological flow regime puts MESOPLUME (and, to lesser degree, MESOGRID) at a serious disadvantage relative to MESOPUFF, the models remain in good agreement at the lowest (most disperse) limits of the concentration field calculations (0.1 $\mu g/m^3$).

However, when stagnation conditions are encountered in a modeling simulation, the inverse wind speed dependence of the MESOPLUME modeling approach can lead to spurious results - as evidenced by several instances when concentrations increased substantially by large downwind distances. MESOPUFF is not as seriously affected in this manner.

Similarly, under conditions of disorganized flow or where significant local convergence occurs, the MESOGRID model also shows spurious increases in concentration at large downwind distances, but apparently to a lesser degree than MESOPLUME. This spurious behavior can arise even when the two-dimensional wind field is nondivergent, because parcels of material are advected at each time step by successive, independent, one-dimensional operations in the east-west and north-south directions, and one-dimensional wind fields may have appreciable local divergence.

The significant differences that are apparent among results of the different models in the near field of sources can be partially explained in terms of the differences in the way the respective modeling algorithms deal with (or ignore) the small-eddy diffusion effects. By contrast, at large distances from the source, plume dispersion (as represented by these models) is dominated by the advective effects of large-scale eddies in the mean wind field, and the differences in the way each model treats small-scale diffusion are much less important.

On the larger regional scales, at least, the effects of numerical pseudodiffusion in the MESOGRID model can be ignored--as can be judged by the overall similarity of the grid model results (for small concentration isopleth values) with the results of the plume and puff models, neither of which is subject to pseudodiffusive effects. Time-discretization errors in all three models can be minimized by conservative choices of advective (or diffusive) time steps. Space-discretization errors in MESOPLUME can be serious in cases of highly variable wind fields.

6.4 Model Sensitivity Results

In interpreting the detailed results of the model sensitivity experiments shown in Sections 4 and 5, their principal limitations should be borne in mind.

First, it will be recalled that the model sensitivity analyses were performed as if the effects of varying one model parameter could be considered as entirely independent of all the other model parameter choices; in reality, many of the model parameters are strongly coupled, either explicity or implicitly. For example, the advective transport, diffusion removal, and chemical transformation processes are treated as formally separable, although they are often strongly (if implicitly) coupled--obviously the mass of SO_2 already converted to $SO_4^=$ is not available to be deposited nor to be transported as SO_2 for subsequent transformation further downwind. Another but subtler case of parameter coupling is the relationship between the diurnal variations in mixing height (hence, in the onset of plume mixing to the ground), and the resulting downwind pattern of surface deposition.

Second, the interpretation of the sensitivity results is complicated by the implicit, but often strong, interaction among meteorological variables that govern large scale dispersion (e.g., mixing depth and wind velocity) and model parameters that control the actual finite-difference calculations (e.g., grid size or time step). When the values of meteorological variables change rapidly in time and space, spatial and temporal discretization errors in the calculation scheme may be expected to cause significant errors, as, for example, in the calculation of individual plume element trajectories. Therefore, values used for the time step or spatial interval should be sufficiently small to permit good approximations to the "exact" plume trajectories in the case of analytically-specified wind fields. In this study, computer core size restrictions precluded the study of space discretization errors. However, it has been shown for MESOPUFF and MESOPLUME (see Figures 5-1 and 5-2) that time discretization errors do not appear to unduly influence the calculated regional-scale 24-hour average SO_2 concentrations, if a time step not larger than 2-4 hours is used.

Next, it must be strongly emphasized that, for a number of reasons concerned with model practicality, the physical parameterizations used in these models are very simple, and do not therefore take into account some of the more detailed (but often only fragmentary) information available. Examples include:

- the use of constant, spatially uniform rates for in-situ plume conversion of SO_2 to $SO_4^=$--no provision has been made for the sensitivity of the conversion rate to humidity, or to the rate with which a plume entrains surrounding cleaner air;
- no provision for wet removal processes has been incorporated; further, a complete and explicit model of wet removal would require consideration of spatially and temporally variable precipitation patterns and associated rainfall rates;
- the use of constant rates of dry deposition, with no provision for factors influencing atmospheric and surface resistances to SO_2 deposition. Such factors may be spatially variable (e.g., soil type, vegetation type and percent coverage) or diurnally variable (e.g., atmospheric stability, plant stomatal resistance).

With the simple parameterizations used in this study the models are shown to be very sensitive to rates of decay and dry deposition (see Figures 4-1 and 4-2). A five-fold increase in either of these removal mechanisms causes about a two-third decrease in Episode 1 24-hour average SO_2 concentrations; in contrast, a five-fold decrease causes about a one-third increase in concentrations. This behavior is highly episode specific, however (see Figures 4-3 and 4-4). Obviously, even when using very simple (e.g., linear, first order) removal rate prescriptions, the model user must choose, with care, values for decay rate and deposition velocity that are appropriate for the regional-scale simulation at hand.

Lastly, it is emphasized that these test results, although providing much valuable information, are not definitive, in view of the strong dependence of the results on the particular choices of meteorological and emission source scenarios.

With these limitations in mind, the detailed set of results presented in Sections 4 and 5 support the following useful general conclusions:

- Uncertainties in the meteorological data will usually exert the dominant influence upon model sensitivity. The tests provide clear evidence that the regional scale results are far more sensitive to typical variations in the larger (meso-)

scales of meteorological flow than to uncertainties in the small scale plume dispersion rates. The analysis has shown that as long as nominally large values of $d\sigma_y/dt$ (for MESOPLUME and MESOPUFF) and K_z (for MESOGRID) are chosen, the regional-scale dispersion of a plume depends only slightly on small-scale diffusion (see Figures 4-7 through 4-10, and 4-14). By contrast, varying the large-scale meteorological variables [e.g., wind speed (Figures 4-12 and 4-13), wind direction (Figures 4-7 through 4-10) and mixing depth (Figure 4-5)] can produce large and highly episode-specific variations in the concentration fields.

- Although the models appear to be highly sensitive both to large scale variations in the meteorological fields, and to physical decay and deposition processes, it is contended here that better prescription of the meteorological variables defining plume dispersion is the more serious issue to be addressed, in order to improve regional-scale SO_2 and $SO_4^=$ modeling techniques. Indeed, more research is needed in both the mesoscale meteorology and transformation/removal areas (Husar et al. 1978); but before significant improvements in regional-scale model performance will be realized solely through use of more complex decay/deposition algorithms, substantial progress must be made in acquiring and using meteorological data for characterization of the regional-scale dispersion.

6.5 Adequacy of Meteorological Data

Judging by the many model sensitivity and comparison analyses performed during this study, the principal limitations to the accuracy of these models for regional-scale simulation appear to be the insufficient spatial and temporal resolution of the meteorological fields. The effective spatial resolution is set by the characteristic distance between rawinsonde stations in the Four Corners area. This distance is of order 400 km, or about 10 grid intervals in each model. The inadequate temporal resolution is a more serious limitation--upper air soundings are only made at 12-hour intervals, and important diurnal variations in wind field, mixing height, and turbulence structure can occur on much shorter time scales. The simple interpolation schemes adapted for convenience in the present MESOPAC model can certainly be improved.

One possible approach to achieving better resolution of the regional scale meteorology is that taken by Heffter and coworkers (Heffter and Taylor 1975, Draxler, 1977); in their approach, the twice-daily upper-air rawinsonde data are supplemented by the much denser set of hourly surface station data, using a prescription for the manner in which the surface winds are interpolated upwards to represent the layer averaged wind field. This approach was not adopted in the MESOPAC model, in part for lack of any interpolation method deemed adequate to handle the strong topographic influences and convective conditions that often dominate mesoscale flow fields in the Four Corners area. If these new dispersion models are to be used in other regions, however, it might be appropriate to modify MESOPAC to use supplementary surface wind data. As another possibility, these models could be driven by a limited-area, Numerical Weather Prediction (NWP) model that has demonstrated prognostic skill in the geographic region of interest over a period of, for example, 12 to 18 hours.

6.6 Comparative Costs

By far the largest factor in the costs of doing regional-scale simulation with one or another of these models is the size of the emissions inventory. As shown in Section 5.3, only for large numbers of sources, for example, 20 to 80 or more, does the grid model (the simulation costs of which are independent of source inventory size) become cost-effective relative to the puff and plume models (the simulation costs of which are proportional to the number of sources). Thus, to model the incremental air quality impact of one or a few point sources on existing ambient air quality in a region, either MESOPUFF or MESOPLUME is appropriate (depending on the meteorology), and MESOGRID would be extremely impractical. If, however, the emissions inventory consists of, for example, 100 sources (and near-field plume resolution is not critical) MESOGRID is likely to be the better choice (again, depending to some extent on the meteorology).

The detailed nature of the meteorological scenario also plays an important role in determining model costs. For MESOPUFF and MESOPLUME, episodes dominated by stagnating or recirculating flows will cost more to simulate than episodes of largely uniform flow conditions:

- For sufficiently stagnating or disorganized flows, MESOPLUME, the model of choice for the more zonal flows may break down and use of the somewhat more expensive (MESOPUFF) model is mandated.

- For the plume and puff models, the execution costs per time step are functions of average number of plume or puff volume elements resident on the grid; under strongly recirculating conditions, volume elements may remain on the grid for several days. For MESOGRID, however, stagnation episodes may be less expensive computationally whenever the Courant condition permits the model to use a longer time step because wind speeds are low.

Because the costs of running these models are so dependent on the specific episode and experience with the models is as yet limited to the two multiday episodes described, it is not possible at present to make reliable, general, quantitative statements about relative costs for different meteorological scenarios.

6.7 Recommended Model Choices

Although it is not possible to make recommendations for use that will, in every circumstance, lead to the right choice of models, some general guidance can be provided. Certainly one guiding principle should be that if two or more models perform comparably, the cheaper or simpler of the models is preferable. For example, under situations of relatively uniform steady zonal flow, the MESOPLUME and MESOPUFF models agree extremely well, but MESOPLUME is cheaper and conceptually simpler.

A second guiding principle should be that it is best to choose if possible, the model that is, for a given application, more appropriate to the widest range of dispersion situations likely to be actually encountered. By this criterion, MESOPUFF is clearly preferable to MESOPLUME - under zonal, uniform flow conditions it is as accurate as MESOPLUME; under disorganized, recirculating, and stagnating flows it is physically much more credible; and the cost differential, roughly a factor of two, is not likely to be a strong impediment in most cases. In situations for which the source inventories are so large as to make the costs of MESOPUFF simulations prohibitive, the use of MESOGRID is dictated. Overall, however, for most point-source applications, it is felt that MESOPUFF is the most generally useful of these mesoscale models. Recommendations that may help guide the user in choosing among MESOPUFF, MESOPLUME, or MESOGRID are presented in Table 6-1.

6.8 Other Applications

Some of the areas of obvious extension for these models include:

- regional-scale sulfate formation as described by first order chemistry and removal (many problems may require addition of wet removal processes;
- regional-scale visibility degradation and plume blight (with further assumptions about plume chemistry and linkage to modules for solar insolation; radiative transfer; target contrast and luminance; human psychovisual response, photographic and other instrument response, etc.);
- acid rain formation (requires addition of wet removal processes);
- long-range transport, decay, and removal of radionuclides and other suitable airborne tracer substances with long residence times and small to negligible ambient background concentrations;

TABLE 6-1

RECOMMENDED MODEL CHOICES

Criterion	Preferred Model(s)
Number of Point Sources	
• Small (N < 20)	• MESOPUFF
• Medium (20 < N < 80)	• Choice is scenario-dependent
• Large (N > 80)	• MESOGRID
Dominant Meteorology	
• Zonal flows, moderate to high wind speeds	• MESOPUFF or MESOPLUME (MESOGRID*)
• Stagnating or recirculating flows	• MESOPUFF (MESOGRID*)
• Variable flow regimes	• MESOPUFF (MESOGRID*)
Model Sensitivity	
• Near-source concentration estimates, including sensitivity to plume diurnal fumigation cycle, small scale diffusion, and plume rise.	• MESOPUFF

*For large inventories.

- regulatory applications, e.g., new source review under the PSD provisions of the 1977 Clean Air Act where (1) the chief concern is the incremental impact on regional air quality of one or several increment-consuming new sources (use of MESOPUFF or MESOPLUME) or (2) where the regional background concentration fields must also be simulated, starting from a sizable emissions inventory containing both point sources and area sources (use of MESOGRID).

REFERENCES

Benkley, C. W. and A. Bass. 1979a. Development of Mesoscale Air Quality Simulation Models. Volume 2. User's Guide to MESOPLUME (Mesoscale Plume Segment) Model. EPA 600/7-79-XXX, Environmental Protection Agency, Research Triangle Park, NC, 141 pp.

Benkley, C. W. and A. Bass. 1979b. Development of Mesoscale Air Quality Simulation Models. Volume 3. User's Guide to MESOPUFF (Mesocale Puff) Model. EPA 600/7-79-XXX. Environmental Protection Agency, Research Triangle Park, NC, 118 pp.

Benkley, C. W. and A. Bass. 1979c. Development of Mesoscale Air Quality Simulation Models. Volume 6. User's Guide to the MESOPAC (Mesoscale Meteorology) Package. EPA 600/7-79-XXX. Environmental Protection Agency, Research Triangle Park, NC, 85 pp.

Benkley, C. W. and L. L. Schulman. 1979. Estimating Hourly Mixing Depths from Historical Meteorological Data. J. Appl. Meteor. 18:772-780.

Blackadar, A. K. 1962. The Vertical Distribution of Wind and Turbulent Exchange in the Neutral Atmosphere. J. Geophys. Res. 67: 3095-3102.

Boris, J. P., and D. L. Book. 1973. Flux-corrected Transport--I. SHASTA, A Fluid Transport Algorithm That Works. Jour. Comp. Phys. 11:38-69.

Briggs, G. S. 1975. Plume Rise Predictions. Lectures on Air Pollution and Environmental Impact Analyses. American Meteorological Society, Boston, MA, p. 67-114.

Clark, T. L. and R. E. Eskridge. 1977. Non-Divergent Wind Analysis Algorithm for the St. Louis RAPS Network. EPA 600/4-77-049. Environmental Protection Agency, Research Triangle Park, NC, 63 pp.

Draxler, R. R. 1977. A Mesoscale Transport and Diffusion Model. NOAA Tech. Memo ERL ARL-74, 31 pp.

Egan, B. A. and J. R. Mahoney. 1972. Numerical Modeling of Advection and Diffusion of Urban Area Source Pollutants. J. Appl. Meteor. 11:312-322.

Egan, B. A., K. S. Rao, and A. Bass. 1976. A Three-Dimensional Advective-Diffusive Model for Long Range Sulfate Transport and Transformation. Seventh International Technical Meeting on Air Pollution Modeling and its Application, Airlie, VA, September 7-10, 1976, p. 697-714.

REFERENCES (Continued)

Golder, P. 1972. Relations Among Stability Parameters in the Surface Layer. Bound. Layer Meteor. 3:47-58.

Hales, J. M., D. C. Powell and T. D. Fox. 1977. STRAM-An Air Pollution Model Incorporating Non-linear Chemistry, Variable Trajectories, and Plume Segment Diffusion. EPA 450/3-77-012. Environmental Protection Agency, Research Triangle Park, NC, 147 pp.

Heffter, J. L. 1965. The Variations of Horizontal Diffusion Parameters with Time for Travel Periods of One Hour or Longer. J. Appl. Meteor. 4:153-156.

Heffter, J. L. and A. D. Taylor. 1975. A Trajectory Model, Part I. A Regional-Continental Scale Transport, Diffusion and Deposition Model. NOAA Tech Memo. ERL ARL-50, 28 pp.

Hilst, G. R. 1970. Sensitivities of Air Quality Prediction to Input Errors and Uncertainties. Proceedings. Symposium on Multiple-Source Urban Diffusion Models. APC No. AP-86. Environmental Protection Agency, Research Triangle Park, NC, pp. 8-1 to 8-40.

Husar, R. B., J. P. Lodge, and D. J. Moore, eds. 1978. Workshop: Sulfur in the Atmosphere. Atmos. Environ. 12:7-23.

Liu, C. Y. and W. R. Goodin. 1976. An Iterative Algorithm for Objective Wind Field Analysis. Mon. Wea. Rev. 104:784-792.

Liu, M-K. and D. D. Durran. 1977. The Development of a Regional Air Pollution Model and Its Application to the Northern Great Plains. EPA-908/1 - 77-001. Environmental Protection Agency, Denver, CO, 281 pp.

Morris, C. S., C. W. Benkley and A. Bass. 1979. Development of Mesoscale Air Qulity Simulation Models. Volume 4. User's Guide to MESOGRID (Mesoscale Grid) Model. EPA 600/7-79-XXX Environmental Protection Agency, Research Triangle Park, NC, 105 pp.

Nappo, C. S. 1978. Workshop on Long-Range Trajectory-Puff and Plume Modeling of Continuous Source Emissions. NOAA Tech. Memo. ERL-ARL-72, 18 pp.

Nuber, J. A., A. Bass, M. T. Mills and C. S. Morris. 1977. A Review of Regional-Scale Air Quality Models for Long Distance Dispersion Modeling in the Four Corners Region. EPA-600/7-78-066, Environmental Protection Agency, Research Triangle Park, NC, 82 pp.

O'Brien, J. J., 1970. A Note on the Vertical Structure of the Eddy Exchange Coefficient in the Planetary Boundary Layer. J. Atmos. Sci. 27:1213-1215.

REFERENCES (Continued)

Pack, D. M., G. J. Ferber, J. L. Heffter, K. Telegadas, J. K. Angell, W. H. Hoecker and L. Machta. 1978. Meteorology of Long-Range Transport. Atmos. Environ. 12:425-444.

Plate, E. J. 1971. Aerodynamic Characteristics of Atmospheric Boundary Layers. U.S. Atomic Energy Commission [NTIS Ref. No. TID-25465], 190 pp.

Scire, J. S., J. E. Beebe, C. W. Benkley and A. Bass. 1979. Development of Mesoscale Air Quality Simulation Models. Volume 5. User's Guide to the MESOFILE Postprocessing Package. EPA 600/7-79-XXX. Environmental Protection Agency, Research Triangle Park, NC, 67 pp.

Sheih, C. M., G. D. Hess and B. B. Hicks. 1978. Design of Network Experiments for Regional-Scale Atmospheric Pollutant Transport and Transformation. Atmos. Environ. 12:1745-1753.

Start, G. E. and L. L. Wendell. 1974. Regional Effluent Dispersion Calculations Considering Spatial and Temporal Meteorological Calculations. NOAA Tech. Memo. ERL-ARL-44, 63 pp.

Turner, D. B. 1970. Workbook of Atmospheric Dispersion Estimates. U.S. Dept. of H.E.W, Public Health Service, Publ. 999-AP-26, 88 pp.

Wilson, W. E. 1978. Sulfates in the Atmosphere: a Progress Report on Project MISTT. Atmos. Environ. 12:537-548.

APPENDIX A

MESOPLUME TECHNICAL DISCUSSION

A.1 Basic Mass Conservation Equations

MESOPLUME, a variable-trajectory version of the conventional straight-line Gaussian plume model, is designed to take into account the spatial and temporal variations in the horizontal advection, diffusion, transformation, and removal mechanisms governing the dispersion of a plume on regional transport scales. In MESOPLUME, a continuous plume is modeled by subdividing the plume into a number of contiguous 'plume segment' elements, as illustrated in Figure A-1. The conservation of pollutant mass over a plume segment of length Δs is expressed by the mass balance equation:

$$\Delta Q = \left\{ \int_{o}^{\infty} \int_{-\infty}^{\infty} G(s,r,z) \, dr \, dz \right\} \Delta s \qquad \text{(A-1)}$$

$$+ \int_{o}^{\infty} \int_{-\infty}^{\infty} u \, C \, dr \, dz \Bigg|_{s+\Delta s} - \int_{o}^{\infty} \int_{-\infty}^{\infty} u \, C \, dr \, dz \Bigg|_{s}$$

where s, r, and z are the longitudinal, lateral, and vertical plume directions, $G(s,r,z)$ ($g \, m^{-3} s^{-1}$) is the rate of change (gain-loss) of pollutant concentration $C(s,r,z)$ ($g \, m^{-3}$) by conversion and removal processes, ΔQ ($g \, s^{-1}$) is the resultant rate of change of pollutant mass and u ($m \, s^{-1}$) is the wind speed. In the MESOPLUME model, $G(s,r,z)$ and u are considered to be constant from s to $s + \Delta s$, where s is the current distance of a plume segment endpoint from the emitting source, measured along the plume axis.

MESOPLUME permits the user to specify two possible vertical distribution functions; (1) a vertical Gaussian profile, ignoring any effects of the mixing lid H; or (2) a uniform vertical distribution below the mixing lid.

For Case 1, the ground-level axial plume concentration $C(s,r,0)$ is defined at the upwind edge of a plume segment by the expression:

$$C(s,r,0) = \frac{Q(s)}{\pi \, u \, \sigma_z(s) \, \sigma_y(s)} \exp\left[\frac{-r^2}{2\sigma_y^{\,2}}\right] \exp\left[\frac{-z^2}{2\sigma_z^{\,2}}\right] \qquad \text{(A-2)}$$

Preceding page blank

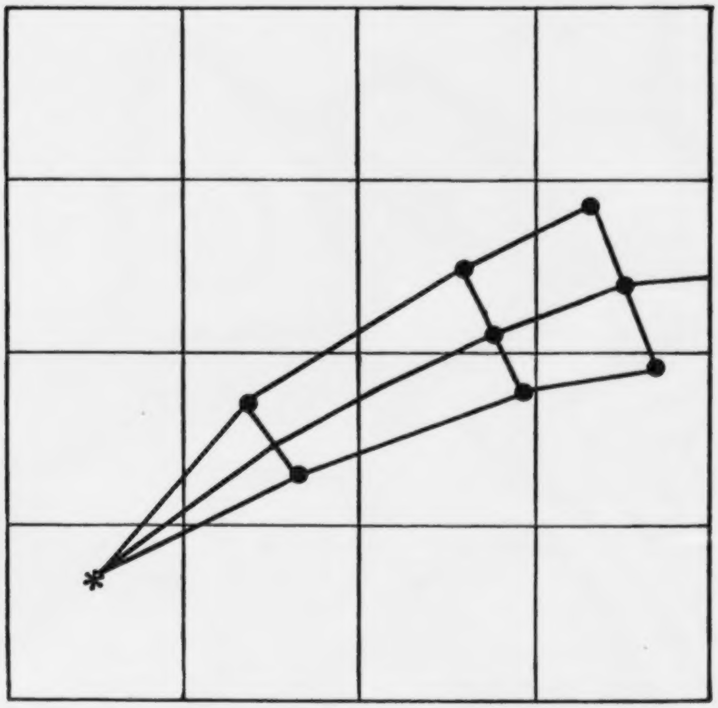

Figure A-1 The Variable Trajectory Plume Model Approach

807098a

where Q(s) is the pollutant mass flux and $\sigma_y(s)$, $\sigma_z(s)$ are the lateral and vertical Gaussian plume dispersion coefficient distributions at downwind distance s. Full reflection from the ground is assumed.

For Case 2, if the plume altitude (z) lies below the mixed lid H, the ground-level axial concentration is expressed at the upwind edge of the plume segment by the expression for uniform vertical mixing:

$$C(s,r,0) = \frac{Q(s)}{\sqrt{2\pi}\; u\; H_m\; \sigma_y(s)} \exp\left[\frac{-r^2}{2\sigma_y^{\,2}}\right] \qquad \text{(A-3)}$$

where H_m is the maximum mixing depth encountered by the plume segment (see Section A.8). If, rather, the plume centerline lies above the mixing lid, no ground-level concentrations are calculated. At the downwind edge (s+Δs) of the plume segment, the ground-level axial concentration (s+Δs,r,0) is expressed as:

$$C(s{+}ds,r,0) = \frac{\{Q(s)+(dQ/dt)\}\Delta t}{\sqrt{2\pi}\; u\; H_m\; \sigma_y(s+\Delta s)} \exp\left[\frac{-r^2}{2\sigma_y^{\,2}}\right] \qquad \text{(A-4)}$$

The MESOPLUME model solves the mass conservation Equation A-1 independently for both sulfur dioxide (SO_2) and sulfate ($SO_4^=$). The gain functions include terms for the loss (gain) of SO_2 ($SO_4^=$) by linear decay of SO_2 to $SO_4^=$ and terms for dry deposition of either species (see Sections A.5 and A.6).

A.2 The Grid System

The original coordinate system used in the STRAM model has been replaced in MESOPLUME by a simple Cartesian coordinate system. All spatial model input data (emission source inventories and meteorological fields) are referenced to the same grid, called the "basic computational" grid. To improve the resolution of the plume sampling function (see Section A.4.3), MESOPLUME uses a sampling grid that is a subset of the basic computational grid. The origin of the sampling grid may be placed anywhere on the basic computational grid (but not on the northern or eastern grid boundaries). The resolution of the sampling grid is a multiple of the resolution of the basic computational grid. Currently, the maximum allowable size of both the basic computational and sampling grids is 40 by 40 horizontal grid points. Figure A-2 illustrates one possible arrangement of basic computational and sampling grids. Note that the grid index of the origin (1,1) is assigned Cartesian coordinates x = 0, y = 0. The sampling grid in this example originates at (i = 2, j = 2) or (x = 1, y = 1) on the basic computational grid, and has a spatial resolution four times finer than the basic computational grid.

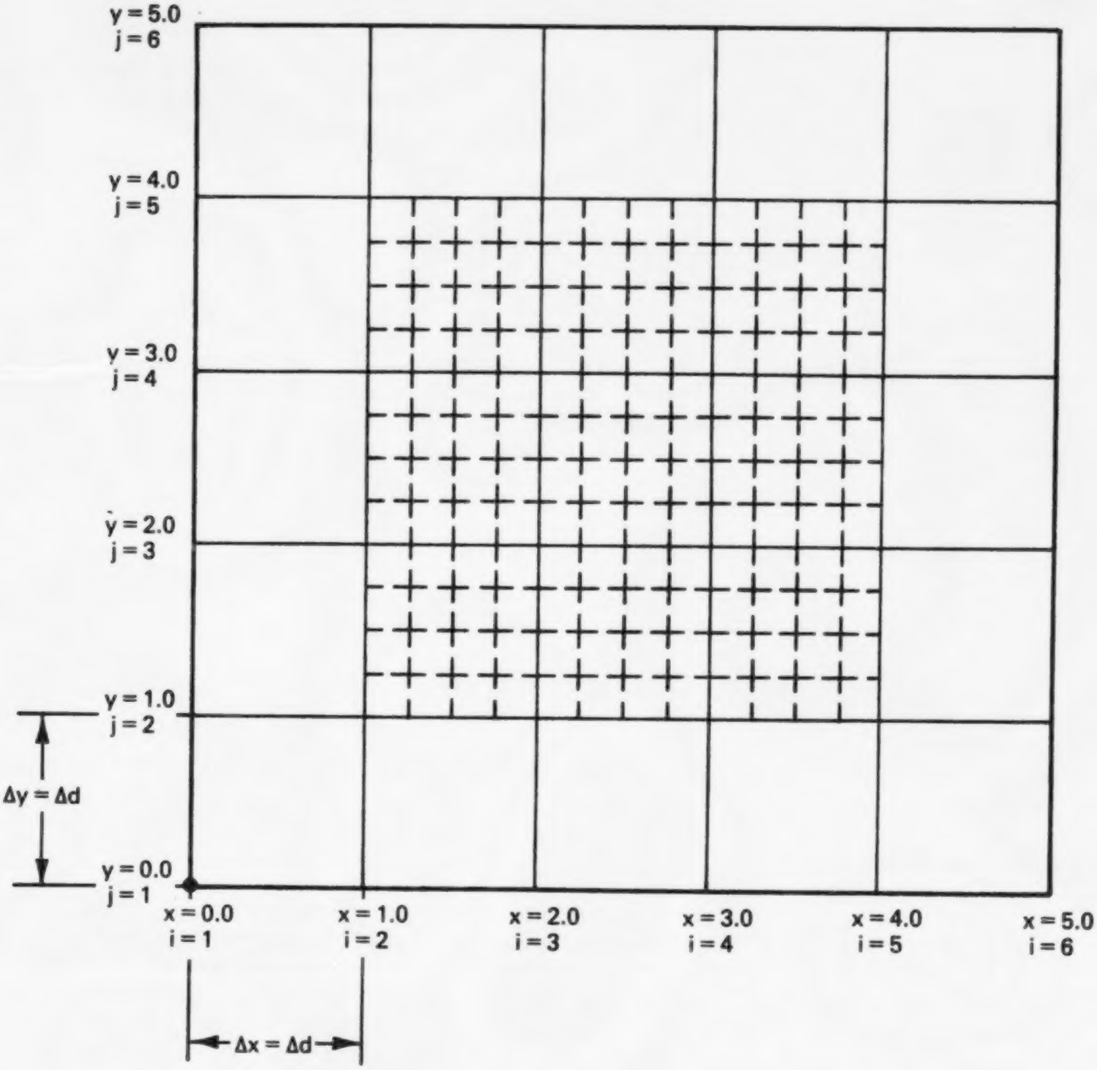
y = 5.0
j = 6
y = 4.0
j = 5
y = 3.0
j = 4
y = 2.0
j = 3
y = 1.0
j = 2
Δy = Δd
y = 0.0
j = 1
x = 0.0
i = 1
x = 1.0
i = 2
x = 2.0
i = 3
x = 3.0
i = 4
x = 4.0
i = 5
x = 5.0
i = 6
Δx = Δd

Figure A-2 One Possible Arrangement of Sampling and Basic Computational Grids

A.3 Specification of Model Inputs

MESOPLUME is, at present, driven by the meteorological fields produced by MESOPAC, a MESOscale meteorology PACkage (Benkley and Bass 1979c), but an alternative meteorological preprocessing system with appropriate grid resolution could be substituted by the user. MESOPLUME requires the following fields (usually at hourly intervals) interpolated to each model grid point:

- horizontal (u,v) wind components,
- mixing depth, and
- Pasquill-Gifford-Turner (PGT) stability class.

Use of MESOPAC model output by the MESOPLUME model is straightforward - the Cartesian coordinate system is identical in both models. Note that the horizontal (u,v) wind components are considered invariant with height. Vertical wind components are not used. The fields of PGT stability class are used by MESOPLUME in doing plume rise and plume growth calculations.

A.4 Plume Trajectory, Dispersion and Sampling Algorithms

The computational scheme of the MESOPLUME model has three distinct functional elements: (1) a Lagrangian plume trajectory function, (2) a plume dispersion function, and (3) a plume sampling function. The Lagrangian trajectory function is used to advect the endpoints of each plume segment during a basic time step; the resultant distance between consecutive endpoints defines the length of each plume segment. The widths at the upwind and downwind ends of each plume segment are determined by the plume dispersion function. Given the size and location of each plume segment, the plume sampling function computes the concentration exposure received during the time interval at each grid point that lies within the plume segment.

2.4.1 Lagrangian Trajectory Function

This section describes how the endpoints of a plume segment are advected during a time step; it has been adapted (but largely verbatim) from Hales et al. (1977, pages 15-18).

Let the components of the wind in the x and y grid directions along the trajectory be designated by $u[t;x(t),y(t)]$ and $v[t;x(t),y(t)]$, respectively,

where

$$x(t) = \frac{1}{\Delta d} \int_{o}^{t} u[t';x(t'),y(t')]dt'$$

$$y(t) = \frac{1}{\Delta d} \int_{o}^{t} v[t';x(t'),y(t')]dt'$$

$$x(0) = x_0 \ ; \ y(0) = y_0$$

$$u(0;x(0),y(0)) = u(x_0,y_0)$$

$$v(0;x(0),y(0)) = v(x_0,y_0)$$

and x_0,y_0 are the initial coordinates (origin) of a trajectory of total length s*. (The grid space unit Δd is used in the program to convert to nondimensional spatial units on the computational grid.) The vectors u(t;...) and v(t;...) provide a Lagrangian description of the velocity field. Increments of advection over a further time interval Δt are therefore given by

$$\Delta x = \frac{1}{\Delta d} \int_{t}^{t+\Delta t} u[t';x(t'),y(t')] \, dt' \ ; \qquad \text{(A-5a)}$$

$$\Delta y = \frac{1}{\Delta d} \int_{t}^{t+\Delta t} v[t';x(t'),y(t')] \, dt' \ . \qquad \text{(A-5b)}$$

After the new coordinates $x(t+\Delta t)$ and $y(t+\Delta t)$ are calculated for each incremented endpoint of a given plume, a check is made to see if any of these values are off the grid. If so, both the affected plume increment and all plume increments emitted from the same source previously are deleted from further consideration.

The integration of the wind components over the trajectory is approximated by a two-step iteration method involving bilinear interpolation in space and in time (see Figure A-3).

The various positions in Figure A-3 are best defined by equations:

$$x_1 = x(t) + u[t;x(t),y(t)] \ \Delta t \ ; \qquad \text{(A-6a)}$$

$$y_1 = y(t) + v[t;x(t),y(t)] \ \Delta t \ ; \qquad \text{(A-6b)}$$

$$x_2 = x_1 + u[t+\Delta t;x_1,y_1] \ \Delta t \ ; \qquad \text{(A-6c)}$$

$$y_2 = y_1 + v[t+\Delta t;x_1,y_1] \ \Delta t \ ; \qquad \text{(A-6d)}$$

---

*In practice, however, the exact definition of s in MESOPLUME is the current along-the-variable-plume-axis distance of a segment endpoint from a source. In time-varying flows, it may be somewhat different from the actual segment endpoint trajectory length.

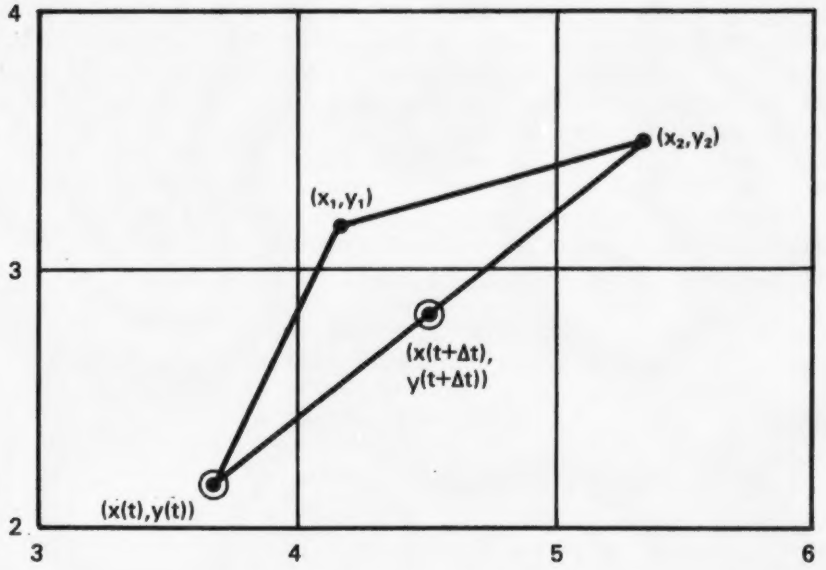
4
3
2
3
4
5
6
(x_1, y_1)
(x_2, y_2)
$(x(t+\Delta t),$
$y(t+\Delta t))$
$(x(t), y(t))$

Figure A-3 Calculation of the Trajectory of a Plume Segment Endpoint

$$x(t+\Delta t) = 0.5[x(t) + x_2] ; \qquad \text{(A-6e)}$$

$$y(t+\Delta t) = 0.5[y(t) + y_2] . \qquad \text{(A-6f)}$$

Thus, the new position $(x(t+\Delta t),y(t+\Delta t))$ is found by adding the vector average of two advection increments to the former position $(x(t),y(t))$. The first advection increment is calculated by advecting the plume increment for the entire interval Δt using the wind effective at $[x(t),y(t)]$ at time t. The addition of this increment to the position $[x(t),y(t)]$ yields the position (x_1,y_1). However, (x_1,y_1) is not assumed to be the actual end of the advection increment because the wind may change along the trajectory. A second advection increment is calculated using (x_1,y_1) as the starting point and the wind at that point effective at the end of the time increment. The addition of this advection increment to position (x_1,y_1) yields position (x_2,y_2). Then the new plume increment position $(x(t+\Delta t),y(t+\Delta t))$ is taken to be the point halfway along the line from $(x(t),y(t))$ to (x_2,y_2).

The bilinear interpolation by which the effective wind components u(t), and v(t) are calculated works as follows. Let t_n and t_{n+1} be the effective times of the two gridded wind fields closest to time t. Time interpolation weights t_1 and t_2 are defined by:

$$t_2 = \frac{t - t_n}{t_{n+1} - t_n} \qquad t_n \leq t < t_{n+1} ; \qquad \text{(A-7a)}$$

$$t_1 = 1 - t_2 . \qquad \text{(A-7b)}$$

Next, the location of $(x(t),y(t))$ is noted on Figure A-3. The coordinate values are between 3 and 4 for x(t) and between 2 and 3 for y(t). Accordingly:

$$X_q = x(t) - 3 ; \qquad \text{(A-8a)}$$

$$X_p = 1 - X_q ; \qquad \text{(A-8b)}$$

$$Y_q = y(t) - 2 ; \qquad \text{(A-8c)}$$

$$Y_p = 1 - Y_q . \qquad \text{(A-8d)}$$

This yields

$$\begin{aligned}u(t) = {} & t_1 X_p Y_p u(t_n;3,2) + t_2 X_p Y_p u(t_{n+1};3,2) \\ & + t_1 X_q Y_p u(t_n;4,2) + t_2 X_q Y_p u(t_{n+1};4,2) \\ & + t_1 X_p Y_q u(t_n;3,3) + t_2 X_p Y_q u(t_{n+1};3,3) \\ & + t_1 X_q Y_q u(t_n;4,3) + t_2 X_q Y_q u(t_{n+1};4,3) \ .\end{aligned} \qquad \text{(A-9)}$$

Similar equations hold for $v(t)$, $u(t+\Delta t)$, and $v(t+\Delta t)$. Therefore, the advection Equation A.5 is calculated from

$$\Delta x = \frac{1}{2\Delta d} \{u(t) + u(t+\Delta t)\}\Delta t; \qquad \text{(A-10a)}$$

$$\Delta y = \frac{1}{2\Delta d} \{v(t) + v(t+\Delta t)\}\Delta t. \qquad \text{(A-10b)}$$

The subsequent positions are given by

$$x(t+\Delta t) = x(t) + \Delta x \ ; \qquad \text{(A-11a)}$$

$$y(t+\Delta t) = y(t) + \Delta y \ . \qquad \text{(A-11b)}$$

A.4.2 The Plume Dispersion Function

This section, describing the evaluation of the plume dispersion parameters, has been taken largely verbatim, with modifications, from Hales et al. (1977, pp. 23-24). The plume dispersion parameters σ_y and σ_z are calculated for distances out to 100 km using plume growth formulas fitted to the curves of Turner (1970). For distances greater than 100 km the plume growth rates given by Heffter (1965) are used. The growth of a plume with travel time t or along the plume trajectory distance s from the source is represented by

$$\sigma_y(s+\Delta s) = \sigma_y(s) + \Delta s \left.\frac{d\sigma_y}{ds}\right|_{s+\Delta s/2} ; \qquad \text{(A-12)}$$

$$\sigma_y(t+\Delta t) = \sigma_y(t) + \Delta t \left.\frac{d\sigma_y}{dt}\right|_{t+\Delta t/2} . \qquad \text{(A-13)}$$

Similar equations for σ_z are used. These terms allow for spatial and temporal changes in stability class to be included, without violating the entropy principle (centerline concentrations cannot increase with downwind distance).

The integral formulas for σ_y and σ_z for travel distances less than 100 km are of the following forms

$$\sigma_y(s,\alpha) = Y_\alpha \, s^{0.9} \text{ (meters)}; \qquad \text{(A-14)}$$

$$\sigma_z(s,\alpha) = Z_\alpha \, s^{b_\alpha} \text{ (meters)}. \qquad \text{(A-15)}$$

Here α is a stability index designated as A, B, C, D, E, or F for the PGT stability categories. The coefficients Y_α, Z_α, and b_α are given in Table A-1 as a function of stability index α and yield σ_y and σ_z in meters when s is specified in meters. Because the integral formulas are not valid if the stability class changes over the travel distance s, the derivative forms are actually used to carry out the computations

$$\frac{d\sigma_y}{ds} = 0.9 \; Y_\alpha \; s^{-0.1} ; \qquad \text{(A-16)}$$

$$\frac{d\sigma_z}{ds} = b_\alpha \; A_\alpha \; s^{(b_\alpha - 1)} . \qquad \text{(A-17)}$$

MESOPLUME assumes that σ_y, σ_z = 0 at the origin (s = 0).

The derivative formulas used to grow σ_y and σ_z for travel distances greater than 100 km are those given by Heffter (1965):

$$\frac{d\sigma_y}{dt} \; (\text{m s}^{-1}) = 0.5 \qquad \text{(A-18)}$$

$$\frac{d\sigma_z}{dt} \; (\text{m s}^{-1}) = 0.5 \; (2K_z)^{1/2} \; t^{-1/2} \qquad \text{(A-19)}$$

TABLE A-1

COEFFICIENTS FOR DISPERSION PARAMETER FORMULAS

Stability Index α	Plume Growth Coefficients		
	Y_α	Z_α	b_α
A	0.36	0.00023	2.10
B	0.25	0.058	1.09
C	0.19	0.11	0.91
D	0.13	0.57	0.58
E	0.096	0.85	0.47
F	0.063	0.77	0.42

A.4.3 The Plume Sampling Function

Each plume segment resident on the grid (at the end of every time step Δt) is sampled, using the plume sampling function, to evaluate the average concentration experienced at each sampling and intersection during the previous time step. For example, consider the hypothetical plume segment depicted in Figure A-4. The plume segment centerline at time $t+\Delta t$ extends from (x,y) to $(x+\Delta x, y+\Delta y)$, the positions of the two consecutive plume segment endpoints at $t+\Delta t$. The plume segment length is $\Delta s = (\Delta x^2 + \Delta y^2)^{1/2}$. The lateral extent of a plume segment is considered to be truncated at $\pm 3\sigma_y$. This is a reasonable simplification--much less than 1% of the area under the Gaussian distribution function lies beyond $\pm 3\sigma_y$ from its center. In this example, plume segment radii of size $3\sigma_y(s)$ at the upwind edge (x,y) of the segment and of size $3\sigma_y(s+\Delta s)$ at the downwind edge $(x+\Delta x, y+\Delta y)$ are indicated. At time $t+\Delta t$, the grid point intersections (21,12), (22,12), (22,13), (23,13), and (22,14) are each impacted by the hypothetical plume segment; each grid point is assigned a certain average concentration $C(i,j)$ resulting from the presence of the plume segment over Δt. This evaluation is illustrated as follows: Suppose the grid point concentration $C(i,j)$ is to be calculated at (22,12). First, the ground-level concentrations $C(x,y)$ and $C(x+\Delta x, y+\Delta y)$ are computed using Equations 2-3 and 2-4 for the case of uniform vertical distribution. Next, a point (x',y') is found such that the line segment of length r constructed from (x',y') to the grid point (i,j) is perpendicular to the plume segment centerline. The effective source strength $C(x',y')$ is then computed by linear interpolation:

$$C(x',y') = \frac{C(x,y)\,\Delta s_2 + C(x+\Delta x,\, y+\Delta y)\,\Delta s_1}{\Delta s_1 + \Delta s_2} \qquad \text{(A-20)}$$

The lateral plume dispersion coefficient $\sigma_y(x,y)$ is similarly interpolated from:

$$\sigma_y(x',y') = \frac{\sigma_y(x,y)\,\Delta s_2 + \sigma_y(x+\Delta x,\, y+\Delta y)\,\Delta s_1}{\Delta s_1 + \Delta s_2} \qquad \text{(A-21)}$$

Finally, the grid point concentration $C(22,12)$ is computed as:

$$C(22,12) = C(x',y') \exp\left(\frac{-r^2}{2\sigma_y^{\,2}(x',y')}\right) \qquad \text{(A-22)}$$

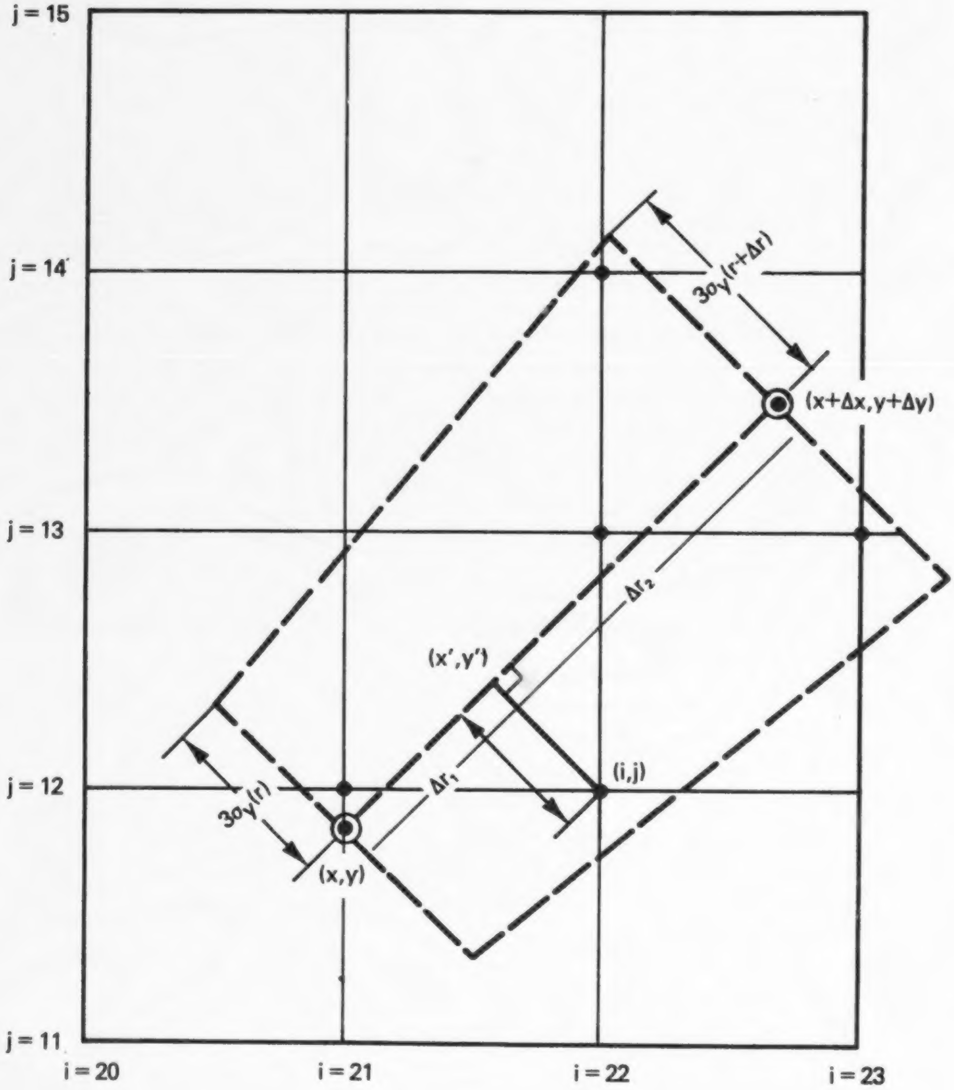
j = 15
j = 14
j = 13
j = 12
j = 11
i = 20
i = 21
i = 22
i = 23
3σy(r+Δr)
(x+Δx,y+Δy)
Δr₂
(x',y')
(i,j)
Δr₁
3σy(r)
(x,y)

Figure A-4 Calculation of the Concentration C(i,j) by the Sampling Function

7902291

If a grid point lies within more than one plume segment at the end of a time step (for example, because plumes of multiple sources overlap), the total concentration at the grid point $C_T(i,j)$ is computed as the sum of the individual contributions:

$$C_T(i,j) = \sum_{m=1}^{m_T} C_m(i,j) \tag{A-23}$$

where m_T is the total number of segments impacting the grid intersection (i,j) during the time step of interest. Note that a plume segment is only sampled beginning with the second time step of its history and at every time step thereafter.

The MESOPLUME model has two peculiarities intrinsic to the basic advective-diffusive scheme of the model, which can present problems when the sampling function is applied. These problems arise from (1) the inverse-wind speed dependence of the concentration algorithm (Equation A-2) and (2) the way in which adjacent plume segments are actually juxtaposed in a curvilinear flow. As an example of the inverse-wind speed dependence problem, consider the case illustrated in Figure A-5, for which the wind flow along the plume axis rapidly decelerates, and suppose u_A, the average wind speed over segment A, is twice u_B, the average wind speed over segment B.* Neglecting removal processes, MESOPLUME evaluates the concentration $C(x_1,y_1)$ at the downwind edge of segment A according to Equation A-4:

$$C(x_1,y_1)\Big|_A = \frac{Q}{\sqrt{2\pi}\, u_A\, \sigma_y(x_1,y_1)\, H_m} \tag{A-24}$$

but can also evaluate the concentration $C(x_1,y_1)\big|_B$ at the same point using Equation A-3 as appropriate to the upwind edge of segment B using u_B instead. Since $u_A = 2u_B$,

$$C(x_1,y_1)\Big|_B = 2C(x_1,y_1)\Big|_A \tag{A-25}$$

If the grid resolution is such that severe discontinuities in the wind field occur, the MESOPLUME model will indeed predict plume centerline concentrations increasing with downwind distance. This prediction, a violation of the second law of thermodynamics, represents a major shortcoming of the plume segment model--it cannot treat stagnation flows correctly.

---

*This does not imply that the two-dimensional wind field is significantly divergent--the local flow about segments A and B may be exactly non-divergent if the mass fluxes through the lateral boundaries are "correct."

To address the second problem, that of juxtaposing adjacent plume segments, consider the situation illustrated in Figure A-6. In this figure two adjacent plume segments are advected in a highly curvilinear flow. In this case, for each plume segment, the lateral lines that define the plume segment widths (at the upwind and downwind end points) are constructed to be perpendicular to the local plume segment axes. Therefore, if the average wind direction used to advect segment B is very different from the average wind direction used to advect segment A, the plume segments will not be perfectly contiguous, as shown. In the example, there is a shaded region in which grid points will receive two concentration doses during one time step and also a region where the plume may actually "pass over" a grid point without impacting it at all. This illustrates a second potentially serious shortcoming of the model - it cannot treat strongly sheared flows (e.g., recirculating flows) correctly.

A.5 Conversion of Sulfur Dioxide to Sulfate

MESOPLUME represents the conversion of SO_2 to $SO_4^=$ as a simple linear rate function--the changes in mass of each pollutant in one time step Δt are given by the time-discretized equations:

$$\Delta Q^n(SO_2) = k_1 Q^n(SO_2) \Delta t \qquad \text{(A-26a)}$$

$$\Delta Q^n(SO_4^=) = -1.5 k_1 Q^n(SO_2) \Delta t \qquad \text{(A-26b)}$$

where $Q^n(SO_2)$ is the mass of SO_2 at the beginning of the nth time step and $k_1(s^{-1})$ is the conversion rate constant. MESOPLUME uses the nominal value $k_1 = -5.56 \times 10^{-6}$, suggested by Hales et al. (1977), unless otherwise specified by the user.

Note that the conversion of SO_2 to $SO_4^=$ represented by Equation A-26 is (1) independent of the vertical or horizontal distribution of SO_2 within a plume and (2) independent of whether a plume lies above or below the mixing height.

For the solutions to be adequate representations of the continuous exponential equations (e.g., $\dot{Q}(SO_2) = k_1 Q(SO_2)$), Q should not change appreciably over the time interval Δt. Since this is frequently not the case, the time interval Δt is automatically subdivided into as many subintervals $\Delta t'$ as are required to ensure that no more than a specified fraction ΔQ_f of the mass Q is removed by decay during a subinterval $\Delta t'$. This process is described further in the next section.

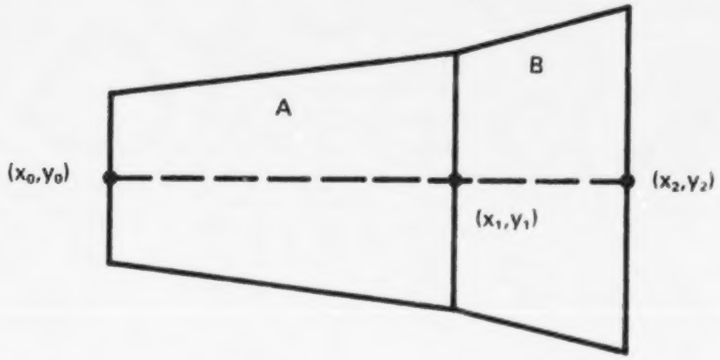
A
B
(x₀,y₀)
(x₁,y₁)
(x₂,y₂)

Figure A-5 A Schematic Representation of Adjacent Plume Segments in Rapidly Decelerating Flow

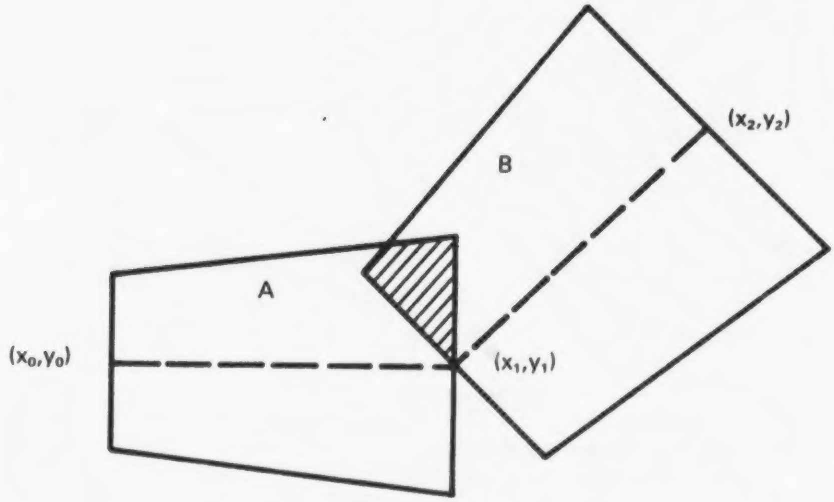
A
B
(x₀,y₀)
(x₁,y₁)
(x₂,y₂)

Figure A-6 A Schematic Representation of Adjacent Plume Segments in Highly Curvilinear Flow

A.6 Dry Deposition of Sulfur Dioxide and Sulfate

The changes of mass ΔQ^n(g) of each pollutant resulting from dry deposition are given by:

$$\Delta Q^n(SO_2) = -(v_d(SO_2)\ Q^n(SO_2)\ \Delta t)\ /\ H_m \qquad \text{(A-27a)}$$

$$\Delta Q^n(SO_4^=) = -(v_d(SO_4^=)\ Q^n(SO_4^=)\ \Delta t)\ /\ H_m \qquad \text{(A-27b)}$$

where $Q^n(SO_2)$ and $Q^n(SO_4^=)$ are the masses of SO_2 and $SO_4^=$, respectively, in the plume segment at the beginning of the time step, $v_d(SO_2)$ and $v_d(SO_4^=)$ are the deposition velocities of each pollutant, and H_m is the vertical depth of the plume segment (see Section A.8). MESOPLUME uses the nominal values $v_d(SO_2) = 0.01$ (m/s) and $v_d(SO_4^=) = 0.001$ (m/s), as suggested by Hales et al. (1977), unless otherwise specified by the user.

As described before, MESOPLUME automatically ensures that the mass Q does not change within one subinterval $\Delta t'$ by more than a user-specified fraction ΔQ_f. Taking into account both SO_2 removal mechanisms (decay and deposition), the expression used by MESOPLUME to specify the subinterval $\Delta t'$ is

$$\Delta t' = \text{MIN}\left\{\frac{\Delta Q_f(SO_2)}{-k_1}\ ,\ \frac{\Delta Q_f(SO_2)\ H_m}{v_d(SO_2)}\right\} \qquad \text{(A-28)}$$

In other words, the subinterval size $\Delta t'$ is chosen automatically by MESOPLUME at the beginning of each basic interval Δt such that no more than a specified fraction ΔQ_f of SO_2 mass is removed by either mechanism (or, no more than $2\Delta Q_f$ by both mechanisms combined) within $\Delta t'$. It should be emphasized that the conversion and removal rates are not affected by this restriction. Also, individual puff trajectories are not updated at each subinterval $\Delta t'$; they remain unchanged over the basic interval Δt.

A.7 Plume Rise

The effective emission height h_e of each plume segment is computed as $h_e = h_s + h_p$, where h_s is the stack height (m) and h_p is the plume rise (m). The plume rise equations used by the MESOPLUME model are those described by Briggs (1975) for equilibrium (final) plume rise. For unstable and neutral conditions with $h' \leq H$ (i.e., the plume does not rise into an elevated stable layer)

$$h_p = h' = 1.6\ F^{1/3}\ (3.5\ x^*)^{2/3}\ u^{-1} \qquad \text{(A-29a)}$$

For unstable and neutral conditions with h' > H (i.e., plume penetrates into on elevated stable layer)

$$h_p = \text{MIN}\ \{h'\ ,\ (z_b^3 + 18.75\ F\ u_m^{-1}\ S^{-1})^{1/3}\}\ ; \qquad \text{(A-29b)}$$

for stable conditions when $u \geq 1.37$ m/s

$$h_p = 2.6\ F^{1/3}\ S^{-1/3}\ u^{-1/3}\ ; \qquad \text{(A-29c)}$$

for stable conditions when $u < 1.37$ m/s

$$h_p = 5.0\ F^{1/4}\ S^{-3/8}\ . \qquad \text{(A-29d)}$$

where:

F = buoyancy flux (m^4/s^3)
x^* = $34.49\ F^{0.4}$ for $F > 55$
= $14.0\ F^{0.625}$ for $F \leq 55$
S = $(g/T)(\partial\theta/\partial z)$
g = $9.8\ m\ s^{-2}$
T = 290°K
$\partial\theta/\partial z$ = $0.0137°K\ m^{-1}$
H = mixing depth (m)
z_b = $H - h_s$ (m)
u = wind speed ($m\ s^{-1}$)
u_m = MAX $\{u\ ,\ 1.37\}$

A.8 Treatment of Plume Fumigation

When the "uniform vertical distribution" option is elected, MESOPLUME takes the spatial and temporal variations in the mixing height into consideration to determine the extent at ground level pollutant impact:

(a) For a plume element centerline less than the mixing height, MESOPLUME arbitrarily assigns the element a height of zero and immediately mixes the mass of the plume element uniformly through the mixing depth, with the mixing lid acting as a perfect reflector. Equations A-3 and A-4 are then applied to compute around level concentrations.

(b) For a plume element centerline greater than the mixing height, no impact of the element is felt at the ground. However, if subsequently the mixing height becomes greater than the height of the plume element centerline, the entire plume element is immediately mixed uniformly through the mixing depth, and Equations A-3 and A-4 again apply.

The mixing depth encountered by a plume element is likely to change over time and space. MESOPLUME assumes that a plume element residing in the mixed layer is always uniformly mixed throughout the maximum mixing depth H_m encountered by the element in its progression through the computational space-time grid.

The restriction of uniform plume element properties through a characterizable depth such as H_m is imperative for a one-layer model such as MESOPLUME to ensure that parcels of material, once entrained, are not bifurcated in the vertical when the height of the mixing lid changes. Therefore, in the MESOPLUME model a plume segment, once entrained, is uniformly mixed through a realistic height, consistent with the following assumptions:

(a) When convection ceases in the late afternoon, turbulent energy in the afternoon mixed layer dissipates. Once the energy of the large convective cells is completely damped, the remaining small scale energy is not sufficient to yield a vertical entrainment rate comparable to the daytime entrainment rate produced by large convective eddies.

(b) The stable lid capping the convective layer most likely maintains some integrity after convection ceases and acts to prohibit any additional vertical entrainment of plume material.

(c) A modeling approach that redistributes mass into a shallower layer when the mixing depth decreases will violate the second law of thermodynamics.

Since no mechanism remains for turbulent transfer of pollutant material either upwards or downwards once the mixing depth decreases, it is asserted that the height most appropriate to define the extent of vertical mixing of a segment is the maximum mixing height H_m that the segment encounters during any portion of its travel.

A hypothetical example is given in Figure A-7 to schematically illustrate the interaction of the MESOPLUME vertical distribution algorithm and the mixing depth progression algorithm used by MESOPAC [Benkley and Bass (1979c), Benkley and Schulman (1979a)]. Here consider two instantaneous parcels of material released at different times from a source with an effective stack height of 250 m; the first release is made at 0300 GMT on the first day; the second release is made at

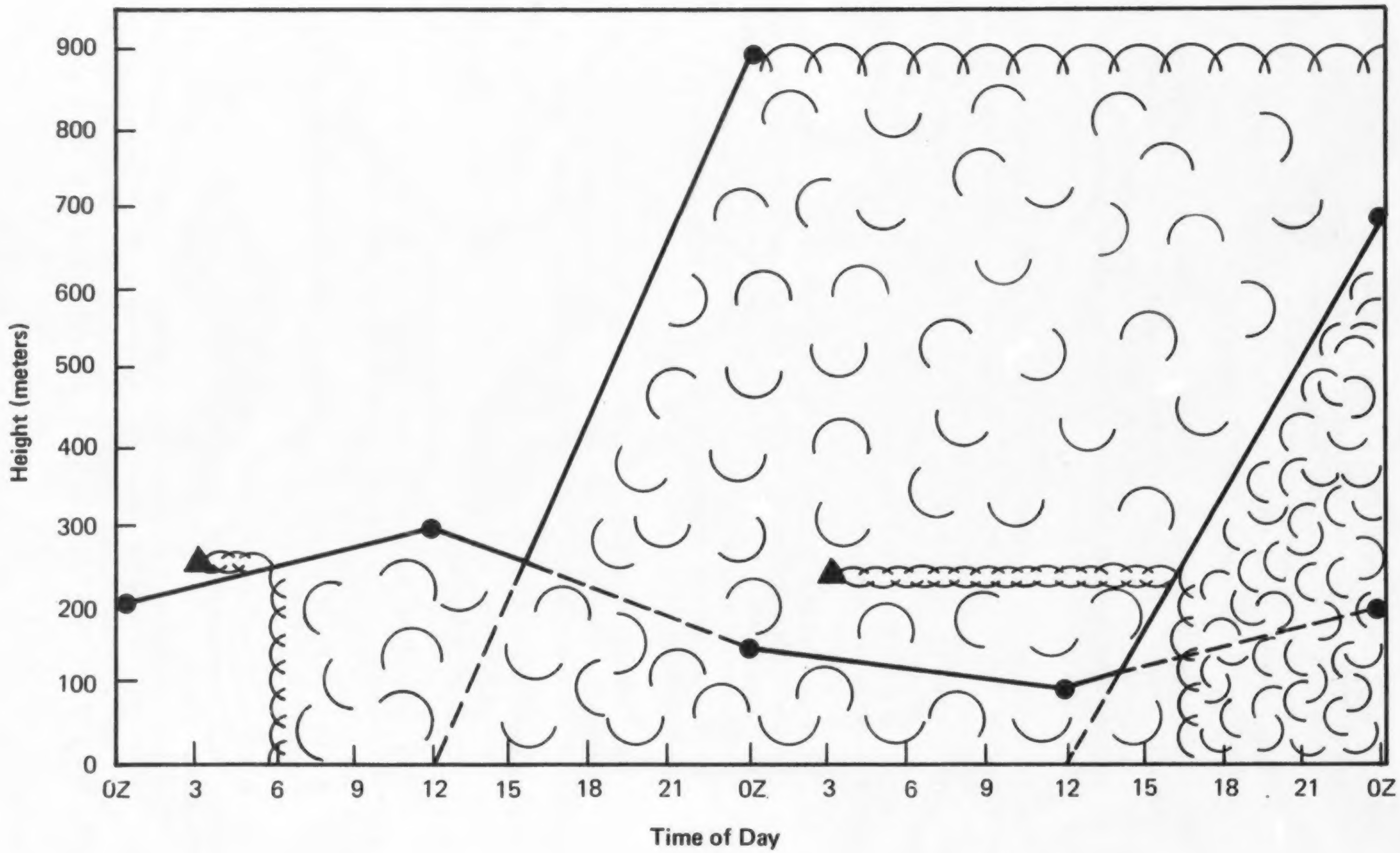

Figure A-7 Response of Two Plume Elements to Changes in Mixing Depth

0300 GMT on the second day. Assume that the hypothetical source is located in the western United States - so that 0000 GMT corresponds to late afternoon -the usual time of maximum mixing depth.

The first parcel is entrained at 0600 GMT on Day 1 as the nocturnal boundary layer oscillates slightly upward in height. MESOPLUME immediately mixes the parcel uniformly throughout this mixing depth. This first parcel is mixed uniformly through 900 m by 0000 GMT on Day 2, and remains mixed through 900 m subsequent to that time, even though the height of the mixed layer collapses. The second parcel, emitted at 0300 GMT on Day 2 is fumigated at 1500 GMT and is mixed uniformly through 700 m by the end of the afternoon. Therefore, the first parcel, emitted at 0300 GMT on Day 1, remains uniformly mixed through a deeper vertical layer than the second parcel; this is consistent with the greater extent of mixing on the first day as compared to the second day.

This mixing depth/fumigation scheme exhibits at least two shortcomings.

- When a plume segment becomes bifurcated in the vertical by collapse of the mixing lid, how should the plume segment lateral dispersion rate be characterized? Because MESOPLUME is a one-layer model, the same set of horizontal dispersion coefficients must be applied to both the above-mixing-lid and the below-mixing-lid portions of the bifurcated segment.

- The dry deposition algorithm (see Section A.6) removes SO_2 and $SO_4^=$ at a rate proportional to the surface concentration--this loss is then redistributed throughout the entire vertical extent of the plume. It would be more realistic to distribute the loss only through the current mixing depth, but this is not possible in a one-layer plume segment model.

It is felt that these limitations of the scheme are necessary for a method that is both computationally practical and yet realistic for use with a one-layer model. The inclusion of a fumigation cycle is very important; the marked effects of plume fumigation on the distribution of regional-scale ground-level concentration patterns are illustrated in Section 3.3.

A.9 Comparison to the Conventional Gaussian Plume Model

From the point of view of possible regulatory applications, one of the most attractive features of MESOPLUME is its ability to recreate the results of the conventional Turner Workbook plume model (using PGT coefficients). When MESOPLUME is run with appropriate uniform steady-state meteorology and fine spatial resolution, it can reproduce the

Turner workbook results to a high degree. This can be demonstrated, for example, under the following test conditions:

- The horizontal grid spacing of the model is reduced, e.g., to 5 km.
- The meteorological fields (wind direction, wind speed, mixing height and PGT stability class) used to drive MESOPLUME are taken to be spatially uniform and constant in time.
- MESOPLUME is run with one source until quasi-steady-state conditions are well established; that is, plume segments are created at the same uniform rate at which they disappear off the edge of the grid.

Under these special test conditions, MESOPLUME simulates very well the Turner Workbook plume concentrations out to distances of 100 km from an emission source. (The PGT σ_y and σ_z curves, represented in the model by piecewise linear power law fits, are only defined to 100 km.) Table A-2 and Figure A-8 provide a representative illustration of how closely MESOPLUME results compare to those obtained for the conventional Gaussian plume model using the PGT "D" curve for σ_y, and a uniform vertical distribution. Overall, the comparison is excellent--the very small fractional differences (typically less than 2%) are attributable mostly to inexact fitting of the PGT σ_y curve by the power law function used in MESOPLUME. The somewhat larger deviations near the source are expected - the results shown here were obtained with a wind velocity and time step corresponding to plume segments about 5 km in length - so, near the source, the linear averaging done by the sampling function does not approximate accurately the power law behavior of the plume centerline concentrations. It is expected that with use of smaller time steps and correspondingly shorter plume segments, the comparison of MESOPLUME to the Turner Workbook plume in the very near field would be even closer.

In its present version, MESOPLUME does not include an option for a reflected Gaussian vertical distribution, so that *at distances where the plume does not yet approach a uniform vertical distribution, MESOPLUME will not give correct results*. Under stable flow conditions, for example, plumes may not approach a uniform vertical distribution for many kilometers downwind. This version of MESOPLUME should therefore only be used at and beyond distances for which the assumption of uniform vertical mixing is appropriate - often only at distances of 100 km or more. [It would be very simple to modify the present version, however, to incorporate an optional Gaussian reflected vertical distribution so as to make MESOPLUME suitable also for near-field computations.]

TABLE A-2

COMPARISON OF Cu/Q VALUES FOR MESOPLUME AND TURNER WORKBOOK-COMPUTED VALUES

($u = 2.78$ m s^{-1}, PGT Class = D, H = 1000 m,
uniform vertical distribution)

Distance (km)	PGT σ_y (m)	Turner Workbook ($C\ u\ Q^{-1}$)	MESOPLUME ($C\ u\ Q^{-1}$)	Fractional Deviation
10	550	7.25×10^{-7}	7.77×10^{-7}	0.07
15	780	5.11	5.94	0.16
20	1,000	3.99	4.11	0.03
25	1,220	3.27	3.47	0.06
30	1,420	2.80	2.83	0.01
35	1,620	2.46	2.50	0.02
40	1,820	2.19	2.19	0.00
45	2,020	1.97	1.97	0.00
50	2,200	1.81	1.78	-0.02
55	2,400	1.66	1.64	-0.01
60	2,600	1.53	1.50	-0.02
65	2,775	1.44	1.42	-0.01
70	2,975	1.34	1.31	-0.02
75	3,200	1.25	1.25	0.00
80	3,375	1.18	1.17	-0.01
85	3,550	1.12	1.11	-0.01
90	3,700	1.08	1.06	-0.02
95	3,850	1.04	1.00	-0.04
100	4,000	1.00	0.95	-0.05

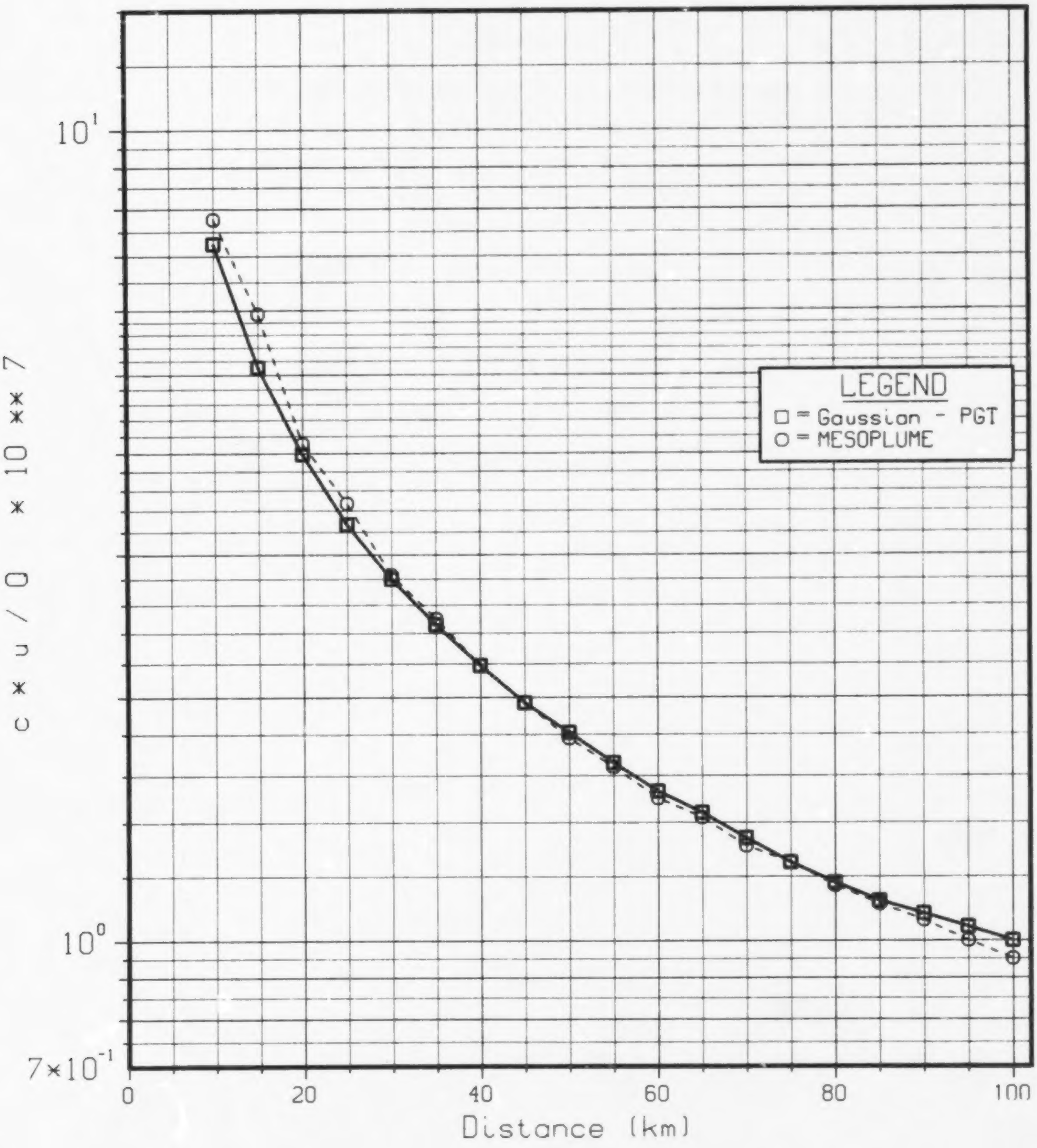

Figure A-8 MESOPLUME vs. the Conventional Gaussian Plume

APPENDIX B

MESOPUFF TECHNICAL DISCUSSION

B.1 Basic Mass Conservation Equations

MESOPUFF, a discretized variable-trajectory version of the conventional straight-line Gaussian plume model, is designed to take into account the spatial and temporal variations in the advection, diffusion, transformation, and removal mechanisms governing plume dispersion on regional transport scales. In MESOPUFF, a continuous plume is modeled by subdivision into a sufficient number of discrete "puffs" of circular horizontal cross section, as illustrated in Figure B-1. The conservation of pollutant mass in a puff transported a distance Δs is expressed by the mass balance equation:

$$\Delta Q = \int_0^{\infty} \int_{-\infty}^{\infty} \int_{-\infty}^{\infty} G(r, \theta, z) \, dr \, d\theta \, dz \tag{B-1}$$

$$= \frac{u}{\Delta s} \int_0^{\infty} \int_{-\infty}^{\infty} \int_{-\infty}^{\infty} C \, dr \, d\theta \, dz \Bigg|_{s+\Delta s} - \frac{u}{\Delta s} \int_0^{\infty} \int_{-\infty}^{\infty} \int_{-\infty}^{\infty} C \, dr \, d\theta \, dz \Bigg|_{s}$$

where r, θ, define points relative to the puff center in cylindrical coordinates, $G(r,\theta,z)$ ($g\ m^{-3}\ s^{-1}$) is the rate of change (gain-loss) of pollutant concentration $C(r,\theta,z)$ ($g\ m^{-3}$), ΔQ ($g\ s^{-1}$) is the resultant rate of change of pollutant mass, and u($m\ s^{-1}$) is the wind speed. In the MESOPUFF model, $G(r,\theta,z)$ and u are constant for s to $s + \Delta s$, where s is defined as the total distance a puff has traveled since it was emitted.*

For a discrete puff lying below the mixing height H, the circularly symmetric ground-level puff concentration $C(r,0;s)$ is defined as

$$C(r,0;s) = \frac{Q(s)}{2\pi \, \sigma_y^{\,2}(s) \, g_1(z)} \exp\left(\frac{-r^2}{2\,\sigma_y^{\,2}(s)}\right) g_2(z) \tag{B-2}$$

where Q(s) is the pollutant mass flux and $\sigma y(s)$ the "radial" Gaussian plume dispersion coefficient at distance s. The use of a "radial" Gaussian dispersion coefficient is a convenient computational device,

---

*By contrast, in the MESOPLUME (plume segment) model, s is the current distance of a plume segment endpoint from the emitting source, measured along the plume axis; for temporally varying flows, the two definitions can yield significantly different values of s.

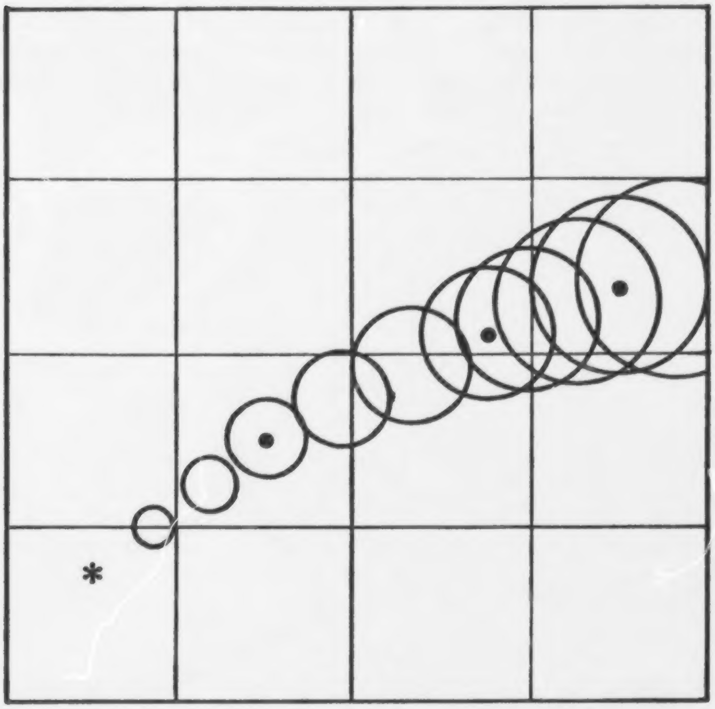

Figure B-1 The Variable Trajectory Puff Model Approach nothing more. The functions $g_1(z)$ and $g_2(z)$ are dependent upon the vertical distribution of concentration in the puff. Replacing H by H_m, the maximum mixing depth encountered by a puff (see Section B.8), MESOPUFF permits the user to specify one of two possible algorithms for the distribution function g(z), namely

1) a uniform vertical distribution algorithm within H_m, such that $g_1(z) = H_m$ and $g_2(z) = 1.0$, and

2) a Gaussian, multiple reflection algorithm where:

   - if $\sigma_z < 2\ H_m$, $g_1(z) = \sqrt{2\pi}\ \sigma_z$ and $g_2(z)$ is a function that accounts for multiple reflection effects and
   - if $\sigma_z \geq 2\ H_m$, $g_1(z) = H$, and $g_2(z) = 1.0$.

For regional-scale transport, e.g., at distances from 100 to 1,000 km from a source, either algorithm will produce substantially similar results, as a rule, because at travel distances $\gtrsim 100$ km σ_z is likely to be greater than $2H_m$.

Using the uniform vertical distribution function (1), the ground level puff concentration C(r,0;s) at distance s is

$$C(r,0;s) = \frac{Q(s)}{2\pi\ \sigma_y^2(s)\ H_m} \exp\left(\frac{-r^2}{2\ \sigma_y^2(s)}\right) \tag{B-3}$$

At distance s+Δs, the ground level concentration becomes

$$C(r,0;s+\Delta s) = \frac{Q(s+\Delta s)}{2\pi\ \sigma_y^2(s+\Delta s)\ H_m} \exp\left(\frac{-r^2}{2\ \sigma_y^2(s+\Delta s)}\right) \tag{B-4}$$

To ensure that a series of discrete puffs overlap along the variable plume axis with sufficient density to approximate a continuous plume, an individual puff (as described by Equation B-2), should not travel a distance Δs greater than $2\ \sigma_y$ in one time step Δt. Where wind speeds are large enough that this condition would be violated, it is necessary to subdivide further the time step used to interpolate puff concentrations to grid points.

The MESOPUFF model solves the mass balance equation (B-1) independently for both sulfur dioxide (SO_2) and sulfate ($SO_4^=$). The "gain" functions for each species include terms for the loss (gain) of SO_2 ($SO_4^=$) by linear decay of SO_2 to $SO_4^=$, and also include terms for dry deposition of either species--see Sections B.5 and B.6.

B.2 The Grid System

To facilitate the interaction of the MESOPUFF model with a number of input and output routines and pre- and postprocessors, a simple Cartesian coordinate system has been adopted for MESOPUFF. All spatial model input data (emission source inventories and meteorological fields) are referenced to the same grid, called the "basic computational" grid. To improve the resolution of the plume sampling function (see Section B.4.3), MESOPUFF uses a sampling grid that is a subset of the basic computational grid. The origin of the sampling grid may be placed anywhere on the basic computational grid (other than on the northern or eastern grid boundaries). The resolution of the sampling grid is a multiple of the resolution of the basic computational grid. Currently, the maximum allowable size of both the basic computational and sampling grids is 40 by 40 horizontal grid indices. Figure B-2 illustrates one possible arrangement of basic computational and sampling grids. Note that the grid index of the origin (1,1) is assigned Cartesian coordinates $x = 0$, $y = 0$. The sampling grid in this example originates at ($i = 2$, $j = 2$) or ($x = 1$, $y = 1$) on the basic computational grid, and a spatial resolution four times finer than the basic computational grid.

B.3 Specification of Model Inputs

MESOPUFF is, at present, driven by the meteorological fields produced by the MESOPAC MESOscale meteorology PACkage (Benkley and Bass 1979c), but an alternative meteorological preprocessing system with appropriate grid resolution could be substituted by the user. MESOPUFF requires the following fields (usually at hourly intervals) interpolated to each model grid point:

- horizontal (u,v) wind components,
- mixing depth, and
- Pasquill-Gifford-Turner (PGT) stability class.

Use of MESOPAC model output by the MESOPUFF model is straightforward-the Cartesian coordinate system is identical in both models. Note that the horizontal (u,v) wind components are considered invariant with height. Vertical wind components are not used. The fields of PGT stability class are used by MESOPUFF in doing plume rise and plume growth calculations.

B.4 Puff Trajectory, Dispersion and Sampling Algorithms

The computational scheme of the MESOPUFF model has three distinct functional elements: (1) a Lagrangian puff trajectory function, (2) a puff dispersion function, and (3) a puff sampling function. The

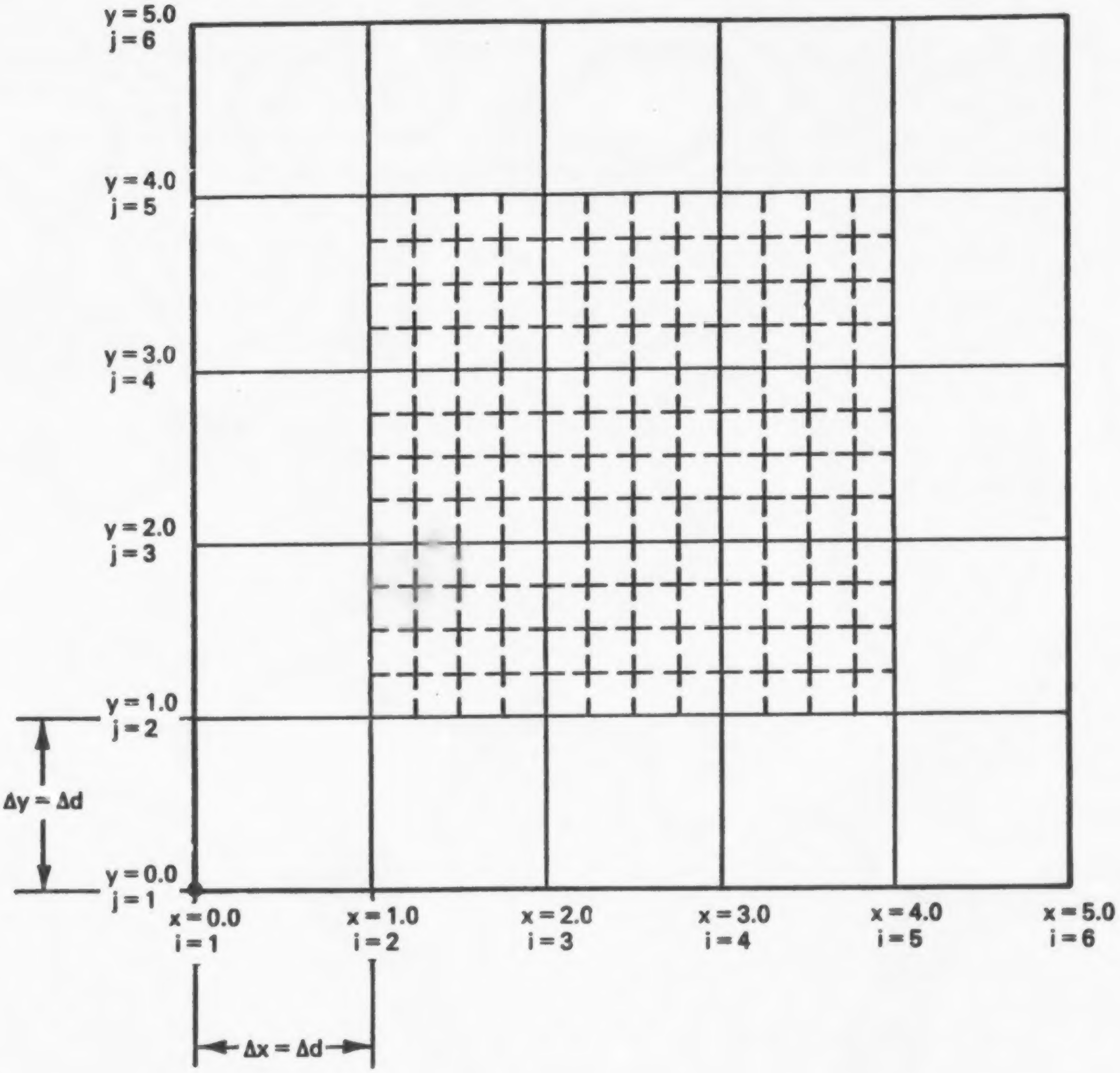
y = 5.0
j = 6
y = 4.0
j = 5
y = 3.0
j = 4
y = 2.0
j = 3
y = 1.0
j = 2
Δy = Δd
y = 0.0
j = 1
x = 0.0
i = 1
x = 1.0
i = 2
x = 2.0
i = 3
x = 3.0
i = 4
x = 4.0
i = 5
x = 5.0
i = 6
Δx = Δd

Figure B-2 One Possible Arrangement of Sampling and Basic Computational Grids

Lagrangian trajectory function is used to advect the centerpoint of each puff during a basic time step. The radius of each puff is determined by the puff dispersion function. Given the size and location of each puff, the puff sampling function computes the concentration exposure received during the time interval at each grid point by summing up the individual puff contributions at each grid point.

B.4.1 Lagrangian Trajectory Function

This section describes how the centerpoint of a puff is advected during a time step; it has been adopted (but largely verbatim) from Hales et al. (1977, pages 15-18).

Let the components of the wind in the x and y grid directions along the trajectory be designated by u[t;x(t),y(t)] and v[t;x(t),y(t)], respectively,

where

$$x(t) = \frac{1}{\Delta d} \int_{o}^{t} u[t';x(t'),y(t')]dt'$$

$$y(t) = \frac{1}{\Delta d} \int_{o}^{t} v[t';x(t'),y(t')]dt'$$

$$x(0) = x_0 \; ; \; y(0) = y_0$$

$$u(0;x(0),y(0)) = u(x_0,y_0)$$

$$v(0;x(0),y(0)) = v(x_0,y_0)$$

and x_0,y_0 are the initial coordinates (origin) of a trajectory of total length s. (The grid space unit Δd is used in the program to convert to nondimensional spatial units on the computational grid.) The vectors u(t;...) and v(t;...) provide a Lagrangian description of the velocity field. Increments of advection over a further time interval Δt are therefore given by

$$\Delta x = \frac{1}{\Delta d} \int_{t}^{t+\Delta t} u[t';x(t'),y(t')] \, dt' \; ; \qquad \text{(B-5a)}$$

$$\Delta y = \frac{1}{\Delta d} \int_{t}^{t+\Delta t} v[t';x(t'),y(t')] \, dt' \; . \qquad \text{(B-5b)}$$

After the new coordinates $x(t+\Delta t)$ and $y(t+\Delta t)$ are calculated for each incremented puff centerpoint, a check is made to see if any of these values are off the grid. If so, the affected puff is deleted from further consideration.

The integration of the wind components over the trajectory is approximated by a two-step iteration method involving bilinear interpolation in space and in time (see Figure B-3).

The various positions in Figure B-3 are best defined by equations:

$$x_1 = x(t) + u[t;x(t),y(t)]\ \Delta t\ ; \tag{B-6a}$$

$$y_1 = y(t) + v[t;x(t),y(t)]\ \Delta t\ ; \tag{B-6b}$$

$$x_2 = x_1 + u[t+\Delta t;x_1,y_1]\ \Delta t\ ; \tag{B-6c}$$

$$y_2 = y_1 + v[t+\Delta t;x_1,y_1]\ \Delta t\ ; \tag{B-6d}$$

$$x(t+\Delta t) = 0.5[x(t) + x_2]\ ; \tag{B-6e}$$

$$y(t+\Delta t) = 0.5[y(t) + y_2]\ . \tag{B-6f}$$

Thus, the new position $(x(t+\Delta t),y(t+\Delta t))$ is found by adding the vector average of two advection increments to the former position $(x(t),y(t))$. The first advection increment is calculated by advecting the plume increment for the entire interval Δt using the wind effective at $[x(t),y(t)]$ at time t. The addition of this increment to the position $[x(t),y(t)]$ yields the position (x_1,y_1). However, (x_1,y_1) is not assumed to be the actual end of the advection increment because the wind may change along the trajectory. A second advection increment is calculated using (x_1,y_1) as the starting point and the wind at that point effective at the end of the time increment. The addition of this advection increment to position (x_1,y_1) yields position (x_2,y_2). Then the new puff position $(x(t+\Delta t),y(t+\Delta t))$ is taken to be the point halfway along the line from $(x(t),y(t))$ to (x_2,y_2).

The bilinear interpolation by which the effective wind components $u(t)$, and $v(t)$ are calculated works as follows. Let t_n and t_{n+1} be the effective times of the two gridded wind fields closest to time t. Time interpolation weights t_1 and t_2 are defined by:

$$t_2 = \frac{t - t_n}{t_{n+1} - t_n} \qquad t_n \leq t < t_{n+1}\ ; \tag{B-7a}$$

$$t_1 = 1 - t_2. \tag{B-7b}$$

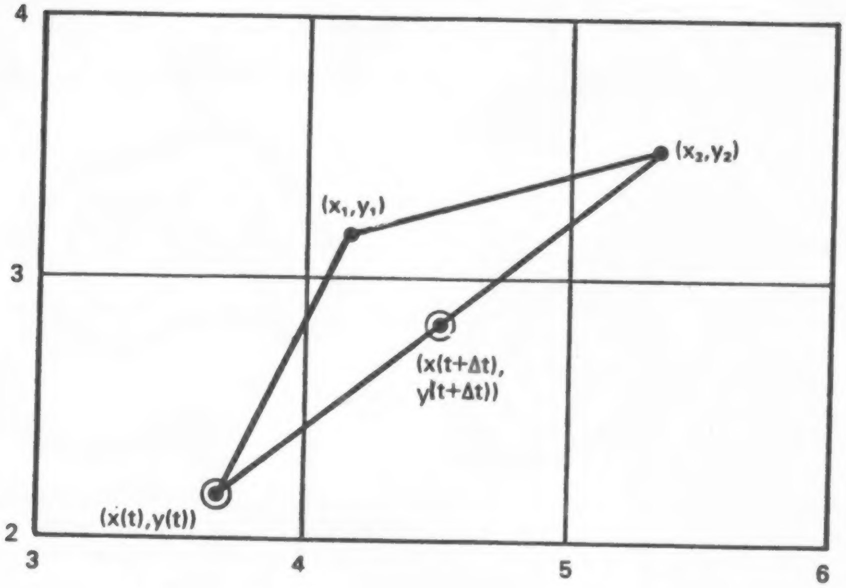
4
3
2
3
4
5
6
(x₁,y₁)
(x₂,y₂)
(x(t+Δt),
y(t+Δt))
(x(t),y(t))

Figure B-3 Calculation of the Trajectory of a Plume Segment Endpoint

Next, the location of (x(t),y(t)) is noted on Figure B-3. The coordinate values are between 3 and 4 for x(t) and between 2 and 3 for y(t). Accordingly:

$$X_q = x(t) - 3 \; ; \tag{B-8a}$$

$$X_p = 1 - X_q \; ; \tag{B-8b}$$

$$Y_q = y(t) - 2 \; ; \tag{B-8c}$$

$$Y_p = 1 - Y_q \; . \tag{B-8d}$$

This yields

$$\begin{aligned} u(t) = \; & t_1 X_p Y_p u(t_n;3,2) + t_2 X_p Y_p u(t_{n+1};3,2) \\ + \; & t_1 X_q Y_p u(t_n;4,2) + t_2 X_q Y_p u(t_{n+1};4,2) \\ + \; & t_1 X_p Y_q u(t_n;3,3) + t_2 X_p Y_q u(t_{n+1};3,3) \\ + \; & t_1 X_q Y_q u(t_n;4,3) + t_2 X_q Y_q u(t_{n+1};4,3) \; . \end{aligned} \tag{B-9}$$

Similar equations hold for v(t), u(t+Δt), and v(t+Δt). Therefore, the advection Equation B-5 is calculated from

$$\Delta x = \frac{1}{2\Delta d} \{u(t) + u(t+\Delta t)\}\Delta t; \tag{B-10a}$$

$$\Delta y = \frac{1}{2\Delta d} \{v(t) + v(t+\Delta t)\}\Delta t. \tag{B-10b}$$

The subsequent positions are given by

$$x(t+\Delta t) = x(t) + \Delta x \; ; \tag{B-11a}$$

$$y(t+\Delta t) = y(t) + \Delta y \; . \tag{B-11b}$$

B.4.2 The Puff Dispersion Function

This section, describing the evaluation of the puff dispersion parameters, has been taken largely verbatim, with modifications, from Hales et al. (1977, pp. 23-24). The puff dispersion parameters σ_y and σ_z are calculated for distances out to 100 km using plume growth formulas fitted to the curves of Turner (1970). For distances greater than 100 km the plume growth rates given by Heffter (1965) are used. The growth of a puff with travel time t or along the plume trajectory distance s from the source is represented by

$$\sigma_y(s+\Delta s) = \sigma_y(s) + \Delta s \left.\frac{d\sigma_y}{ds}\right|_{s+\Delta s/2} ; \qquad \text{(B-12)}$$

$$\sigma_y(t+\Delta t) = \sigma_y(t) + \Delta t \left.\frac{d\sigma_y}{dt}\right|_{t+\Delta t/2} . \qquad \text{(B-13)}$$

Similar equations for σ_z are used. These terms allow for spatial and temporal changes in stability class to be included, without violating the entropy principle (puff centerpoint concentrations cannot increase with downwind distance).

The integral formulas for σ_y and σ_z for travel distances less than 100 km are of the following forms

$$\sigma_y(s,\alpha) = Y_\alpha \, s^{0.9} \text{ (meters)}; \qquad \text{(B-14)}$$

$$\sigma_z(s,\alpha) = Z_\alpha \, s^{b_\alpha} \text{ (meters)}. \qquad \text{(B-15)}$$

Here α is a stability index designated as A, B, C, D, E, or F corresponding to the PGT stability categories. The coefficients Y_α, Z_α, and b_α are given in Table B-1 as a function of stability index α and yield values of σ_y and σ_z in meters when s is specified in meters. Because the integral formulas are not valid if the stability class changes over the travel distance s, differentiated forms of equations B-14 and B-15 are actually used to carry out the computations.

$$\frac{d\sigma_y}{ds} = 0.9 \; Y_\alpha \; s^{-0.1} ; \qquad \text{(B-16)}$$

TABLE B-1

COEFFICIENTS FOR DISPERSION PARAMETER FORMULAS

Stability Index α	Puff Growth Coefficients		
	Y_α	Z_α	b_α
A	0.36	0.00023	2.10
B	0.25	0.058	1.09
C	0.19	0.11	0.91
D	0.13	0.57	0.58
E	0.096	0.85	0.47
F	0.063	0.77	0.42

$$\frac{d\sigma_z}{ds} = b_\alpha Z_\alpha s^{(b_\alpha - 1)} \quad . \qquad \text{(B-17)}$$

MESOPUFF assumes that σ_y, $\sigma_z = 0$ at the origin $(s = 0)$.

The derivative formulas used to grow σ_y and σ_z for travel distances greater than 100 km are those given by Heffter (1965):

$$\frac{d\sigma_y}{dt} (m\ s^{-1}) = 0.5 \qquad \text{(B-18)}$$

$$\frac{d\sigma_z}{dt} (m\ s^{-1}) = 0.5\ (2K_z)^{1/2}\ t^{-1/2} \qquad \text{(B-19)}$$

B.4.3 The Plume Sampling Function

Each puff resident on the grid is sampled, using the plume sampling function, to evaluate the average concentration experienced at each sampling grid intersection during the previous time step. For example, consider the hypothetical puff depicted in Figure B-4. The puff centerpoint is at (x,y) and the puff radius is truncated at 3 σ_y. This is a reasonable simplification - much less than 1% of the area under a Gaussian distribution function lies beyond 3 σ_y from the peak value. During the time step considered, the grid point intersections (21,12) (22,12) and (22,13) are each impacted by the hypothetical puff; each grid point is assigned a certain average concentration resulting from the presence of the puff during the time step Δt. The grid point concentration C(i,j) calculated at (22,12) is computed by Equation B-2:

$$C(22,12) = \frac{Q(x,y)}{2\pi\ \sigma_y^{\ 2}(x,y)\ g_1(z)} \ \exp\left[\frac{-r^2}{2\ \sigma_y^{\ 2}(x,y)}\right] g_2(z) \qquad \text{(B-20)}$$

If a continuous plume has been properly simulated, a grid point impacted by the plume will receive individual doses from more than one puff (as was previously depicted in Figure B-1). It is also possible that two plumes overlap; in this case, puffs from both plumes can impact a grid point. The total concentration, $C_T(i,j)$ at each grid point is therefore computed as the sum of individual puff contributions:

$$C_T(i,j) = \sum_{M=1}^{M_T} C_M(i,j) \qquad \text{(B-21)}$$

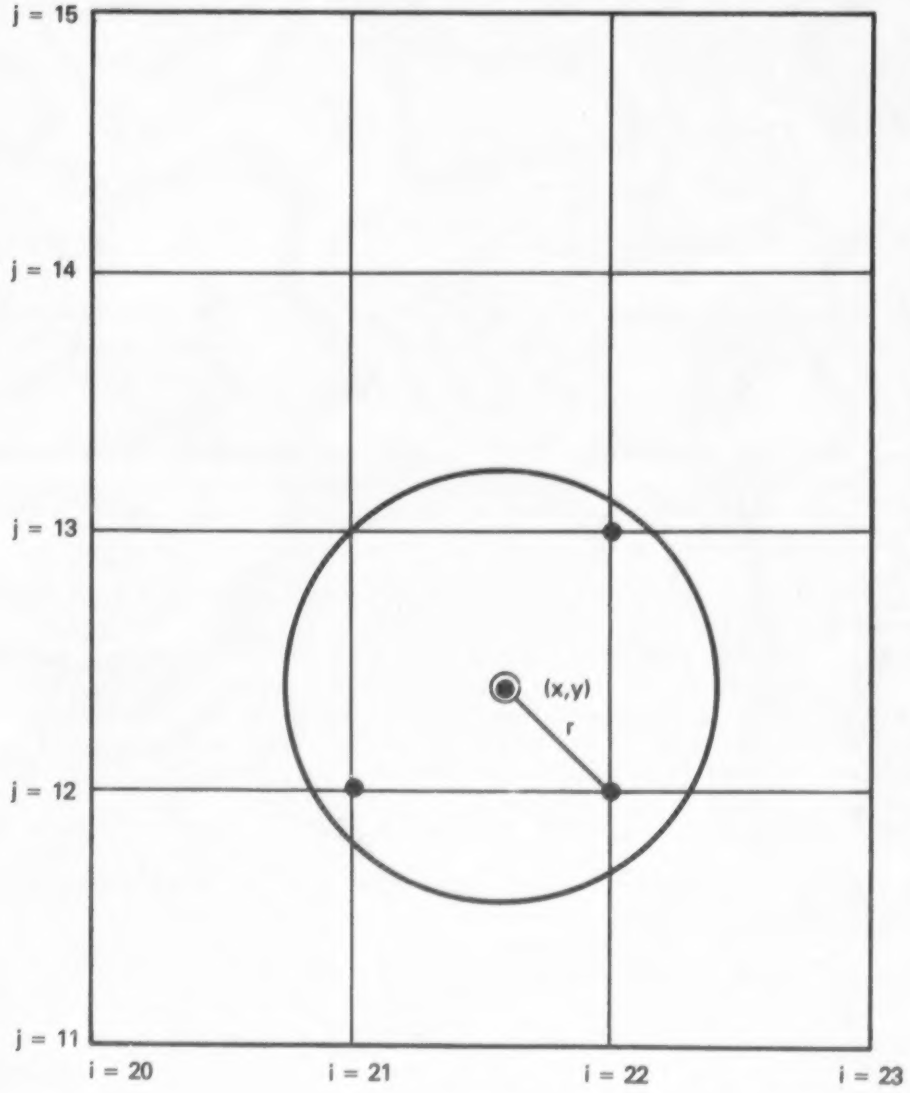
j = 15
j = 14
j = 13
j = 12
j = 11
i = 20
i = 21
i = 22
i = 23
(x,y)
r

Figure B-4 Calculation of the Concentration C(i,j) by the Sampling Function where M_T is the total number of puffs impacting the grid intersection (i,j) during the time step of interest.

B.5 Conversion of Sulfur Dioxide to Sulfate

MESOPUFF represents the conversion of SO_2 to $SO_4^=$ as a simple linear rate function--the changes in mass of each pollutant in one time step Δt are given by the time-discretized equations:

$$\Delta Q^n(SO_2) = k_1 \; Q^n(SO_2) \; \Delta t \tag{B-22a}$$

$$\Delta Q^n(SO_4^=) = -1.5 \; k_1 \; Q^n(SO_2) \; \Delta t \tag{B-22b}$$

where $Q^n(SO_2)$ is the mass of SO_2 at the beginning of the nth time step and $k_1(s^{-1})$ is the conversion rate constant. MESOPUFF uses the nominal value $k_1 = -5.56 \times 10^{-6}$ (that is, 2% per hour) suggested by Hales et al. (1977), unless otherwise specified by the user.

Note that the conversion of SO_2 to $SO_4^=$ represented by Equation B-22 is (1) independent of the vertical or horizontal distribution of SO_2 within a plume and (2) independent of whether a plume lies above or below the mixing height.

For the solutions to be adequate representations of the continuous exponential equations (e.g., $\dot{Q}(SO_2) = k_1 Q(SO_2)$), Q should not change appreciably over the time interval Δt. Since this is frequently not the case, the time interval Δt is optionally subdivided into as many subintervals $\Delta t'$ as are required to ensure that no more than a specified fraction ΔQ_f of the mass Q is removed by decay during a subinterval $\Delta t'$. This process is described further in the next section.

B.6 Dry Deposition of Sulfur Dioxide and Sulfate

The changes of mass $\Delta Q^n(g)$ of each pollutant resulting from dry deposition are given by:

$$\Delta Q^n(SO_2) = -(v_d(SO_2) \; Q^n(SO_2) \; \Delta t) \; / \; H_m \tag{B-23a}$$

$$\Delta Q^n(SO_4^=) = -(v_d(SO_4^=) \; Q^n(SO_4^=) \; \Delta t) \; / \; H_m \tag{B-23b}$$

where $Q^n(SO_2)$ and $Q^n(SO_4^=)$ are the masses of SO_2 and $SO_4^=$, respectively, in the puff at the beginning of the nth time step, $v_d(SO_2)$ and $v_d(SO_4^=)$ are the deposition velocities of each pollutant, and H is the vertical depth of the puff element (see Section B.8). MESOPLUME uses the nominal values $v_d(SO_2) = 0.01$ (m/s) and $v_d(SO_4^=) = 0.001$ (m/s), as suggested by Hales et al. (1977), unless otherwise specified by the user.

As described before, MESOPUFF can optionally ensure that the mass Q does not change within one subinterval $\Delta t'$ by more than a user-specified fraction ΔQ_f. Taking into account both SO_2 removal mechanisms (decay and deposition), the expression used by MESOPUFF to specify the subinterval $\Delta t'$ is

$$\Delta t' = \mathrm{MIN}\left\{ \frac{\Delta Q_f(SO_2)}{-k_1} \; , \; \frac{\Delta Q_f(SO_2)\; H_m}{v_d(SO_2)} \right\} \qquad \text{(B-24)}$$

In other words, the subinterval size $\Delta t'$ can optionally be chosen by MESOPUFF at the beginning of each basic interval Δt such that no more than a specified fraction ΔQ_f of SO_2 mass is removed by either mechanism (or, no more than $2\Delta Q_f$ by both mechanisms combined) within $\Delta t'$. It should be emphasized that the conversion and removal rates are not affected by this restriction. Further discussion of the optional sampling mechanism is contained in Section B.9.

B.7 Plume Rise

The effective emission height h_e of each puff is computed as $h_e = h_s + h_p$, where h_s is the stack height (m) and h_p is the plume rise (m). The plume rise equations used by the MESOPUFF model are those described by Briggs (1975) for equilibrium (final) plume rise. For unstable and neutral conditions with $h' \leq H$ (i.e., the plume does not rise into an elevated stable layer)

$$h_p = h' = 1.6\; F^{1/3}\; (3.5\; x^*)^{2/3}\; u^{-1} \; ; \qquad \text{(B-25a)}$$

For unstable and neutral conditions with $h' > H$ (i.e., the plume penetrates into an elevated stable layer)

$$h_p = \mathrm{MIN}\{h' \; , \; (z_b^3 + 18.75\; F\; u_m^{-1}\; S^{-1})^{1/3} \} \; ; \qquad \text{(B-25b)}$$

for stable conditions when $u \geq 1.37$ m/s

$$h_p = 2.6\, F^{1/3}\, S^{-1/3}\, u^{-1/3}\ ; \qquad \text{(B-25c)}$$

for stable conditions when $u < 1.37$ m/s

$$h_p = 5.0\, F^{1/4}\, S^{-3/8}\ . \qquad \text{(B-25d)}$$

where:

F = buoyancy flux (m^4/s^3)
x^* = $34.49\, F^{0.4}$ for $F > 55$
= $14.0\, F^{0.625}$ for $F \leq 55$
S = $(g/T)(\partial\theta/\partial z)$
g = $9.8\ m\ s^{-2}$
T = 290°K
$\partial\theta/\partial z$ = $0.137°K\ m^{-1}$
H = mixing depth (m)
z_b = $H - h_s$ (m)
u = wind speed ($m\ s^{-1}$)
u_m = MAX $\{u\ ,\ 1.37\}$

B.8 Treatment of Plume Fumigation

When the "uniform vertical distribution" option is elected, MESOPUFF takes the spatial and temporal variations in the mixing height into consideration to determine the height extent of ground level impact:

(a) For a puff element which is emitted at an effective stack height which is less than the mixing height, MESOPUFF assigns the element a height of zero and immediately mixes the entire mass of the puff uniformly through the mixing depth (the mixing lid acts as a perfect reflector). Equations B-3 and B-4 are then applied to compute ground level concentrations.

(b) For a puff element which is emitted at an effective stack height which is greater than the mixing height, no effect of the puff is felt at ground. However, if subsequently the mixing height becomes greater than the height of the puff centerpoint, the entire puff element is immediately mixed uniformly through the mixing depth, the puff height is set equal to zero, and Equation B-3 and B-4 again apply.

The mixing depth encountered by a puff element is likely to change over time and space. MESOPUFF assumes that a puff element residing in the mixed layer is mixed through the maximum mixing depth H_m encountered by the puff in its progression through the computational space-time grid.

The restriction of a uniform puff element through a characterizable depth such as H_m is imperative for a one-layer model such as MESOPUFF - so it is imperative for a one-layer model such as MESOPUFF - so that parcels of material, once entrained, are not bifurcated in the vertical when the height of the mixing lid changes (as sensed by a parcel in transport). Therefore, in the MESOPUFF model, a puff, once entrained, is uniformly mixed through a realistic height, consistent with the following assumptions:

(a) When convection ceases in the late afternoon, turbulent energy in the afternoon mixed layer dissipates. Once the energy of the large convective cells is completely damped, the remaining small scale energy is not sufficient to yield a vertical entrainment rate comparable to the daytime entrainment rate produced by large convective eddies.

(b) The stable lid capping the convective layer most likely maintains some integrity after convection ceases, and acts to prohibit any additional vertical entrainment of plume material.

(c) A modeling approach that redistributes mass into a shallower layer when the mixing depth decreases will violate the second law of thermodynamics.

Since no mechanism remains for turbulent transfer of pollutant material either upwards or downwards once the mixing depth decreases, it is asserted that the height most appropriate to define the extent of vertical mixing of a puff is the maximum mixing height that the puff encounters during any portion of its travel.

To schematically illustrate the interaction of the MESOPUFF vertical distribution algorithm and the mixing depth progression algorithm used by MESOPAC (Benkley and Bass (1979b), Benkley and Schulman 1979)) consider the hypothetical example given in Figure A-7 of Appendix A.

Here, consider two puffs of material released at different times from a source with an effective stack height of 250 m; the first puff release is made at 0300 GMT on the first day, the second puff release at 0300 GMT on the second day. Assume that the hypothetical source is located in the western United States so that 0000 GMT corresponds to late afternoon--the usual time of maximum mixing depth.

The first puff is entrained at 0600 GMT on Day 1 as the nocturnal boundary layer oscillates slightly upward in height. MESOPUFF immediately mixes the puff uniformly throughout this mixing depth.

This puff is mixed uniformly through 900 m by 0000 GMT on Day 2, and remains mixed through 900 m subsequent to that time, even though the height of the mixed layer collapses. The second puff, emitted at 0300 GMT on Day 2 is fumigated at 1500 GMT and is mixed uniformly through 700 m by the end of the afternoon. Therefore, the first puff, emitted at 0300 GMT on Day 1, remains uniformly mixed through a deeper vertical layer than the second puff; this is consistent with the greater extent of mixing on the first day as compared to the second day.

This mixing depth/fumigation scheme exhibits at least two shortcomings.

- When a puff becomes bifurcated in the vertical by collapse of the mixing lid, how should the puff radial dispersion rate be characterized? Because MESOPUFF is a one-layer model, the same set of horizontal dispersion coefficients must be applied to both the above-mixing-lid and the below-mixing-lid portions of the bifurcated puff.

- The dry deposition algorithm (see Section B.6) removes SO_2 and $SO_4^=$ at a rate proportional to the surface concentration--this loss is then redistributed throughout the entire vertical extent of the plume. It would be more realistic to distribute the loss only through the current mixing depth, but this is not possible in a one-layer puff element model.

It is felt that these limitations of the scheme are necessary for a method that is both computationally practical and yet realistic for use with a one-layer model. The inclusion of the fumigation cycle is very important; the marked effects of plume fumigation on the distribution of regional-scale ground level concentration patterns are illustrated in Section 3.3.

B.9 Accurate Simulation of the Continuous Plume

Because MESOPUFF simulates a continuous plume by means of a series of discrete puffs, care must be exercised so that puffs overlap sufficiently to allow the plume to appear smooth and continuous to the sampling function. There are two methods by which this can be accomplished: (1) by subdividing the distance Δs that a puff travels in one time step, and (2) by subdividing effective distance $\Delta s'$ between consecutive puffs.

The first method allows for sampling each puff on the grid at a rate n_s times more frequently than that with which the puff is advected. For $n_s > 1$ MESOPUFF will choose a sampling time step $\Delta t_s = \Delta t \; n_s^{-1}$

where Δt_s is the basic model time step. Therefore, the distance Δs_s traveled by a puff between consecutive plume samples is $\Delta s_s = \Delta s\ n_s^{-1}$.

The second method allows for releasing puffs at a rate n_p times more often than the basic time step; each puff released will have an initial mass of SO_2 assigned as $Q_p(SO_2) = Q(SO_2)\ n_p^{-1}$ where $Q(SO_2)$ is the mass of SO_2 emitted by a source in one 'basic' time step; the corresponding distance Δs_p between two consecutive puffs is $\Delta s_p = \Delta s'\ n_p^{-1}$. MESOPUFF updates the Lagrangian trajectory of each puff resident on the grid at each 'puff release' time step.

In practice, both options appear about equally effective in simulating a smooth and continuous plume (See Section 5.3). The puff release method is slightly more expensive but may yield more accurate puff trajectories in strongly curvilinear or temporally varying flows.

Both options can be exercised jointly; however, the larger of (n_p, n_s) should be an even multiple of the smaller. As an example, suppose the basic time step is 1 hour, with $n_p = 2$ and $n_s = 4$; puffs will be released every half-hour from each source, puff trajectories will also be updated every half-hour, and puffs will be sampled every quarter-hour, or twice per puff release step.

If the dynamic sampling step option is invoked in MESOPUFF (see Section B.6) the actual samplings step n_p used by MESOPUFF during any basic model time step will be taken as the larger of (a) the user-specified n_p and (b) the dynamically-computed n_p.

Some guidance in selecting the appropriate puff release and sampling rates for a MESOPUFF simulation is provided by Figure B-5, which depicts the strong effect of increasing the distance between adjacent puff centerpoints upon the ability of MESOPUFF to recreate a continuous plume. It is seen that when adjacent puff centerpoints are separated by no more than 2 σ_y, concentrations computed by MESOPUFF will differ by no more than about ±2% from concentrations as computed by MESOPUFF in the limit as puff separation distances go to zero; if the centerpoints at adjacent puffs are separated by about 4 σ_y, deviations can be a large as 50% or more.

Because puffs are assigned zero width when released, it follows that for a given combination of puff release rate, sampling rate, and wind speed, a certain amount of time must elapse before adjacent puffs have grown wide enough to provide the degree of overlap necessary to simulate a continuous plume. But, because high rates of puff release and puff sampling quickly become cost-prohibitive (see Section 5.2.3), some near-field inaccuracies must be tolerated if long-distance transport is to be modeled in a cost-effective manner. Therefore, if one wishes to model plume impact at distances greater than 100 km, for example, the puff relase rate and puff sampling rate should be chosen so that, for the maximum expected wind speeds, adjacent puffs will overlap sufficiently within, say a downwind range of 50-100 km.

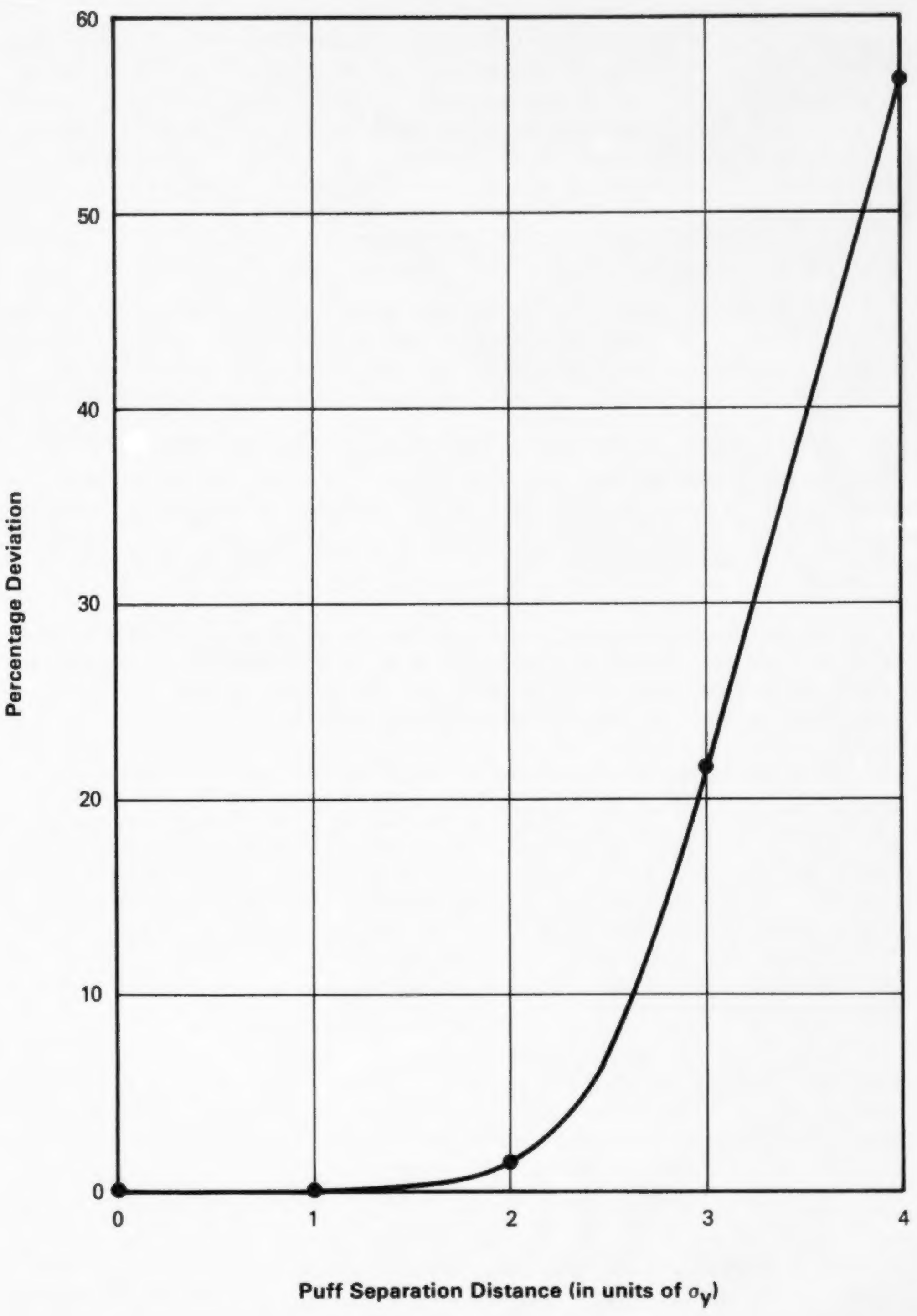

7909073

Figure B-5 MESOPUFF Model: Percentage Deviation with Puff Separation Distance

B.10 Comparison to the Conventional Gaussian Plume Model

From the point of view of possible regulatory applications, one of the most attractive features of MESOPUFF is its ability to recreate the results of the conventional Turner Workbook plume model (using PGT coefficients). When MESOPUFF is run with appropriate uniform steady-state meteorology and fine spatial resolution it can reproduce the Turner Workbook to a high degree. This can be demonstrated under the following test conditions:

- The horizontal grid spacing of the model is reduced, e.g., to 5 km.
- The meteorological fields (wind direction, wind speed, mixing height and PGT stability class) used to drive MESOPUFF are taken to be spatially uniform and constant in time.
- MESOPUFF is run with one source until quasi-steady-state conditions are well established; that is, puffs are created at the same uniform rate at which they disappear off the edge of the grid.
- Consecutive puffs are emitted (or sampled) with sufficient frequency to simulate a continuous plume (see Section B.9).

Under these special test conditions, MESOPUFF simulates very well the Turner Workbook plume concentrations out to distances of 100 km from an emission source. (The PGT coefficient curves, represented in the model by piecewise linear power law fits, are only defined to 100 km.) Table B-2 and Figure B-6 provide a representative illustration of how closely MESOPUFF results compare to those obtained for the conventional Gaussian plume model using the PGT "D" curve for σ_y and a uniform vertical distribution. Overall, the comparison is excellent--the very small fractional differences (typically less than 2%) are attributable mostly to inexact fitting of the PGT curves by the power law functions used in MESOPUFF.

MESOPUFF includes the option for a Gaussian distribution in the vertical with multiple reflections (see Section A-1). MESOPUFF is therefore applicable both in the near field of a source (where a vertical Gaussian profile is appropriate) and in the far field of a source (where a uniform vertical distribution is normally assumed). The current version of MESOPUFF does not, however, include a transitional plume rise algorithm but transitional plume rise is not important beyond 5 km, even for the largest power plants.

TABLE B-2

COMPARISON OF Cu/Q VALUES FOR MESOPUFF AND TURNER WORKBOOK-COMPUTED VALUES

($u = 2.78$ m s^{-1}, PGT Class = D, H = 1000 m,
uniform vertical distribution)

Distance (km)	PGT σ_y (m)	Turner Workbook ($C\ u\ Q^{-1}$)	MESOPUFF ($C\ u\ Q^{-1}$)	Fractional Deviation
5	300	11.80×10^{-7}	12.01×10^{-7}	0.02
10	550	7.25	7.47	0.03
15	780	5.11	5.18	0.01
20	1,000	3.99	4.02	0.01
25	1,220	3.27	3.28	0.00
30	1,420	2.80	2.80	0.00
35	1,620	2.46	2.43	-0.01
40	1,820	2.19	2.15	-0.02
45	2,020	1.97	1.94	-0.02
50	2,200	1.81	1.77	-0.02
55	2,400	1.66	1.62	-0.02
60	2,600	1.53	1.49	-0.03
65	2,775	1.44	1.39	-0.03
70	2,975	1.34	1.30	-0.03
75	3,200	1.25	1.22	-0.02
80	3,375	1.18	1.15	-0.03
85	3,550	1.12	1.09	-0.03
90	3,700	1.08	1.04	-0.04
95	3,850	1.04	1.00	-0.04
100	4,000	1.00	0.96	-0.04

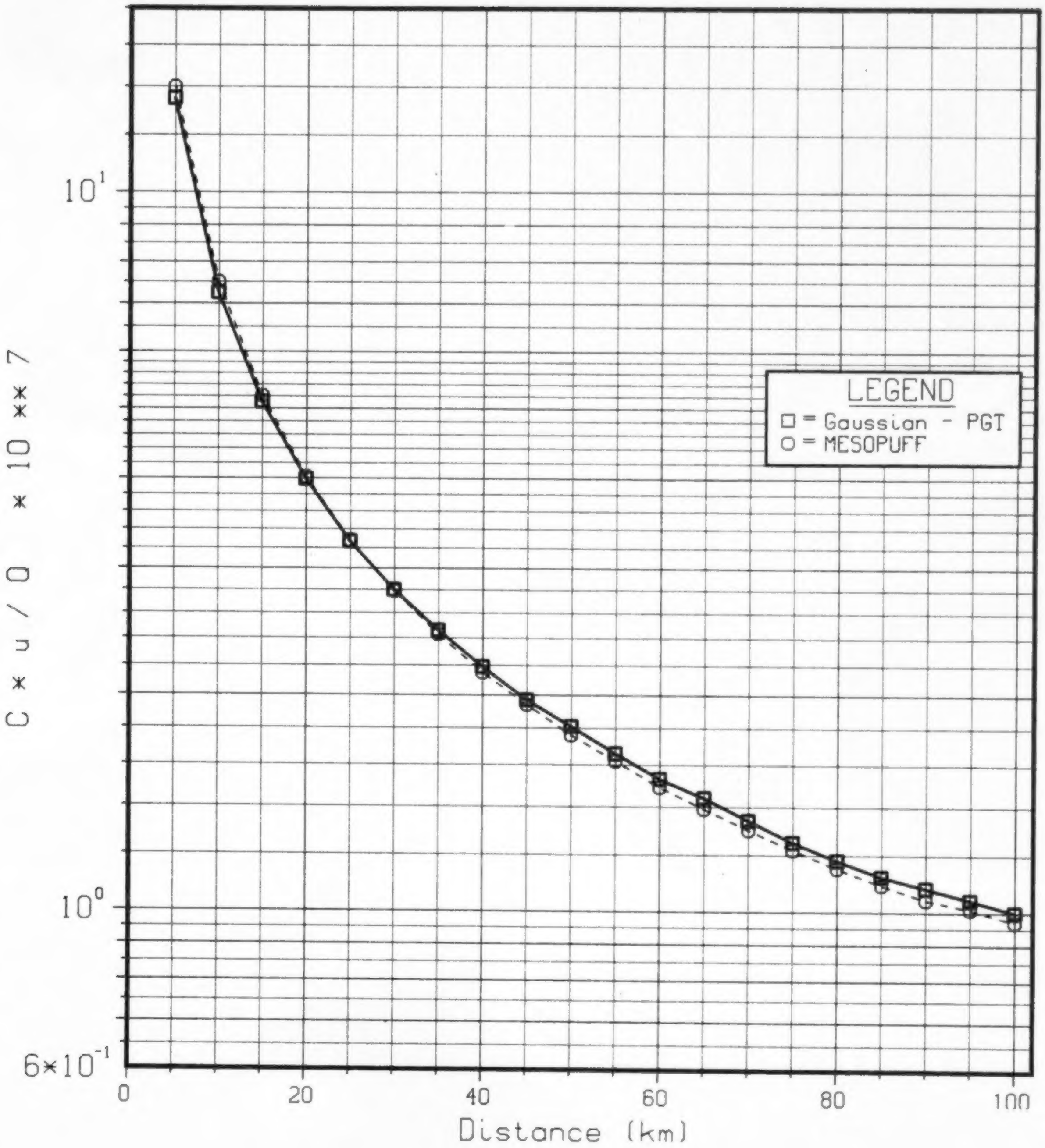

Figure B-6 MESOPUFF vs. the Conventional Gaussian Plume

APPENDIX C

MESOGRID TECHNICAL DISCUSSION

C.1 Model Formulation

The horizontal advection, vertical diffusion, linear decay, and dry deposition of sulfur dioxide (SO_2) and sulfate ($SO_4^=$) species on regional scales are represented in MESOGRID by a discrete-level numerical representation of the continuous equations describing the mass conservation of the respective pollutant species:

$$\frac{\partial C_1}{\partial t} = -u\frac{\partial C_1}{\partial x} - v\frac{\partial C_1}{\partial y} + \frac{\partial}{\partial z}\left(K_z\frac{\partial C_1}{\partial z}\right) - k_1C_1 - f_1C_1\delta(z,H,\Delta z_k) + \frac{Q_1}{\Delta z_k} \qquad \text{(C-1)}$$

$$\frac{\partial C_2}{\partial t} = -u\frac{\partial C_2}{\partial x} - v\frac{\partial C_2}{\partial y} + \frac{\partial}{\partial z}\left(K_z\frac{\partial C_2}{\partial z}\right) + \frac{3}{2}k_1C_1 - f_2C_2\delta(z,H,\Delta z_k) \qquad \text{(C-2)}$$

where

x is the east-west horizontal coordinate (m);

y is the north-south horizontal coordinate (m);

z is the vertical coordinate (m);

t is the time (s);

C_1, C_2 are the ambient concentrations of sulfur dioxide (SO_2) and sulfate ($SO_4^=$) respectively ($g\ m^{-3}$);

Q_1 is the source emission rate of SO_2 ($g\ m^{-2}s^{-1}$) within a vertical cell of height Δz_k (the $SO_4^=$ emission rate is assumed to be zero);

$u(x,y)$, $v(x,y)$ are, respectively, the x and y components of horizontal wind velocity ($m\ s^{-1}$);

K_z is the vertical eddy diffusivity ($m^2\ s^{-1}$);

k_1 is the rate (s^{-1}) of linear decay of SO_2 to $SO_4^=$;

f_1, f_2 are the dry deposition rate functions (s^{-1}) of SO_2 and $SO_4^=$, respectively. Dry deposition is considered only when the height z of a parcel of pollutant is below the mixing height H; and

$\delta(z,H,\Delta z_k) = 1$ for $z \leq$ and $k = 1$; $\delta(z,H,\Delta z_k) = 0$ for $z > H$ or $k \neq 1$.

The set of equations used by MESOGRID invokes these important assumptions:

- the advective wind field is two-dimensional (horizontal) only; thus if the model is to conserve mass strictly, it must be driven by a horizontally nondivergent wind field.
- horizontal diffusion is negligible compared to advective transport.

The MESOGRID model solves the set of discretized advection-diffusion equations on a three-dimensional grid with either two or three vertical levels (as desired). The Egan-Mahoney (1972) method of moments is used to minimize pseudodiffusive errors by conservation of the lower order moments of the pollutant distribution. The grid cell resolution is user-specifiable (to a maximum of 26x26x3 cells). The horizontal grid size is uniform; the vertical cell dimensions may vary between levels. The choice of grid cell dimensions will reflect the following considerations:

1) the overall size of the area to be modeled, and required spatial resolution of concentration fields,
2) the advective and diffusive numerical stability criteria, and
3) the relative model execution costs as dictated by items 1 and 2 above.

C.2 The Grid System

MESOGRID is referenced to a simple Cartesian coordinate system for easy interaction with a variety of input/output (I/O) routines, as well as pre- and postprocessors. The MESOGRID grid cell system is illustrated in Figure C-1. Each grid cell is denoted by an ordered triple of indices (i,j,k) where i is the east-west (x-direction) index (i=1 is the westernmost cell), j is the north-south (y-direction) index (j=1 is the southernmost cell), and k is the vertical (z-direction) index (k=1 is the lowest level). For example, the center of the southwesternmost and lowest grid cell (with indices 1,1,1) corresponds to the physical location $(x=0,\ y=0,\ z=\Delta z_1/2)$. All emission source data and meteorological data input to the MESOGRID model are referenced to this grid system.

C.3 Specification of Model Inputs

The meteorological fields required to drive the MESOGRID model are generated by the MESOPAC model (Benkley and Bass 1979c), a meteorological preprocessing package developed specifically for this purpose. MESOPAC produces gridded hourly interpolated fields of:

- horizontal (u,v) wind components ($m\ s^{-1}$),

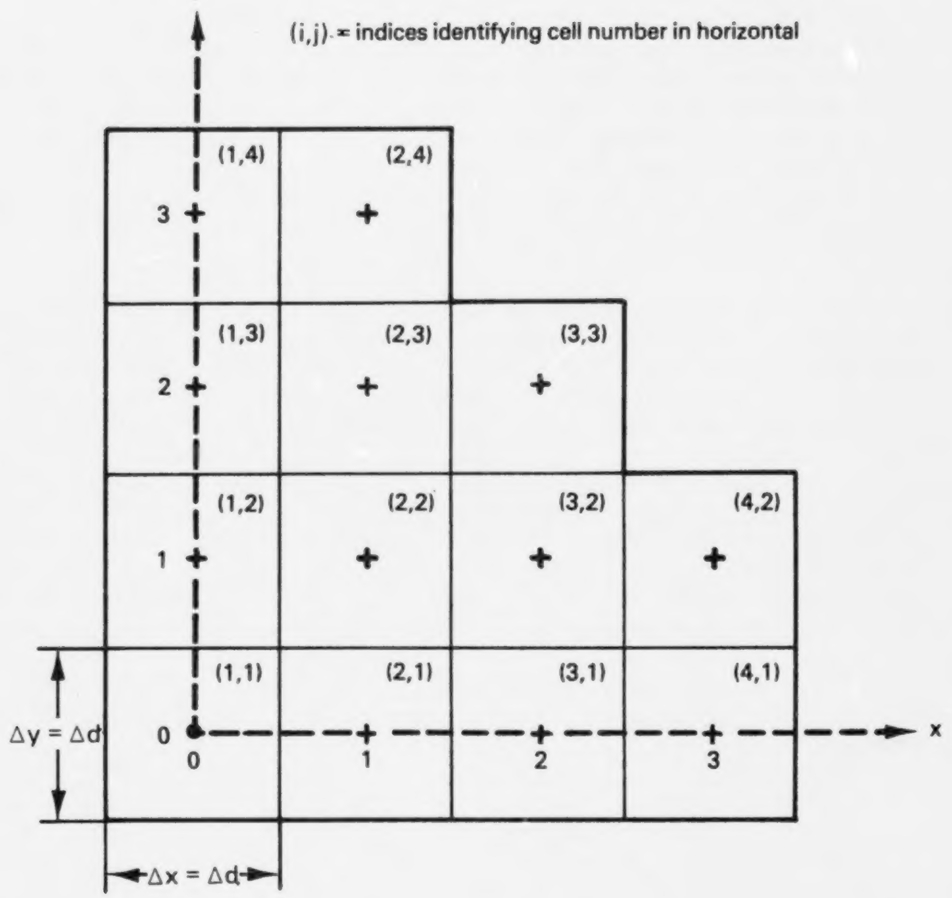
y
(i,j) = indices identifying cell number in horizontal
(1,4)
(2,4)
(1,3)
(2,3)
(3,3)
(1,2)
(2,2)
(3,2)
(4,2)
(1,1)
(2,1)
(3,1)
(4,1)
3
2
1
0
0
1
2
3
x
Δy = Δd
Δx = Δd

Figure C-1 A Schematic Representation of the MESOGRID Cartesian Coordinate System

- mixing depth (m), and
- Pasquill-Gifford-Turner (PGT) stability class.

Interaction of the MESOGRID model with the MESOPAC preprocessor is straightforward--the coordinate system is identical in both models and the grid point values of meteorological variables produced by MESOPAC apply directly to the center of each MESOGRID cell. At present, the horizontal wind components generated by MESOPAC are treated as invariant with height, although the MESOGRID model itself can accommodate vertically layered wind fields. The mixing depth and stability fields are used by MESOGRID to determine eddy diffusivity (K_z) vertical profiles (see a detailed discussion in Section C.4.3).

Emission source locations are user-specified through a three-dimensional Cartesian coordinate system (x,y,z coordinates), and MESOGRID assigns the appropriate (i,j,k) grid cell. For example (see Figure C-1), a source with x,y coordinates (0.6, 1.4) is assumed to fall within a grid cell with horizontal indices (2,2). Acceptable ranges of x and y are $(-0.5 \leq x \leq i_{max} -0.5)$ and $(-0.5 \leq y \leq j_{max} -0.5)$; if x or y values are specified beyond those limits, a MESOGRID run will terminate with the error message SOURCE NOT IN GRID. Source locations are assigned vertical indices (k) as illustrated in Figure C-2. Thus, a source with an effective release height, $h_e = h_s + h_p = 600$ m, where h_s is the stack height and h_p the plume rise (see Section C.8), is assumed to fall within the second (k=2) vertical layer.

Point source emissions Q(g s^{-1}) are assumed to be distributed uniformly throughout a grid cell; an equivalent volume emission source rate is defined by:

$$\overline{Q} = \frac{Q}{\Delta z_k (\Delta d)^2} \qquad \text{(C-3)}$$

where $\overline{Q}$ is the cell-averaged source emission rate (g $m^{-3}s^{-1}$), Q is the point-source emission rate (g s^{-1}), Δz_k is the vertical depth (m) of the k-th cell, and Δd is the size of a horizontal grid cell. As an example, if $Q = 10^3$(g s^{-1}), $\Delta z_2 = 10^3$ m, and $\Delta d = 4 \times 10^4$ m (typical values), then $\overline{Q} = 6.25 \times 10^{-10}$ (g $m^{-3}s^{-1}$).

C.4 Solution of the Advection-Diffusion Equations

The tracer equations for each pollutant (Equations C-1 and C-2) are solved in finite difference representations. The solution proceeds in two sequential steps. In the first step, pollutant mass is advected by the wind field. Immediately thereafter, in the second step, pollutant mass is diffused in the vertical at a rate proportional to the layer values of the K_z field. These computational steps are described next.

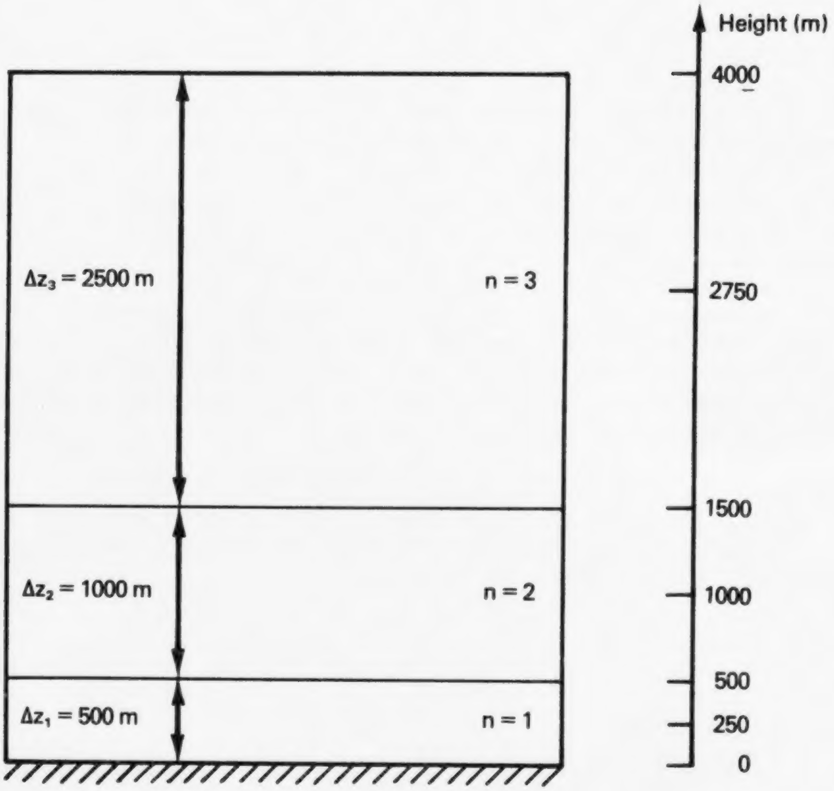
Height (m)
4000
2750
1500
1000
500
250
0
Δz₃ = 2500 m
n = 3
Δz₂ = 1000 m
n = 2
Δz₁ = 500 m
n = 1

Figure C-2 Vertical Structure of the MESOGRID Computation Grid Assuming Default Values

C.4.1 Horizontal Advection

Conventional finite-difference approximations to the two advection terms, $u\partial C/\partial x$ and $v\partial C/\partial y$ in Equations C-1 and C-2, produce truncation errors; these errors can introduce spurious, pseudodiffusive effects in the predicted concentration terms. This artificial diffusion by the numerical scheme can be, in some instances, orders of magnitude larger than that resulting from the real atmospheric mixing process. Various special finite-differencing methods have been proposed for control of numerical diffusion (e.g., SHASTA--see Boris and Book 1973). In the present model, the approach adopted is a unique mixture of both Eulerian and Lagrangian approaches, called the Method of Moments (Egan and Mahoney 1972). This method substantially reduces the pseudodiffusion associated with numerical advection term by using one or more statistical moments of the concentration distribution within a grid element scheme. This section describes this procedure in detail. To keep the explanation as simple as possible, the discussion of horizontal advection will be initially limited to the description of advection in the east-west direction only.

Defining C as the average concentration within a grid element, the forward-in-time, backward-in-space, finite-difference approximation to the horizontal advection for a uniform wind field $u > 0$ (neglecting diffusive, source, and sink terms) is

$$C^{T+1}_{m,k} = (1 - \sigma)\, C^{T}_{m,k} + \sigma C^{T}_{m-1,k} \qquad \text{(C-4)}$$

where T denotes the T^{th} time step such that $t = T\Delta t$, m and k denote the m^{th} (i^{th} or j^{th}) horizontal and the k^{th} vertical grid elements and $\sigma = u\Delta t/\Delta d$, the ratio of the advection distance per unit time step to the grid element dimension. The Courant advective criterion stability requires that $\sigma \leq 1$. After many time steps, the resulting horizontal advection can be likened to advection with velocity u and upwind-downwind mixing with a pseudodiffusive coefficient of magnitude $u\Delta d(1 - \sigma)/2$. A substantial reduction in this diffusive effect can be achieved if the first and second moments of the material within a cell are calculated after each time step and used to adjust the amount of material advected downwind during the next time step. Specifically, the procedure calculates the first and second moments of the concentration distribution after material has been advected into and out of a grid cell. These moments are then used to define a simple rectangular concentration distribution in the grid cell having the same amount of total mass and identical first and second moments.

Suppose ξ_m denotes the relative displacement of material within the m^{th} cell from the center of the cell, such that ξ_m ranges from -0.5 at the left hand to +0.5 at the right-hand extreme boundary of a cell. The zeroth, first, and centered second moments of the grid cell concentration distributions, corresponding to the mean concentration, the center of mass, and the scaled distribution variance are given by

$$
\begin{aligned}
C_m &= \int_{-0.5}^{0.5} C(\xi_m)\, d\xi_m \\
F_m &= \int_{-0.5}^{0.5} C(\xi_m)\, \xi_m \, d\xi_m / C_m \qquad \text{(C-5)} \\
R_m^2 &= \int_{-0.5}^{0.5} C(\xi_m)\, (\xi_m - F_m)^2 \, d\xi_m / C_m
\end{aligned}
$$

For simple rectangular concentration distributions, these integrals are readily evaluated by summation for each grid element in terms of the material distributions of the portions remaining and newly advected in after each successive time step. It may be seen that the nature of the downwind transfer depends on the value of the "portioning" parameter,

$$P_m = (F_m + \sigma + 0.5\, R_m - 0.5)/R_m \qquad \text{(C-6)}$$

For $P_m \leq 0$ none of the material is advected into the m+1 cell. If $P_m \geq 1$ all of the material is advected into the downwind cell. For $1 > P_m > 0$, an amount of material $P_m C_m$ is advected to the downwind cell, and $(1 - P_m)C_m$ remains in the m^{th} cell. Considering now the general case for the m^{th} cell with inflow from the m-1 cell, outflow to the m+1 cell, and continuous source addition during the time step, the forward-time computation procedure at grid element m can be represented as

$$
\begin{aligned}
C_m^{T+1} &= C_r + C_a + \overline{Q_m}\Delta T \\
C_m^{T+1}\, F_m^{T+1} &= C_r F_r + C_a F_a + \overline{Q_m}\Delta t(\sigma/2) \\
C_m^{T+1}\, (R^2)_m^{T+1} &= C_r[R_r^{\,2} + 12(F_m^{T+1} - F_r)^2] \qquad \text{(C-7)} \\
&\quad + C_a[R_a^2 + 12(F_m^{T+1} - F_a)^2] \\
&\quad + \overline{Q_m}\Delta t[1 + 12(F_m^{T+1} - \sigma/2)^2],
\end{aligned}
$$

where subscripts r and a indicate quantities remaining and newly advected in, respectively. This procedure completely eliminates pseudo-diffusive effects for a simple rectangular concentration distribution. Small diffusive errors will remain when more complicated distributions are advected.

In the MESOGRID model, the scheme described above has been generalized to two-dimension horizontal advection. Figure C-3 illustrates in top view the advection of a block of material with a uniform concentration distribution. In analogy to the one-dimensional advection procedure, one may define (suppressing the horizontal grid element subscripts (i,j)

$$\begin{aligned} P_i &= (F_i + \sigma_i + 0.5\ R_i - 0.5)/R_i \\ P_j &= (F_j + \sigma_j + 0.5\ R_j - 0.5)/R_j \end{aligned} \tag{C-8}$$

Then (imagining a newly emitted parcel of material contained within one grid cell), for the case illustrated in Figure C-3, where $0 < P_i$, $P_j < 1$, the contribution to the new concentrations at each of the four grid cells sharing the material after advection is

$$\begin{aligned} C^{T+1}_{i+1,j} &= C^{T}_{i,j}\ P_i(1 - P_j), \\ C^{T+1}_{i,j+1} &= C^{T}_{i,j}(1 - P_i)P_j, \\ C^{T+1}_{i+1,j+1} &= C^{T}_{i,j}\ P_iP_j, \\ C^{T+1}_{i,j} &= C^{T}_{i,j}(1 - P_i)(1 - P_j). \end{aligned} \tag{C-9}$$

The rules for advection for $P < 0$ or $P > 1$ follow those derived for one-dimensional advection, as do the expressions for calculating the first and second moments. In general the moments are evaluated from the concentration distributions advected into a cell from more than one adjacent cell. The computation procedure determines which neighboring cells contribute to the moment calculations and computes ΣC_m, ΣC_mF_m, $\Sigma C_mR_m{}^2$, and then the new values for each element:

$$C^{T+1} = \Sigma C_m \tag{C-10}$$

$$F^{T+1} = \frac{\Sigma C_mF_m}{C^{T+1}} \tag{C-11}$$

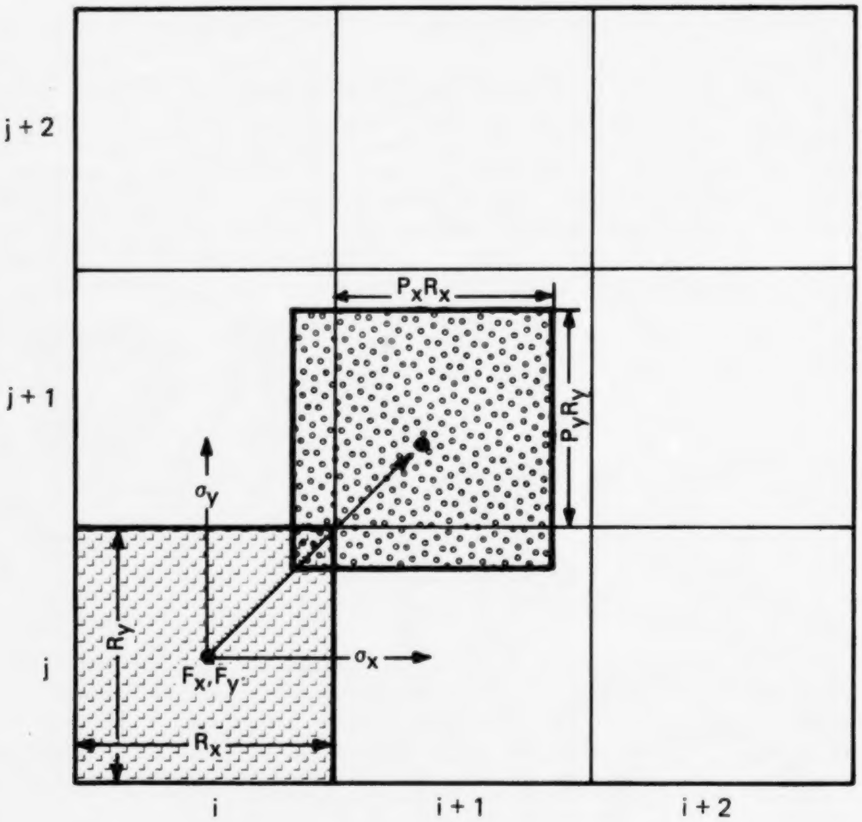
j + 2
j + 1
j
i
i + 1
i + 2
P_xR_x
P_yR_y
σ_y
σ_x
R_y
R_x
F_x, F_y

Figure C-3   Scale Parameters for the Advection of a Rectangular Block of Uniformly Mixed Material

$$\left(R^{T+1}\right)^2 = \frac{\Sigma C_m R_m^2}{C^{T+1}} - 12\left(F^{T+1}\right)^2 + 12\,\frac{\Sigma F_m^2 C_m}{C^{T+1}} \qquad \text{(C-12)}$$

C.4.2 Vertical Diffusion

The vertical diffusion terms $\partial/\partial z(K_z \partial C/\partial z)$ in Equations C-1 and C-2 are simulated by a conventional forward-time, centered-difference technique modified so that the vertical grid spacing can be variable. (The MESOGRID model is easily modified to include more vertical levels if computer resources and budgets permit.) In regions where parameters or concentrations change rapidly with height, resolution and accuracy can be improved with smaller vertical grid spacing. The vertical diffusion calculation may be represented by $C_k^{T+1} = (1 - \gamma_{k+1} - \gamma_{k-1})\, C_k^T + \gamma_{k+1}\, C_{k+1}^T + \gamma_{k-1}\, C_{k-1}^T$, where the horizontal subscript m is now suppressed, and

$$\gamma_{k+1} = \frac{(K_k + K_{k+1})\Delta t}{\Delta z_k\,(\Delta z_k + \Delta z_{k+1})}$$

$$\gamma_{k-1} = \frac{(K_k + K_{k-1})\Delta t}{\Delta z_k\,(\Delta z_k + \Delta z_{k-1})} \qquad \text{(C-13)}$$

The diffusivities K_k are calculated at the center of each grid element, and Δz_k denotes the depth of the kth grid element. The diffusive computational stability criterion requires that the γ's are less than 0.5. The first and second moments of the horizontal distribution are maintained in the diffusive transfer by two additional equations:

$$F_k^{T+1} = \left[\left(1 - \gamma_{k+1} - \gamma_{k-1}\right) C_k^T F_k^T + \gamma_{k+1}\, C_{k+1}^T F_{k+1}^T + \gamma_{n-1}\, C_{n-1}^T F_{n-1}^T\right] /\, C_k^{T-1} \qquad \text{(C-14)}$$

$$\begin{aligned}\left(R^2\right)_k^{T+1} = \Bigg\{ & C_k^T \left[\left(R^2\right)_k^T + 12\left(F_k^T - F_k^{T+1}\right)^2\right]\left(1 - \gamma_{k+1} - \gamma_{k-1}\right) \\ & + \gamma_{k+1}\, C_{k+1}^T \left[\left(R^2\right)_{k+1}^T + 12\left(F_{k+1}^T - F_{k+1}^{T+1}\right)^2\right] \\ & + \gamma_{k-1}\, C_{k-1}^T \left[\left(R^2\right)_{k-1}^T + 12\left(F_{k-1}^T - F_{k-1}^{T+1}\right)^2\right]\Bigg\} /\, C_k^{T+1}\end{aligned} \qquad \text{(C-15)}$$

C.4.3 Calculation of Spatially Variable K_z Profiles

MESOGRID computes spatially variable profiles of vertical eddy diffusivity for use in the vertical dispersion algorithms. The scheme uses the mixing depth, wind speed, and stability class information provided by MESOPAC to compute K_z profiles in each of two altitude regimes: (1) the surface layer of depth S = 0.1H and (2) the Ekman layer extending from the top of the surface layer to the mixing height H.

To develop the profiles of K_z in the boundary layer, it is assumed that atmospheric pollutants diffuse in the same manner as heat. The vertical eddy diffusivity in the surface boundary layer is then given by:

$$K_z = \frac{0.35\ u_* z}{\phi_h\left(\frac{z}{L}\right)} \qquad \text{(C-16)}$$

where

u_* is the friction velocity,

z is height above ground,

L is the Monin-Obukhov length,

ϕ_h is the nondimensional potential temperature gradient.

By definition, $\phi_h\left(\frac{z}{L}\right)$ equals 1 for neutral conditions $\left(\frac{z}{L} = 0\right)$ in the surface layer.

For stable conditions

$$\phi_h\left(\frac{z}{L}\right) = 1 + 4.7\ \frac{z}{L}\ ; \qquad \text{(C-17a)}$$

and for unstable conditions $(z/L > 0)$

$$\phi_h\left(\frac{z}{L}\right) = \left(1 - 15\ \frac{z}{L}\right)^{-1/2} . \qquad \text{(C-17b)}$$

Substitution of Equations (C-17a and C-17b) into Equation (C-16) yields for stable conditions

$$K_z = \frac{0.35\ ku_* z}{1 + 4.7\ \frac{z}{L}}\ ; \qquad \text{(C-18a)}$$

and for unstable conditions

$$K_z = 0.35u_*z\left(1 - 15\,\frac{z}{L}\right)^{1/2} \quad . \tag{C-18b}$$

The value of u_* is taken to be 0.035 u_f, where u_f is the "free stream" wind velocity (Blackadar 1962). If the MESOPAC model is used to compute wind fields, the winds may not be significantly less than the free stream wind speeds as long as the reference level chosen to describe the wind fields falls typically within the upper two-thirds of the boundary layer.

If the Monin-Obukhov length L is assigned a value dependent on the PGT stability class estimated by MESOPAC, the surface layer K_z profiles become stability-dependent as well. Table C-1 depicts values of L^{-1} as a function of PGT stability class for a typical roughness length z_o = 25 cm, as suggested by Golder (1972).

TABLE C-1

INVERSE MONIN-OBUKHOV LENGTH $L^{-1}(m^{-1})$ AS A FUNCTION OF
PGT STABILITY CLASS, FOR ROUGHNESS
LENGTH z_o = 25 cm (AFTER GOLDER 1972)

	PGT Stability Class					
	A	B	C	D	E	F
L^{-1}	-0.11	-0.05	-0.01	-	0.01	0.05

To develop the K_z profiles in the Ekman layer, MESOGRID uses an interpolation method suggested by O'Brien (1970) to determine diffusivities between the top of the surface layer (S) and the top of the mixed layer (H). Taking into account the physical requirement that the first derivative of K_z be continuous with height in the Ekman layer, O'Brien formulated the second-order equation

$$K_z = \frac{(z - H)^2}{(H - S)^2} \cdot \left\{ K_S + (z - S) \cdot \left[\left.\frac{\partial K_z}{\partial z}\right|_S + 2\,\frac{K_S}{H - S} \right] \right\} \tag{C-19}$$

where

z is the height at which K_z is to be determined
H is the height of the mixed layer (from MESOPAC)
S is the height of the surface layer
K_S is the value of K_z at the top of the surface layer (from Equation C-16)
$\left.\frac{\partial K_z}{\partial z}\right|_S$ is the derivative of K_z evaluated at S.

Here, it is assumed that K_z approaches zero at the top of the mixed layer. Three stability-dependent equations for $\partial K_z/\partial z|_S$ are formulated by differentiating Equation C-16 and evaluating at height S:

For unstable conditions

$$\left.\frac{\partial K_z}{\partial z}\right|_S = 0.35u_* \left(1 - 22.5 \frac{S}{L}\right) \left(1 - 15 \frac{S}{L}\right)^{-1/2} \quad ; \qquad \text{(C-20a)}$$

for neutral conditions

$$\left.\frac{\partial K_z}{\partial z}\right|_S = 0.35u_* \; ; \qquad \text{(C-20b)}$$

and for stable conditions

$$\left.\frac{\partial K_z}{\partial z}\right|_S = 0.35u_* \left(1 + 4.7 \frac{S}{L}\right)^2 . \qquad \text{(C-20c)}$$

Table C-2 contains formulations for surface-layer K_z (Equation C-16) and $\partial K_z/\partial z|_S$ (Equation C-20) appropriate to each PGT stability class, using the stability-dependent values of L^{-1} from Table C-1.

Equations C-16 through C-20 are used by MESOGRID to calculate values of K_z at the mean height z_k of each vertical grid element whenever the meteorological data is updated by MESOPAC. Because of the way the MESOGRID model characterizes vertical diffusion the mixing depth, H cannot be used directly as the depth through which pollutants diffuse in the vertical. However, the effect of a mixing lid can be simulated

TABLE C-2

STABILITY-DEPENDENT EXPRESSIONS FOR K_z IN THE SURFACE LAYER AND $\left.\frac{\partial K_z}{\partial z}\right|_S$

PGT Stability	K_z (surface layer)	$\left.\frac{\partial K_z}{\partial z}\right\|_S$
A	$0.35u_*z(1 + 1.65\ z)^{1/2}$	$0.35u_*(1 + 2.48\ S)(1 + 1.65\ S)^{-1/2}$
B	$0.35u_*z(1 + 0.75\ z)^{1/2}$	$0.35u_*(1 + 1.13\ S)(1 + 0.75\ S)^{-1/2}$
C	$0.35u_*z(1 + 0.15\ z)^{1/2}$	$0.35u_*(1 + 0.23\ S)(1 + 0.15\ S)^{-1/2}$
D	$0.35u_*z$	$0.35u_*$
E	$0.35u_*z(1 + 0.05\ z)^{-1}$	$0.35u_*(1 + 0.05\ S)^2$
F	$0.35u_*z(1 + 0.23\ z)^{-1}$	$0.35u_*(1 + 0.23\ S)^2$

approximately--MESOGRID sets K_z in a grid cell essentially to zero if the mean grid cell lies above the mixing height. Referring to the example in Figure C-2, if the mixing depth H lies between 1,000 and 2,750 meters, K_z is set to zero in the uppermost layer but is left unchanged in the two lower layers. But because diffusive transfer of mass by two contiguous vertical grid cells is made proportional to the average of the K_z values for each cell (Equation C-13), without further modification of the K_z profiles, mass transfer would take place between Levels 2 and 3 even though Level 3 lies entirely above the mixing depth. MESOGRID will correct partially for this behavior; the average of K_z for Levels 2 and 3 will be set equal to zero if $1{,}000 \leq H < 1{,}500$ m, but will be unchanged if $1{,}500 \leq H < 2{,}750$ m.

C.4.4 Numerical Stability Criteria

As described before, computational stability of the computational scheme is ensured only if:

$$\frac{u\Delta t}{\Delta d} \leq 1 \qquad \text{(C-21)}$$

and

$$\frac{(K_k + K_{k\pm1})\ \Delta t}{\Delta z_k(\Delta z_k + \Delta z_{k\pm1})} \leq 0.5 \qquad \text{(C-22)}$$

Equation (C-21), the advective stability criterion (Courant condition) means that a parcel of mass must not be advected, in either horizontal direction, through a distance greater than one grid space Δd within a time step Δt. Equation (C-22) means that the effective vertical diffusion velocity $(K_k + K_{k\pm1})/(\Delta z_k + \Delta z_{k\pm1})$ cannot be such that a parcel is displaced vertically (by diffusion) more than a distance $\Delta z_k/2$ within Δt.

Given the maximum values of u and K_z at the beginning of each hour, MESOGRID calculates the maximum time step allowed by the more stringent of these stability criteria, except that the actual time steps used by MESOGRID are constrained to be even fractions of one hour; thus the possible choices for Δt are 5, 6, 7.5, 10, 15, 20, 30, and 60 minutes. Note that, notwithstanding the above, MESOGRID does not currently allow selection of a time step shorter than 5 minutes.

Table C-3 lists the maximum values wind velocity $\underline{u}$ and K_z values (expressed as averages between adjacent levels, e.g., $\overline{K}_{1.5} = (K_1 + K_2)/2$, for the nominal choices ($\Delta d = 40{,}000$ m, $\Delta z_1 = 500$ m, $\Delta z_2 = 1{,}000$ m, and $\Delta z_3 = 2{,}500$ m). Under stable conditions, the advective criterion will normally dominate, whereas for unstable conditions (resulting in computed K_z values up to 10^3 in test simulations), the vertical diffusion

TABLE C-3

MAXIMUM VALUES OF u AND $\overline{K}_{1.5}$, $\overline{K}_{2.5}$ VS. TIME STEP Δt, FOR NOMINAL MODEL PARAMETERS

Model Time Step Δt (min)	Advective Stability Criterion ($m\ s^{-1}$)	Diffusive Stability Criterion $\overline{K}_{1.5}$ ($m^2\ s^{-1}$)	$\overline{K}_{2.5}$ ($m^2\ s^{-1}$)
5	135	625	2,916
15	45	208	972
30	22	104	486
60	11	52	293

Assumptions: Δd = 40,000 m

Δz_1 = 500 m

Δz_2 = 1,000 m

Δz_3 = 2,500 m

stability criterion may dominate. Specific choices of horizontal and vertical grid cell dimensions can yield stability criteria significantly different from those of the hypothetical example. For instance, if the desired near-ground vertical resolution dictates choice of a small Δz value, the maximum time step may be determined by the diffusion criteria, whatever the stability class.

In the MESOGRID model simulations, it was often found that for unstable conditions, K_z would be so large that the time steps necessary to ensure computational stability were smaller than the minimum value deemed reasonable for regional-scale transport (Δt = 5 minutes). Because such small time steps result in very expensive computing costs, a method, explained next, has been provided to give the user a degree of control over the diffusion-specified time step by systematically decreasing very large values of K_z. Such a procedure may be justifiable if the MESOGRID model is used for regional-scale simulations (as distinct from near-source impacts). Because, in a grid model, the magnitude of K_z values determines the rapidity with which vertical mixing will occur by diffusion--as long as the reduced K_z values lead to uniform vertical mixing within travel distances that are small compared to the regional transport scales of interest, the effect on regional-scale concentration patterns should be minimal (unless ground-level removal processes are of dominant importance).

The approach taken here forces the model to reduce large values of K_z to within a range consistent with both the advective stability time step Δt_a (Equation C-21) and a user-specified "requested" time step Δt_r. There are six distinct cases delineated in Table C-4 for modification or nonmodification of K_z; these six cases are the six possible orderings of Δt_r, Δt_a and the diffusive stability time step Δt_d (Equation C-22) by increasing magnitude. No modification of K_z is required in Cases 1, 2, and 3, because the advective stability criterion is at least as stringent as the diffusive stability criterion, thus the model selects a time step shorter than that required by the largest K_z values. In Case 4, the diffusive stability criteria is more stringent than the advective stability criteria, but no K_z modification is necessary because $\Delta t_r \leq \Delta t_d$. For Cases 5 and 6, both Δt_a and Δt_r are greater than Δt_d, and modification of K_z profiles is required. In Case 5, large K_z values are reduced to within a range acceptable to Δt_r, whereas in Case 6, large values are reduced in accordance with Δt_a. In both cases, a K_z profile that violates either of the diffusive stability criteria in Table C-3 is uniformly reduced by an appropriate scaling factor--the shape of the profile is maintained.

The "requested" time step procedure gives the user a measure of control over the time steps selected by the model and, thus, the cost of a model simulation. The procedure results in the modification of the fewest number of K_z profiles by the smallest amount necessary to enable use of either Δt_r or Δt_a.

TABLE C-4

DETERMINING WHEN MESOGRID WILL MODIFY K_z PROFILES

Case Number	Possible Time Step Orderings	Modify K_z?
1	$\Delta t_a \leq \Delta t_d \leq \Delta t_r$	No
2	$\Delta t_a \leq \Delta t_r \leq \Delta t_d$	No
3	$\Delta t_r \leq \Delta t_a \leq \Delta t_d$	No
4	$\Delta t_r \leq \Delta t_d \leq \Delta t_a$	No
5	$\Delta t_d < \Delta t_r \leq \Delta t_a$	Yes, in accordance with Δt_r
6	$\Delta t_d < \Delta t_a < \Delta t_r$	Yes, in accordance with Δt_a

C.5 Boundary Conditions

The MESOGRID model permits horizontal boundary concentrations of SO_2 and $SO_4^=$ to be specified independently for each vertical level and at each east-west and north-south boundary face of the computational region. The boundary value concentrations are assumed to occupy fictitious grid cells adjacent to the boundary of the regular grid. These concentrations are then advected into the grid using the procedure described in Section C.4.1. These boundary values, which have default values of zero, are assumed to be time independent.

The boundary condition describing mass transfer through the "top" of the computational region is specified in terms of a reflection coefficient. The reflection coefficient is user-specified and can range from complete reflection of mass from the upper boundary (value of unity) to total loss of material through the upper boundary (value of zero). The boundary condition describing mass transfer out of the bottom of the grid is user-specified through the 'deposition velocity' concept. Section C.7 gives a more detailed description of the bottom boundary condition.

C.6 Conversion of Sulfur Dioxide to Sulfate

MESOGRID represents the conversion of SO_2 to $SO_4^=$ as a simple linear rate function. The changes in mass of each pollutant in one time step Δt are given by:

$$\Delta Q^n(SO_2) = k_1 Q^n(SO_2) \Delta t \tag{C-23a}$$

$$\Delta Q(SO_4^=) = -1.5 k_1 Q^n(SO_2) \Delta t \tag{C-23b}$$

where $Q^n(SO_2)$ is the mass of SO_2 at the beginning of the nth time step, and k_1 (s^{-1}) is the conversion rate constant. MESOGRID uses the nominal value $k_1 = -5.56 \times 10^{-6}$, as suggested by Hales et al. (1977), unless otherwise specified by the user.

It should be noted that the conversion of SO_2 to $SO_4^=$ represented by Equation C-23 is (1) made independent of the vertical or horizontal distribution of SO_2 within a plume, and (2) independent of whether a plume lies above or below the mixing height.

When Equation C-23 is applied to an individual grid cell after the advection calculation and prior to the diffusion calculation, the changes in concentrations of SO_2 and $SO_4^=$ resulting from linear conversion are:

$$\Delta C^n(SO_2) = k_1 C^n(SO_2) \Delta t \tag{C-24a}$$

$$\Delta C^n(SO_4^=) = -1.5 k_1 C^n(SO_2) \Delta t \tag{C-24b}$$

where, for example, $C^n(SO_2)$ is the grid cell concentration of SO_2 at time step n, following the horizontal advection operation.

C.7 Dry Deposition of Sulfur Dioxide and Sulfate

The changes of mass $\Delta Q^n(g)$ of each pollutant at time step n resulting from dry deposition are given by:

$$\Delta Q^n(SO_2) = -\left\{v_d(SO_2)\ Q_1^n(SO_2)\ \Delta t\right\}/\Delta z_1 \qquad \text{(C-25a)}$$

$$\Delta Q^n(SO_4^=) = -\left\{v_d(SO_4^=)\ Q_1^n(SO_4^=)\ \Delta t\right\}/\Delta z_1 \qquad \text{(C-25b)}$$

where $Q^n(SO_2)$ and $Q^n(SO_4^=)$ are the total masses of SO_2 and $SO_4^=$, respectively, in a vertical column at the beginning of time step n (Q_1^n is the mass in the lowest cell); $v_d(SO_2)$ and $v_d(SO_4^=)$ are the deposition velocities of SO_2 and $SO_4^=$ respectively; and Δz_1 is the vertical depth of the the lowest grid layer. MESOGRID uses the nominal values $v_d(SO_2) = 0.01\ (m\ s^{-1})$ and $v_d(SO_4^=) = 0.001\ (m\ s^{-1})$, as suggested by Hales et al. (1977), unless otherwise specified by the user.

There is an important difference in the way mass is depleted by MESOGRID as compared to the plume and puff models; although the amounts of SO_2 and $SO_4^=$ removed by dry deposition are the same in each model for vertically uniform distributions, MESOGRID depletes mass in only the lowest of its vertical layers rather than throughout the entire mixing depth (as do the other models). However, since MESOGRID exercises the dry depostion algorithm before the vertical diffusion algorithm, mass loss in a cell in the lowest level is redistributed through cells in the upper layers (as long as they are below the mixing lid). Therefore, if the effective "diffusion velocity" (see Section C.4.4) is large, the dry deposition algorithm in MESOGRID yields the equivalent results as the algorithm in the other models.

C.8 Plume Rise

The effective emission height h_e of each point source is computed as $h_e = h_s + h_p$, where h_s is the stack height (m) and h_p is the plume rise (m). The plume rise equations used by the MESOGRID model are those described by Briggs (1975) for equilibrium (final) plume rise.
For unstable and neutral conditions with $h' \leq H$ (i.e., the plume does not rise into an elevated stable layer).

$$h_p = h' = 1.6\ F^{1/3}\ (3.5\ x^*)^{2/3}\ u^{-1}; \qquad \text{(C-26a)}$$

For unstable and neutral conditions with h' > H (i.e., the plume penetrates into an elevated stable layer)

$$h_p = \text{MIN} \left\{ h', \quad (z_b^3 + 18.75\ F\ u_m^{-1}\ S^{-1})^{1/3} \right\} ; \qquad \text{(C-26b)}$$

for stable conditions when $u \geq 1.37$ m s^{-1}

$$h_p = 2.6\ F^{1/3}\ S^{-1/3} u^{-1/3}; \qquad \text{(C-26c)}$$

for stable conditions when $u < 1.37$ m s^{-1}

$$h_p = 5.0\ F^{1/4}\ S^{-3/8}; \qquad \text{(C-26d)}$$

where:

F = buoyancy flux (m^4 s^{-3})

x^* = $34.49\ F^{0.4}$ for $F > 55$

= $14.0\ F^{0.625}$ for $F \leq 55$

S = $(g/T)(\partial\theta/\partial z)$

g = 9.8 m s^{-2}

T = 290°K

$\partial\theta/\partial z$ = 0.0137°K m^{-1}

H = mixing depth (m)

z_b = $H - h_s$ (m)

u = wind speed (m s^{-1})

u_m = MAX $\{u , 1.37\}$

APPENDIX D

SCALE ANALYSIS FOR TERMS IN MASS CONTINUITY EQUATION

Consider the mass continuity equation with decay:

$$\frac{\partial C}{\partial \tau} = -\nabla \cdot (\overline{v}C) - kC + C\nabla \cdot \overline{v}$$

where

$\frac{\partial C}{\partial \tau}$ is the time rate of change of concentration,

$-\nabla \cdot (\overline{v}c)$ is the advective term in flux form,

$-k_1C$ is the decay term, and

$C\nabla \cdot \overline{v}$ is the divergence term.

Using worst-case scaling values, an order of magnitude estimate for the time scale of the advective term is approximately:

$$\tau_{ad} \sim \frac{L}{U} \quad \frac{2 \times 10^4 m}{2m/s} \sim 3 \text{ hours}$$

where L is a length scale typically containing most of the lateral concentration gradient of the plume, and U is a typical stagnation wind speed velocity. By comparison, the time scale for decay is much longer:

$$\tau_d \sim -\frac{1}{\ln(0.98)} \sim 50 \text{ hours}$$

the e-folding time for a rate of decay of 2% per hour.

But, for the divergence term taken as 10^{-4} sec^{-1}, the time scale for mass change resulting from the absolute divergence of the horizontal wind field is given by:

$$\tau_{div} \sim 3 \text{ hours}$$

or of the same order as the advective time step. Therefore, the results of the MESOGRID model (in common with any Eulerian grid model) can be significantly influenced by divergence presented in the wind field.